Model Order Reduction for Computational Aeroelasticity

Matteo Ripepi

Ph.D. Thesis

Cover: Aircraft flying in the sky between the clouds.
Designed by Antonio and Matteo Ripepi.

POLITECNICO DI MILANO
Dipartimento di Scienze e Tecnologie Aerospaziali
Doctoral Programme in Aerospace Engineering

Model Order Reduction for Computational Aeroelasticity

Doctoral Dissertation of:
Matteo RIPEPI

Supervisor:
Prof. Paolo Mantegazza

Tutor:
Prof. Sergio Ricci

The Chair of the Doctoral Program:
Prof. Luigi Vigevano

2014–XXVI cycle

This dissertation has been completed in partial fulfillment of the requirements for the doctoral program in Aerospace Engineering of the *Dipartimento di Scienze e Tecnologie Aerospaziali* (DSTA).

Keywords: Model Order Reduction, System Identification, Aeroelasticity, Unsteady Aerodynamics, Computational Fluid Dynamics, Gust Modeling

Printed in Germany
Author's email: matteo.ripepi@mail.polimi.it

“True is much too complicated to allow anything but approximations”

— John von Neumann, 1903 - 1957

Acknowledgments

It is always a difficult task to include all the people that, during a three years work towards a doctoral degree, have contributed in a major or minor measure to be part of your laborious and fascinating journey.

I will start with my supervisor Prof. Paolo Mantegazza, who has provided me with an invaluable amount of technical knowledge in aeroservoelasticity beginning from his teachings in the graduate classes, continuing with his support during the master thesis, and ending with my Ph.D. research. It has been great working with you. Thank you.

I wish to express my gratitude to Prof. Sergio Ricci, always available in helping me with suggestions and recommendation, from when I was a graduate student. Thank you to put me into contact with the DLR for my visiting research experience. For that, in some sense, you gives me a new direction to my life. I am also grateful to Prof. Pierangelo Masarati, always ready to teach me something new whenever there was occasion. I must say I have always admired you and the way you passionately and tirelessly work. Thanks to Prof. Marco Morandini, who helped me with the use of SLEPc, and provided me with the needed computational power for run some of my calculations.

I want to thank Prof. Dr. Norbert Kroll, who accepted me in the Institute of Aerodynamics and Flow Technology of DLR to work with Dr. Stefan Görtz on model reduction and gust modeling. Thank you to offer me a job position. And thank you Stefan for all the help you give me during my experience, ranging from basic things as give me a ride to Ikea, passing from the professional support with the TAU-code, to the talks we had about living abroad. You are a very smart, respectful and kind person. I am also grateful to Dr. Ralph Heinrich for the support with the implementation of the gust modeling, and to my officemate Vamshi who helped me with the settings of the TAU-code. Thanks to Adrien and all "der mittagessen group" for the nice time spent together during lunch time. And a special mention to Till, who introduces me to the Triathlon group. I had great time with you guys. I want to thank also the research group of the DLR Institute of Aeroelasticity of Göttingen, for the interesting exchange of ideas and the nice talks about research topics in aeroelasticity. You are a group of very smart guys.

I wish to express my gratitude to Prof. Charbel Farhat, who accepted me in his lab at Stanford University to work with Dr. David Amsallem. It has been an honor to work in your research group and be part of Stanford, even if for a while. Thank you David for your support during my visiting experience, and for the valuable exchange of ideas on model reduction. I hope we can continue to collaborate on nonlinear model reduction. I had a great experience and learnt many new things, attending the group meetings and the

seminars, and working side by side with the smart people of the group. Thanks to Philip, for the support you give me with the finite element formulation. A particular thanks to Maciej, for the interesting exchange of ideas about the nonlinear identification methods and Volterra theory, and beside that for the good discussions during lunch time, together with Radek and Jari. I really appreciate your efforts for accommodate me in the group. I wish also thank my Stanford colleagues, Todd, Matt, Kyle, Alex, and Hubert for sharing the office, sometimes until late night. Thanks to all the international friends, most of them Italians and Frenches, that I met at Stanford and Palo Alto. I really enjoyed the time spent together with you in California. You gave me many good memories to bring back home.

A very special thanks goes to all my colleagues and friends of the Politecnico di Milano. To Giulio, for the help with your CFD code AeroFoam, for the stimulating discussions about computational aeroelasticity, and for your enthusiastic way in approaching the development and implementation of new thing. I have always admired your skills and capacities. To Andrea, continually available in helping people whenever they need, thank you for providing me with suggestions about the Matlab implementations and to provide me with your Full Potential code. Beside that, your cheerful behavior have always revived the office mood. To Sebastiano, for the hint you give me about the harmonic balance method that I developed in Stanford. To Andrea, for the exchange of ideas about identification techniques and to provide me the training data for the nonlinear identification. To Fabio, for the downgrading of my computer. To Dario and Andrea who gives me their templates for this thesis. Thanks to Riccardo, Vincenzo, Alessandro, Tommy, Federica, Valentina, Francesca, Barbara, Claudio, Michele. You all are very special person and I will miss you and the typical happy environment you bring in our offices. A special thanks to Andrea, for the discussions we hold in Delft about what walking through a doctoral program means. I guess you give me a last motivation and incentive to start my Ph.D. You are a very smart person, I admired your talent since the time of undergraduate studies. I have been fortunate to meet during my education so many talented individuals.

Thanks to my closest friends: Luca, Antonietta, Fabio, Giulia, Maurizio, Laura, Francesca, Eleonora. Somewhere I read that good friends are like good books: they know to wait, but they are always available when you search for them. So I want to thank all of my friends that, despite sometimes I did not dedicated them the time I wished, for traveling and study reasons, are always present. You know life will split you apart from your friends, but you will always have a place in you heart for them and they will always have time for you when you really need.

Un ringraziamento profondo alla mia famiglia, in particolare i miei genitori, che con i loro sacrifici mi han permesso di raggiungere alte vette, dandomi le ali per volare verso i miei sogni e i miei traguardi, e lasciandomi viaggiare senza farmi mancare e pesare nulla. Non vi ho mai ringraziato abbastanza per il mio carattere introverso, ma sappiate che apprezzo molto tutto quello che avete fatto per me. Vi ringrazio di cuore. Vi voglio bene.

Last but not least, my gratitude goes to my beloved Cristina, to be patience in waiting for my stuff, my studies and my travels around the world, and to be still beside me, ready to put in discussion her life for the sake of my passions. Thanks my Love. It is now time to walk together through life.

Milano, March 2014
Matteo Ripepi

Contents

Preface

Objective and Outline

The main objective of this thesis is to develop model order reduction techniques suitable for computational aeroelasticity. In particular, we will propose methods to tackle different aspects of this framework, i.e. the approximation of the generalized aerodynamic forces of linearized aeroelastic systems, the simulation of aeroelastic dynamic responses to gusts and atmospheric turbulence, the aerodynamics and structural nonlinearities, and the generation of parametrized low-order models.

This thesis consists of seven chapters. Chapter 1 is the introduction to the computational aeroelastic framework for the aircraft design loads calculation and to the model reduction techniques for dynamical systems, whereas the others chapters form the main material of the thesis:

Chapter 2 deals with state space modeling. In this chapter we introduce the state-space framework for aeroelastic systems subjected to external disturbances (e.g. gusts) and its transformation to a flight mechanics point of view.

Chapter 3 presents the linear model order reduction strategies. In particular, in this chapter we develop a projection-based method using Schur subspaces and we propose an identification technique of state space models through a matrix fraction approximation.

Chapter 4 introduces an alternative gust modeling approach. In this chapter we develop a method aiming to reduce the complexity in the identification of gust aerodynamic transfer matrices and allowing a systematic investigation of a large number of gusts without regenerating the reduced model.

Chapter 5 analyzes the methods proposed in the Chapter 3 and 4. In this chapter we apply the proposed linear model reduction methods and gust modeling to aeroelastic systems for flutter calculations and dynamic responses.

Chapter 6 investigates model reduction and identification techniques for nonlinear dynamic systems. In particular, in this chapter we identify a nonlinear state space model approximating the behavior of nonlinear aeroelastic systems and we use an element-based hyper-reduction method to reduce the complexity of the nonlinear terms.

Chapter 7 studies parameterized model order reduction. In this chapter the hyper-reduction method is applied to obtain a global basis over a set of given parameters.

Contributions

The following are the main contributions of the thesis.

Chapter 2: State Space Aeroelastic Modeling

- We propose an linear time invariant state space formulation with a unified framework for the aerodynamic generalized forces arising from both the structural motion and the gust disturbance.
- We apply a first/second order dynamic residualization respectively in the state and in the output equations, meant to recover the low frequency contribution of the high frequency content of generalized aerodynamic forces.
- We illustrate a possible procedure to easily transform the aeroelastic state space model framework to a flight mechanics point of view.

Chapter 3: Linear Model Order Reduction

- We propose the use of Schur subspaces of the linearized aerodynamic subsystem as reduced basis onto which to project the model.
- We make use of residual bases complementing the slow frequency subspaces of interest to decouple completely the slow/fast dynamics.
- We introduce a residualization of the fast dynamics which exploit the very same factorization used for the power iterations that led us the Schur subspaces, so saving computational time.
- We select the Schur subspaces likely to contribute more to the input-output behavior using a dominant pole criterion on the basis of the controllability and observability concepts.
- We improve a previous matrix fraction description formulation through: the adoption of a more appropriate performance index, the avoidance of a tweaked iterated weighting to ensure the identification of a stable model, the obtainment of either lower order models for an assigned precision or a better fitting for a given order, and the omission of a costly final constrained nonlinear optimization.

Chapter 4: Reducing Gust Modeling Complexity

- We propose an alternative gust modeling approach via spatially fixed shape functions, named gust modes, which allows to calculate unsteady gust forces using the very same formulation adopted for flutter calculations, with the embedded possibility of treating even heterogeneous gust fields. Moreover it leads to smoothed gust aerodynamic transfer matrices and it provides a systematic investigation of a large number of gusts with a low number of full order simulations.

- We introduce the concept of optimal gust entry point, mitigating the delay oscillations of the gust aerodynamic transfer matrix associated to the gust penetration, and thus ensuring an adequate approximation with a low number of states.
- We propose to adopt a discrete shaping filter approach for any finite duration gust profile, e.g. 1-cos gusts, so providing possible benefits in designing optimal multi-plant MIMO controllers aimed at gust loads alleviation.

Chapter 5: Simulations of Linear Reduced Order Aeroelastic Systems

- We demonstrate the features, capabilities and behavior of the proposed linear model order reduction methods in solving flutter and gust/turbulence response problems of two dimensional and three dimensional aeroelastic systems in subsonic and transonic flows.
- We apply the alternative gust modeling approach to complex aircraft configurations modeled using high fidelity computational fluid dynamic.

Chapter 6: Nonlinear Model Order Reduction

- We extend the proposed linear identification approach, based on the matrix fraction approximation of the aerodynamic transfer matrices, with polynomial terms, in the state and the input, approximating the aerodynamic/structural nonlinearities of aeroelastic systems.
- We propose a selection technique of the nonlinear monomials based on a greedy algorithm.
- We develop the nonlinear state-space identification procedure for continuous-time models.
- We perform the fitting procedure of the nonlinear part avoiding to touch the state matrix identified with the matrix fraction approximation, so maintaining the stability of the linear subsystem.
- We apply a projection-based hyper-reduction approach, where in the online phase the nonlinear function is evaluated only at a few locations of the spatial domain and reconstructed implicitly using the pre-computed basis vectors, to a nonlinear aeroelastic system with structural nonlinearities, and whose structural subsystem is modeled by using finite elements.

Chapter 7: Parametric Model Order Reduction

- We implement a parametric model reduction approach coupling the element-based hyper-reduction with a global basis, generated from the proper orthogonal decomposition of a snapshot matrix containing the time history responses of the full order system for a given set of parameters.

Chapter 1

Introduction

The present chapter provides an account of the relevant literature on the subject of model order reduction and system identification. The reader should be aware that such account is far from being a complete review. It only mentions the literature that has had a major impact on the present work.

In section 1.1 the main challenges in the generation of the dynamic aeroelastic loads database for aircraft design are highlighted together with the motivation for the present research work, in section 1.2 the main approaches and numerical methods used in computational aeroelasticity are described, and in section 1.3 the state of the art in model order reduction and system identification techniques for dynamic systems is briefly presented.

1.1 Dynamic aeroelastic loads process for aircraft design

Modern aircraft are characterized by large flexible structures subjected to high speed flows, whose aerodynamic flow regimes during their critical flight loads conditions may include complex aeroelastic phenomena, shock interactions, flow separation, and other nonlinear flow phenomena (e.g. limit-cycle oscillations involving structural and aerodynamic nonlinearities, transonic flow with shocks and flow separation, buffeting phenomena and gust).

An accurate prediction of these load conditions plays a crucial role in the design and development of the aircraft, and thus require the use of high-fidelity models, such as those provided by computational fluid dynamics (CFD) based aeroelasticity, also named computational aeroelasticity (CAE), which would be able to reduce risk, design costs and operational flight costs.

However high-fidelity modeling of aerodynamic systems involves hundreds (e.g. in 2D simulations of airfoils in compressible potential flow) to millions of degrees of freedom (e.g. in 3D simulations of a complete aircraft in compressible viscous flow), thus being extremely time consuming and requiring huge storage resources for their direct numerical simulation, thus imposing significant constraint to their applications in optimal design and system control. Moreover, load databases imply a large amount of aeroelastic analyses since several aircraft configurations and flight conditions (perhaps a priori unknown) have

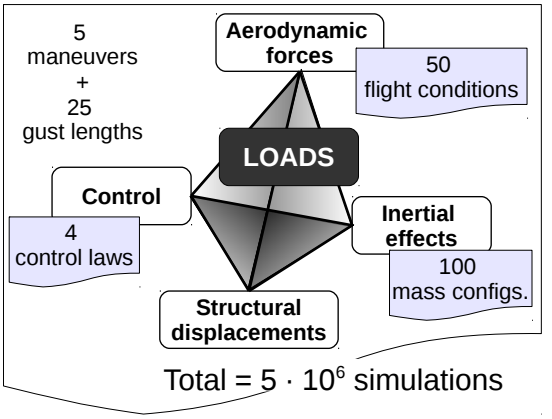

Figure 1.1: *Collar diagram of aeroservoelasticity showing an example of the parameter combinations and number of computations needed for the aircraft design*

to be analyzed to identify and obtain the maximum loads the aircraft will experience, and these analyses have to be repeated for every structural design update.

For their high potential in critical flight loads prediction, high-fidelity CFD-based aeroelastic analysis should be adopted also during the preliminary design stage so to address new challenges in aircraft design. However they are still computationally too expensive, so that, usually, flight load envelopes are determined with low fidelity methods, high-fidelity methods being confined to a limited set of design points (e.g. cruise or flutter calculation), along with the investigation of aeroelastic stability boundaries by means of fluid structure interaction (FSI) analysis during the verification phases of new aircraft design [1, 2].

Model reduction techniques aim at overcoming these issues by carrying-out medium to low fidelity models able to represent the characteristic behavior of the system under investigation within an acceptable level of approximation, but with far less computational requirements. The resulting reduced order model is thus suitable to be employed in an integrated multidisciplinary framework, to design control systems and/or for real time applications, therefore reducing the loads analysis cost of conventional aircraft, the evaluation time of innovative designs and the overall aircraft development cost/time.

Therefore this Ph.D. research project aims at reducing the overall cost/time associated with the critical flight loads calculation process necessary for an aircraft design. Reduced order modeling methods and procedures have been developed and implemented to accelerate and improve efficiency and accuracy of high-fidelity full order computational aeroservoelastic analyses. These enhancements will reduce the computational time required by each individual analysis, and therefore they will accelerate the aircraft design and allow the evaluation of innovative non-conventional configurations at a lower risk.

The developed acceleration technologies can be assembled in a general purpose, CFD-based, nonlinear aeroelastic simulation tool, and integrated in a multidisciplinary environment so to perform accurate computational aeroservoelastic maneuver simulations, up to a virtual flight testing (i.e. the so called “Digital Flight”). The CAE tool arising from these technologies can be used in the preliminary design stage, predicting loads and per-

formance, and investigating the aeroelastic behavior of the complete aircraft, from stability to nonlinear dynamics, in level-flight and during maneuvers.

1.2 Approaches and strategies in computational aeroelasticity

In the present section a brief description of the most important approaches and strategies in computational aeroelasticity (CAE) are presented.

The term computational aeroelasticity is generally referred to the coupling of aerodynamic, structural deformation, and dynamics disciplines, in order to perform aeroelastic analysis, ranging from maneuver simulations to gust responses, usually required in loads prediction processes.

The CASE field include a large body of research [1–8] where strategies and techniques are developed and addressed to solve aeroelastic problems. All of the subsystems may be modeled at different levels of fidelity. Aerodynamic may be modeled using linear unsteady aerodynamics as well as nonlinear high-fidelity methods arising from computational fluid dynamics. Likewise structural dynamics may be modeled ranging from simple beam theory up to the state-of-the-art finely detailed three-dimensional Finite Element Modeling (FEM). The control system may be designed either with a simple, yet effective, single loop controller or with more robust techniques which consider uncertainties arising from aerodynamic, structural parameters and modeling errors.

The progresses in the development of numerical methods for the solution of the nonlinear aerodynamic flow equations, from the solution of full potential flows through Euler to Navier-Stokes simulations, together with the increased computational resources has endorsed the computational fluid dynamics as an accepted tool for airplane design.

CFD research efforts are directed to investigate better numerical schemes, faster solution methods, parallel processing, more accurate turbulence models, and unsteady aerodynamic, which has a central role in dynamic aeroelastic simulations [2, 9–12]. Research is also addressed to implementing flexible ways of generating and deforming computational meshes [13–18] and developing accurate techniques to perform the interaction with the structural dynamic [19–24].

Further developments in computational aeroelasticity are also related to progresses in nonlinear structural dynamic finite element methods. From the side of the computational structural dynamics (CSD) challenges include the solution of linear and nonlinear large scale structural finite element equations, for example using substructuring techniques [] (where the solution of large finite problems is performed on sets of coupled substructure problems), and the automated identification of the damping ratios and frequencies of the resulting dynamic response [25].

The high computational cost of CFD simulations has driven also an extensive research effort toward developing model order reduction (MOR) methods for unsteady CFD and for coupled CFD/CSD models, to allow nonlinear aeroelastic simulation within reasonable time and cost limitations. This is the research topic of the present work.

Computational aeroelasticity can be nowadays applied to model and analyze a complex aircraft full configurations with an impressive level of accuracy. Aeroelastic analyses car-

ried out by coupling CFD/CSD simulations are able in capturing highly complex nonlinear static and dynamic fluid/structure interaction phenomena, such as transonic flows with shock wave motion, which are otherwise difficult to simulate.

Typical nonlinear CFD-based aeroelastic applications are flutter simulations, where the equations of motion are linearized about a nonlinear aeroelastic steady state solution and a small-perturbation linear stability analysis is carried out using the linear methods.

1.2.1 Structural model

Structural models for aeroelastic systems may be realized using either linear or nonlinear beam theories, shell theories, or plate theories as the Kirchhoff-Love theory for thin plate or the Mindlin-Reissner theory for thick plates. The Finite Element Method (FEM) is typically used as approximation to build the numerical model. The structural displacements at the finite element nodes are usually expressed in term of a small set of generalized modal coordinates $\mathbf{q}$, being $\mathbf{s} = \mathbf{N}_q\mathbf{q}$, as well the finite element (FE) matrices are projected onto the modal subspace $\mathbf{N}_q$. Typically, the first few lowest frequency modes to the first hundred or so for a highly complex aircraft structure are necessary to capture the static and dynamic flexibility of the structure accurately.

The generalized nonlinear aeroelastic equation of motion projected onto the modal subspace is given by:

$$\mathbf{M}\ddot{\mathbf{q}}(t) + \mathbf{C}\dot{\mathbf{q}}(t) + \mathbf{K}\mathbf{q}(t) + \mathbf{f}_{\mathsf{nl}}(\mathbf{q}) = \mathbf{Q}(\mathbf{x}, \mathbf{q}, \dot{\mathbf{q}}, \mathbf{v}_g, t, M_\infty, Re_\infty) \tag{1.1}$$

where $\mathbf{M}$, $\mathbf{C}$, $\mathbf{K}$ are respectively the mass, damping and linear stiffness modal matrices and $\mathbf{f}_{\mathsf{nl}}$ is the modal projected vector of nonlinear internal forces of the structure (e.g. arising from in-plane/out-plane structural coupling behavior, strain hardening, structural free-play). The generalized aerodynamic forces $\mathbf{Q}$ correspond to the aerodynamic loads projected onto the structural modes $\mathbf{N}_q$ and couple the unsteady aerodynamics and inertial loads with the structural dynamics. They depend on the flow variables $\mathbf{x}$, the structural motion and dynamics, gusts and atmospheric turbulence $\mathbf{v}_g$, and the flow parameters Mach number M_∞ and Reynolds number Re_∞.

1.2.2 A hierarchy of aerodynamic models

Aerodynamics may be modeled with different levels of fidelity. Some of the mathematical models and numerical methods commonly adopted within the framework of computational aeroelasticity are described hereafter. More complete surveys and informations on the topic may be found in Refs. [1–3, 26].

The time-dependent fluid flow equations, from which the aerodynamic forces to be applied to the structure are obtained, may generally be written as:

$$\dot{\mathbf{x}} = \mathbf{F}(\mathbf{x}) + \mathbf{G}(t) \tag{1.2}$$

where $\mathbf{x}$ is the solution vector over the flow field domain, the right-hand vector $\mathbf{F}(\mathbf{x})$ includes terms due to flow field nonlinearity (i.e. the inviscid fluxes), flow field viscosity

and other body forces, and the vector $\mathbf{G}(t)$ represents the motion of the boundaries at the fluid-structure interfaces, which can be coupled to the structural model to be integrated forward in time. In this case the boundary motion will be function of the structural motion as $\mathbf{G}(t) = \mathbf{G}(\mathbf{q}(t), \dot{\mathbf{q}}(t))$.

To solve the full nonlinear flow field equations in a time-marching manner, both spatial and temporal discretizations are applied. Spatial discretizations are most often based on the finite volume and finite element methods [27, 28], using application oriented structured meshes [29–32], more flexible and efficiently generated unstructured meshes [33, 34] or hybrid meshes [35, 36] combining the advantages of the previous two typologies. For temporal discretization, various approaches can be used ranging from explicit methods with multistage Runga-Kutta schemes, to implicit temporal schemes with dual time-stepping [37]. Traditional solution acceleration techniques are usually used such as residual smoothing [38] and multigrid acceleration [39].

Owing to the extreme challenges in computing time-varying aeroelastic behavior and the wide range of phenomena to be simulated, there are many ways in which the fluid dynamics equations are formulated and solved. The methods range from the use of well-established lower fidelity linear approaches to the use of high fidelity full Navier-Stokes equations. Hereafter some of the aerodynamic models used in computational aeroelasticity, introduced by an increasing level of approximation, are briefly described.

Navier-Stokes equations

The conservative form of the governing equations for a compressible, viscous, conductive fluid with constant properties are given by:

$$\frac{\partial \mathbf{x}}{\partial t} + \boldsymbol{\nabla}\cdot \mathbf{f}(\mathbf{x}) = \boldsymbol{\nabla}\cdot \mathbf{d}(\mathbf{x}) \qquad \forall\,(\boldsymbol{x}, t) \in [\Omega \times \mathcal{T}] \tag{1.3}$$

which are written within an Eulerian framework in differential form for a confined space-time domain $\Omega \subseteq \mathbb{R}^d$, with $d = 2, 3$, and $\mathcal{T} \subseteq \mathbb{R}^+$. The conservative variables vector $\mathbf{x}(\boldsymbol{x}, t)$, the inviscid fluxes $\mathbf{f}(\mathbf{x})$ and viscous fluxes $\mathbf{d}(\mathbf{x})$ are defined respectively as:

$$\mathbf{x} = \begin{bmatrix} \rho \\ \rho \boldsymbol{v} \\ E^{\mathrm{t}} \end{bmatrix} \quad \mathbf{f} = \begin{bmatrix} \rho \boldsymbol{v} \\ \rho \boldsymbol{v} \otimes \boldsymbol{v} + P[\mathbf{I}] \\ \boldsymbol{v}\,(E^{\mathrm{t}} + P) \end{bmatrix} \quad \mathbf{d} = \begin{bmatrix} 0 \\ \boldsymbol{\tau} \\ \boldsymbol{\tau}\cdot \boldsymbol{v} + \boldsymbol{q} \end{bmatrix} \tag{1.4}$$

with $\rho(\boldsymbol{x}, t)$, $\boldsymbol{v}(\boldsymbol{x}, t)$ and $E^{\mathrm{t}}(\boldsymbol{x}, t)$ being respectively the density, the flow velocity and the total energy per unit volume, and $P(\boldsymbol{x}, t)$, $\boldsymbol{\tau}(\boldsymbol{x}, t)$ and $\boldsymbol{q}(\boldsymbol{x}, t)$ being the pressure, the viscous stresses tensor product and the power exchanged by conduction, and $[\mathbf{I}] \in \mathbb{R}^{d\times d}$ the identity matrix. The equation of state for the pressure P and the constitutive equations for the viscous stresses tensor $\boldsymbol{\tau}$ and the power exchanged by conduction $\boldsymbol{q}$ lead to the closure of the problem. The resulting system of mixed non-linear Partial Differential Equations (PDEs) is then completed providing the properly boundary and initial conditions.

The application of a local time averaging operator, leading to the so called Reynolds Averaged Navier-Stokes (RANS) equations, is a common approximation of the original model in order to overcome the computational costs associated to the direct solution of the Navier-Stokes equations. The unknowns of the problem will thus become the physical

variables of the mean flow-field, while the diffusion due to the turbulence fluctuations will be recovered by modeling the symmetric tensor of the Reynolds stresses [40, 41].

A modification of the RANS leading to a more accurate, yet numerically feasible, approach is the so-called Detached Eddy Simulation (DES) [40, 42, 43], which overcome the limitations of the RANS in predicting massively separated flows by switching to a subgrid scale formulation in regions fine enough for Large-Eddy Simulation (LES) [44], i.e. treating near-wall regions using RANS and directly simulating the rest of the flow. The accuracy of DES predictions has typically been far superior to RANS calculations while at the same time avoiding the Reynolds-number limitations that plague the LES.

Euler equations

The viscous stress tensor and the power exchanged by conduction can be neglected from the Navier-Stokes momentum and energy equations when the dynamic effects associated to the viscous diffusion and thermal conduction are confined just within the boundary layer. This lead to the Euler equations:

$$\frac{\partial \mathbf{x}}{\partial t} + \boldsymbol{\nabla} \cdot \mathbf{f}(\mathbf{x}) = 0 \qquad \forall\,(\boldsymbol{x}, t) \in [\Omega \times \mathcal{T}] \tag{1.5}$$

which are a set of hyperbolic non-linear PDEs completed by setting the proper inflow and slip boundary conditions.

The eventual loss effects of the viscosity effects may be recovered by means of approaches coupling the inviscid Euler equations flow model with a viscous boundary layer model [45].

Full Potential equations

Considering the further approximation of irrotational flow (i.e. $\boldsymbol{\nabla} \times \boldsymbol{v} = 0$), under the hypothesis of a singly connected domain, the velocity $\boldsymbol{v}$ may be expressed as a gradient of a scalar potential ϕ, which is governed by two scalar equations [26], mass conservation:

$$\frac{\partial \rho}{\partial t} + \boldsymbol{\nabla} \cdot (\rho \boldsymbol{\nabla} \phi) = 0 \qquad \forall\,(\boldsymbol{x}, t) \in [\Omega \times \mathcal{T}] \tag{1.6}$$

and energy conservation i.e. Bernoulli equation (a first integral of the Euler equations):

$$\frac{\partial \phi}{\partial t} + \frac{\|\boldsymbol{\nabla}\phi\|^2}{2} - \frac{{V_\infty}^2}{2} + \frac{c_\infty^2}{\gamma - 1}\left[\left(\frac{\rho}{\rho_\infty}\right)^{\gamma-1} - 1\right] = 0 \tag{1.7}$$

being V_∞ and c_∞ respectively the free-stream velocity and speed of sound, and γ the heat capacity ratio. Considering an isentropic flow, the coefficient of the aerodynamic loads is evaluated as $C_p = 2(\rho^\gamma - 1)/(\gamma M_\infty^2)$, being M_∞ the free-stream Mach number.

Under the hypothesis of irrotational flow, the local vorticity production is zero. Nevertheless a finite circulation is allowed around lifting bodies. Then, if multiple connected domain are considered, a nonuniqueness is present, giving rise to a discontinuity in the potential function ϕ [46]. The vorticity is associated to this discontinuity, which for lifting

bodies is confined into a zero-thickness vortex layer (i.e. the wake) originating from the the trailing edge of the wing. The discontinuity is advected along such a wake [46], being the resultant of the aerodynamic forces null on the wake. The potential flow model is thus completed adding to this wake condition, the tangential flow boundary conditions on the body and the nonreflecting farfield boundary conditions.

As a further consequence of the irrotational flow assumption, the Full Potential (FP) model does not admit nonhomentropic flow-field conditions, and thus it loses validity in presence of shock waves, across which the Rankine-Hugoniot relations [26] show a rise in the entropy. Indeed Crocco's equation [47] shows that irrotational flows can be only omoentropic, thus irreversible phenomena are not allowed.

Weak FP formulations allow a shock discontinuity to appropriately occur for mass and energy, but the shock remains isentropic and the momentum balance is not satisfied. Nonetheless the entropy production through a weak/moderate shocks can be shown to be proportional to the cubic power of the local Mach number [26], thus it is relatively negligible up to local Mach numbers $M = 1.3 \div 1.4$. So the potential model represents an acceptable and effective approximation, even for transonic flows, for a moderate upstream Mach range.

Such weak full-potential formulation may be framed using an independent approximation of the density and velocity potential fields. In this way the problem can be formulated in state space form, with the two fields (ρ, ϕ) as state functions, considerably simplifying the development of a numerical approximation, and leading to a robust resolution highly sparse scheme. Moreover embedded shocks may be sharply captured, even within relatively coarse meshes, by simply introducing a density change across the shock while keeping the potential continuous.

Nonisentropic FP formulations have been also introduced [48, 49] where a nonisentropic Bernoulli equation leading to a nonisentropic wake equation is used. In this formulation a thin entropy layer surround the ensemble of body and wake, and the related convected entropy equation ensure an effective unsteady correction, approaching Euler solutions.

Alternatively the density may be evaluated using Bernoulli equation, which substituted in the mass conservation give rise to a conservative mixed nonlinear second-order PDE in the unknown potential ϕ only:

$$\frac{\partial^2 \phi}{\partial t^2} + \frac{\partial (\boldsymbol{\nabla}\phi)^2}{\partial t} + \boldsymbol{\nabla}\phi \cdot \boldsymbol{\nabla}\left(\frac{\|\boldsymbol{\nabla}\phi\|^2}{2}\right) - c^2 \boldsymbol{\nabla}^2 \phi = 0 \qquad \forall\, (\boldsymbol{x}, t) \in [\Omega \times \mathcal{T}] \tag{1.8}$$

being $c(\boldsymbol{x}, t)$ the local celerity of sound.

Methods have been also developed that use the full potential equation for the inviscid region coupled with a viscous boundary layer in order to incorporate viscous effects [50, 51].

Integral-equation-based methods

The potential flow around a body of arbitrary shape is governed by the equation for the velocity potential which is a non-linear wave equation. Neglecting the non-linear terms,

the following integral representation for the velocity potential can be obtained [46]:

$$E(\boldsymbol{x},t)\phi(\boldsymbol{x},t) = \int_0^t \int_{\mathbb{R}^3} G_{\mathsf{A}} \boldsymbol{\nabla}_{\boldsymbol{y}}\phi \cdot \boldsymbol{\nabla}_{\boldsymbol{y}} E \, d\mathcal{V} \, d\tau + \boldsymbol{\nabla}_{\boldsymbol{x}} \cdot \int_0^t \int_{\mathbb{R}^3} G_{\mathsf{A}} \phi \, \boldsymbol{\nabla}_{\boldsymbol{y}} E \, d\mathcal{V} \, d\tau$$
$$- \frac{1}{c^2} \int_0^t \int_{\mathbb{R}^3} G_{\mathsf{A}} \frac{\partial \phi}{\partial \tau} \frac{\partial E}{\partial \tau} \, d\mathcal{V} \, d\tau - \frac{1}{c^2} \frac{\partial}{\partial t} \int_0^t \int_{\mathbb{R}^3} G_{\mathsf{A}} \phi \frac{\partial E}{\partial \tau} \, d\mathcal{V} \, d\tau \quad (1.9)$$

where the domain function $E(\boldsymbol{x},t)$ takes value 1 outside the body surface $\mathcal{S}_{\mathsf{b}}$ and 0 inside $\mathcal{S}_{\mathsf{b}}$ and the fundamental solution for acoustic waves equation is $G_{\mathsf{A}} = G\,\delta(\tau - t + r/c)$, with $G(\boldsymbol{x},\boldsymbol{y}) := -1/4\pi r$ and $r := \|\boldsymbol{x} - \boldsymbol{y}\|$, with $\boldsymbol{x} \in \mathcal{V}_{\mathsf{f}} \setminus \mathcal{S}_{\mathsf{w}}$, i.e. the fluid volume $\mathcal{V}_{\mathsf{f}}$ except the wake surface $\mathcal{S}_{\mathsf{w}}$. The boundary condition on $\mathcal{S}_{\mathsf{b}}$ is $\partial\phi/\partial n = \boldsymbol{v}_{\mathsf{b}} \cdot \boldsymbol{n} + \boldsymbol{v}_t$, where $\boldsymbol{v}_{\mathsf{b}}$ is the velocity of the boundary at $\boldsymbol{x}$, $\boldsymbol{n}$ is the normal to $\mathcal{S}_{\mathsf{b}}$ at $\boldsymbol{x}$, and $\boldsymbol{v}_t$ is the transpiration velocity through the surface, equal to zero for impermeable surfaces. The potential is null at infinity whereas it is discontinue across the wake, $\Delta\phi = \text{const}$ following a wake point and $\Delta(\partial\phi/\partial n) = 0$.

Considering only the body surface a the Morino's boundary integral equation is obtained. In the integral representation of Eq. (1.9) $\phi(\boldsymbol{x})$ on $\mathcal{S}_{\mathsf{b}}$ is not known. However, if $\boldsymbol{x}$ is a smooth point of $\mathcal{S}_{\mathsf{b}}$, one obtains $E(\boldsymbol{x},t) = 1/2$. The boundary conditions of tangential flow are not applied directly to the potential but are inserted into the source term in Green's theorem. Requiring continuity of tangential flow near the surface insures that the boundary conditions are satisfied. So the potential ϕ on $\mathcal{S}_{\mathsf{b}}$ may be computed, and then, after determining the velocity on $\mathcal{S}_{\mathsf{b}}$ (the tangential components from $\phi(\boldsymbol{x})$ on $\mathcal{S}_{\mathsf{b}}$, the normal one from the boundary condition on $\partial\phi/\partial n$), the pressure on the body surface is obtained with the Bernoulli's theorem.

The further assumption of incompressible ($\boldsymbol{\nabla} \cdot \boldsymbol{v} = 0$) flow field leads to the Laplace equation

$$\boldsymbol{\nabla}^2 \phi = 0 \qquad \forall\,(\boldsymbol{x},t) \in [\Omega \times \mathcal{T}] \quad (1.10)$$

which is a linear elliptic PDE whose time dependence is carry on by the boundary conditions and Bernoulli equation and the non-linearities appear only in the evaluation of the pressure via Bernoulli's theorem, where they appear respectively as a derivative and as an algebraic nonlinearity. This linear flow field equation is usually solved converting the solution over the full domain into a simplified boundary value problem, where the body surface is represented by a distribution of virtual singularity of unknown value. Fundamental solutions ϕ are the source, the doublet and the vortex, or a linear combination of them. Approximate solutions are obtained discretizing the integral equation using a finite element approach, which corresponds to subdivide the body surface as an ensemble of panels (planar or curvilinear) and assuming a shape function (e.g. constant, linear, quadratic) for the unknowns singularity strengths. Imposing the boundary conditions at a discrete set of points, a linear system of equations is obtained and solved for the singularity strengths.

Different methods can be devised depending on the singularity chosen, among the most noticeable the Doublet Lattice Method (DLM) and the Vortex Lattice Method (VLM) [52], which are usually applicable for subsonic flows even if transonic flows may be handle through the use of correction procedures making use of wind tunnel data or other approaches. Integral equations for supersonic flows are obtained considering the linearizing compressible potential flow equations [53].

Integral-based equations can easily compute unsteady aerodynamic loads and are used for preliminary investigations on gust response problems or wind tunnel testing, enabling comparisons with more advanced high fidelity CFD results [54].

1.2.3 Aeroelastic interface

The structural and aerodynamic models may be coupled into a set of equations to be integrated forward in time. The simulation may be carried out by solving a single set of coupled equations in a monolithic approach or solving two system of equations, in a partitioned approach [55–57].

Usually a monolithic approach is applied when the aerodynamics have a low-level of fidelity (still is accurate enough to properly catch the aeroelastic problem under examination), as for example in the case of a geometrically nonlinear structure interacting with linear unsteady aerodynamics [58], or small structural problems are considered, as for example in two-degrees of freedom aeroelastic problems [59]. However for more complex aeroelastic problems monolithic procedures, strictly marching the aeroelastic equations simultaneously in each iteration, is in general more computationally challenging, having the different CFD/CSD domains different mathematical and numerical properties.

A partitioned approach is in these cases preferred, usually guaranteeing a greater flexibility in term of the possibility to model the different subsystems with the ad-hoc tools and numerical approaches. Indeed the methods for the solution of both the domains, i.e. CFD and CSD, have independently reached a high level of sophistication and degree of problem specific adaptation. Being the structural and aerodynamic formulations mutually independent, a variable fidelity modeling approach may be readily realized, with the different models promptly matching the problem under analysis without changing the overall formulation of the equations of motion.

Using a partitioned approach the equations may be marched forward in time in a staggered manner with information exchanged between the two systems at specific time steps and either with or without subiterations at each time step to ensure convergence (i.e. loosely coupled or strongly coupled).

In the partitioned approach for CFD-based aeroelasticity a coupled solution is solved, where an aerodynamic model, a structural model and a mesh motion solver must interact together and mutually exchange information in time and space.

Temporal coupling

The temporal coupling is related to the way the aerodynamic model and the structural model are cycled as the solution is advanced in time. There are several time-marching procedures ranging from fully explicit to fully implicit. References [59–61] provide an analysis of various coupling methods. Among the different methods, time advancement may be realized through explicit lagged procedures, implicit iterative methods, conventional serial staggered approaches or central staggered differencing and backward second-order differencing of the fluid and structure with predictor/corrector steps. Strongly coupled schemes which conserve the overall second-order accuracy of the solution may be obtained with

the application of appropriate constraints [34, 62]. For steady state solutions where a time marching approach using a pseudo-time is used to converge to the equilibrium time accuracy is not an issue.

Spatial coupling

Spatial coupling involves the procedure used to project quantities from one side of the interface to the other, i.e. structural displacements from the structural model to the aerodynamic model, and aerodynamic loads from the aerodynamic model to the structural one.

Coupling issues arise from the fact that the models do not have coincident interface node points. Therefore an interpolation step satisfying the requirement of energy conservation [62, 63] is necessary. In Refs. [19, 23, 24] different coupling methods are evaluated and the relative advantages and disadvantages for the overall accuracy and behavior of the aeroelastic solution are presented. Among the vary approaches there are: the infinite-plate spline [64], the multiquadratic biharmonic, the non-uniform B-spline, the thin-plate spline, the finite-plate spline and the inverse isoparametric mapping. Other recently proposed methods include the interpolation-based algorithm (IBA) [65], the non-uniform rational B-spline (NURBS) [63], the common refinement [66] and the quadrature projection [67].

1.2.4 Mesh motion

Numerical simulations for computational aeroelasticity applications must often deal with issues arising from moving boundaries. Strong distortions of the computational domain must be tackle by an appropriate kinematic description of the continuum under consideration. This has a major impact over the overall accuracy of the method and over the capabilities to complete the simulation, which may be fail in case of an excessive distortion of the computational mesh.

Two classical descriptions of motion are adopted in the framework of continuum mechanics: the Lagrangian description [68], typically used in structural mechanics and the Eulerian description [69], which finds its natural application in fluid dynamics. In computational meshes based on the Lagrangian approach the grid nodes are moved at the local velocity of the associated material particles, allowing an easy tracking of free surfaces and interfaces between different materials, but leading to large distortions of the computational domain (if a remeshing technique is not applied) when large motions (e.g those arising from by shear movements and vorticity) are involved. Whereas, the motion of the continuum using the Eulerian approach is described with respect to a spatially fixed computational mesh, through which the material flows, allowing large distortions but comporting not accurate interface tracking and not precise resolution of flow details.

The Arbitrary Lagrangian-Eulerian (ALE) description [70, 71] of the fluid motion is an intermediate formulation developed to combine the advantages of the above classical approaches, minimizing their respective drawbacks when applied to fluid-structure coupled problems described with different kinematic formulations.

Arbitrary Lagrangian-Eulerian methods

The Arbitrary Lagrangian-Eulerian description may be seen as a generalization of the classical kinematic descriptions, mapping the material and spatial domains onto a referential domain, whose motion is defined so as to preserve the mesh quality and therefore the accuracy of the solution. The RANS equations in integral conservative form described within the ALE formulation framework, expressing the balance of the conservative variables with respect to a an arbitrary control volume $\Omega(t)$ moving with mesh velocity $\boldsymbol{v}_{\mathsf{b}}$, are:

$$\frac{d}{dt}\int_{\Omega(t)} \mathbf{x}\, d\Omega + \oint_{\mathcal{S}(t)} [\mathbf{f}(\mathbf{x}) - \mathbf{x}\, \boldsymbol{v}_{\mathsf{b}}] \cdot \boldsymbol{n}\, d\mathcal{S} + \oint_{\mathcal{S}(t)} \mathbf{d}(\mathbf{x}) \cdot \boldsymbol{n}\, d\mathcal{S} = 0, \qquad \forall \Omega(t) \subseteq \mathbb{R}^d \quad (1.11)$$

where $\mathcal{S}(t) = \partial\Omega(t) \subseteq \mathbb{R}^{d-1}$ is the boundary with normal unit vector $\boldsymbol{n}(\boldsymbol{x}, t)$, assumed positive when pointing outside the fluid domain, and $\boldsymbol{v}_{\mathsf{b}}(\boldsymbol{x}, t)$ is the local velocity of the moving boundaries.

The local grid velocities and the definition of the geometric quantities necessary to compute the fluxes across a given portion of the domain cannot be chosen independently [72]. Therefore the control volume must satisfy an additional constraint during the movement [73]. A constraint, usually referred to as the Geometric Conservation Law (GCL) [74], on the interface velocity is then applied, which imposes that a uniform flow field must be reproduced exactly.

Satisfying the GCL (or its discrete version) is a necessary and sufficient condition to guarantee the nonlinear stability of the integration scheme [75]. However, the GCL is neither a necessary nor a sufficient condition to preserve time accuracy [76] (it is just a sufficient condition to obtain a scheme that is at least first order accurate [77]), but schemes violating this constraint usually are polluted by spurious oscillations [78]. Therefore, it is generally accepted that enforcing the GCL results in improving the accuracy and the stability of the numerical scheme. An updated review of the literature on the subject can be found in [74].

Mesh deformation

In the three-field formulations proposed in Ref. [79] the CFD mesh nodes in the fluid field are modeled as finite element nodal points in an artificial structural finite element model in which all CFD mesh points are connected to each other by nonlinear springs, and thus fluid mesh points are moved together with the motion of the structural surfaces in such a way to ensure regularity of the CFD mesh throughout the simulation. In other works [22, 80] spring network-like approaches [14, 80, 81], which may fail in keeping the grid valid when non-tetrahedral elements are used, are avoided and mesh motion is handle using an elastic analogy where however the grid is represented as an elastic continuum. introducing a natural mechanisms to prevent node-face collisions.

Improvements have been achieved by utilizing a hierarchical strategy of mesh deformation tools [82], where a convenient intermediate frame in the kinematic description of the grid motion is introduced between the reference and target configurations, and combining the identification of a linear tensor mapping the rigid motion contribution with a modified

version of the Inverse Distance Weighting (IDW) [83] multivariate interpolation kernel for the elastic contribution, and a transpiration boundary conditions technique minimizing the small remaining residual errors (if any) of the previous steps.

The procedure is somehow similar to the approach used in aeroelasticity where the structural problem is rewritten in a mean axes floating reference frame by decoupling the rigid and elastic degrees of freedom (DOFs) associated with flight mechanics and aeroelasticity respectively.

This hierarchical strategy is particularly suited for the aeroservoelastic simulations of free flying aircraft [82], because the control surfaces deflection (that cannot always be reproduced accurately by means of mesh deformation techniques, especially at the interface between moving and fixed components), takes advantage of the final transpiration correction step to improve the numerical prediction of the control stability derivatives [5].

Research efforts for fluid-structure systems with large motion, like in rotorcraft applications where is of primary importance to perform efficient unsteady computations while highlighting relevant flow features, such as shocks, wakes or vortices, have been directed towards the use of adaptive grids involving local modification of the grid [84] and topology modifications [85], obtained by resorting to a suitable mix of mesh deformation, edge-swapping, node insertion and removal. The adaptation procedure is driven by the boundary conditions and error estimators based on the gradient or the Hessian matrix of the solution.

Transpiration

At a solid/wall boundary, such as the surface of a wing immersed in a fluid flow, it is necessary to enforce the slip boundary condition by setting to zero the normal component of the local velocity.

However, as a viable alternative when small displacements perturbations are involed, it is possible to assign a non-zero value to the normal component of the local velocity, called transpiration velocity, in order to simulate the geometric and kinematic effects of a given displacement law of the boundary, without actually deforming the computational grid.

1.3 A survey of model reduction techniques for dynamic systems

In the present section a brief description of the most important approaches and techniques for model order reduction and system identification are presented. The extent of the subject is such that it is difficult to give a really comprehensive description of it. Therefore only some key points have been covered with a specific focus on the works that are specifically relevant to the present research.

Model order reduction (MOR) techniques aim in reducing the order n of a generic set of differential algebraic equations (DAEs)[1]

$$\begin{aligned} \mathbf{E}\dot{\mathbf{x}}(t) &= \mathbf{f}(\mathbf{x}(t),\, \mathbf{u}(t)) \\ \mathbf{y}(t) &= \mathbf{g}(\mathbf{x}(t),\, \mathbf{u}(t)) \end{aligned} \tag{1.12}$$

[1] If $\mathbf{E}$ is non singular the system may be easily recast as a system of ordinary differential equations (ODEs).

where $\mathbf{u}$, $\mathbf{y}$ and $\mathbf{x}$ are respectively the input, output and state variable of the system, to a lower order $r \ll n$ set of equations:

$$\begin{aligned} \mathbf{E}_r \dot{\mathbf{x}}_r(t) &= \mathbf{f}_r(\mathbf{x}_r(t),\, \mathbf{u}(t)) \\ \mathbf{y}(t) &= \mathbf{g}_r(\mathbf{x}_r(t),\, \mathbf{u}(t)) \end{aligned} \tag{1.13}$$

capturing the main behavior and all the relevant properties of the system, and retaining the accuracy of the approximation. Considering the special case of a generic Linear Time Invariant (LTI) system in descriptor form in the time domain:

$$\begin{aligned} \mathbf{E}\dot{\mathbf{x}} &= \mathbf{A}\mathbf{x} + \mathbf{B}\mathbf{u} \\ \mathbf{y} &= \mathbf{C}\mathbf{x} + \mathbf{D}\mathbf{u} \end{aligned} \tag{1.14}$$

the reduced system will be:

$$\begin{aligned} \mathbf{E}_r \dot{\mathbf{x}}_r &= \mathbf{A}_r \mathbf{x}_r + \mathbf{B}_r \mathbf{u} \\ \mathbf{y} &= \mathbf{C}_r \mathbf{x}_r + \mathbf{D}_r \mathbf{u} \end{aligned} \tag{1.15}$$

where $\mathbf{A}$, $\mathbf{B}$, $\mathbf{C}$ and $\mathbf{D}$ are the state space representation matrices of the LTI system. In carrying out such a reduction, besides obtaining a reduced order model having an acceptable approximation error, care must be taken in preserving the properties of the original system (stability, passivity[2], positive definiteness, etc.). The reduction procedure must also be computationally efficient, so building the reduced model employing a low computational cost.

Several reduced order modeling (ROM) techniques may be found in the literature. Extensive references are available in [86–91]. In general, ROM methods may be divided into two main categories, projection methods [92] and identification techniques, both applicable in the time and frequency domains [87].

Projective methods accomplish the model reduction by projecting the DAE system[3] onto a certain (orthonormal) basis spanning a generic subspace (of the original phase space) $\mathcal{Y}_r$ of size $O(r)$, and redefining the state as a linear combination of the basis of the subspace $\mathcal{X}_r$, where $\mathcal{X}_r = \text{Range}(\mathbf{X}_r)$, $\mathcal{Y}_r = \text{Range}(\mathbf{Y}_r) \subset \mathbb{C}^n$. The states put aside by the projection may be truncated or dynamic residualized. Projective methods are model-based reduction techniques, carrying out the reduction directly of the model matrices, of which therefore have the opportunity to preserve certain properties.

Considering a LTI system, the model order reduction procedure consist of finding a reduced state vector $\hat{\mathbf{x}}(t) = \mathbf{X}_r^T \mathbf{x}_r(t) \in \mathbf{X}_r$, where in general $\mathbf{x}_r(t) \in \mathbb{C}^r$, such that the residual $\mathbf{r} = \mathbf{E}_r \dot{\hat{\mathbf{x}}} - \mathbf{A}_r \hat{\mathbf{x}} - \mathbf{B}_r \mathbf{u}$, be orthogonal to the subspace $\mathcal{Y}_r$. So that:

$$\begin{aligned} &\mathbf{Y}_r^* \left(\mathbf{E}\mathbf{X}_r \dot{\mathbf{x}}_r - \mathbf{A}\mathbf{X}_r \mathbf{x}_r - \mathbf{B}\mathbf{u}\right) = 0 \\ &\mathbf{y} = \mathbf{C}\mathbf{X}_r \mathbf{x}_r + \mathbf{D}\mathbf{u} \end{aligned} \tag{1.16}$$

and the corresponding reduced order matrices would be: $\mathbf{E}_r = \mathbf{Y}_r^* \mathbf{E} \mathbf{X}_r$, $\mathbf{A}_r = \mathbf{Y}_r^* \mathbf{A} \mathbf{X}_r$, $\mathbf{B}_r = \mathbf{Y}_r^* \mathbf{B}$, $\mathbf{C}_r = \mathbf{C}\mathbf{X}_r$, and $\mathbf{D}_r = \mathbf{D}$, with $\mathbf{X}_r$, $\mathbf{Y}_r \in \mathbb{C}^{n \times r}$ projection matrices. This

[2] The system does not generate energy and only absorbs energy from the sources used to excite it.

[3] The projection may be also performed directly on the continuous or semi-discrete representation of the governing Partial Differential Equations (PDEs) [93], thus having a global validity.

framework is commonly named Petrov-Galërkin projective approximation, whilst the so called Bubnov-Galërkin projections methods are those obtained by setting $\mathbf{X}_r = \mathbf{Y}_r$.

Determining the reduced basis usually requires perhaps several off-line solutions of the high-fidelity system. This large off-line cost will be amortized over the many calculations, optimizations or real-time simulations the reduced model will allow to perform. Moreover, control synthesis and design is not feasible using too large high-fidelity models.

Usually the knowledge of the Jacobian matrix is needed to build the subspace and therefore a system linearization is implied. However, the Jacobian matrix is provided only when implicit approximation are used to finely discretize the DAEs. When explicit algorithms are employed the Jacobian matrix is missing, then "snapshots" methods [94] have to be used.

The different projection methods are then classified depending on the choice of the subspaces $\mathcal{X}_r$ and $\mathcal{Y}_r$, and on the selected basis (i.e. projection matrices) spanning these spaces. In literature two main categories of subspaces may be found: the Krylov and the Singular Value Decomposition (SVD) based subspace. Krylov subspaces are attractive for large-scale sparse systems, since only matrix-vector multiplications are required to generate them. The standard Krylov subspace generated by a matrix $\mathbf{A}$ and a vector $\mathbf{b}$ is given by $K_r(\mathbf{A}, \mathbf{b}) = \text{span}\left\{\mathbf{b}, \mathbf{A}\mathbf{b}, \ldots, \mathbf{A}^{r-1}\mathbf{b}\right\}$, but many others may be found. For example:

- Standard Krylov subspace:
  $K_r(\mathbf{A}, \mathbf{B}) = \text{span}\left\{\mathbf{B}, \mathbf{A}\mathbf{B}, \ldots, \mathbf{A}^{r-1}\mathbf{B}\right\}$
- Shift-Invert Krylov subspace:
  $K_r((\mathbf{A} - \alpha\mathbf{I})^{-1}, \mathbf{B}) = \text{span}\left\{\mathbf{B}, (\mathbf{A} - \alpha\mathbf{I})^{-1}\mathbf{B}, \ldots, (\mathbf{A} - \alpha\mathbf{I})^{-(r-1)}\mathbf{B}\right\}$; where often $\alpha = 0$.
- Extended Krylov subspace:
  $EK_r(\mathbf{A}, \mathbf{B}) = K_r(\mathbf{A}, \mathbf{B}) + K_r(\mathbf{A}^{-1}, \mathbf{A}^{-1}\mathbf{B})$
- Rational Krylov subspace:
  $K_r(\mathbf{A}, \mathbf{B}, \mathbf{s}) = \text{span}\left\{(\mathbf{A} - s_1\mathbf{I})^{-1}\mathbf{B}, (\mathbf{A} - s_2\mathbf{I})^{-1}\mathbf{B}, \ldots, (\mathbf{A} - s_r\mathbf{I})^{-1}\mathbf{B}\right\}$, with the chosen poles $s = [s_1, \ldots, s_r]$ a-priori.

Moment matching approximation methods [95] are based on Krylov subspaces (which may be carried out by using Lanczos [96] and Arnoldi [97] procedures) or their rational variants [98]. Moment matching consists in finding a reduced order model whose transfer function $\mathbf{H}_r$ matches a certain number of moments[4] of the original model $\mathbf{H} = \mathbf{C}(s\mathbf{E} - \mathbf{A})^{-1}\mathbf{B} + \mathbf{D}$ at the selected frequencies $s_i,\ i = 1, \ldots, r$. Moment matching may be obtained also through realization techniques or by means of interpolatory methods.

Among the many projection methods based on SVD found in literature, it is worthwhile highlight the Hankel norm approximation [99] and the balanced truncation [100–103] (or more general balance MOR), whose projection bases are "balanced modes" obtained by solving two Lyapunov equations related to controllability and observability Gramians. For

[4] The k-th, $k \geq 0$, moment of a system at $s \in \mathbb{C}$ is given by the k-th derivative of the transfer function at s.

a generalized stable LTI state-space system $(\mathbf{E}, \mathbf{A}, \mathbf{B}, \mathbf{C})$, the solutions $\mathbf{G}_c = \mathbf{X}\mathbf{X}^T$, controllability Gramian, and $\mathbf{G}_o = \mathbf{Y}\mathbf{Y}^T$, observability Gramian, of the dual generalized Lyapunov equations

$$\mathbf{A}\mathbf{G}_c\mathbf{E}^T + \mathbf{E}\mathbf{G}_c\mathbf{A}^T = -\mathbf{B}\mathbf{B}^T \tag{1.17a}$$

$$\mathbf{A}^T\mathbf{G}_o\mathbf{E} + \mathbf{E}^T\mathbf{G}_o\mathbf{A} = -\mathbf{C}^T\mathbf{C} \tag{1.17b}$$

are used to generate truncated balancing transformations right $\mathbf{T}_r = \mathbf{X}^T\mathbf{V}_1\mathbf{\Sigma}_1^{-1/2}$, and left $\mathbf{T}_l = \mathbf{Y}^T\mathbf{U}_1\mathbf{\Sigma}_1^{-1/2}$, where $\mathbf{U}_1$, $\mathbf{V}_1$ contains the eigenvectors corresponding to the r largest singular values $\Sigma_1 = \mathcal{D}(\sigma_1, \ldots, \sigma_r)$, and

$$\mathbf{Y}^T\mathbf{E}\mathbf{X} = \begin{bmatrix}\mathbf{U}_1 & \mathbf{U}_2\end{bmatrix}\begin{bmatrix}\mathbf{\Sigma}_1 & 0\\ 0 & \mathbf{\Sigma}_2\end{bmatrix}\begin{bmatrix}\mathbf{V}_1 & \mathbf{V}_2\end{bmatrix}^T \tag{1.18}$$

Note that if $\mathbf{E}$ is singular, then the generalized Lyapunov equations may have no solutions even for a stable system, and if solutions exist they are always nonunique [104]. In this case the projected generalized Lyapunov equation must be solved, giving the generalized proper and improper Gramians [105] as solutions. A balanced truncation is not optimal, in the sense that there may be other reduced-order models with smaller error norms, however it guarantees an a priori upper bound of the error of:

$$\|\mathbf{H} - \mathbf{H}_r\|_{\mathcal{H}_\infty} \leq 2\sum_{j=r+1}^{n}\sigma_i \tag{1.19}$$

It must be noted that Lyapunov equations cannot be solved exactly when large $(\mathbf{E}, \mathbf{A})$ matrices are involved, therefore leading to approximate balanced reduction [106–112].

Alternatively one may use the state matrix eigenvectors thus realizing an eigenmode-based order reduction [113, 114] (such as modal truncation or residualization is equivalent to singular perturbation approximation [115–117]), which implies a sort of time scale separation. Modal approximations require the selection of dominant eigenvalues (and eigenvectors), that for large-scale systems may be computed via iterative subspace methods, focusing on the computation of a few specific eigenvalues and eigenvectors instead of the complete spectrum. A Krylov-Schur method [118, 119] is suitable in finding a few eigenpairs of a large-scale matrix, and is preferred to the implicit restart Arnoldi algorithm being more efficient and less prone to numerical issues. Moreover the resulting Schur matrix structure allows, as will be successively presented in section 3.1, to obtain an advantageous form for residualizing the discarded fast dynamic. If needed, the controllability and the observability concepts may be combined to these spectral-based methods thus leading to the extraction of the so called dominant poles [91, 120], i.e. the most important eigenvalues in term of their contribution on the input-output relation, whose projective subspace carry out an accurate modal-equivalent of the transfer function of the original large-scale system.

These methods are suitable for linear systems. When nonlinear systems are involved the snapshot method may be used, where empirical time series data $\mathbf{x}(t_i)$, or frequency domain data $\mathbf{x}(\omega_i)\, i = 1, \ldots, N$, arising from measurement are exploited using the SVD, picking the relevant directions of the correlation matrix $\mathbf{K} = \mathbf{X}\mathbf{X}^T \in \mathbb{R}^{n\times n}$, being $\mathbf{X} =$

$[\mathbf{x}_1, \ldots, \mathbf{x}_N] \in \mathbb{R}^{n \times N}$, with $N \ll n$. This leads to the empirical Gramians method and the Proper Orthogonal Decomposition (POD) [121], also known as Karhunen-Loève decomposition (K-L) [122–124] or Principal Component Analysis (PCA) [125–127]. The method of snapshots [94] avoid to solve the infeasible eigenvalue problem for the large matrix $\mathbf{K}$. Instead it considers the matrix $\mathbf{x}^T\mathbf{x} \in \mathbb{R}^{N \times N}$, having same singular values of $\mathbf{K}$, and eigenvectors that, after normalization, are just the POD modes. Hybrid techniques may also be found, such as Balanced POD [128, 129]. It must be observed that the POD is a linear technique, but it is able to handle nonlinearity because it can account for nonlinear coupling of terms acting within the linear space defined by the basis functions.

Among other approaches capable of handling nonlinear problems there is the Harmonic Balance (HB) [130–132], where the time dependence of the solution is assumed to be a Fourier series in time. Harmonic Balance is not a reduced order modeling technique in a strict sense, but it may be of help in reducing the computational time for nonlinear, time-periodic, unsteady problems.

Alternatives to PCA, which relying on Gaussian features utilizes the first and second moments of the measured data (i.e. exploit correlation and covariance properties), is the Independent Component Analysis (ICA) [133], which exploits the inherently non-Gaussian features of the data and employs higher moments.

System identification methods are black-box data-driven reduction techniques which build reduced order models, whose behavior matches (within a chosen norm) the response of the larger model, by fitting observed input-output data. Rather than directly reducing the dimensions of the model matrices, they construct a model for the input-output map, bypassing the computation of the state system. The Jacobian matrix knowledge is not required[5], and therefore neither is the linearization of the DAE, being the system only used to provide time histories data.

System identification [87–89] is a very broad field involving many techniques arising from different application areas. A simple classification of it is not easy. Identification methods may be divided depending on the character of the models to be estimated: linear, nonlinear, parametric, nonparametric, hybrid, global, local, etc.. However the approach chosen, the prediction of the output at a time instant is carried out by considering all or some previously measured inputs and outputs.

Two typical approaches to the fitting problem whom identification relies on, are the parametric approach and the non-parametric approach. Parametric methods postulate an underlying mathematical structure of the system, which is associated to some parameters, usually determined by minimizing the error between the model and the fitting data. Nonparametric methods construct the model without specifying any structure a priori, which is instead determined from the data. They direct estimate the system responses using correlation analysis (if the impulse response or the step response are estimated) or spectral analysis (if the system frequency response is estimated). In carrying-out the fitting process Least-Squares (LS) techniques may be used. According to the error minimization criteria LS methods belong to Equation Error (EE) methods. Others criteria are the Output Error (OE) and Prediction Error (PE) methods, the Extended Kalman Filter (EKF) [134],

[5] Knowledge of the internal structure of the model is generally not required, except for some cases where partial information of the system is known (e.g. gray-box methods [87] estimate models using some ideas about the character of the process generating the data).

Bayesian Analysis [135] and Maximum-Likelihood Estimation (MLE) [87, 136]. These estimation methods differs about the time horizon over which they are restricted, and therefore in their ability in providing good prediction models rather than good simulation models. Whatever the criteria chosen, they can be applied to quite arbitrary parametrizations.

Parametric methods are divided also on the model structure chosen. They include different structures of Linear Time Invariant (LTI) models, which being characterized entirely by their impulse response, may be estimated through transient and frequency analyses. For example linear state-space models may be estimated using subspace projection approaches, based on geometric operations on subspaces spanned by matrices obtained from the data, or vector fitting methods, which build rational approximations of the transfer function that can be used to adaptively build reduced order models. Other common structure models are the regression methods which describe the systems by means of difference equations. Among them there are the Finite Impulse Response (FIR), which make use only of past inputs, the Auto-Regressive model with eXternal input (ARX) [137], which use use past inputs and outputs data, the Average model with eXternal input (ARMAX) [138], which use inputs, outputs and predicted outputs, the Output Error (OE) model, which use past inputs and past simulated outputs, and the Box-Jenkins (BJ) model, which use past inputs, outputs, simulated outputs and predicted outputs. All these regression methods have their nonlinear counterparts (NARX, NARMAX, ...). More recent models relies on black-box nonlinear structures, able to perform a nonlinear mapping of the input-output data, such as Artificial Neural Network (ANN) [139], Fuzzy models [140], machine learning, manifold learning, etc.

The different model structures are special cases of the generic input-output model structure:

$$\mathbf{y}(t) = \mathbf{H}(\delta, \boldsymbol{\theta})\, \mathbf{u}(t) + \mathbf{H}_w(\delta, \boldsymbol{\theta})\, \mathbf{w}(t) \tag{1.20}$$

where $\mathbf{H}$ is the transfer function from input $\mathbf{u}(t)$ to output $\mathbf{y}(t)$, and $\mathbf{H}_w$ a linear filter shaping the white noise disturbance $\mathbf{w}(t)$, $\boldsymbol{\theta}$ is the parameter vector, and δ is the backward-shift (delay) operator (i.e. $\delta^{-n}\,\mathbf{u}(t) \equiv \mathbf{u}(t-n)$) if discrete-time systems are considered or, equivalently, δ denotes a discrete-time approximation to the continuous-time differentiation operator d/dt if continuous-time representations are considered, with the notational freedom of using t both as discrete-time and continuous-time. Describing the transfer functions as rational matrix approximations, the model may be rewritten as the polynomial black-box model:

$$\mathbf{A}(\delta, \boldsymbol{\theta})\, \mathbf{y}(t) = \frac{\mathbf{B}(\delta, \boldsymbol{\theta})}{\mathbf{E}(\delta, \boldsymbol{\theta})}\, \mathbf{u}(t) + \frac{\mathbf{C}(\delta, \boldsymbol{\theta})}{\mathbf{D}(\delta, \boldsymbol{\theta})}\, \mathbf{w}(t) \tag{1.21}$$

where matrices $\mathbf{A}$, $\mathbf{B}$, $\mathbf{C}$, $\mathbf{D}$, $\mathbf{E}$ are polynomials matrices in δ, whose coefficients are stored in $\boldsymbol{\theta}$. Specific cases of these polynomials lead to the particular models previously cited (ARX, OE, and so on).

The most popular nonparametric methods there are the functional series approaches. Among these there are the nonparametric regression methods, which represents nonlinear systems by means of a convolution integral of Volterra [89, 141] or Wiener kernels [142] and the system input. In these kernel methods, the kernel function is estimated as a mean over a local neighborhood of the data. A more sophisticated approach would be to compute a

more advanced estimate within the neighborhood, such as using local polynomial approximations whose coefficients are computed using a weighted least squares fitting.

Chapter 2

State-Space Aeroelastic Modeling

Aeroelastic analysis, such as flutter stability and time responses to external disturbances (e.g. gust/turbulence), may exploit full advantages of high-fidelity CFD, however an effort in the reduction of its computational cost is required. This may be performed through the use of corrections of classical subsonic DLM, the application of less sophisticated CFD models (e.g. full potential coupled to a boundary layer theory), or linearized CFD models, coming from a direct linearization of the aerodynamic formulation or accounted through their transfer functions, to which a successive model order reduction technique (e.g. a Proper Orthogonal Decomposition) may be further applied.

Linearized aerodynamic models maintain a core position in the aircraft aeroelastic analysis where computations have to be performed for a wide range and combinations of many parameters. The linearization is performed through small perturbations of the aerodynamic state vector and small perturbations of the solid/wall boundaries belonging to the interface aeroelastic domain. This small linear perturbations are applied about the (nonlinear) mean flow field, which may comprise shock waves and flow separation. The motion of shock waves or separation bubbles are nearly proportional to the boundary perturbation, justifying the use of linearized approximation.

Moreover a linearized aerodynamic subsystem can be easily coupled to the structural model in order to obtain an aeroelastic model is a state-space formulation, which can fully take advantage of modern techniques arising from the control system community.

2.1 Linear(ized) aerodynamic subsystem

In this section the formulation of a Linearized Computational Fluid Dynamics (LCFD) model is presented, in order to provide a framework for searching a linear Reduced Order Model (ROM), which it will be subsequently used in chapter 3 in the derivation of a finite states Linear Time Invariant (LTI) aerodynamic subsystem. The linearization of the fluid equations for a subsonic, supersonic or hypersonic flow field is a technique widely used to simplify an otherwise complex and expensive flow field analysis.

A linearized aerodynamic model of a nonlinear high fidelity CFD formulation, whether based on Full Potential, Euler, RANS, will ends with the following (very) large set of LTI

of n equations:

$$\begin{aligned} \mathbf{E}\,\dot{\mathbf{x}} &= \mathbf{A}\,\mathbf{x} + \mathbf{B}_q\,\mathbf{q} + \mathbf{B}_{\dot{q}}\,\dot{\mathbf{q}} + \mathbf{B}_g\,\frac{\mathbf{v}_g}{V_\infty} \\ \mathbf{Q}_a &= q_\infty \mathbf{C}\,\mathbf{x} \end{aligned} \tag{2.1}$$

where $\mathbf{q}$ are the discretized free structural coordinates, $\mathbf{v}_g$, the gust/turbulence, q_∞ the freestream dynamic pressure. Calling ρ, $\rho\boldsymbol{v}$, E^{t} and ϕ respectively: the fluid density, momentum, the total energy per unit volume [1] and velocity potential, the state vector $\mathbf{x}$ will be either a stacking of discretized $\begin{bmatrix}\rho & \rho\boldsymbol{v} & T\end{bmatrix}^T$, for Euler and RANS, $\begin{bmatrix}\rho & \phi\end{bmatrix}^T$ for a two fields FP formulation or $\begin{bmatrix}\phi & \dot{\phi}\end{bmatrix}^T$ for a potential only formulation. Such a model should be asymptotically stable, so $\mathbf{A}$ is not singular. Moreover, since both the pressure and the tangential stresses applied to the structure are dependent just on $\mathbf{x}$ the output generalized forces, $\mathbf{Q}_a$, are strictly proper. A way to a ROM of order $l \ll n$, representing a response of interest for a set of responses related to a relatively low frequency excitations, can be obtained by rewriting the above state equation as:

$$\mathbf{A}^{-1}\mathbf{E}\,\dot{\mathbf{x}} = \mathbf{x} + \mathbf{A}^{-1}\mathbf{B}_q\,\mathbf{q} + \mathbf{A}^{-1}\mathbf{B}_{\dot{q}}\,\dot{\mathbf{q}} + \mathbf{A}^{-1}\mathbf{B}_g\,\frac{\mathbf{v}_g}{V_\infty} \tag{2.2}$$

It should be noticed that, apart from a few symbols used to dress our formulae so to convey an LCFD feeling, what above is applicable to any asymptotically stable linear system. Moreover the details omitted in the development of the above ROM formulae will show that all of the involved numerical calculations can be carried out by fully preserving the high level of sparsity often characterizing large LTI system and LCFD models in particular, so that what will be presented is fairly usable as it is.

The linearization is carried out about a steady-state flow condition associated to a full nonlinearly trimmed solution of the high fidelity model (FP, Euler or RANS equations). Therefore the linearized model may be seen as a combination of a linearization of the unsteady part of the solution combined with a nonlinear and non-uniform steady mean flow. This allows the full nonlinear unsteady equations to be cast as one set of nonlinear steady-state equations and another set of linear unsteady equations that depend on the underlying steady flow [143, 144].

In this case the simulation of the linearized form of the high fidelity equations involves the solution over the complete flow domain. A further reduction in the complexity of the flow physics may be obtained by eliminating the need to compute the motion of a full flow field mesh. This is performed by considering the aerodynamic transfer matrix which represents a mapping between the input (the structural boundary displacements and eventually gust/turbulence) and the output (the aerodynamic loads projected onto the structural modes) of the aerodynamic subsystem.

The generalized aerodynamic forces associated to the aerodynamic transfer matrix can be calculated for sinusoidal motions of a set of mode shapes about the fully non-linear trimmed steady solution for a range of input frequencies, otherwise considering the output/input ratio in frequency domain of the aerodynamic force obtained from impulsive, step or blended step[2] input functions. Such a local numerical linearization approach is

[1] The absolute temperature may be used in the state vector as an alternative to the total energy.

[2] The blended step is computationally efficient because it does not require excessive time resolution to be described, otherwise needful for an impulse, and prevents Gibbs phenomena in the transient, typical of a step.

compatible with the strongly non-linear flow field of many aeroelastic problems, only when the steady flow effects dominate the aeroelastic behavior and the unsteady generalized aerodynamic forces are satisfactorily linear with respect to small structural displacements. For example, in the transonic case, it may be sufficient to capture the locations of shock waves of the steady-state solutions and carry out linear perturbations about that to produce accurate prediction of the transonic flutter dip (i.e. the reduction in flutter speed due to transonic flow effects) [12, 145, 146].

The resulting frequency-dependent linear unsteady aerodynamic transfer matrix may be used coupled to the structure in its direct form, i.e. following the classic aeroelasticity approach, or cast as a state-space model through techniques based on rational function approximations, i.e. following a modern aeroelasticity approach. Thus the complicated fluid/structure system may be reduced to a Multi-Input-Multi-Output (MIMO) system to which, when a linear modal structure is considered, the classical methods of linear analysis can be applied.

The linearization of the high-fidelity CFD equations leads to an approximation which holds its effectiveness in aeroelastic stability and response analysis. Nevertheless there are difficulties and limits in the use of linearized CFD models in computational aeroelasticity. For example Limit Cycle Oscillations (LCO), large shock motion or separation motion, may be hardly simulated. Moreover it is difficult to obtain a linearized model for separated flows, where there is no a clear understanding on how performing the linearization of turbulence models and transition models.

2.2 State-Space Formulation

Following the structural analyst point of view of the classic frequency approach, a linear(ized) aeroelastic formulation around a trimmed rectilinear motion is written in generalized, not necessarily proper, absolute modal coordinates:

$$\left(s^2\mathbf{M} + s\mathbf{C} + \mathbf{K} - q_\infty \mathbf{H}_{am}(p, M_\infty)\right)\mathbf{q} = q_\infty \mathbf{H}_{ag}(p, M_\infty)\mathbf{u}_g(s) + \mathbf{B}_h \mathbf{Q}_h \qquad (2.3)$$

with q_∞ and M_∞ being respectively the freestream dynamic pressure and Mach number, $p = sl_a/V_\infty = h + jk$ the complex reduced frequency, $j = \sqrt{-1}$, s the circular complex frequency, l_a an appropriate aerodynamic reference length, and V_∞ the constant aircraft speed.

The system matrices are:

$\mathbf{M} = \mathbf{M}_s + \mathbf{M}_c$ the system mass matrix combining the overall physical mass, $\mathbf{M}_s$, and a possible control contribution, $\mathbf{M}_c$;

$\mathbf{C} = \mathbf{C}_s + \mathbf{C}_g + \mathbf{C}_c$ the system damping matrix comprising: the structural damping, $\mathbf{C}_s$, gyroscopic effects associated to spinning rotors, $\mathbf{C}_g$, control terms, $\mathbf{C}_c$;

$\mathbf{K} = \mathbf{K}_s + \mathbf{K}_\sigma + \mathbf{K}_{at} + \mathbf{K}_T + \mathbf{K}_G + \mathbf{K}_c$ the overall stiffness matrix taking into account: the linear(ized) structural and prestress stiffnesses, $\mathbf{K}_s$ and $\mathbf{K}_\sigma$, the reference trim aerodynamic stiffness associated to the related steady aerodynamic load, $\mathbf{K}_{at}$, the follower thrusts stiffness, $\mathbf{K}_T$, the gravity stiffness $\mathbf{K}_G$, control elements, $\mathbf{K}_c$;

and the vector $\mathbf{q}$ is an appropriate set of N generalized coordinates, extended to include control states. Generalized external forcing loads, $\mathbf{Q}_h$, are applied to the system through the load distribution influence matrix $\mathbf{B}_h$.

The aerodynamic loads appear in terms of transfer matrices associated to the generalized forces related to structural motions, $\mathbf{Q}_{am}$, and gusts, $\mathbf{Q}_{ag}$:

$$\mathbf{Q}_{am}(p, M_\infty) = q_\infty \mathbf{H}_{am}(p, M_\infty)\mathbf{q} \tag{2.4a}$$

$$\mathbf{Q}_{ag}(p, M_\infty) = q_\infty \mathbf{H}_{ag}(p, M_\infty)\mathbf{u}_g \tag{2.4b}$$

Recalling the previous section, $\mathbf{u}_g(t)$ could be either generalized coordinates $\mathbf{q}_g(t)$related to the gust velocity (as it will be shown in section 4.2) or the angle of attack variation due to the gust velocity $\mathbf{v}_g(t)/V_\infty$, thus providing the following two gust transfer matrices:

$$\mathbf{Q}_{ag}(p, M_\infty) = q_\infty \mathbf{H}_{av_g}(p, M_\infty)\, \frac{\mathbf{v}_g(p)}{V_\infty} \tag{2.5a}$$

$$\mathbf{Q}_{ag}(p, M_\infty) = q_\infty \mathbf{H}_{aq_g}(p, M_\infty)\, \mathbf{q}_g(p) \tag{2.5b}$$

The aerodynamic transfer matrices are calculated at a discrete set of harmonic reduced frequencies, $k = \omega l_a / V_\infty$, and extended to any value p through causal inter-extrapolations. Such matrices can be obtained numerically through many linear(rized) formulations, e.g.: unsteady integral equations related only to the body surface, direct/indirect linearizations of flow solutions obtained through Computational Fluid Dynamics (CFD), ranging from Full-Potential to Euler and Reynolds Averaged Navier-Stokes [49, 82, 147].

The above classic aeroelastic formulation requires the peculiar solution techniques mentioned in the introduction, where we referred also to the quest of a more systematic approach leading to LTI state models. Thus, on the basis of the same raw aerodynamic data available in classic aeroelasticity, such an approach identifies a finite state approximation of the aerodynamic subsystem. This is carried out by recasting the aerodynamic transfer matrices in the form of a linear asymptotically stable system having the generalized unsteady aerodynamic forces $\mathbf{Q}_{amg} = \mathbf{Q}_{am} + \mathbf{Q}_{ag}$ as an output.

Adopting a unified approach for determining a single state space approximation for all of the aerodynamic forces [148], we define: $\mathbf{H}_{amg} = [\mathbf{H}_{am}\ \mathbf{H}_{ag}]$ and proceed toward a possible state approximation of the type:

$$\dot{\mathbf{x}}_{amg}(t) = \frac{V_\infty}{l_a}\mathbf{A}_{amg}\mathbf{x}_{amg}(t) + \frac{V_\infty}{l_a}\mathbf{B}_{0amg}\begin{Bmatrix}\mathbf{q}(t)\\ \mathbf{u}_g(t)\end{Bmatrix} + \mathbf{B}_{1amg}\begin{Bmatrix}\dot{\mathbf{q}}(t)\\ \dot{\mathbf{u}}_g(t)\end{Bmatrix} \tag{2.6a}$$

$$\begin{aligned}\mathbf{Q}_{amg}(t) = {} & \mathbf{C}_{amg}\mathbf{x}_{amg}(t) + \mathbf{E}_{0amg}\begin{Bmatrix}\mathbf{q}(t)\\ \mathbf{u}_g(t)\end{Bmatrix} + \frac{l_a}{V_\infty}\mathbf{E}_{1amg}\begin{Bmatrix}\dot{\mathbf{q}}(t)\\ \dot{\mathbf{u}}_g(t)\end{Bmatrix} \\ & + \left(\frac{l_a}{V_\infty}\right)^2 \mathbf{E}_{2amg}\begin{Bmatrix}\ddot{\mathbf{q}}(t)\\ \ddot{\mathbf{u}}_g(t)\end{Bmatrix}\end{aligned} \tag{2.6b}$$

whose associated aerodynamic transfer matrix is:

$$\mathbf{H}_{amg} = \mathbf{E}_{0amg} + p\mathbf{E}_{1amg} + p^2\mathbf{E}_{2amg} + \mathbf{C}_{amg}\left(p\mathbf{I} - \mathbf{A}_{amg}\right)^{-1}\left(\mathbf{B}_{0amg} + p\mathbf{B}_{1amg}\right) \tag{2.7}$$

The above formula can be quite useful also as a causal interpolation for the classical approach. In particular, its (am) part can be adopted as a substitute for first/second order causal $p-k$ approximations [149] in continued solutions of the flutter equation [150, 151], thus ending in providing results like those given by the Generalized Aeroelastic Analysis Method (GAAM) [152]. Apart from the new residual term $\mathbf{B}_{1amg}$ the above unified model is embedded in any linearized unsteady aerodynamic field based formulation [148]. Hence it is retained as the most suitable choice from a conceptual point of view.

Equation (2.3) may be translated into an LTI model in the descriptor form:

$$\mathbf{E}_{ae}\dot{\mathbf{x}}_{ae}(t) = \mathbf{A}_{ae}\mathbf{x}_{ae}(t) + \mathbf{B}_{aeg}\begin{Bmatrix}\mathbf{u}_g(t)\\ \dot{\mathbf{u}}_g(t)\\ \ddot{\mathbf{u}}_g(t)\end{Bmatrix} + \mathbf{B}_{aeh}\mathbf{Q}_h \tag{2.8}$$

Adopting the partitions: $\mathbf{B}_{.amg} = [\mathbf{B}_{.am}\ \mathbf{B}_{.ag}]$, $\mathbf{E}_{.amg} = [\mathbf{E}_{.am}\ \mathbf{E}_{.ag}]$, where the dummy dots $(.)$ can be either 0, 1 or 2, and defining $\mathbf{x}_{ae}^T = \{\mathbf{q}^T,\ \dot{\mathbf{q}}^T,\ \mathbf{x}_{amg}^T\}$, the related matrices are:

$$\mathbf{E}_{ae} = \begin{bmatrix}\mathbf{I} & \mathbf{0} & \mathbf{0}\\ \mathbf{0} & \mathbf{M}_{ae} & \mathbf{0}\\ \mathbf{0} & \mathbf{0} & \mathbf{I}\end{bmatrix}, \qquad \mathbf{A}_{ae} = \begin{bmatrix}\mathbf{0} & \mathbf{I} & \mathbf{0}\\ -\mathbf{K}_{ae} & -\mathbf{C}_{ae} & q_\infty\mathbf{C}_{amg}\\ (V_\infty/l_a)\,\mathbf{B}_{0am} & \mathbf{B}_{1am} & (V_\infty/l_a)\,\mathbf{A}_{amg}\end{bmatrix}$$

$$\mathbf{B}_{aeg} = \begin{bmatrix}\mathbf{0} & \mathbf{0} & \mathbf{0}\\ q_\infty\mathbf{E}_{0ag} & q_\infty\left(l_a/V_\infty\right)\mathbf{E}_{1ag} & q_\infty\left(l_a/V_\infty\right)^2\mathbf{E}_{2ag}\\ (V_\infty/l_a)\,\mathbf{B}_{0ag} & \mathbf{B}_{1ag} & \mathbf{0}\end{bmatrix}, \qquad \mathbf{B}_{aeh} = \begin{bmatrix}\mathbf{0}\\ \mathbf{B}_h\\ \mathbf{0}\end{bmatrix}$$

$$\begin{aligned}\mathbf{M}_{ae} &= \mathbf{M} - q_\infty\left(l_a/V_\infty\right)^2\mathbf{E}_{2am}\\ \mathbf{C}_{ae} &= \mathbf{C} - q_\infty\left(l_a/V_\infty\right)\mathbf{E}_{1am}\\ \mathbf{K}_{ae} &= \mathbf{K} - q_\infty\mathbf{E}_{0am}\end{aligned} \tag{2.9}$$

The above LTI formulation contains first/second order dynamic residualizations [153] respectively in the state and in the output equations, meant to recover the low frequency contribution of the high frequency content of generalized aerodynamic forces (GAFs), similarly to the static correction provided by mode accelerations in structural problems.

Despite improving the fitting accuracy, a second order residualization of the gust terms might be unsuitable when dealing with continuous turbulence. Indeed most of the usually adopted shaping filters models their Power Spectral Density (PSD) roll off as $1/s$ [154, 155], thus leading to an unacceptable white noise differentiation in time. That can be verified with shaping filters, whose matrices $\mathbf{A}_w$, $\mathbf{B}_w$,$\mathbf{C}_w$ provide the following state space realization [154, 155]:

$$\dot{\mathbf{x}}_w(t) = \mathbf{A}_w\mathbf{x}_w(t) + \mathbf{B}_w\mathbf{w}(t) \tag{2.10a}$$

$$\mathbf{u}_g(t) = \mathbf{C}_w\mathbf{x}_w(t) \tag{2.10b}$$

$$\dot{\mathbf{u}}_g(t) = \mathbf{C}_w\mathbf{A}_w\mathbf{x}_w(t) + \mathbf{C}_w\mathbf{B}_w\mathbf{w}(t) \tag{2.10c}$$

$$\ddot{\mathbf{u}}_g(t) = \mathbf{C}_w\mathbf{A}_w^2\mathbf{x}_w(t) + \mathbf{C}_w\mathbf{A}_w\mathbf{B}_w\mathbf{w}(t) + \mathbf{C}_w\mathbf{B}_w\dot{\mathbf{w}}(t) \tag{2.10d}$$

which clearly shows that $\ddot{\mathbf{u}}_g$ will drag an unacceptable $\dot{\mathbf{w}}$ into the state model. So it seems almost compulsory to omit the second order gust terms when the state space identification has to be used for turbulence responses. Nonetheless, omitting $\mathbf{Q}_h$ for sake of simplicity, we write the full finite state gust/turbulence model as:

$$\begin{bmatrix}\mathbf{E}_{ae} & \mathbf{0}\\ \mathbf{0} & \mathbf{I}\end{bmatrix}\begin{Bmatrix}\dot{\mathbf{x}}_{ae}(t)\\ \dot{\mathbf{x}}_w(t)\end{Bmatrix} = \begin{bmatrix}\mathbf{A}_{ae} & \mathbf{A}_{aew}\\ \mathbf{0} & \mathbf{A}_w\end{bmatrix}\begin{Bmatrix}\mathbf{x}_{ae}(t)\\ \mathbf{x}_w(t)\end{Bmatrix} + \begin{bmatrix}\mathbf{B}_{0aew}\\ \mathbf{B}_w\end{bmatrix}\mathbf{w}(t) + \begin{bmatrix}\mathbf{B}_{1aew}\\ \mathbf{0}\end{bmatrix}\dot{\mathbf{w}}(t) \tag{2.11}$$

with:

$$\mathbf{A}_{aew} = \mathbf{B}_{aeg}\begin{bmatrix}\mathbf{C}_w\\ \mathbf{C}_w\mathbf{A}_w\\ \mathbf{C}_w\mathbf{A}_w^2\end{bmatrix}, \quad \mathbf{B}_{0aew} = \mathbf{B}_{aeg}\begin{bmatrix}\mathbf{0}\\ \mathbf{C}_w\mathbf{B}_w\\ \mathbf{C}_w\mathbf{A}_w\mathbf{B}_w\end{bmatrix}, \quad \mathbf{B}_{1aew} = \mathbf{B}_{aeg}\begin{bmatrix}\mathbf{0}\\ \mathbf{0}\\ \mathbf{C}_w\mathbf{B}_w\end{bmatrix} \tag{2.12}$$

and discard the term $\mathbf{B}_{1aew}$ to avoid any white noise differentiation. Despite the availability of analytical expressions of the $1/s$ type, a full second order residualization could be retained by fitting turbulence power spectra with rational filters rolling off as $1/s^2$, while maintaining the correct $1/s$ behavior over the frequency range of interest for the aeroelastic responses. It will lead to the same formal set of equations, with $\mathbf{B}_{1aew} = \mathbf{0}$, and the following output and definitions of $\mathbf{A}_{aew}$ and $\mathbf{B}_{0aew}$:

$$\begin{Bmatrix}\mathbf{u}_g(t)\\ \dot{\mathbf{u}}_g(t)\\ \ddot{\mathbf{u}}_g(t)\end{Bmatrix} = \begin{bmatrix}\mathbf{C}_w\\ \mathbf{C}_{\dot{w}}\\ \mathbf{C}_{\dot{w}}\mathbf{A}_w\end{bmatrix}\mathbf{x}_w(t) + \begin{bmatrix}\mathbf{0}\\ \mathbf{0}\\ \mathbf{C}_{\dot{w}}\mathbf{B}_w\end{bmatrix}\mathbf{w}(t) \tag{2.13a}$$

$$\mathbf{A}_{aew} = \mathbf{B}_{aeg}\begin{bmatrix}\mathbf{C}_w\\ \mathbf{C}_{\dot{w}}\\ \mathbf{C}_{\dot{w}}\mathbf{A}_w\end{bmatrix}, \qquad \mathbf{B}_{0aew} = \mathbf{B}_{aeg}\begin{bmatrix}\mathbf{0}\\ \mathbf{0}\\ \mathbf{C}_{\dot{w}}\mathbf{B}_w\end{bmatrix} \tag{2.13b}$$

Instead, the term $\ddot{\mathbf{u}}_g(t)$ causes no troubles in case of deterministic gust responses, whether the gust profile to be used has or not a continuous first time derivative, as for a sharp-edged gust. Indeed, defining the following partitions:

$$\mathbf{B}_{aeg} = [\mathbf{B}_{0aeg}\ \mathbf{B}_{1aeg}\ \mathbf{B}_{2aeg}] \tag{2.14}$$

omitting $\mathbf{Q}_h$ once more, Eq. (2.8) can be rewritten as:

$$\mathbf{E}_{ae}\dot{\mathbf{x}}_{ae}(t) = \mathbf{A}_{ae}\mathbf{x}_{ae}(t) + \mathbf{B}_{0aeg}\mathbf{u}_g(t) + \mathbf{B}_{1aeg}\dot{\mathbf{u}}_g(t) + \mathbf{B}_{2aeg}\ddot{\mathbf{u}}_g(t) \tag{2.15}$$

so that, calling $H(t)$ the Heaviside step function, it can be specialized to a single sharp-edged gust by writing $u_g(t) = H(t)\,V_g$:

$$\mathbf{E}_{ae}\dot{\mathbf{x}}_{ae}(t) = \mathbf{A}_{ae}\mathbf{x}_{ae}(t) + V_g\,\mathbf{B}_{0eag}H(t) + V_g\,\mathbf{B}_{1eag}\delta(t) + V_g\,\mathbf{B}_{2eag}\dot{\delta}(t) \tag{2.16}$$

$\delta(t)$ being the impulse function. Its solution will be of the type:

$$\mathbf{x}_{ae}(t) = \mathbf{x}_{ae_\delta}\delta(t) + \mathbf{x}_{ae_r}(t)H(t) \tag{2.17}$$

Therefore, assuming $\mathbf{x}_{ae_r}(0^-)$, for $t > 0$ we have:

$$\mathbf{E}_{ae}\mathbf{x}_{ae_\delta}\dot{\delta} + \mathbf{E}_{ae}\mathbf{x}_{ae_r}(0^+)\delta + \mathbf{E}_{ae}\dot{\mathbf{x}}_{ae_r} = \mathbf{A}_{ae}\mathbf{x}_{ae_\delta}\delta + \mathbf{A}_{ae}\mathbf{x}_{ae_r} + V_g\,\mathbf{B}_{0eag} + V_g\,\mathbf{B}_{1eag}\delta + V_g\,\mathbf{B}_{2eag}\dot{\delta} \quad (2.18)$$

Equating the terms multiplying $\dot{\delta}$ is: $\mathbf{x}_{ae_\delta} = V_g\mathbf{E}_{ae}^{-1}\mathbf{B}_{2eag}$. Then, the full solution comes from integrating the following LTI system, starting from the shown initial condition:

$$\mathbf{E}_{ae}\dot{\mathbf{x}}_{ae_r} = \mathbf{A}_{ae}\mathbf{x}_{ae_r} + V_g\,\mathbf{B}_{0eag} \quad (2.19a)$$

$$\mathbf{x}_{ae_r}(0^+) = V_g\,\mathbf{E}_{ae}^{-1}\left(\mathbf{A}_{ae}\mathbf{E}_{ae}^{-1}\mathbf{B}_{2eag} + \mathbf{B}_{1eag}\right) \quad (2.19b)$$

It is remarked that, because of the block diagonal structure of $\mathbf{E}_{ae}$, and the structure of $\mathbf{B}_{2eag}$ it results:

$$\begin{aligned}\mathbf{x}_{ae_\delta} = V_g\mathbf{E}_{ae}^{-1}\mathbf{B}_{2eag} &= V_g\begin{bmatrix}\mathbf{I} & \mathbf{0} & \mathbf{0}\\ \mathbf{0} & \mathbf{M}_{ae} & \mathbf{0}\\ \mathbf{0} & \mathbf{0} & \mathbf{I}\end{bmatrix}^{-1}\begin{Bmatrix}\mathbf{0}\\ q_\infty\left(l_a/V_\infty\right)^2\mathbf{E}_{2ag}\\ \mathbf{0}\end{Bmatrix}\\ &= V_g\begin{bmatrix}\mathbf{I} & \mathbf{0} & \mathbf{0}\\ \mathbf{0} & \mathbf{M}_{ae}^{-1} & \mathbf{0}\\ \mathbf{0} & \mathbf{0} & \mathbf{I}\end{bmatrix}\begin{Bmatrix}\mathbf{0}\\ q_\infty\left(l_a/V_\infty\right)^2\mathbf{E}_{2ag}\\ \mathbf{0}\end{Bmatrix} = V_g\begin{Bmatrix}\mathbf{0}\\ q_\infty\left(l_a/V_\infty\right)^2\mathbf{M}_{ae}^{-1}\mathbf{E}_{2ag}\\ \mathbf{0}\end{Bmatrix}\end{aligned} \quad (2.20)$$

so that the impulsive part of the solution has no $\mathbf{q}_\delta$ neither $\mathbf{x}_{a_\delta}$ terms, but only $\dot{\mathbf{q}}_\delta$. Moreover, $\dot{\mathbf{q}}_\delta = \mathbf{q}(0^+)$, so that none of the aeroelastic states will contain a truly impulsive part, $\mathbf{x}_{a_\delta}$.

This illustrates why a first order gust residualization is strictly needed just for continuous turbulence responses.

2.2.1 Transformation to a flight mechanics point of view

We conclude with a brief comment on the possibility of tackling the LTI aeroelastic model in the alternative attached-stability axes form, i.e. closer to a flight mechanics point of view, which will mostly affect the states associated to the aircraft reference frame. Even if it could be easily developed by a first hand transformation of the GAFs to attached-stability axes [156, 157], nothing is lost with the just presented approach as it can be recovered also by applying to Eq. (2.8) the simple state transformation shown in [157, 158].

Symmetric case

It is here provided the way to transform the aeroelastic model from absolute plunge and pitching to incidence and pitching rate. First of all it is remarked that the generalized forces associated to the rigid-plunge modes will correspond to a physical downward force, F_h, and a pitch up moment, M_θ, only if the plunge, h, is a pure unit rigid downward vertical translation, of one meter, and θ a pure upward rigid plane rotation, of one radian, around an assigned reference point.

The preferred downward and pitch up directions have been chosen to follow the standard convection of the body axes and related kinematic states used in flight mechanics. It will entail a further change of sign if F_h has to be transformed into lift, L, as it will commented later. Since from vibration modes calculation symmetric body frame motions can be obtained as any combination of a pure vertical translation and rotation, whatever of the available rigid body modes have to be translated into h and θ. For that defining $\boldsymbol{r}_1(\bar{\boldsymbol{x}})r_1$ and $\boldsymbol{r}_2(\bar{\boldsymbol{x}})r_2$ the available generic symmetric rigid body modes with shapes, $\boldsymbol{r}_1(\bar{\boldsymbol{x}})$ and $\boldsymbol{r}_2(\bar{\boldsymbol{x}})$, given at a set of points ≥ 2, $\bar{\boldsymbol{x}}$ typically the nodes in the case of a finite element analysis, having amplitudes, r_1 and r_2. So, calling $\mathbf{H}_a^{r_1 r_2}$ the partition of the available modal aerodynamic transfer matrix, associated to r_1 and r_2, defining $\mathbf{Q}_a^{r_1 r_2} = \begin{bmatrix} Q_{r_1} & Q_{r_2} \end{bmatrix}^T$ the related generalized forces and $\mathbf{q}_{r_1 r_2}^T = \begin{bmatrix} r_1 & r_2 \end{bmatrix}^T$, the related generalized modal coordinates, it can be write

$$\mathbf{Q}_a^{r_1 r_2} = \begin{Bmatrix} Q_{r_1} \\ Q_{r_2} \end{Bmatrix} = \mathbf{H}_a^{r_1 r_2} \begin{Bmatrix} r_1 \\ r_2 \end{Bmatrix} \tag{2.21}$$

Equation (2.21) is transformed to:

$$\mathbf{Q}_a = \begin{Bmatrix} F_h \\ M_\theta \end{Bmatrix} = \mathbf{H}_a^{h\theta} \begin{Bmatrix} h \\ \theta \end{Bmatrix} \tag{2.22}$$

by defining the vector $\pm\mathbf{1}_h := \begin{bmatrix} 0 & 0 & 1 \end{bmatrix}^T$, and the vector $\pm\boldsymbol{x} := \begin{bmatrix} z & 0 & -x \end{bmatrix}^T$, of the offsets with respect to an aerodynamic reference point $\bar{\boldsymbol{x}}$. The $\pm$ signs above have to be chosen so to make it consistent the imposed h and θ with possible different orientations of the related axes used in the structural modes calculations. Then the relation between the different representations of the symmetric rigid modes is recovered by writing the corresponding point wise modes transformation, followed by the solution of the related, possibly overdetermined, linear system of equations, as follows:

$$\mathbf{R} \begin{Bmatrix} r_1 \\ r_2 \end{Bmatrix} = \begin{bmatrix} \pm\mathbf{1}_h & \pm\boldsymbol{x} \end{bmatrix} \begin{Bmatrix} h \\ \theta \end{Bmatrix} \qquad \Rightarrow \qquad \begin{Bmatrix} r_1 \\ r_2 \end{Bmatrix} = \mathbf{T}_a \begin{Bmatrix} h \\ \theta \end{Bmatrix} \tag{2.23}$$

with $\mathbf{R} := \begin{bmatrix} \mathbf{r}_1 & \mathbf{r}_2 \end{bmatrix}$, and $\mathbf{T}_a := (\mathbf{R}^T\mathbf{R})^{-1}\mathbf{R}^T \begin{bmatrix} \pm\mathbf{1}_h & \pm\boldsymbol{x} \end{bmatrix}$. So that, maintaining the equivalence of the related virtual works, it finally results:

$$\begin{Bmatrix} F_h \\ M_\theta \end{Bmatrix} = \mathbf{T}_a^T \begin{Bmatrix} Q_{r_1} \\ Q_{r_2} \end{Bmatrix} \qquad \Rightarrow \qquad \mathbf{H}_a^{h\theta} = \begin{bmatrix} \mathbf{H}_h & \mathbf{H}_\theta \end{bmatrix} = \mathbf{T}_a^T \mathbf{H}_a^{r_1 r_2} \mathbf{T}_a \tag{2.24}$$

It would be clearly sufficient to determine the conversion on the base of just two points, but choosing an overdetermined set $\bar{\boldsymbol{x}}$ and solving for it in the above least squares averaged sense will remove any bias related to the choice of the points, also smoothing away any, small, numerical error of the available $(\boldsymbol{r}_1, \boldsymbol{r}_2)$ modes.

Since in flight mechanics the symmetric equations of motion are written in terms of the aircraft incidence α, and pitching rate q, while in aeroelastic calculations they are in terms of the absolute motion (h, θ), after having removed any indeterminacy about the possible absolute symmetric rigid modes available, the aerodynamic transfer matrix $\mathbf{H}_a^{h\theta} = \begin{bmatrix} \mathbf{H}_h & \mathbf{H}_\theta \end{bmatrix}$ must be translated to $\mathbf{H}_a^{\alpha q} = \begin{bmatrix} \mathbf{H}_\alpha & \mathbf{H}_q \end{bmatrix}$. It must be noted that since we are referring to small perturbations, along a level rectilinear motion, the generalized forces associated to (h, θ) and (α, q) will remain the same, i.e. F_h and M_θ.

In order to convert the aeroelastic (h, θ) transfer matrices, into the ones for (α, q), a setting of the related boundary conditions must be done, so to have the very same F_h and M_θ. This is done using the following transformations:

$$\begin{Bmatrix} \alpha \\ q/V_\infty \end{Bmatrix} = \mathbf{T}^{\alpha q}_{h\theta} \begin{Bmatrix} h \\ \theta \end{Bmatrix} = \begin{bmatrix} jk/l_a & 1 \\ 0 & jk/l_a \end{bmatrix} \begin{Bmatrix} h \\ \theta \end{Bmatrix} \tag{2.25a}$$

$$\begin{Bmatrix} h \\ \theta \end{Bmatrix} = (\mathbf{T}^{\alpha q}_{h\theta})^{-1} \begin{Bmatrix} \alpha \\ q/V_\infty \end{Bmatrix} = \mathbf{T}^{h\theta}_{\alpha q} \begin{Bmatrix} \alpha \\ q/V_\infty \end{Bmatrix} = \begin{bmatrix} l_a/(jk) & -l_a^2/(jk)^2 \\ 0 & l_a/(jk) \end{bmatrix} \begin{Bmatrix} \alpha \\ q/V_\infty \end{Bmatrix} \tag{2.25b}$$

Then the following relations hold:

$$\begin{bmatrix} \mathbf{H}_h & \mathbf{H}_\theta \end{bmatrix} = \begin{bmatrix} \mathbf{H}_\alpha & \mathbf{H}_q \end{bmatrix} \mathbf{T}^{\alpha q}_{h\theta} = \begin{bmatrix} jk\,\mathbf{H}_\alpha/l_a & (\mathbf{H}_\alpha + jk\,\mathbf{H}_q/l_a) \end{bmatrix} \tag{2.26a}$$

$$\begin{bmatrix} \mathbf{H}_\alpha & \mathbf{H}_q \end{bmatrix} = \begin{bmatrix} \mathbf{H}_h & \mathbf{H}_\theta \end{bmatrix} \mathbf{T}^{h\theta}_{\alpha q} = \begin{bmatrix} l_a\mathbf{H}_h/(jk) & l_a(\mathbf{H}_\theta - \mathbf{H}_\alpha)/(jk) \end{bmatrix} \tag{2.26b}$$

which can be adopted to obtain the needed (α, q) quasi steady derivatives. Indeed:

$$\begin{bmatrix} \mathbf{H}'_h & \mathbf{H}'_\theta \end{bmatrix} = \begin{bmatrix} (\mathbf{H}_\alpha + jk\,\mathbf{H}'_\alpha)/l_a & (\mathbf{H}'_\alpha + (\mathbf{H}_q + jk\,\mathbf{H}'_q)/l_a) \end{bmatrix} \tag{2.27a}$$

$$\begin{bmatrix} \mathbf{H}''_h & \mathbf{H}''_\theta \end{bmatrix} = \begin{bmatrix} (2\mathbf{H}'_\alpha + jk\,\mathbf{H}''_\alpha)/l_a & (\mathbf{H}''_\alpha + (2\mathbf{H}'_q + jk\,\mathbf{H}''_q)/l_a) \end{bmatrix} \tag{2.27b}$$

$$\begin{bmatrix} \mathbf{H}'''_h & \mathbf{H}'''_\theta \end{bmatrix} = \begin{bmatrix} (3\mathbf{H}''_\alpha + jk\,\mathbf{H}'''_\alpha)/l_a & (\mathbf{H}'''_\alpha + (3\mathbf{H}''_q + jk\,\mathbf{H}'''_q)/l_a) \end{bmatrix} \tag{2.27c}$$

being $(\,\cdot\,)' := d(\,\cdot\,)/d(jk)$, so ending with:

$$\mathbf{H}_\alpha(0) = l_a\mathbf{H}'_h(0) = \mathbf{H}_\theta(0) \qquad \mathbf{H}_q(0) = l_a(\mathbf{H}'_\theta(0) - \mathbf{H}'_\alpha(0)) \tag{2.28a}$$

$$\mathbf{H}'_\alpha(0) = l_a\mathbf{H}''_h(0)/2 \qquad \mathbf{H}'_q(0) = l_a(\mathbf{H}''_\theta(0) - \mathbf{H}''_\alpha(0))/2 \tag{2.28b}$$

$$\mathbf{H}''_\alpha(0) = l_a\mathbf{H}'''_h(0)/3 \qquad \mathbf{H}'_q(0) = l_a(\mathbf{H}'''_\theta(0) - \mathbf{H}'''_\alpha(0))/3 \tag{2.28c}$$

with the missing $\mathbf{H}'''_\alpha$ to be calculated with a further derivative.

Antisymmetric case

It is here provided the way to transform the aeroelastic model from absolute side slip, yaw, and roll to side slip angle, yaw and roll rates. Analogously to what done previously for the symmetric case, the generalized forces associated to the frame absolute side-yaw-roll modes, whose corresponding physical side force F_y, yaw and roll moments M_ψ and M_ϕ, must be related to pure unit rigid side motion v, rigid yaw ψ and rigid roll ϕ around assigned reference axes through a given point. Once more the related directions must been chosen to follow the standard convention of the body axes and related kinematic states used in flight mechanics. Since from vibration modes calculations rigid body motions can be obtained as any combination of a pure side translation and yaw, roll rotations, whatever of the rigid body modes into v, ψ and ϕ. Naming $\boldsymbol{r}_1(\bar{\boldsymbol{x}})r_1$, $\boldsymbol{r}_2(\bar{\boldsymbol{x}})r_2$ and $\boldsymbol{r}_3(\bar{\boldsymbol{x}})r_3$ the available antisymmetric rigid body modes having shapes $\boldsymbol{r}_1(\bar{\boldsymbol{x}})$, $\boldsymbol{r}_2(\bar{\boldsymbol{x}})$ and $\boldsymbol{r}_3(\bar{\boldsymbol{x}})$, given at a set of points ≥ 3, $\bar{\boldsymbol{x}}$ typically the nodes in the case of a finite element analysis, and amplitudes r_1, r_2 and r_3. So calling $\mathbf{H}_a^{r_1 r_2 r_3}$ the partition of the available modal aerodynamic

transfer matrix, associated to r_1, r_2 and r_3, defining $\mathbf{Q}^T_{r_1 r_2 r_3} = \begin{bmatrix} Q_{r_1} & Q_{r_2} & Q_{r_3} \end{bmatrix}^T$ the related generalized forces and $\mathbf{q}^T_{r_1 r_2 r_3} = \begin{bmatrix} r_1 & r_2 & r_3 \end{bmatrix}^T$ the related generalized modal coordinates, it can be written:

$$\mathbf{Q}_a^{r_1 r_2 r_3} = \begin{Bmatrix} Q_{r_1} \\ Q_{r_2} \\ Q_{r_3} \end{Bmatrix} = \mathbf{H}_a^{r_1 r_2 r_3} \begin{Bmatrix} r_1 \\ r_2 \\ r_3 \end{Bmatrix} \tag{2.29}$$

The needed transfer matrix is:

$$\mathbf{Q}_a = \begin{Bmatrix} F_v \\ M_\psi \\ M_\phi \end{Bmatrix} = \mathbf{H}_a^{v\psi\phi} \begin{Bmatrix} v \\ \psi \\ \phi \end{Bmatrix} \tag{2.30}$$

Defining the vector $\pm\mathbf{1}_h := \begin{bmatrix} 0 & 1 & 0 \end{bmatrix}^T$, and the vectors $\pm\boldsymbol{x} := \begin{bmatrix} y & -x & 0 \end{bmatrix}^T$, and $\pm\boldsymbol{y} := \begin{bmatrix} 0 & z & -y \end{bmatrix}^T$ of the offsets with respect to an aerodynamic reference point $\bar{\boldsymbol{x}}$. The $\pm$ signs above have to be chosen so to make it consistent the imposed v, ψ and ϕ with possible different orientations of the related axes used in the structural modes calculations. Then the relation between the different representations of the antisymmetric rigid modes is recovered by writing the corresponding point wise modes transformation, followed by the solution of the related, possibly overdetermined, linear system of equations, as follows:

$$\mathbf{R} \begin{Bmatrix} r_1 \\ r_2 \\ r_3 \end{Bmatrix} = \begin{bmatrix} \pm\mathbf{1}_h & \pm\boldsymbol{x} & \pm\boldsymbol{y} \end{bmatrix} \begin{Bmatrix} v \\ \psi \\ \phi \end{Bmatrix} \qquad \Rightarrow \qquad \begin{Bmatrix} r_1 \\ r_2 \\ r_3 \end{Bmatrix} = \mathbf{T}_a \begin{Bmatrix} v \\ \psi \\ \phi \end{Bmatrix} \tag{2.31}$$

with $\mathbf{R} := \begin{bmatrix} \mathbf{r}_1 & \mathbf{r}_2 & \mathbf{r}_3 \end{bmatrix}$, and $\mathbf{T}_a := (\mathbf{R}^T\mathbf{R})^{-1}\mathbf{R}^T \begin{bmatrix} \pm\mathbf{1}_h & \pm\boldsymbol{x} & \pm\boldsymbol{y} \end{bmatrix}$. So that, maintaining the equivalence of the related virtual works, it finally results:

$$\begin{Bmatrix} F_v \\ M_\psi \\ M_\phi \end{Bmatrix} = \mathbf{T}_a^T \begin{Bmatrix} Q_{r_1} \\ Q_{r_2} \\ Q_{r_3} \end{Bmatrix} \qquad \Rightarrow \qquad \mathbf{H}_a^{v\psi\phi} = \begin{bmatrix} \mathbf{H}_v & \mathbf{H}_\psi & \mathbf{H}_\phi \end{bmatrix} = \mathbf{T}_a^T \, \mathbf{H}_a^{r_1 r_2 r_3} \, \mathbf{T}_a \tag{2.32}$$

It would be clearly sufficient to determine the transformation on the base of just three points, but choosing an overdetermined set $\bar{\boldsymbol{x}}$ and solving for it in the above least squares averaged sense will remove any bias related to the choice of the points, also smoothing away any, small, numerical error of the available $(\boldsymbol{r}_1, \boldsymbol{r}_2, \boldsymbol{r}_3)$ modes.

Since in flight mechanics the symmetric equations of motion are written in terms of the aircraft side slip angle β, yaw r, and roll p rates while in aeroelastic calculations they are in terms of the absolute motion, having removed any indeterminacy about the possible absolute symmetric rigid modes available, the aerodynamic transfer matrix $\mathbf{H}_a^{h\psi\phi} = \begin{bmatrix} \mathbf{H}_v & \mathbf{H}_\psi & \mathbf{H}_\phi \end{bmatrix}$ must be translated to $\mathbf{H}_a^{\beta rq} = \begin{bmatrix} \mathbf{H}_\beta & \mathbf{H}_r & \mathbf{H}_p \end{bmatrix}$.

As for the symmetric case, in order to convert the aeroelastic (v, ψ, ϕ) transfer matrices, into the ones for (β, r, p), a setting of the related boundary conditions must be done, so to

have the very same F_y, M_ψ and M_ϕ. This is done using the following transformation:

$$\begin{Bmatrix} \beta \\ r/V_\infty \\ p/V_\infty \end{Bmatrix} = \mathbf{T}^{\beta rp}_{v\psi\phi} \begin{Bmatrix} v \\ \psi \\ \phi \end{Bmatrix} = \begin{bmatrix} jk/l_a & -1 & 0 \\ 0 & jk/l_a & 0 \\ 0 & 0 & jk/l_a \end{bmatrix} \begin{Bmatrix} v \\ \psi \\ \phi \end{Bmatrix} \tag{2.33}$$

Then the following relation hold:

$$\begin{aligned} \begin{bmatrix} \mathbf{H}_v & \mathbf{H}_\psi & \mathbf{H}_\phi \end{bmatrix} &= \begin{bmatrix} \mathbf{H}_\beta & \mathbf{H}_r & \mathbf{H}_p \end{bmatrix} \mathbf{T}^{\beta rp}_{v\psi\phi} \\ &= \begin{bmatrix} jk\,\mathbf{H}_\beta/l_a & (-\mathbf{H}_\beta + jk\,\mathbf{H}_r/l_a) & jk\,\mathbf{H}_p/l_a \end{bmatrix} \end{aligned} \tag{2.34}$$

which can be adopted to obtain the needed (β, r, p) quasi steady derivatives, given by the following staggered recursions:

$$\mathbf{H}^{(i)}_\beta(0) = l_a \mathbf{H}^{(i+1)}_v(0)/(i+1) \tag{2.35a}$$

$$\mathbf{H}^{(i)}_r(0) = l_a (\mathbf{H}^{(i+1)}_\psi(0) + \mathbf{H}^{(i+1)}_\beta(0))/(i+1) \tag{2.35b}$$

$$\mathbf{H}^{(i)}_p(0) = l_a \mathbf{H}^{(i+1)}_\phi(0)/(i+1) \tag{2.35c}$$

It is remarked, signs apart, the complete analogy of the results for (h, θ) to (α, q) with those of (v, ψ, ϕ) to (β, r, p), along with the similarity of the roll ϕ with pure plunge h and/or side slip v.

2.3 Aeroelastic analysis

Stability and response analyses of aeroelastic systems can be based either on a frequency domain formulation, here referred to as classic approach, or on the so called modern approach, i.e. using a Linear Time Invariant (LTI) state space formulations [159, 160]. The classic approach stands on well established models of harmonic aerodynamic transfer matrices related to motions and gusts, also known as Generalized Aerodynamic Force (GAF) matrices, usually determined at a finite set of Mach numbers and frequencies, which are afterward causally interpolated[3] and expanded to obtain any value of interest [161, 162]. It naturally leads to response calculations in the frequency domain, which are subsequently inverse transformed to the time domain, while, because of the harmonic only knowledge of GAFs, flutter analyses require specialized numerical techniques [150–152, 164]. The modern approach can instead adopt well developed, efficient and widely available, solution tools for LTI systems. Both of them are capable of treating aeroservoelastic systems, but only the modern approach can, fully and straightforwardly, exploit powerful, state of the art Multi Input Multi Output (MIMO) design techniques for possible active controls.

[3] A causal interpolation [161–163] of a tabulated transfer matrix $\mathbf{H}(\omega)$ is an interpolation scheme capable of generating new points of $\mathbf{H}(\omega)$ in such a way that its inverse Fourier transform provides an impulse response matrix $\mathbf{h}(t)$ which is identically null for $t < 0$.

2.3.1 Flutter

Flutter is a typical dynamic instability phenomenon in fluid structural interaction systems. High fidelity computational aeroelasticity has been successfully employed in the prediction of flutter onset, mainly focusing on critical conditions in the flight envelope at which flutter onset is known to be sensitive to flow field nonlinearity. Several flight regimes in which nonlinearity must be taken into account are the transonic range and at high angle of attack. The growing use of higher fidelity tools at such critical points has allowed designers to gain greater confidence earlier in a design cycle by providing insight into the sensitivity of a design to nonlinear effects. This has resulted in cost savings by reducing the changes that would otherwise be required as a result of flight test failures. Nonlinear flutter analysis with structural nonlinearities may be performed through a tightly coupled aeroelastic analysis by using a time-domain unsteady aerodynamic computation.

However, despite the success of high fidelity CAE tools, flutter analyses carried out with the study of the stability properties of the aeroelastic system linearized about a reference condition maintain a core position in the computation of the aircraft flutter clearance. Indeed, the assumption of linearity (locally at least) of the aeroelastic system is crucial to reduce the computational costs, allowing a rapid assessment of the flutter onset of an aircraft over a broad part of the flight envelope.

In transonic flow regime aerodynamic nonlinearities grow more important, but, if the local angle of attack is sufficiently small, the aerodynamic forces and shock motion behave linearly with respect to the angle of attack and, furthermore, this range of linearity increases as the frequency of the angle of attack motion increases [146]. Hence, the assumption of local linearity can be applied even in transonic conditions, allowing the use of linear Reduced Order Models (ROMs) of the high-fidelity aerodynamic subsystem as the Generalized Aerodynamic Forces (GAF).

Linear flutter analysis concerns the study of the system eigenvalues. In particular, a flutter occurs when the damping of a structural eigenvalue becomes null under the interaction with the surrounding fluid.

Hence, considering the equation governing the dynamics of the motion, Eq. (2.3), in the absence of external excitation besides aerodynamic forces generated by structural vibration only:

$$\underbrace{\left(s^2\mathbf{M} + s\mathbf{C} + \mathbf{K} - q_\infty \mathbf{H}_{am}(p, M_\infty)\right)}_{\boldsymbol{\mathcal{Z}}(s,M_\infty)} \mathbf{q} = 0 \tag{2.36}$$

flutter appears at the flight conditions and the reduced frequency for which the equations coefficient matrix $\boldsymbol{\mathcal{Z}}(s, M_\infty)$ is singular, i.e. the determinant is null. Different techniques have been devised to obtain the solution to this nonlinear eigenvalue problem. The main difficulty is that the aerodynamic matrix $\mathbf{H}_{am}$ is a complicated transcendental function of the frequency of oscillations.

The V-g method

The V-g method, known also as American k flutter method, solves the transcendental eigenvalue problem considering harmonic oscillations, i.e. using just the imaginary part jk

of the complex reduced frequency $p = sl_a/V_\infty = h + jk$ with $k = \omega b/V_\infty$, assuming the absence of the structural damping, $\mathbf{C} = 0$, and introducing a fictitious structural damping proportional to the generalized stiffness matrix so that the governing equation in frequency domain:

$$\left(-k^2 \frac{V_\infty^2}{l_a^2}\mathbf{M} + (1+jg)\mathbf{K} - q_\infty \mathbf{H}_{am}(k, M_\infty)\right)\mathbf{q} = 0 \tag{2.37}$$

becomes an eigenvalue problem that can be rewritten as:

$$\left(\mathbf{K}^{-1}\mathbf{A} - \lambda\mathbf{I}\right)\mathbf{q} = 0 \tag{2.38}$$

with:

$$\mathbf{A}(k, M_\infty) := \left(\mathbf{M} + \frac{\rho l_a^2}{2k^2}\mathbf{H}_{am}(k, M_\infty)\right) \tag{2.39a}$$

$$\lambda(k) := \frac{1+jg}{k^2}\frac{l_a^2}{V_\infty^2} \tag{2.39b}$$

The method does not allow rigid-body modes (i.e. a singular stiffness matrix $\mathbf{K}$) nor a null reduced frequency $k = 0$. In order to take into account the rigid modes, the problem may be partitioned between rigid-body and elastic modes and be rewritten as:

$$\left(\begin{bmatrix}\mathbf{A}_{rr} & \mathbf{A}_{re}\\ \mathbf{A}_{er} & \mathbf{A}_{ee}\end{bmatrix} - \lambda\begin{bmatrix}\mathbf{0} & \mathbf{0}\\ \mathbf{0} & \mathbf{K}_e\end{bmatrix}\right)\begin{Bmatrix}\mathbf{q}_r\\ \mathbf{q}_e\end{Bmatrix} = 0 \tag{2.40}$$

and obtaining the rigid modes as $\mathbf{q}_r = -\mathbf{A}_{rr}^{-1}\mathbf{A}_{re}\mathbf{q}_e$, the problem becomes:

$$\left(\mathbf{K}_e^{-1}(\mathbf{A}_{ee} - \mathbf{A}_{er}\mathbf{A}_{rr}^{-1}\mathbf{A}_{re}) - \lambda\mathbf{I}\right)\mathbf{q}_e = 0 \tag{2.41}$$

Then, given a flight condition with air density ρ, the eigenvalues λ and the related quantities $\omega = 1/\sqrt{\mathrm{Re}(\lambda)}$, $V = \omega l_a/k$, and $g = \mathrm{Im}(\lambda)/\mathrm{Re}(\lambda)$, are calculated for a set of reduced frequencies k. Hence the $V - g - \omega$ diagrams may be constructed, allowing to determine the flutter airspeed V_F, i.e. the lowest V at which a g branch becomes positive, together with the related flutter frequency ω_F and complex flutter mode $\mathbf{q}_F$, and determine the divergence airspeed V_D, i.e. the lowest V at which an ω branch and the corresponding g branch approach zero when $k \to 0$.

The British k Method

The k method operate directly in the Laplace domain, but still using harmonic aerodynamic, and assuming a fictitious damping proportional to structural stiffness, so that the eigenvalue problem becomes:

$$\left(\mathbf{M}^{-1}\mathbf{A} - \lambda\mathbf{I}\right)\mathbf{q} = 0 \tag{2.42}$$

where, writing explicitly the airspeed dependence, it is:

$$\mathbf{A}(k, M_\infty) := \left((\mathbf{I} + j2\boldsymbol{\zeta})\mathbf{K} - \frac{1}{2}\rho V_\infty^2 \mathbf{H}_{am}(k, M_\infty)\right) \tag{2.43a}$$

$$\lambda(p) := s^2 = \frac{p^2 V^2}{l_a^2} \tag{2.43b}$$

which allows the use of rigid-body modes and it holds also for $k = 0$. Given a set of reduced frequencies k, the solution at desired airspeed and density is represented by the eigenvalues $\lambda = p^2 V_\infty^2 / l_a^2$ satisfying $k = \mathrm{Im}(p)$. Calculating the related $\omega = k V_\infty / l_a$ and $\gamma = h/k = \mathrm{Re}(p)/k$, the diagrams $V - \gamma - \omega$ for a fixed air density ρ, or $\rho - \gamma - \omega$ for a fixed airspeed V, may be used to perform structural parametric studies.

The p-k Method

The p-k method, instead of solving an eigenvalue problem, uses an iterative numerical algorithm to find the roots, $p = \gamma k + jk$, to the problem

$$\det(\mathbf{A}(p)) = 0 \tag{2.44}$$

being:

$$\mathbf{A}(p) := p^2 \frac{V_\infty^2}{l_a^2}\mathbf{M} + p\frac{V_\infty}{l_a}\mathbf{C} + \mathbf{K} - q_\infty \mathbf{H}_{am}(p, M_\infty) \tag{2.45}$$

The aerodynamic transfer matrix is approximated by evaluating it on the restricted domain $p \approx jk$, i.e. the imaginary part of the Laplace domain: $\mathbf{H}_{am}(p, M_\infty) \approx \mathbf{H}_{am}(k, M_\infty)$. This is essentially due to the fact that typically the unsteady aerodynamic codes operates in frequency domain instead of Laplace domain. However this approximation is weaker as the evaluated eigenvalues are more distant from the imaginary axis. Therefore the decay rate computed by the p-k method is only valid near the critical flutter speed.

Alternatively, in order to better represent non-harmonic aerodynamics, the transfer matrix is approximated as $\mathbf{H}_{am}(p, M_\infty) \approx \mathbf{H}_{am}(k, M_\infty) + j\frac{g}{k}\mathbf{H}_{am}(k, M_\infty)$, where the term $\mathbf{H}_{am}(k, M_\infty)/k$ is not singular for $k \to 0$, because generally the aerodynamic transfer matrix presents a quadratic trend for the real part and a linear trend for the imaginary part for values of the reduced frequency k in the neighborhood of the origin.

The method yields realistic damping and frequency variations without the need for assumption about the structural damping, however small steps may be required in the iterative process to ensure the convergence for all the roots, i.e. an aeroelastic root per each modal coordinate taken into account, being aerodynamic-lag roots not considered. The p-k method can be also used for finding roots in a closed-loop aeroservoelastic stability analysis, when the aeroelastic model is coupled to a control system, however the search is not robust because there are more roots than modes.

The g Method

The g method assumes, based on analytic continuation, that:

$$\mathbf{H}_{am}(p, M_\infty) \approx \mathbf{H}_{am}(k, M_\infty) + g\mathbf{H}'_{am}(k, M_\infty) \tag{2.46}$$

where it is defined $g = \gamma k$ such that $p = g + jk$, so giving the following frequency-domain equation in the g term:

$$\left(g^2\widehat{\mathbf{M}} + g\widehat{\mathbf{C}}(k, M_\infty) + \widehat{\mathbf{K}}(k, M_\infty)\right)\mathbf{q} = 0 \tag{2.47}$$

with:

$$\widehat{\mathbf{M}} := \left(\frac{V_\infty}{l_a}\right)^2 \mathbf{M} \tag{2.48a}$$

$$\widehat{\mathbf{C}} := 2jk\left(\frac{V_\infty}{l_a}\right)^2 \mathbf{M} + \frac{V_\infty}{l_a}\mathbf{C} - q_\infty \mathbf{H}'_{am}(k, M_\infty) \tag{2.48b}$$

$$\widehat{\mathbf{K}} := -k^2\left(\frac{V_\infty}{l_a}\right)^2 \mathbf{M} + jk\frac{V_\infty}{l_a}\mathbf{C} + \mathbf{K} - q_\infty \mathbf{H}_{am}(k, M_\infty) \tag{2.48c}$$

It is noted that the aerodynamic transfer matrix approximation is the same of the both introduced in the p-k method when $g = 0$, and agrees with the aerodynamic non-harmonic correction of the p-k method when $\mathbf{H}_{am}(k, M_\infty)$ is a linear function of jk, that is in the case of quasi-steady aerodynamics. Equation (2.47) can be rewritten in a state space form as:

$$(\mathbf{A} - g\mathbf{I})\,\mathbf{x} = 0 \tag{2.49}$$

with:

$$\mathbf{A} := \begin{bmatrix} \mathbf{0} & \mathbf{I} \\ -\widehat{\mathbf{M}}^{-1}\widehat{\mathbf{C}} & -\widehat{\mathbf{M}}^{-1}\widehat{\mathbf{K}} \end{bmatrix} \qquad \text{and} \qquad \mathbf{x} := \begin{Bmatrix} \mathbf{q} \\ g\mathbf{q} \end{Bmatrix} \tag{2.50}$$

Solutions to the flutter analysis exist when g is a real eigenvalue, i.e. it must be satisfied the assumption $\mathrm{Im}(g) = 0$. Therefore, solving the eigenvalue problem for a set of reduced frequencies, sweeping from zero to a given maximum value, it is searched the reduced frequency k for which $\mathrm{Im}(g) = 0$, so that the associate $\mathrm{Re}(g)$ value are the actual solutions for the given k, and moreover it is $\gamma = g/k$ for $k \neq 0$, and $\gamma = (g l_a)/(2\ln(2)\, V_\infty)$. Conversely to the p-k methods, the g method is capable in detecting extra roots due to unsteady aerodynamic lag. Moreover it facilitates an efficient Predictor-Corrector eigenvalue tracking scheme and it yields robust aeroservoelastic analysis when the aeroelastic model is augmented with a control system.

Stability via Finite-State approximation

The linearized equation of aeroelasticity can be reduced in a state-space form using a rational fraction approximation, as it has been shown in the present chapter (Eq. (2.8)). The free aeroelastic response is given by the following descriptor form:

$$\mathbf{E}_{ae}\dot{\mathbf{x}}_{ae}(t) = \mathbf{A}_{ae}\mathbf{x}_{ae}(t) \tag{2.51}$$

where $\mathbf{x}_{ae}$ is the state-space vector including the structural displacements and dynamics and the aerodynamic states, and $\mathbf{A}_{ae}$) is the aeroelastic state-space matrix as obtained by the finite-state modeling, explicitly depending on the airspeed V_∞ and the air density ρ_∞ and implicitly dependent by the Mach number M_∞.

As well known by the the theory of the linear ODE, the stability of such a dynamical system can be completely described studying the corresponding eigenproblem, here written in both a generalized form and standard form:

$$\left(\mathbf{A}_{ae} - \lambda \mathbf{E}_{ae}\right) \mathbf{x}_{ae} = 0 \qquad \text{generalized} \tag{2.52a}$$

$$\left(\mathbf{E}_{ae}^{-1}\mathbf{A}_{ae} - \lambda \mathbf{I}\right) \mathbf{x}_{ae} = 0 \qquad \text{standard} \tag{2.52b}$$

Hence the state space framework establish a very flexible and robust framework for aeroelastic and aeroservoelastic stability analysis, allowing the use of modern MIMO control system techniques.

The μ Method

The μ-based methods aim to determine the flutter airspeed for aeroelastic systems with deterministic uncertainty and variation of aeroelastic models, by performing a robust flutter analysis using the so-called μ-analysis.

The μ method introduces a structured singular value (SSV) μ into the aeroelastic system, which is thus parameterized at a nominal dynamic pressure with a perturbation to the dynamic pressure. However this does not guarantee to compute match-point flutter speeds, because the robust analysis computes a worst-case perturbation to a single parameter, the dynamic pressure, whereas the model is function of both dynamic pressure and airspeed. This implies that the model needs to consider multiple perturbations, or uncertainties, that are nonlinearly related. An alternative μ formulation is thus devised where nonlinear uncertainties that affect coupled parameters in the equation of motion are included through feedback loops that are coupled through the feedthrough matrix of the plant. The formulation expresses the dynamic pressure as a polynomial function of the airspeed, so that the flight condition is described entirely through a single-parameter dependency. This results in match-point flutter speeds solutions from the μ-analysis.

The frequency domain aerodynamic transfer matrix may be approximated using a finite-state approximation or used directly as it is, thus leading to the μ-k formulation. In this last case the flight condition is treated in a traditional manner, i.e. the perturbation to dynamic pressure is excluded, to facilitate the robust flutter analysis. As a result, the robust analysis can be performed using existing numerical models, resembling a p-k or g-method flutter analysis, and inherently produces match-point flutter solutions, and allows for detailed aerodynamic uncertainty descriptions.

The μ-p method is a generalization of the μ-k method to the Laplace domain to allow for robust analysis at any flight condition, so extending the standard linear flutter analysis to take deterministic uncertainty and variation into account.

Therefore the concept of robust flutter analysis is introduced by considering the Laplace-domain equations of motion with uncertainty and/or variation:

$$\mathbf{Z}(p,\delta)\mathbf{q} = \left(p^2 \frac{V_\infty^2}{l_a^2}\mathbf{M}(\delta) + p\frac{V_\infty}{l_a}\mathbf{C}(\delta) + \mathbf{K}(\delta) - q_\infty \mathbf{H}_{am}(p, M_\infty, \delta)\right)\mathbf{q} = 0 \tag{2.53}$$

being $\delta \in \mathcal{D}$ normalized uncertainty parameters and $\mathcal{D} = \{\delta : \|\delta\|_\infty \leq 1\}$.

In case of linear perturbations the uncertain parameters are assembled in a block-structured uncertainty matrix $\mathbf{\Delta} \in \mathcal{B}$, with $\mathcal{B} = \{\mathbf{\Delta} : \mathbf{\Delta}$ structured and $\bar{\sigma}(\mathbf{\Delta}) \leq 1\}$ and $\bar{\sigma}$ being the maximum singular value. Hence the robust flutter equation is obtained through the uncertainty feedback form:

$$(\mathbf{I} - \mathbf{P}(p)\mathbf{\Delta})\mathbf{z} = 0 \tag{2.54}$$

with:

$$\mathbf{P}(p) := -\mathbf{W}(p)^T \mathbf{Z}_0^{-1}(p)\mathbf{V}(p) \tag{2.55a}$$

$$\mathbf{Z}_0(p) := p^2 \frac{V_\infty^2}{l_a^2}\mathbf{M} + p\frac{V_\infty}{l_a}\mathbf{C} + \mathbf{K} - q_\infty \mathbf{H}_{am}(p, M_\infty) \tag{2.55b}$$

where $\mathbf{W}$ and $\mathbf{V}$ are scaling matrices that determine the magnitude and influence of the uncertainty.

Then a set of feasible eigenvalues is computed using the μ analysis, allowing robust analysis of the flutter speed, and also determining subcritical properties such as the frequency and damping of a particular mode. The robust flutter speed represents the worst-case flight condition with respect to potential modeling errors.

2.3.2 Gust response

Numerical linearized models can be effectively applied in order to compute accurately classical aeroelastic phenomena. Besides the flutter boundary prediction, even the gust response calculation can exploit the use of linearized methods in the frequency domain [165]. The frequency-domain formulation of the aeroelastic equation of motion in generalized coordinates is used in these procedures to calculate discrete transient gust response, via Fourier and inverse Fourier transforms (or Laplace and inverse Laplace transforms).

The main advantage of the frequency domain approach is that it is based on the use of aerodynamic transfer matrices, which can be generated by common, well established, panel-method aerodynamics (e.g. the Doublet-Lattice method or the constant pressure panel method) which are implemented also in commercial codes like Nastran [166] and ZAERO [167]. The gust velocity input is hence expressed as a combination of harmonic excitations of various reduced frequencies, and the gust-generalized aerodynamic forces are computed using the aerodynamic transfer matrix at these reduced frequencies.

Adopting the Taylor's hypothesis, also known as frozen gust assumption, i.e. the gust profile (random) spatial distribution does not significantly change during the time interval for which the aircraft is penetrating the gust field (assumption which holds for sufficiently high aircraft speed), the gust time history, deterministic or stochastic, is expressed in the form:

$$v_g(x, t) = v_g(V_\infty t - x) \tag{2.56}$$

being v_g the gust vertical velocity distribution encountered by the aircraft having a fixed reference frame with coordinate axis x opposite to its flight direction. In the Laplace domain it results:

$$v_g(x, s) = v_g(s)\, \mathrm{e}^{-j\omega \frac{x}{V_\infty}} \tag{2.57}$$

with $v_g(s)$ being the Laplace transform of the gust profile: $v_g(s) = \int_{0^-}^{\infty} v_g(t) e^{-st}\, dt$.

Hence the frequency response of the aeroelastic state vector is obtained from the aeroelastic governing equation (2.3), and then, if needed, the time history is calculated via inverse Laplace transform.

Following this classic frequency domain approach, the variance matrix of a generic output $\mathbf{y}$ (e.g. a dynamic load) induced on the structure by a stochastic gust having a Power Spectral Density (PSD) function[4] $\mathbf{\Phi}_{gg}(\omega)$, comes from the standard formula:

$$\mathbf{\Sigma}_{yy} = \frac{1}{2\pi} \int_{-\infty}^{\infty} \mathbf{\Phi}_{yy}(\omega) d\omega \tag{2.60}$$

with:

$$\Phi_{yy}(\omega) = \mathbf{H}^{*}_{aeg}(\omega)\, \mathbf{\Phi}_{gg}(\omega)\, \mathbf{H}^{T}_{aeg}(\omega) \tag{2.61}$$

and where $\mathbf{H}_{aeg}$ is the aeroelastic transfer matrix from the gust input to the output y.

Alternatively to the use of the Fourier inverse transformation, gust responses in the time domain may be calculated by expressing the aerodynamic transfer matrix as a state space model, making use of rational function approximation methods [163, 168, 169]. The state-space model can be directly augmented to the aeroelastic system in state-space formulation (Eq. (2.8) or Eq. (2.11)) for rapid aeroelastic response analysis trough a direct integration in time. From the determined generalized aerodynamic forces, the structural sectional loads required for the aircraft design may be then recovered through a summation-of-forces approach (i.e. by summation of the aerodynamic forces with the inertial loads) or a mode-displacement approach (i.e. calculating the elastic forces from the elastic deformations using the stiffness matrix). When stochastic gusts are considered and only variance quantities of the output are demanded, Lyapunov and generalized Sylvester equations [104, 170] may be straightforwardly used, as it will be presented in section 4.2.2.

The accurate prediction of dynamic gust loads is very important to ensure structural integrity. Hence recent research aims at exploiting the use of high-fidelity CFD tools for dynamic gust-response analysis, introducing prescribed vertical gust velocities with the Field Velocity Method (FVM) [171] or the Split Velocity Method (SVM) [172], and relying on the use of reduced order modeling techniques.

Concerning model reduction, the representation of unsteady aerodynamic flow fields in terms of global aerodynamic modes has proven to be a useful method for reducing the size of the aerodynamic model over those representations that use local variables at discrete grid points in the flow field. Eigenmodes and proper orthogonal decomposition modes [173] have been used for this purpose with good effect. Alternatively to the eigenmodes of the aerodynamic subsystem, information on the eigenspectrum of the linearized coupled aeroelastic system may be used, projecting then the full order nonlinear aeroelastic model through a Taylor series expansion onto a small basis of eigenvectors which is

[4] It is reminded that the power spectral density function is given by:

$$\mathbf{\Phi}_{gg}(\omega) = \frac{1}{\pi} \int_{-\infty}^{\infty} \phi(\tau)\, e^{-j\omega\tau} d\tau \tag{2.58}$$

being $\phi(\tau)$ the correlation function defined as:

$$\phi_{gg}(\tau) = \lim_{T\to\infty} \frac{1}{2T} \int_{-T}^{T} v_g(x,t)\, v_g(x, t-\tau)\, dt \tag{2.59}$$

capable of representing the full order model dynamics [174]. In this case the gust term in the reduced model can be introduced in a manner consistent with standard synthetic gust definitions, allowing a systematic investigation of the influence of a large number of gusts without regenerating the reduced model. Time-domain aerodynamic gust responses may be also obtained using system identification methods [173, 175]. In this case the aerodynamic models are obtained from a set of input-output training data of CFD responses to random gust excitations.

A different approach computes the generalized gust forces $\mathbf{Q}_{ag}(t)$ due to arbitrary gust profiles via convolution with a proper aerodynamic indicial function, obtained using a rigid sharp-edge gust response $\widehat{\mathbf{Q}}_{ag}(t)$ (which for a incompressible two-dimensional flow is nothing else that the Küssner function [176]) of the CFD aerodynamic model [175, 177]. Hence using the Duhamel's integral concept it is:

$$\mathbf{Q}_{ag}(t) = \dot{v}_g(0)\,\widehat{\mathbf{Q}}_{ag}(t) + \int_0^t \frac{\partial v_g(\tau)}{\partial \tau}\,\widehat{\mathbf{Q}}_{ag}(t-\tau)\,d\tau = \int_0^t v_g(\tau)\,\frac{\partial \widehat{\mathbf{Q}}_{ag}(t-\tau)}{\partial \tau}\,d\tau \tag{2.62}$$

having v_g a constant value for $t > x/V_\infty$ and a null value elsewhere. The indicial sharp-edge gust response may be also expressed in the Laplace domain with exponential terms [178] of the form $s\mathbf{A}_i \mathrm{e}^{-\beta_i t}$ and $\mathbf{A}_j \mathrm{e}^{-\beta_j t}$, or represented in a state space form using rational function approximations [179], with the coefficients involving the indicial function determined numerically via a fitting procedure. The aeroelastic gust responses are then computed applying a linear aeroelastic feedback loop (Eq. (2.8)). The method is highly computationally efficient, as only one relatively short computational fluid dynamics run is required for the computation of the sharp-edge gust response, after which responses to arbitrary gust profiles can be simulated instantly, compared with the time computation of the full CFD simulations.

A recent approach [180] develops an auto-regressive moving-average (ARMA) reduced order gust model using a gust with a Gaussian profile. Then, POD bases are combined with the ARMA modeling technique to predict the time varying pressure coefficient increment distribution due to a novel gust profile.

2.3.3 Limit Cycle Oscillations (LCOs)

In a nonlinear differential equation, a bifurcation occurs when a small smooth change made to a set of parameter values (the bifurcation parameters) of the system causes a sudden qualitative or topological change in its solution behavior. Limit cycle oscillation (LCO) is one of the simplest dynamic bifurcation phenomenon encountered in the analysis of nonlinear dynamic systems. Among the other bifurcations there are higher harmonic and subharmonic resonances, jump-resonances, entrainment, beating, and period doubling.

In aeroelasticity LCOs can be due to either nonlinear aerodynamics effects (e.g. transonic shock waves and shock-induced trailing edge separation) or structural nonlinearities (e.g. concentrated, as control surface free-play, hinges friction and hysteresis, or distributed, as material or geometric nonlinearity).

An LCO is a closed trajectory in the phase space which can occurs beyond a linear flutter onset, i.e. Hopf bifurcation point, of the dynamic system of interest. Considering an

autonomous nonlinear dynamic system governed by the differential equation

$$\dot{\mathbf{x}} = \mathbf{R}(\mathbf{x}, \beta) \tag{2.63}$$

being $\mathbf{R}(\mathbf{x}) : \mathbb{R}^N \rightarrow \mathbb{R}^N$ a nonlinear function and β the bifurcation parameters, the Hopf bifurcation is a local bifurcation point in which the dynamical system loses stability (i.e. a pair of complex conjugate eigenvalues of the Jacobian matrix of the linearized system about the point has a vanishing real part, while the real component of the other eigenvalues is negative[5]).

The nonlinear system presents a set of equilibrium solutions $\widehat{\mathbf{x}}$ satisfying the relation $\mathbf{R}(\widehat{\mathbf{x}}, \beta) = 0$. Hence the linearized (local) stability study of an equilibrium solution consists in the analysis of the set of eigenvalues λ of the system Jacobian matrix, $\mathbf{J}$, evaluated at the equilibrium point:

$$\mathbf{J}(\mathbf{x}, \beta)|_{\widehat{\mathbf{x}}} := \left.\frac{\partial \mathbf{R}}{\partial \mathbf{x}}\right|_{\widehat{\mathbf{x}}} \tag{2.64}$$

A pair $(\widehat{\mathbf{x}}, \widehat{\beta})$ is an equilibrium point from which it will emerge a branch of unsteady solutions with limit-cycle behavior if the Jacobian matrix has a pair of purely imaginary eigenvalues, with no other eigenvalue having vanishing or positive real part. For values $\beta > \widehat{\beta}$ there is at least one exponentially growing solution of the linearized system, which is limited (stable LCO) or increased (unstable LCO) by the nonlinearity of the original problem.

The behavior of the nonlinear system near the bifurcation point may be represented by a set of dynamical equations for the amplitudes of the unstable eigenvectors, the so called normal forms, which in case of an Hopf bifurcation, are the supercritical and the subcritical. In the former the nonlinearities are saturating, a constant equilibrium point solution is unstable and a new, stable solution develops whose trajectory in the phase space is the limit cycle. In the latter the nonlinearities are destabilizing, a constant equilibrium point solution is unstable and also unstable limit cycles develop.

The bifurcation point can be tracked through the examination of all the eigenvalues of the Jacobian matrix $\mathbf{J}$ with the varying parameter β. Although linear techniques can be used to predict the LCO frequency, they cannot consistently predict where within the flight envelope the onset of the oscillation will occur. An LCO response may be obtained through a direct numerical integration of the full order high fidelity system, or by exploring approximation techniques, such as the harmonic balance method, which allow small computational costs, otherwise by enforcing a periodic solution collocating the periodic response in the time domain. This last approach is less expensive, from a computational point of view, than a direct integration but it requires a good initial guess of the LCO solution of interest.

[5]It is noted that the presence of a pair of purely imaginary eigenvalues implies that a Hopf bifurcation can only occur in systems of dimension two or higher.

Chapter 3

Linear Model Order Reduction

Research efforts in model order reduction of unsteady CFD models for aeroelasticity were first directed to searching an equivalent aerodynamic analogy of the dynamic modes used in the field of finite element methods for structural models. Thus aerodynamic modes obtained from eigenanalyis were used in a projection-based framework in order to find aerodynamic ROMs. Research on minimum state aerodynamic models has been performed using global eigenmodes and Singular Value Decomposition (SVD) of a linearized aerodynamic system, leading to aerodynamic modal representations [181–185]. Static corrections were included in order to compensate for the truncation errors in the dynamic behavior arising from the lower order of modal bases used.

Successive research in order reduction methods for CFD-based aeroelasticity were directed in the use of methods borrowed and adapted from the field of nonlinear systems dynamics. A number of researchers have used the Proper Orthogonal Decomposition (POD) technique [94, 186–195] and Karhunen-Loève expansions [124] to determine and model coherent structures in turbulent flow fields. The POD-based methods have their origin in the area of turbulent flow research where they were used to identify reduced order mechanisms which would capture the behavior of high dimensional flow models. Using this approach, a series of "snapshots" of experimental or computational data, at discrete instants in time [195] or in the frequency domain [196–198], are used to form a small eigenvalue problem that is solved to determine a set of optimal basis functions for representing the aerodynamic flow field. Various variants of POD may be found, such as the balanced POD [128, 129], which try to overcome the drawback of balanced truncation, which is unfeasible for very large systems, by approximating it from snapshots of linearized and adjoint simulations. Eigensystem Realization Algorithm (ERA) [199] is used when adjoint information is not available, such us for experimental snapshots data.

In this thesis both a projection-based model order reduction technique as well as an improved identification based method have been investigated for the reduction of the linearized aerodynamic subsystem. The projection-based aerodynamic model order reduction procedure, presented in section 3.1, consists in transforming the system so to obtain a decoupled slow-fast frequency model, and projecting it onto a double (Petrov-Galërkin projection) or a single (Bubnov-Galërkin projection) Schur subspace. The projected system is afterwards residualized, where the residualization is applied to the state residual, and a final balanced reduction is carried out to further reduce the complexity of the system. In

section 3.2 an identification method based on an improved Rational Matrix Fraction Approximation (RMFA) is developed, where a stable finite state space system is identified starting from the harmonic aerodynamic transfer matrix and carried out by a balanced reduction followed by a refitting process. A comparison against the Schur-based projection method is proposed with some examples. The linear ROMs approaches presented will be just a notationally specific applications of techniques and methods applicable to any asymptotically stable linear system. As a further method to decrease the complexity of computational aeroelastic simulations for gust responses, a novel method for gust modeling by using spatially fixed shape functions, named gust modes, is introduced in section 4.

3.1 Model order reduction by projection onto Schur subspaces

3.1.1 Petrov-Galërkin projection

A generic linear time invariant (LTI) system in descriptor form in the s frequency domain is given by:

$$\begin{aligned} s\mathbf{E}\mathbf{x} &= \mathbf{A}\mathbf{x} + \mathbf{B}\mathbf{u} \\ \mathbf{y} &= \mathbf{C}\mathbf{x} + \mathbf{D}\mathbf{u} \end{aligned} \tag{3.1}$$

It should be noticed that the choice of the frequency domain has been taken just for sake of brevity and simplicity, its translation to the time domain is done with the usual substitution of $s^i(.)$ with $(.)^{(i)}$, the exponent $^{(i)}$ standing for the i-th time derivatives of whatever$(.)$.

Our aim is that of reducing, either by truncation or residualization, the order of our model by using a fairly limited subspace associated to the lowest frequencies of the systems, as we assume that such a range is the one mostly excited by the applied boundary conditions. Even we will use left/right Schur subspaces as our reduction way, any other base more or less covering the very same subspaces will do it. So they can be obtained through Arnoldi [97], Lanczos [96], snapshots [94] and Principal Component Analyses (PCA) [125–127], Principal Orthogonal Decomposition (POD) [121], or Karhunen-Loève decomposition (K-L) [122–124].

Any of them can be put in the final working form needed for the model reduction as:

$$\begin{aligned} \mathbf{E}\mathbf{X}_s\mathbf{S}_x &= \mathbf{A}\mathbf{X}_s & \mathbf{X}_s^T\mathbf{X}_s &= \mathbf{I} \\ \mathbf{E}^T\mathbf{Y}_s\mathbf{S}_y &= \mathbf{A}^T\mathbf{Y}_s & \mathbf{Y}_s^T\mathbf{Y}_s &= \mathbf{I} \end{aligned} \tag{3.2}$$

with $\mathbf{S}_x$ and $\mathbf{S}_y$ being real matrices whose eigenvalues are the slowest, say l, of interest, $\mathbf{X}_s$ and $\mathbf{Y}_s$ being the related right/left subspaces. It should be remarked that order reduction is usually quite strong, to the point that it is possible to assume that l is just a very small fraction of n. The above, inverse, power iterations will not suffer for null eigenvalues, i.e. when $\mathbf{A}$ is singular, as it will be explained later. It should be noticed that a system reduction can be obtained by using only the right subspace. The implications of using either both the left/right or only the right subspace are described in the following.

On the other hand we postpone to a later section a summary of the numerical approaches to be used to determine the left/right Schur subspaces of interest we will use.

Then, assuming we have obtained the slow frequency subspaces of interest, we have now to search for the separated residual bases complementing them in such a way to span $\mathbf{A}$ and $\mathbf{E}$ completely. To such an end we will now show the construction of such a complementing spaces in a way that will decouple the slow and fast parts completely. For sake of brevity only the essential steps of the spaces construction along with the verification that they do decouple our system will be reported. Let us beginning with defining a matrix $\mathbf{X}_r$, with $\mathbf{X}_r^T\mathbf{X}_r = \mathbf{I}$, made of $(n-l)$ columns having a number of rows equal to number of the original state components n, with just a 1 in the position corresponding to the original state component chosen to complement $\mathbf{X}_s$. To have it clearer we notice that any post multiplication of a matrix by $\mathbf{X}_r$ will reduce its number of columns to that of the kept states $\mathbf{x}_s$ with the extraction of the columns corresponding to the ones in each column of $\mathbf{X}_r$. The choice of $\mathbf{X}_r$ is arbitrary but, since any possible subspace with the null eigensolutions of $\mathbf{A}$ must be wholly included in $\mathbf{X}_s$, it must satisfy the constraint of granting that $\mathbf{A}\mathbf{X}_r$ has a full column rank.

Then a similar matrix $\mathbf{Y}_r$, with $\mathbf{Y}_r^T\mathbf{Y}_r = \mathbf{I}$, must be found for the left subspace. It will be made of columns having a number of rows equal to number of the original state equations, with just a 1 in the position corresponding to the original state equation chosen to complement those defining the response in term of $\mathbf{x}_s$. To have it clearer once more, we notice that any pre multiplication of a matrix by $\mathbf{Y}_r$ will reduce its number of rows to that of the kept original state equations, with the extraction of the rows corresponding to the ones in each columns of $\mathbf{Y}_r$. The choice of $\mathbf{Y}_r$ is arbitrary, but it must satisfy the constraint of granting that $\mathbf{Y}_r^T\mathbf{A}$ has a full row rank. It should be noted that their pre-post multiplication of sparse matrices will fully preserve the sparsity of the related results and, while the simple setting $\mathbf{Y}_r = \mathbf{X}_r$ will be the simplest legitimate choice, it might be possible that the adoption of different partitioning structures can further improve the resulting sparsity.

Using the just defined matrices, this can be seen by applying the following state transformation:

$$\begin{aligned}\mathbf{x} &= \begin{bmatrix}\mathbf{X}_s & (\mathbf{I}-\mathbf{X}_s(\mathbf{Y}_s^T\mathbf{E}\mathbf{X}_s)^{-1}\mathbf{Y}_s^T\mathbf{E})\mathbf{X}_r\end{bmatrix}\begin{Bmatrix}\mathbf{x}_s\\ \mathbf{x}_f\end{Bmatrix}\\ &= \begin{bmatrix}\mathbf{X}_s & \mathbf{T}_x\mathbf{X}_r\end{bmatrix}\begin{Bmatrix}\mathbf{x}_s\\ \mathbf{x}_f\end{Bmatrix} = \begin{bmatrix}\mathbf{X}_s & \mathbf{X}_f\end{bmatrix}\begin{Bmatrix}\mathbf{x}_s\\ \mathbf{x}_f\end{Bmatrix}\end{aligned} \tag{3.3}$$

having defined $\mathbf{T}_x := \mathbf{I}-\mathbf{X}_s(\mathbf{Y}_s^T\mathbf{E}\mathbf{X}_s)^{-1}\mathbf{Y}_s^T\mathbf{E}$, and projection transformation:

$$\begin{aligned}\mathbf{P} &= \begin{bmatrix}\mathbf{Y}_s & (\mathbf{I}-\mathbf{Y}_s(\mathbf{X}_s^T\mathbf{E}^T\mathbf{Y}_s)^{-1}\mathbf{X}_s^T\mathbf{E}^T)\mathbf{Y}_r\end{bmatrix}\\ &= \begin{bmatrix}\mathbf{Y}_s & \mathbf{T}_y\mathbf{Y}_r\end{bmatrix} = \begin{bmatrix}\mathbf{Y}_s & \mathbf{Y}_f\end{bmatrix}\end{aligned} \tag{3.4}$$

having defined $\mathbf{T}_y := \mathbf{I}-\mathbf{Y}_s(\mathbf{X}_s^T\mathbf{E}^T\mathbf{Y}_s)^{-1}\mathbf{X}_s^T\mathbf{E}^T$, with $\mathbf{T}_x$ and $\mathbf{T}_y$ being non-symmetric, idempotent, so singular, $(n-l)$ *by* $(n-l)$ matrices.

It is then possible to verify that after applying to Eq. (3.1) the following change of state

and linear combination of its equations:

$$\begin{aligned}\mathbf{P}^T(s\mathbf{E}-\mathbf{A})\begin{bmatrix}\mathbf{X}_s & \mathbf{X}_f\end{bmatrix}\begin{Bmatrix}\mathbf{x}_s\\ \mathbf{x}_f\end{Bmatrix} &= \mathbf{P}^T\mathbf{B}\mathbf{u}\\ \mathbf{y} = \mathbf{C}\begin{bmatrix}\mathbf{X}_s & \mathbf{X}_f\end{bmatrix}\begin{Bmatrix}\mathbf{x}_s\\ \mathbf{x}_f\end{Bmatrix} &+ \mathbf{D}\mathbf{u}\end{aligned} \tag{3.5}$$

taking into account Eq. (3.2), the following decoupled slow-fast frequency model will be obtained:

$$\begin{aligned}s\begin{bmatrix}\mathbf{Y}_s^T\mathbf{E}\,\mathbf{X}_s & 0\\ 0 & \mathbf{Y}_f^T\mathbf{E}\,\mathbf{X}_f\end{bmatrix}\begin{Bmatrix}\mathbf{x}_s\\ \mathbf{x}_f\end{Bmatrix} &= \begin{bmatrix}\mathbf{Y}_s^T\mathbf{A}\,\mathbf{X}_s & 0\\ 0 & \mathbf{Y}_f^T\mathbf{A}\mathbf{X}_f\end{bmatrix}\begin{Bmatrix}\mathbf{x}_s\\ \mathbf{x}_f\end{Bmatrix} + \begin{bmatrix}\mathbf{Y}_s^T\mathbf{B}\\ \mathbf{Y}_f^T\mathbf{B}\end{bmatrix}\mathbf{u}\\ \mathbf{y} &= \mathbf{C}\mathbf{X}_s\mathbf{x}_s + \mathbf{C}\mathbf{X}_f\mathbf{x}_f + \mathbf{D}\mathbf{u}\end{aligned} \tag{3.6}$$

which is eventually synthesized in the following:

$$\begin{aligned}s\begin{bmatrix}\mathbf{E}_s & \mathbf{0}\\ \mathbf{0} & \mathbf{E}_f\end{bmatrix}\begin{Bmatrix}\mathbf{x}_s\\ \mathbf{x}_f\end{Bmatrix} &= \begin{bmatrix}\mathbf{A}_s & \mathbf{0}\\ \mathbf{0} & \mathbf{A}_f\end{bmatrix}\begin{Bmatrix}\mathbf{x}_s\\ \mathbf{x}_f\end{Bmatrix} + \begin{bmatrix}\mathbf{B}_s\\ \mathbf{B}_f\end{bmatrix}\mathbf{u}\\ \mathbf{y} &= \mathbf{C}_s\mathbf{x}_l + \mathbf{C}_f\mathbf{x}_f + \mathbf{D}\mathbf{u}\end{aligned} \tag{3.7}$$

with an easy to imply definitions of the newly defined matrix symbols.

Since the slow and fast parts are completely decoupled a simple truncation:

$$\begin{aligned}s\mathbf{E}_s\mathbf{x}_s &= \mathbf{A}_s\mathbf{x}_s + \mathbf{B}_s\mathbf{u}\\ \mathbf{y} &= \mathbf{C}_s\mathbf{x}_s + \mathbf{D}\mathbf{u}\end{aligned} \tag{3.8}$$

becomes quite a viable model reduction. Nevertheless, in view of safeguarding a desired precision with the smallest order reduction, we can resort to a more appropriate residualization, which is quite simple and allow a more correct recovery of the steady responses, often a fact of paramount importance. In such a way, instead of discarding $\mathbf{x}_f = (s\mathbf{E}_f - \mathbf{A}_f)^{-1}\mathbf{B}_f\mathbf{u}$ we approximate its contribution at low frequencies through a series expansion around $s = 0$ so that its residualization of order m will be:

$$\mathbf{x}_f = -\sum_{i=0}^{m} s^i(\mathbf{A}_f^{-1}\mathbf{E}_f)^i\mathbf{A}_f^{-1}\mathbf{B}_f\mathbf{u} \tag{3.9}$$

which, when substituted in the previously given $l - f$ state and output equations, gives:

$$\begin{aligned}s\mathbf{E}_s\mathbf{x}_s &= \mathbf{A}_s\mathbf{x}_s + \mathbf{B}_s\mathbf{u}\\ \mathbf{y} &= \mathbf{C}_s\mathbf{x}_s + (\mathbf{D} - \mathbf{C}\mathbf{X}_f\mathbf{A}_f^{-1}\mathbf{B}_f)\mathbf{u} - \mathbf{C}\mathbf{X}_f\sum_{i=1}^{m} s^i(\mathbf{A}_f^{-1}\mathbf{E}_f)^i\mathbf{A}_f^{-1}\mathbf{B}_f\mathbf{u}\end{aligned} \tag{3.10}$$

which will return us to a simple truncation by omitting all of the $\sum$ation term, including the addition to $\mathbf{D}$.

To preserve sparsity, the numerical operations related to the fast part, must be carried out

without actually explicitly determining $\mathbf{E}_f$ and $\mathbf{A}_f$, which will be full matrices of large order. To such an end any product of the type $\mathbf{E}_f\mathbf{M}$, $\mathbf{M}$ being any matrix with consistent dimensions, must be carried out using the most appropriate component matrices of $\mathbf{E}_f$. They can be defined after giving the not yet given explicit expression of $\mathbf{E}_f$, i.e.:

$$\mathbf{E}_f = \mathbf{E}_r - \mathbf{E}_{yr}\mathbf{E}_s^{-1}\mathbf{E}_{xr} \tag{3.11}$$

with: $\mathbf{E}_r = \mathbf{Y}_r^T\mathbf{E}\mathbf{X}_r$, $\mathbf{E}_{yr} = \mathbf{Y}_r^T\mathbf{E}\mathbf{X}_s$ and $\mathbf{E}_{xr} = \mathbf{Y}_s^T\mathbf{E}\mathbf{X}_r$; $\mathbf{E}_r$ being highly sparse and $\mathbf{E}_{yr}$ and $\mathbf{E}_{xr}$ reduced order, $(n-l)\times l$, matrices, easy to evaluate because of the high sparsity of $\mathbf{Y}_r^T\mathbf{E}$ and $\mathbf{E}\mathbf{X}_r$. Using them we will work out any of the mentioned products as:

$$\mathbf{E}_f\mathbf{M} = \mathbf{E}_r\mathbf{M} - \mathbf{E}_{yr}(\mathbf{E}_s^{-1}(\mathbf{E}_{xr}\mathbf{M})) \tag{3.12}$$

Along the same line, after defining the following new support matrices:

$$\mathbf{A}_r := \mathbf{Y}_r^T\mathbf{A}\,\mathbf{X}_r \tag{3.13a}$$

$$\mathbf{A}_{xr} := \mathbf{Y}_s^T\,\mathbf{A}\,\mathbf{X}_r \tag{3.13b}$$

and the dense, but small $l\ by\ l$:

$$\mathbf{T}_{ea} := \mathbf{E}_s - \mathbf{A}_{xr}\mathbf{A}_r^{-1}\mathbf{E}_{yr} \tag{3.14}$$

we can make it explicit the once more not given yet matrix: $\mathbf{A}_f = \mathbf{A}_r - \mathbf{E}_{yr}\mathbf{E}_s^{-1}\mathbf{A}_{xr}$, so that, resorting to the matrix inversion, lemma we write:

$$\begin{aligned}\mathbf{A}_f^{-1} &= \mathbf{A}_r^{-1} + \mathbf{A}_r^{-1}\mathbf{E}_{yr}\mathbf{T}_{ea}^{-1}\mathbf{A}_{xr}\mathbf{A}_r^{-1}\\ &= \mathbf{A}_r^{-1}(\mathbf{I} + \mathbf{E}_{yr}\mathbf{T}_{ea}^{-1}\mathbf{A}_{xr}\mathbf{A}_r^{-1})\\ &= (\mathbf{I} + \mathbf{A}_r^{-1}\mathbf{E}_{yr}\mathbf{T}_{ea}^{-1}\mathbf{A}_{xr})\mathbf{A}_r^{-1}\end{aligned} \tag{3.15}$$

afterward proceeding as previously explained for any operation of the type: $\mathbf{A}_f^{-1}\mathbf{M}$.

Clearly there will be no explicit evaluation of the inverses of $\mathbf{T}_{ea}$ and $\mathbf{A}_r$, which will be substituted by their LU factorizations, with the products of inverses to the right of any matrix substituted by a forward-backward substitution.

Nonetheless, because of the small order reduction, $l \ll n$, we have to resort to a new factorization of a large and sparse $\mathbf{A}_r$, quite a viable but costly operation, whose cost will roughly correspond to that of the already available factorization of the matrix $\mathbf{A}$, as we will see is needed for the determination of the reduction subspace using a power based iteration. To avoid such a drawback we prefer to follow the path of evaluating the residualization by getting to the whole state residual: $\mathbf{r} = \mathbf{x} - \mathbf{X}_s\mathbf{x}_s$; so we write:

$$\mathbf{r} = (s\mathbf{E} - \mathbf{A})^{-1}\mathbf{B}\mathbf{u} - \mathbf{X}_s\mathbf{x}_s = (s\mathbf{E} - \mathbf{A})^{-1}\mathbf{B}\mathbf{u} - \mathbf{X}_s(s\mathbf{E}_s - \mathbf{A}_s)^{-1}\mathbf{B}_s\mathbf{u} \tag{3.16}$$

or:

$$(s\mathbf{E}-\mathbf{A})\mathbf{r} = (\mathbf{I}-(s\mathbf{E}-\mathbf{A})\mathbf{X}_s(s\mathbf{E}_s-\mathbf{A}_s)^{-1}\mathbf{Y}_s^T)\mathbf{B}\mathbf{u} = (\mathbf{I}-\mathbf{E}\mathbf{X}_s\mathbf{E}_s^{-1}\mathbf{Y}_s^T)\mathbf{B}\mathbf{u} \tag{3.17}$$

from which:

$$\mathbf{r} = (s\mathbf{E} - \mathbf{A})^{-1}(\mathbf{I} - \mathbf{E}\mathbf{X}_s\mathbf{E}_s^{-1}\mathbf{Y}_s^T)\mathbf{B}\mathbf{u} \tag{3.18}$$

Since with the residualization we want to recover the slow part of the fast response it is not strictly necessary to obtain it through a series around $s = 0$, but a value $s = -\alpha$, with $|\alpha|$ being adequately small, may suffice. Then, defining $\mathbf{A}_\alpha := \alpha\mathbf{E} + \mathbf{A}$ and $\mathbf{B}_r := (\mathbf{I} - \mathbf{E}\mathbf{X}_s\mathbf{E}_s^{-1}\mathbf{Y}_s^T)\mathbf{B}$, such a residualization is:

$$\mathbf{r} = -\sum_{i=0}^{m}(s+\alpha)^i(\mathbf{A}_\alpha^{-1}\mathbf{E})^i\mathbf{A}_\alpha^{-1}\mathbf{B}_r\mathbf{u} \tag{3.19}$$

In such way it is possible to exploit the very same factorization used for the power iterations that led us to $\mathbf{X}_s$ and $\mathbf{Y}_s$, For a non singular $\mathbf{A}$ it is clearly possible to use $\alpha = 0$, in which case we will obtain the same result provided by Eq. (3.9) albeit in a much simpler and less costly way.

The new residualized state and output equation will be:

$$\begin{aligned} s\mathbf{E}_s\mathbf{x}_s &= \mathbf{A}_s\mathbf{x}_s + \mathbf{B}_s\mathbf{u} \\ \mathbf{y} &= \mathbf{C}_s\mathbf{x}_s + (\mathbf{D} - \mathbf{C}\mathbf{A}_\alpha^{-1}\mathbf{B}_r)\mathbf{u} - \mathbf{C}\sum_{i=1}^{m}(s+\alpha)^i(\mathbf{A}_\alpha^{-1}\mathbf{E})^i\mathbf{A}_r^{-1}\mathbf{B}_r\mathbf{u}^{(i)} \end{aligned} \tag{3.20}$$

It should nonetheless be noted that in the case of a nonsingular $\mathbf{A}$ it would be possible to use an $\mathbf{A}_f$ based residualization without the need of a new factorization for $\mathbf{A}_\alpha$. In fact, as it will be shown later on, we could anticipate such a factorization using it for the mentioned power iterations. Whatever the approach chosen a typical second order residualization will eventually end with the following:

$$\begin{aligned} s\mathbf{E}_s\mathbf{x}_s &= \mathbf{A}_s\mathbf{x}_s + \mathbf{B}_s\mathbf{u} \\ \mathbf{y} &= \mathbf{C}_s\mathbf{x}_s + \mathbf{D}_{s0}\mathbf{u} + s\mathbf{D}_{s1}\mathbf{u} + s^2\mathbf{D}_{s2}\mathbf{u} \end{aligned} \tag{3.21}$$

with the related transfer matrix being:

$$\mathbf{H} = \mathbf{D}_{s0} + s\mathbf{D}_{s1} + s^2\mathbf{D}_{s2} + \mathbf{C}_s(s\mathbf{E}_s - \mathbf{A}_s)^{-1}\mathbf{B}_s \tag{3.22}$$

3.1.2 Bubnov-Galërkin projection

What above has shown that a double iteration permits the full uncoupling of the slow and fast part of a LTI system. It would be interesting to know what can be done by adopting a single invariant subspace, i.e. one in which the previously give scheme will use only the sole right subspace:

$$\mathbf{E}\mathbf{X}_s\mathbf{S}_x = \mathbf{A}\mathbf{X}_s \qquad \mathbf{X}_s^T\mathbf{X}_s = \mathbf{I} \tag{3.23}$$

once more to be complemented with the same, previously seen, residual subspace $\mathbf{X}_r$, with $\mathbf{X}_r^T\mathbf{X}_r = \mathbf{I}$, associated to the fast frequency range.

Using $\mathbf{X}_r$ we set up the following state:

$$\begin{aligned}\mathbf{x} &= \begin{bmatrix}\mathbf{X}_s & (\mathbf{I}-\mathbf{X}_s(\mathbf{X}_s^T\mathbf{E}\mathbf{X}_s)^{-1}\mathbf{X}_s^T\mathbf{E})\mathbf{X}_r\end{bmatrix}\begin{Bmatrix}\mathbf{x}_s\\ \mathbf{x}_f\end{Bmatrix}\\ &= \begin{bmatrix}\mathbf{X}_s & \mathbf{T}_x\mathbf{X}_r\end{bmatrix}\begin{Bmatrix}\mathbf{x}_s\\ \mathbf{x}_f\end{Bmatrix} = \begin{bmatrix}\mathbf{X}_s & \mathbf{X}_f\end{bmatrix}\begin{Bmatrix}\mathbf{x}_s\\ \mathbf{x}_f\end{Bmatrix}\end{aligned} \tag{3.24}$$

having defined $\mathbf{T}_x := \mathbf{I}-\mathbf{X}_s(\mathbf{X}_s^T\mathbf{E}\mathbf{X}_s)^{-1}\mathbf{X}_s^T\mathbf{E}$, and projection transformation:

$$\begin{aligned}\mathbf{P} &= \begin{bmatrix}\mathbf{X}_s & (\mathbf{I}-\mathbf{X}_s(\mathbf{X}_s^T\mathbf{E}^T\mathbf{X}_s)^{-1}\mathbf{X}_s^T\mathbf{E}^T)\mathbf{X}_r\end{bmatrix}\\ &= \begin{bmatrix}\mathbf{X}_s & \mathbf{T}_y\mathbf{X}_r\end{bmatrix} = \begin{bmatrix}\mathbf{X}_s & \mathbf{Y}_f\end{bmatrix}\end{aligned} \tag{3.25}$$

having defined $\mathbf{T}_y := \mathbf{I}-\mathbf{X}_s(\mathbf{X}_s^T\mathbf{E}^T\mathbf{X}_s)^{-1}\mathbf{X}_s^T\mathbf{E}^T$, with $\mathbf{T}_x$ and $\mathbf{T}_y$ being non-symmetric, idempotent, so singular, $(n-l)\times(n-l)$ matrices. It is then possible to verify that after applying to Eq. (3.1) the following change of state and linear combination of its equations:

$$\begin{aligned}\mathbf{P}^T(s\mathbf{E}-\mathbf{A})\begin{bmatrix}\mathbf{X}_s & \mathbf{X}_f\end{bmatrix}\begin{Bmatrix}\mathbf{x}_s\\ \mathbf{x}_f\end{Bmatrix} &= \mathbf{P}^T\mathbf{B}\mathbf{u}\\ \mathbf{y} = \mathbf{C}\begin{bmatrix}\mathbf{X}_s & \mathbf{X}_f\end{bmatrix}\begin{Bmatrix}\mathbf{x}_s\\ \mathbf{x}_f\end{Bmatrix} &+ \mathbf{D}\mathbf{u}\end{aligned} \tag{3.26}$$

the following, partially decoupled, low-high frequency model will be obtained,

$$\begin{aligned}s\begin{bmatrix}\mathbf{X}_s^T\mathbf{E}\mathbf{X}_s & \mathbf{0}\\ \mathbf{0} & \mathbf{Y}_f^T\mathbf{E}\mathbf{X}_f\end{bmatrix}\begin{Bmatrix}\mathbf{x}_s\\ \mathbf{x}_f\end{Bmatrix} &= \begin{bmatrix}\mathbf{X}_s^T\mathbf{A}\mathbf{X}_s & \mathbf{X}_s^T\mathbf{A}\mathbf{X}_f\\ \mathbf{0} & \mathbf{Y}_f^T\mathbf{A}\mathbf{X}_f\end{bmatrix}\begin{Bmatrix}\mathbf{x}_l\\ \mathbf{x}_h\end{Bmatrix} + \begin{bmatrix}\mathbf{X}_s^T\mathbf{B}\\ \mathbf{Y}_f^T\mathbf{B}\end{bmatrix}\mathbf{u}\\ \mathbf{y} = \mathbf{C}\mathbf{X}_s\mathbf{x}_s + \mathbf{C}\mathbf{X}_f\mathbf{x}_f &+ \mathbf{D}\mathbf{u}\end{aligned} \tag{3.27}$$

which is eventually synthesized in the following:

$$\begin{aligned}s\begin{bmatrix}\mathbf{E}_s & \mathbf{0}\\ \mathbf{0} & \mathbf{E}_f\end{bmatrix}\begin{Bmatrix}\mathbf{x}_s\\ \mathbf{x}_f\end{Bmatrix} &= \begin{bmatrix}\mathbf{A}_s & \mathbf{A}_{sf}\\ \mathbf{0} & \mathbf{A}_f\end{bmatrix}\begin{Bmatrix}\mathbf{x}_s\\ \mathbf{x}_f\end{Bmatrix} + \begin{bmatrix}\mathbf{B}_s\\ \mathbf{B}_f\end{bmatrix}\mathbf{u}\\ \mathbf{y} = \mathbf{C}_s\mathbf{x}_s + \mathbf{C}_f\mathbf{x}_f &+ \mathbf{D}\mathbf{u}\end{aligned} \tag{3.28}$$

with the implied definitions of the new symbols for the component matrices.

We then see that the fast part is completely uncoupled from the slow part, but contributes to the slow response. A simple truncation:

$$\begin{aligned}s\mathbf{E}_s\mathbf{x}_s &= \mathbf{A}_s\mathbf{x}_s + \mathbf{B}_s\mathbf{u}\\ \mathbf{y} &= \mathbf{C}_s\mathbf{x}_s + \mathbf{D}\mathbf{u}\end{aligned} \tag{3.29}$$

would be possible, but $\mathbf{x}_f$ should be really negligible, which might not be the case for a small order reduction. Therefore, in view of safeguarding a desired precision with the smallest order reduction, resorting to a more appropriate residualization in this case is even more appropriate than with the fully decoupled reduction, presented previously. In such a way the fast part will be coupled to the slow part of the eigenspectrum, bu just through the

input $\mathbf{u}$. The related residualization of order n for the state $\mathbf{x}$ will be the same as before, but will affect both the state and output equations, as given by:

$$\begin{aligned} s\mathbf{E}_s\mathbf{x}_s &= \mathbf{A}_s\mathbf{x}_s + (\mathbf{B}_s - \mathbf{A}_{sf}\mathbf{A}_f^{-1}\mathbf{B}_f)\mathbf{u} - \mathbf{A}_{sf}\sum_{i=1}^{n+1} s^i(\mathbf{A}_f^{-1}\mathbf{E}_f)^i\mathbf{A}_f^{-1}\mathbf{B}_f\mathbf{u} \\ \mathbf{y} &= \mathbf{C}_s\mathbf{x}_s + (\mathbf{D} - \mathbf{C}\mathbf{X}_f\mathbf{A}_f^{-1}\mathbf{B}_f)\mathbf{u} - \mathbf{C}\mathbf{X}_f\sum_{i=1}^{n} s^i(\mathbf{A}_f^{-1}\mathbf{E}_f)^i\mathbf{A}_f^{-1}\mathbf{B}_h\mathbf{u} \end{aligned} \tag{3.30}$$

which will return us to a simple truncation by omitting all the $\sum$ation terms, including the contributions to $\mathbf{B}_s$ and $\mathbf{D}$.

Along the same line of the fully decoupled systems we can take care of keeping the sparsity of the implied matrices to make what above fully viable, the only changes being in the definitions of the supporting matrices, now being: $\mathbf{E}_r = \mathbf{X}_r^T\mathbf{E}\mathbf{X}_r$, $\mathbf{E}_{yr} = \mathbf{X}_r^T\mathbf{E}\mathbf{X}_s$, $\mathbf{E}_{xr} = \mathbf{X}_s^T\mathbf{E}\mathbf{X}_r$, $\mathbf{A}_r = \mathbf{X}_r^T\mathbf{A}\,\mathbf{X}_r$, $\mathbf{A}_{xr} = \mathbf{X}_s^T\,\mathbf{A}\,\mathbf{X}_r$, $\mathbf{T}_{ea} = \mathbf{E}_s - \mathbf{A}_{xr}\mathbf{A}_r^{-1}\mathbf{E}_{yr}$.

We are thus once more interested in looking for a residualization getting to the whole $\mathbf{x}$ state residual: $\mathbf{r} = \mathbf{x} - \mathbf{X}_s\mathbf{x}_s$, based on the same very matrices $\mathbf{E}$ and $\mathbf{A}^{-1}$ used for the single power iteration. Nevertheless, because of the $\mathbf{A}_{sf}$ coupling, such a way will result in being somewhat less straightforward than that of the fully decoupled case, as it can be seen with the following steps:

$$\begin{aligned} \mathbf{r} &= (s\mathbf{E} - \mathbf{A})^{-1}\mathbf{B}\mathbf{u} - \mathbf{X}_s\mathbf{x}_s \\ &= (s\mathbf{E} - \mathbf{A})^{-1}\mathbf{B}\mathbf{u} - \mathbf{X}_s(s\mathbf{E}_s - \mathbf{A}_s)^{-1}\mathbf{X}_s^T(\mathbf{A}\mathbf{r} + \mathbf{B}\mathbf{u}) \end{aligned} \tag{3.31}$$

or

$$\begin{aligned} (s\mathbf{E} - \mathbf{A})\mathbf{r} &= \mathbf{B}\mathbf{u} - (s\mathbf{E} - \mathbf{A})\mathbf{X}_s(s\mathbf{E}_s - \mathbf{A}_s)^{-1})\mathbf{X}_s^T(\mathbf{A}\mathbf{r} + \mathbf{B}\mathbf{u}) \\ &= (\mathbf{I} - \mathbf{E}\mathbf{X}_s\mathbf{E}_s^{-1}\mathbf{X}_s^T)\mathbf{B}\mathbf{u} - \mathbf{E}\mathbf{X}_s\mathbf{E}_s^{-1}\mathbf{X}_s^T\mathbf{A}\mathbf{r} \end{aligned} \tag{3.32}$$

from which:

$$(s\mathbf{E} - \mathbf{A} + \mathbf{E}\mathbf{X}_s\mathbf{E}_s^{-1}\mathbf{X}_s^T\mathbf{A})\mathbf{r} = (\mathbf{I} - \mathbf{E}\mathbf{X}_s\mathbf{E}_s^{-1}\mathbf{X}_s^T)\mathbf{B}\mathbf{u} := \mathbf{B}_r\mathbf{u} \tag{3.33}$$

Unfortunately, since the slow and fast part are not totally decoupled any more, the coefficient matrix at the left hand side will be always singular for $s = 0$. So if we want to avoid the factorization of $\mathbf{A}_f$ we have to use a shifted power iteration even if the problem has no zero eigenvalues and residualized for at $s = -\alpha$ anyhow. Then $\mathbf{B}_r$ will be as defined for the totally decoupled case while redefining $\mathbf{A}_\alpha := (\alpha\mathbf{E} + \mathbf{A} - \mathbf{E}\mathbf{X}_s\mathbf{E}_s^{-1}\mathbf{X}_s^T\mathbf{A})$ we are lead to the already seen residualization:

$$\mathbf{r} = -\sum_{i=0}^{n}(s+\alpha)^i(\mathbf{A}_\alpha^{-1}\mathbf{E})^i\mathbf{A}_\alpha^{-1}\mathbf{B}_r\mathbf{u} \tag{3.34}$$

ending with the following residualized set:

$$\begin{aligned} s\mathbf{E}_s\mathbf{x}_s &= \mathbf{A}_s\mathbf{x}_s + (\mathbf{B}_s - \mathbf{X}_s^T\mathbf{A}\mathbf{A}_\alpha^{-1}\mathbf{B}_r)\mathbf{u} - \mathbf{X}_s^T\mathbf{A}\sum_{i=1}^{n+1}(s+\alpha)^i(\mathbf{A}_\alpha^{-1}\mathbf{E})^i\mathbf{A}_\alpha^{-1}\mathbf{B}_r\mathbf{u} \\ \mathbf{y} &= \mathbf{C}_s\mathbf{x}_s + (\mathbf{D} - \mathbf{C}\mathbf{A}_\alpha^{-1}\mathbf{B}_r)\mathbf{u} - \mathbf{C}\sum_{i=1}^{n}(s+\alpha)^i(\mathbf{A}_\alpha^{-1}\mathbf{E})^i\mathbf{A}_\alpha^{-1}\mathbf{B}_r\mathbf{u} \end{aligned} \tag{3.35}$$

Naturally, once more to preserve sparsity and reuse the factorization of the power iteration, the inversion of $\mathbf{A}_r$ has to be applied using the matrix inversion lemma:

$$\mathbf{A}_r^{-1} = (\alpha\mathbf{E}+\mathbf{A})^{-1}+(\alpha\mathbf{E}+\mathbf{A})^{-1}\mathbf{E}\mathbf{X}_s(\mathbf{E}_s-\mathbf{X}_s^T\mathbf{A}(\alpha\mathbf{E}+\mathbf{A})^{-1}\mathbf{E}\mathbf{X}_s)^{-1}\mathbf{X}_s^T\mathbf{A}(\alpha\mathbf{E}+\mathbf{A})^{-1} \tag{3.36}$$

Clearly their remain the mentioned possibility of working with $\mathbf{A}_f$, by anticipating also in this case the factorization of $\mathbf{A}_\alpha$ for the inverse powers of a nonsingular $\mathbf{A}$.

To be noticed the fact that the residualization applied to the state equation in Eq. (3.35) is an order higher that the one used for the output equation. Because of the integration implied in the state equation, such a choice is fully consistent in term of the overall output residualization, as it can be seen by referring to a third-second order residualization of the type used for our aerodynamic application:

$$\begin{aligned} s\mathbf{E}_s\mathbf{x}_s &= \mathbf{A}_s\mathbf{x}_s + \mathbf{B}_{s0}\mathbf{u} + s\mathbf{B}_{s1}\mathbf{u} + s^2\mathbf{B}_{s2}\mathbf{u} + s^3\mathbf{B}_{s3}\mathbf{u} \\ \mathbf{y} &= \mathbf{C}_s\mathbf{x}_s + \mathbf{D}_{s0}\mathbf{u} + s\mathbf{D}_{s1}\mathbf{u} + s^2\mathbf{D}_{s2}\mathbf{u} \end{aligned} \tag{3.37}$$

along with its transfer matrix:

$$\mathbf{H} = \mathbf{D}_{s0} + s\mathbf{D}_{s1} + s^2\mathbf{D}_{s2} + \mathbf{C}_s(s\mathbf{E}_s - \mathbf{A}_s)^{-1}(\mathbf{B}_{s0} + s\mathbf{B}_{s1} + s^2\mathbf{B}_{s2} + s^3\mathbf{B}_{s3}) \tag{3.38}$$

where the implied definitions should be clear without adding any further detail. In fact, carrying out the right matrix binomial division related to $(s\mathbf{E}_s - \mathbf{A}_s)$, the transfer matrix $\mathbf{H}$ becomes:

$$\begin{aligned} \mathbf{H} = &\left[\mathbf{D}_{s0} + \mathbf{C}_s\mathbf{E}_s^{-1}(\mathbf{B}_{s1} + \mathbf{A}_s\mathbf{E}_s^{-1}(\mathbf{B}_{s2} + \mathbf{A}_s\mathbf{E}_s^{-1}\mathbf{B}_{s3}))\right] \\ &+ s(\mathbf{D}_{s1} + \mathbf{C}_s\mathbf{E}_s^{-1}(\mathbf{B}_{s2} + \mathbf{A}_s\mathbf{E}_s^{-1}\mathbf{B}_{s3})) + s^2(\mathbf{D}_{s2} + \mathbf{C}_s\mathbf{E}_s^{-1}\mathbf{B}_{s3}) \\ &+ \mathbf{C}_s(s\mathbf{E}_s + \mathbf{A}_s)^{-1}\left[\mathbf{B}_{s0} + \mathbf{A}_s\mathbf{E}_s^{-1}(\mathbf{B}_{s1} + \mathbf{A}_s\mathbf{E}_s^{-1}(\mathbf{B}_{s2} + \mathbf{A}_s\mathbf{E}_s^{-1}\mathbf{B}_{s3}))\right] \end{aligned} \tag{3.39}$$

which, with an obvious reuse of redefined symbols, can be rewritten as:

$$\mathbf{H} = \mathbf{D}_{s0} + s\mathbf{D}_{s1} + s^2\mathbf{D}_{s2} + \mathbf{C}_s(s\mathbf{E}_s - \mathbf{A}_s)^{-1}\mathbf{B}_s \tag{3.40}$$

ending with a second order only final residualization:

$$\begin{aligned} s\mathbf{E}_s\mathbf{x}_s &= \mathbf{A}_s\mathbf{x}_s + \mathbf{B}_s\mathbf{u} \\ \mathbf{y} &= \mathbf{C}_s\mathbf{x}_s + \mathbf{D}_{s0}\mathbf{u} + s\mathbf{D}_{s1}\mathbf{u} + s^2\mathbf{D}_{s2}\mathbf{u} \end{aligned} \tag{3.41}$$

i.e. the same formal result of the fully decoupled case. Nonetheless, it should be remarked that, because of the different projection used, the coefficient matrices will not be the same.

Comparing the two presented approaches we can say that the right and left subspace iterations will cost the double of a right only iteration, a cost that is often partly compensated because of a faster convergence of the double iterations. On the other hand the use of the right and left reduction provides both a better truncation and a simpler, and less costly, residualization scheme. In fact it is often better to avoid a simple truncation with a single subspace reduction and its residualization will anyhow be a bit more complicated.

3.1.3 Discrete formulation

The projection framework and the related eigenanalyis may be formulated either in continuous or discrete time. The discretized linear time invariant system in descriptor form in the z discrete frequency domain is obtained by adopting time discretization techniques, resulting in relations between s and z. These relations, together with the corresponding discrete LTI equations, are summarized in Table 3.1.

Discretization formulae	**z to s mapping**	**discrete system**
Forward Euler	$s = \dfrac{z-1}{\Delta t}$	$z\mathbf{E}\mathbf{x} = (\mathbf{A}\Delta t + \mathbf{E})\,\mathbf{x} + \mathbf{B}\Delta t\,\mathbf{u}$
Backward Euler	$s = \dfrac{z-1}{z\Delta t}$	$z\,(\mathbf{E} - \mathbf{A}\Delta t)\,\mathbf{x} = \mathbf{E}\mathbf{x} + z\mathbf{B}\Delta t\,\mathbf{u}$
Crank-Nicholson (Tustin)	$s = \dfrac{2}{\Delta t}\dfrac{z-1}{z+1}$	$z\,(2\mathbf{E} - \mathbf{A}\Delta t)\,\mathbf{x} = (2\mathbf{E} + \mathbf{A}\Delta t) + \mathbf{B}\Delta t\,\mathbf{u} + z\mathbf{B}\Delta t\,\mathbf{u}$
BDF	$s = \dfrac{3z^2 - 4z + 1}{2\Delta t}$	$z^2\,3\mathbf{E}\mathbf{x} - z\,4\mathbf{E}\mathbf{x} + (\mathbf{E} - 2\mathbf{A}\Delta t)\,\mathbf{x} = 2\mathbf{B}\Delta t\,\mathbf{u}$ $z\begin{bmatrix}\mathbf{I} & \mathbf{0}\\ \mathbf{0} & 3\mathbf{E}\end{bmatrix}\bar{\mathbf{x}} = \begin{bmatrix}\mathbf{0} & \mathbf{I}\\ 2\mathbf{A}\Delta t - \mathbf{E} & 4\mathbf{E}\end{bmatrix}\bar{\mathbf{x}} + \begin{bmatrix}\mathbf{0}\\ 2\mathbf{B}\Delta t\end{bmatrix}\mathbf{u}$

Table 3.1: *Discrete LTI systems.*

Anyhow the discretization technique used, it ends up with a system in the discrete frequency z of the type:

$$z\mathbf{E}\,\mathbf{x} = \mathbf{A}\,\mathbf{x} + \mathbf{B}_0\,\mathbf{u} + z\mathbf{B}_1\,\mathbf{u} \tag{3.42}$$

where the new redefined matrices $\mathbf{E}$, $\mathbf{A}$, $\mathbf{B}_0$, and $\mathbf{B}_1$ are easily inferable from Table 3.1. In the discrete time it results:

$$\begin{aligned}\mathbf{E}\,\mathbf{x}(k+1) &= \mathbf{A}\,\mathbf{x}(k) + \mathbf{B}_0\,\mathbf{u}(k) + \mathbf{B}_1\,\mathbf{u}(k+1)\\ \mathbf{y}(k) &= \mathbf{C}\,\mathbf{x}(k) + \mathbf{D}\,\mathbf{u}(k)\end{aligned} \tag{3.43}$$

to which the discussed Petrov-Galërkin and Galërkin model reduction procedures may be easily applied.

3.1.4 Numerical calculation of the slow left/right subspaces

Referring for a while to a standard eigenvalue problem in the form: $s\mathbf{I}\mathbf{x} = \mathbf{A}\mathbf{x}$ any left/right subspace associated to the slow spectrum of the matrix $\mathbf{A}$ will satisfy the following equations:

$$\mathbf{X}_s\mathbf{S}_x = \mathbf{A}\mathbf{X}_s \qquad \mathbf{X}_s^T\mathbf{X}_s = \mathbf{I} \tag{3.44a}$$

$$\mathbf{Y}_s\mathbf{S}_y = \mathbf{A}^T\mathbf{Y}_s \qquad \mathbf{Y}_s^T\mathbf{Y}_s = \mathbf{I} \tag{3.44b}$$

the matrices $\mathbf{S}_x$ and $\mathbf{S}_y$ having the low eigenvalues we are looking for. They will differ in structure according to the basis chosen to represent the related subspaces. The above solution is inevitably searched for by using an iterated numerical procedure which at a generic stage (k) will provide just an approximations for the searched: $\mathbf{X}_s^{(k)}$, $\mathbf{X}_s^{(k)}$, $\mathbf{S}_x^{(k)}$, $\mathbf{S}_y^{(k)}$. Omitting for simplicity of notation both the slow suffix and the iteration index we can write both of the approximation as a single overdetermined system of equations, with a block diagonal unknown matrix, as:

$$\begin{bmatrix}\mathbf{X} & \mathbf{Y}\end{bmatrix}\begin{bmatrix}\mathbf{R}_x & \mathbf{0}\\ \mathbf{0} & \mathbf{R}_y\end{bmatrix} = \begin{bmatrix}\mathbf{A}\mathbf{X} & \mathbf{A}^T\mathbf{Y}\end{bmatrix} \tag{3.45}$$

Its Least Squares (LS) solution being provided by:

$$\begin{bmatrix}\mathbf{I} & \mathbf{X}^T\mathbf{Y}\\ \mathbf{Y}^T\mathbf{X} & \mathbf{I}\end{bmatrix}\begin{bmatrix}\mathbf{R}_x & \mathbf{0}\\ \mathbf{0} & \mathbf{R}_y\end{bmatrix} = \begin{bmatrix}\mathbf{X}^T\mathbf{A}\mathbf{X} & \mathbf{X}^T\mathbf{A}^T\mathbf{Y}\\ \mathbf{Y}^T\mathbf{A}\mathbf{X} & \mathbf{Y}^T\mathbf{A}^T\mathbf{Y}\end{bmatrix} = \begin{bmatrix}\mathbf{R}_x & (\mathbf{X}^T\mathbf{Y})\mathbf{R}_y\\ (\mathbf{Y}^T\mathbf{X})\mathbf{R}_x & \mathbf{R}_y\end{bmatrix} \tag{3.46}$$

from which it can be seen that, because of the constraint imposed by the block diagonal structure of the unknown matrices, $\mathbf{R}_x$ and $\mathbf{R}_y$ can be determined in multiple ways:

1. dependently on each other through the two-sided iteration,

$$\mathbf{R}_x = (\mathbf{Y}^T\mathbf{X})^{-1}\mathbf{Y}^T\mathbf{A}\mathbf{X} \tag{3.47a}$$

$$\mathbf{R}_y = (\mathbf{X}^T\mathbf{Y})^{-1}\mathbf{X}^T\mathbf{A}^T\mathbf{Y} \tag{3.47b}$$

   which corresponds to the search for a stationary point of the true Rayleigh coefficient: $\lambda_R = \frac{\mathbf{y}^T\mathbf{A}\,\mathbf{x}}{\mathbf{y}^T\mathbf{E}\,\mathbf{x}}$. with respect to variations for both $\mathbf{x}$ and $\mathbf{y}$;

2. a hybrid solution first, i.e. a single iteration to full convergence for $\mathbf{R}_x$ and $\mathbf{X}$, just a projection in LS sense, followed by the search for a true Rayleigh stationary point for variations with respect to $\mathbf{y}$, using the previous fully converged $\mathbf{R}_x$ and $\mathbf{X}$:

$$\mathbf{R}_x = \mathbf{X}^T\mathbf{A}\mathbf{X} \tag{3.48a}$$

$$\mathbf{R}_y = (\mathbf{X}^T\mathbf{Y})^{-1}\mathbf{X}^T\mathbf{A}^T\mathbf{Y} \tag{3.48b}$$

3. a trivial second hybrid alternative:

$$\mathbf{R}_y = \mathbf{Y}^T\mathbf{A}^T\mathbf{Y} \tag{3.49a}$$

$$\mathbf{R}_x = (\mathbf{Y}^T\mathbf{X})^{-1}\mathbf{Y}^T\mathbf{A}^{-1}\mathbf{E}\mathbf{Y} \tag{3.49b}$$

4. just two LS solutions, i.e. $\mathbf{R}_x$ and $\mathbf{R}_y$ determined independently:

$$\mathbf{R}_x = \mathbf{X}^T\mathbf{A}\mathbf{X} \tag{3.50a}$$
$$\mathbf{R}_y = \mathbf{Y}^T\mathbf{A}^T\mathbf{Y} \tag{3.50b}$$

   whereas each of which can be used in the case one is interested just either to the left or right subspace.

Once $\mathbf{R}_x$ and $\mathbf{R}_y$ are available they are transformed to a chosen subspace spectral representations, i.e.: $\mathbf{R}_x = \mathbf{Q}_x\mathbf{S}_x\mathbf{Q}_x^{-1}$ and $\mathbf{R}_y = \mathbf{Q}_y\mathbf{S}_y\mathbf{Q}_y^{-1}$, with the $\mathbf{Q}_{(\cdot)}$ matrices being orthogonal for Schur $\mathbf{S}_{(\cdot)}$, so that new improved approximations are given through the following substitutions: $\mathbf{X} = \mathbf{X}\mathbf{Q}_x$ and $\mathbf{Y} = \mathbf{Y}\mathbf{Q}_y$. We go even further and will not care of choosing the most effective of the algorithms providing either just Eq. (3.44a) or both Eq. (3.44a), and Eq. (3.44b). We just notice that against an abundance of methods providing just right subspaces there are far less for the so called two-sided eigensolutions, integrating the simultaneous obtainment of both $\mathbf{X}$ and $\mathbf{Y}$, as for Eq. (3.47) above. It is stated that two-sided iterations can expedite convergence of the determination of a right subspace but mostly at a higher computational cost, because of the larger set of calculations implied. That said a viable solution in our case could be the use of Eq. (3.50). Nevertheless our preference will go to Eqs. (3.48), simply because the first part is the one needed for the partial decoupling and because our experience shows that the availability of the $\mathbf{X}$ expedites the following determination of $\mathbf{Y}$, with a reduction of the cost of its determination to a fraction of that of $\mathbf{X}$. Moreover, even if it might not be a very effective approach, e.g. both single or bi-iterated left/right scalar and block Arnoldi and Lanczos methods are reportedly assumed as better solutions fitting the structure of Eqs. (3.44), we will adopt two easily available FORTRAN routines, SRRIT and EB22 [1]. Both of them provide a single subspace, i.e. Eq. (3.48b), but are easy to modify, so to append the solution of Eq. (3.48a), through the easy addition of a single test and two subroutine calls at the point where the pseudo Rayleigh projection associated to Eq. (3.48a) is applied.

The above optimization of the approximation available at a certain iteration stage (k) needs to be complemented by a power iteration, i.e. $\mathbf{X}^{(k+1)} = \mathbf{A}\mathbf{X}^{(k)}$, which makes it progressing toward the desired part of the eigenspectrum more and more. In view of our interest for the slowest eigenvalues we are compelled to adopt inverse power schemes of the type:

$$\begin{aligned}\mathbf{X}_s^{(k+1)} &= (\mathbf{A}+\alpha\mathbf{E})^{-1}\mathbf{E}\mathbf{X}_s^{(k)}\\ \mathbf{Y}_s^{(k+1)} &= (\mathbf{A}+\alpha\mathbf{E})^{-T}\mathbf{E}^T\mathbf{Y}_s^{(k)}\end{aligned} \tag{3.51}$$

with the change of the eigenvalues origin α being adopted in the case of a singular $\mathbf{A}$, i.e. when there are null eigenvalues. In such a way our subspace iteration will eventually converge to the following, shifted, raw result:

$$\begin{aligned}\mathbf{E}\mathbf{X}_s &= (\mathbf{A}+\alpha\mathbf{E})\mathbf{X}_s\hat{\mathbf{S}}_x\\ \mathbf{E}^T\mathbf{Y}_s &= (\mathbf{A}+\alpha\mathbf{E})^T\mathbf{Y}_s\hat{\mathbf{S}}_y\end{aligned} \tag{3.52}$$

[1] SRRIT is a public domain piece of software while EB22 is proprietary but, at least for academic use, readily available thanks to: HSL, a collection of Fortran codes for large-scale scientific computation. See http://www.hsl.rl.ac.uk/".

which, defining $\mathbf{S}_x := (\mathbf{I} - \alpha\hat{\mathbf{S}}_x)\hat{\mathbf{S}}_x^{-1}$ and $\mathbf{S}_y := (\mathbf{I} - \alpha\hat{\mathbf{S}}_y)\hat{\mathbf{S}}_y^{-1}$, can be put in the final working form of the Eqs. (3.2) needed for our model reductions. It should be remarked that order reduction, say l, is usually quite strong, to the point that it is possible to assume that l is just a very small fraction of n.

As usual, the inverse of $(\mathbf{A} + \alpha\mathbf{E})$ will be never calculated. Instead, the determination of its $\mathbf{LU}$ factorization will be to be carried out just once and direct-transposed forward-backward substitutions will be used in place of the products with its direct and transposed inverses, so to preserve any sparsity as far as possible. In such a view it should be noticed that the direct and transposed products associated to $\mathbf{E}$ will not be a problem, because of the matrices $\mathbf{X}$ being $\mathbf{Y}$ being substantially dense always, so that there will be no index matching problem in using any sparse storage scheme for them. For the case of a nonsingular $\mathbf{A}$ we can finally show how we can help the following residualizations by providing a factorization of $\mathbf{A}_r$ anticipating it for our power iterations. In fact, exemplifying it for the right vectors, we can work out each power iteration step by partitioning $\mathbf{A}$ and $\mathbf{X}$ according to the following:

$$\mathbf{A} = \begin{bmatrix} \mathbf{A}_a & \mathbf{A}_{ar} \\ \mathbf{A}_{ra} & \mathbf{A}_r \end{bmatrix}, \qquad \mathbf{X} = \begin{Bmatrix} \mathbf{X}_a \\ \mathbf{X}_r \end{Bmatrix}, \tag{3.53}$$

so that we can write:

$$\mathbf{Z} = \mathbf{A}_r^{-1}(\mathbf{E}\mathbf{X}^{(k)})_r \tag{3.54a}$$

$$\mathbf{X}_a^{(k+1)} = (\mathbf{A}_a - \mathbf{A}_{ar}\mathbf{A}_r^{-1}\mathbf{A}_{ra})^{-1}((\mathbf{E}\mathbf{X}^{(k)})_a - \mathbf{A}_{ar}\mathbf{Z}) \tag{3.54b}$$

$$\mathbf{X}_r^{(k+1)} = \mathbf{Z} - \mathbf{A}_r^{-1}\mathbf{A}_{ra}\mathbf{X}_a^{(k+1)} \tag{3.54c}$$

as usual clearly working with the $\mathbf{LU}$ factorizations of the sparse $\mathbf{A}_r$ and dense, but very small, $(\mathbf{A}_a - \mathbf{A}_{ar}\mathbf{A}_r^{-1}\mathbf{A}_{ra})^{-1}$. In such a way we will pay a little cost more at the power iterations time while being ready to use the residualizations based on $\mathbf{A}_f$, without any further added cost.

3.2 Improved matrix fraction approximation of aerodynamic transfer matrices

Despite the success of reduced order model formulations applied directly to the high-fidelity aerodynamic model in time-domain, the classic harmonic aerodynamics maintains nonetheless a core position in many modern aeroelastic formulations, where the aerodynamic subsystem is approximated [200] through the identification of a Rational Matrix Fraction Approximation (RMFA) of the GAFs [168, 201–212] having the following structure:

$$\begin{aligned}\mathbf{H}_a(p, M_\infty) = \mathbf{E}_{0a}(M_\infty) + p\mathbf{E}_{1a}(M_\infty) + p^2\mathbf{E}_{2a}(M_\infty) \\ + \mathbf{C}_a(M_\infty)\left(p\mathbf{I} - \mathbf{A}_a(M_\infty)\right)^{-1}\mathbf{B}_{0a}(M_\infty)\end{aligned} \tag{3.55}$$

with M_∞ being the freestream Mach number, $p = sl_a/V_\infty = h + jk$ the complex reduced frequency, $j = \sqrt{-1}$, s the circular complex frequency, l_a an appropriate aerodynamic

reference length, and V_∞ the constant aircraft speed. Calling n_k the number of harmonic reduced frequencies, k, at which $\mathbf{H}_a$ has been determined, an RMFA is usually identified by minimizing a Least Squares (LS) norm, $\|.\|_{LS}$, of the fit error:

$$\min_{\substack{\mathbf{E}_{0a},\mathbf{E}_{1a},\mathbf{E}_{2a}\\ \mathbf{C}_a,\mathbf{A}_a,\mathbf{B}_{0a}}} \sum_{1}^{n_k} \|(\mathbf{H}_a(jk_i) - \mathbf{E}_{0a} - jk_i\mathbf{E}_{1a} - (jk_i)^2\mathbf{E}_{2a} - \mathbf{C}_a\,(jk_i\mathbf{I} - \mathbf{A}_a)^{-1}\,\mathbf{B}_{0a}\|_{LS} \tag{3.56}$$

The ensuing nonlinear minimization aims at the lowest possible order, say l, of $\mathbf{A}_a$, capable of granting an adequate fit precision, under the constraints that $\mathbf{A}_a$ is asymptotically stable and, at least, an exact match of steady state. Because of the nonlinear term, $\mathbf{H}_{a_{nl}} = \mathbf{C}_a\,(jk\mathbf{I} - \mathbf{A}_a)^{-1}\,\mathbf{B}_{0a}$, such a task is far from being trivial. The literature presents various parametrizations leading to $\mathbf{C}_a, \mathbf{A}_a, \mathbf{B}_{0a}$ through simpler initial raw forms of $\mathbf{H}_{a_{nl}}$, aimed at compromising the order l against computational simplicity.

For example in [213] each coefficient of $\mathbf{H}_{a_{nl}}$ is effectively minimized using a rational function, therefore ending with a large order $\mathbf{A}_a$. Conversely other approaches use initializing poles-residues sums in matrix form, e.g.:

$$\mathbf{H}_{a_{nl}}(p) = \sum_{i=1}^{nl} \mathbf{H}_i \frac{\prod_{k=1}^{i} p_k}{\prod_{k=1}^{i}(1+p_k)} \qquad p_k, p_i \in \mathbb{R}^+ \tag{3.57a}$$

$$\mathbf{H}_{a_{nl}}(p) = \sum_{i=1}^{nl} \mathbf{H}_i \frac{p}{1+p_i} \qquad p_i \in \mathbb{R}^+ \tag{3.57b}$$

Equation (3.57a) is a slight modification of what is presented in [214] and leads to structuring $\mathbf{A}_a$ as a set of cascaded dynamics with real scalar blocks [215], while Eq. (3.57b) [202, 203] corresponds to a matrix $\mathbf{A}_a$ having uncoupled real scalar blocks. Their simplest implementation imposes suitable stable poles to make possible a trivial and fast linear LS fit for each matrix element. A further method, the so called Minimum State (MS) formulation [210–212], assigns a negative real diagonal $\mathbf{A}_a$ matrix (thus being equivalent to a residualized non symmetric modal formulation) and requires a nonlinear fitting. One of the simplest approaches used for such a minimization follows sets the matrices $\mathbf{E}_a$ as functions of $\mathbf{C}_a$ and $\mathbf{B}_{0a}$, typically by imposing an exact real fit at $k = 0$ and a complex one at an estimated reduced flutter frequency, and proceeds by alternating linear LS fitting for $\mathbf{C}_a$, keeping $\mathbf{B}_{0a}$ constant, and vice versa. Nowadays all of the above parametrizations aim only at providing an initial guess apt to start a constrained nonlinear optimization over the whole set of unknown parameter matrices [216].

A final approach carries out Eq. (3.55) starting through an initial Left/Right Matrix Fraction Description (LMFD/RMFD) [163]. It should be remarked that the so called Matrix Padé Approximation (MPA), [204–209] is often presented as a poles-residues form of the type of Eq. (3.57). Nevertheless, specific details of the related fitting algorithms apart, MPA formulations are nothing but a Matrix Fraction Description (MFD) in disguise.

Referring by way of example to an LMFD we can write it in two ways:

$$\mathbf{H}_a(p) = \mathbf{D}^{-1}(p)\,\mathbf{N}(p) \tag{3.58a}$$

$$\mathbf{D}(p)\mathbf{H}_a(p) = \mathbf{N}(p) \tag{3.58b}$$

so that using Eq. (3.58b) the identification can be cast into the following weighted linear LS fit:

$$\min_{\mathbf{N},\mathbf{D}} \sum_{1}^{n_k} \|\mathbf{W}(jk_i)\,(\mathbf{D}(jk_i)\mathbf{H}_a(jk_i) - \mathbf{N}(jk_i))\|_{LS} \tag{3.59}$$

$\mathbf{W}$ being an appropriately assigned weighting matrix. The LMFD so determined can be converted to state space, e.g. through a block controllable canonical form and reduced to the form of Eq. (3.55) through a balanced reduction, ending with a constrained nonlinear optimization for its final improvement. The just highlighted approach has been successfully applied to a unified determination of a single LTI subsystem for motion and gust GAFs [148, 163]. However, the above linear LS procedure neither minimizes the true fit error, i.e. $\|\mathbf{H}_a - \mathbf{D}^{-1}\mathbf{N}\|$, nor guarantees to obtain a stable system. Such problems are settled by using some tweaking, e.g. through few iterations with properly adapted $\mathbf{W}$ [148], so to start a final optimization with a model already close to the optimal result.

This work aims at improving the above identification of an MFD by using efficient nonlinear least squares identification schemes, applied to true fit error in a way ensuring the asymptotic stability of the identified system. A state space representation of the identified MFD is obtained through a balanced reduction followed by a second order double dynamic residualization, i.e. a residualization applied to both the state and output equations. Afterwards the new procedure is completed with a final linear refitting of this residualization having a richer set of parameters. Such a revised approach provides improved RMFAs without any tweaking and can be used as a black box.

3.2.1 Identification of the Matrix Fraction Description

In the present subsection the identification of the aerodynamic transfer matrix $\mathbf{H}_a$ as a Matrix Fraction Description (MFD) [163] is presented. A unified formulation where the aerodynamic forces due to structural displacements and gust perturbations is considered, together with the preference towards a Left Matrix Fraction Description (LMFD), because in this unified case the number of rows of $\mathbf{H}_a$ is less or equal to its number of columns. In order to grant the imposition of a desired order n, the LMFD denominator is normalized to its maximum power and written as:

$$\mathbf{H}_a(p) = \mathbf{D}^{-1}(p)\,\mathbf{N}(p) = \left(\mathbf{I}\,p^n + \sum_{i=0}^{n-1} \mathbf{D}_i\,p^i\right)^{-1} \left(\sum_{i=0}^{n+2} \mathbf{N}_i\,p^i\right) \tag{3.60}$$

to which, discarding the number of gusts, usually much smaller than N, we can roughly associate $(2n+3)N^2$ unknowns. Applying a matrix polynomial division we have:

$$\mathbf{H}_a(p) = \mathbf{E}_0 + p\mathbf{E}_1 + p^2\mathbf{E}_2 + \left(\mathbf{I}\,p^n + \sum_{i=0}^{n-1} \mathbf{D}_i\,p^i\right)^{-1} \left(\sum_{i=0}^{n-1} \mathbf{R}_i\,p^i\right) \tag{3.61}$$

where $\mathbf{D}_i$ and $\mathbf{R}_i$ are the quotient and remainder terms related to Eq. (3.60). Thus, the transfer matrix of the state space is:

$$\mathbf{H}_a = \mathbf{E}_{0a} + p\mathbf{E}_{1a} + p^2\mathbf{E}_{2a} + \mathbf{C}_a\,(p\mathbf{I} - \mathbf{A}_a)^{-1}\,\mathbf{B}_a \tag{3.62}$$

with:

$$\mathbf{A}_a = \begin{bmatrix} -\mathbf{D}_{n-1} & \mathbf{I} & \mathbf{0} & \dots & \mathbf{0} \\ -\mathbf{D}_{n-2} & \mathbf{0} & \mathbf{I} & \dots & \mathbf{0} \\ \vdots & \vdots & \vdots & \ddots & \vdots \\ -\mathbf{D}_1 & \mathbf{0} & \mathbf{0} & \dots & \mathbf{I} \\ -\mathbf{D}_0 & \mathbf{0} & \mathbf{0} & \dots & \mathbf{0} \end{bmatrix}, \quad \mathbf{B}_a = \begin{bmatrix} \mathbf{R}_{n-1} \\ \mathbf{R}_{n-2} \\ \vdots \\ \mathbf{R}_1 \\ \mathbf{R}_0 \end{bmatrix}, \quad \mathbf{C}_a^T = \begin{bmatrix} \mathbf{I} \\ \mathbf{0} \\ \vdots \\ \mathbf{0} \\ \mathbf{0} \end{bmatrix} \tag{3.63}$$

The missing matrices $\mathbf{B}_{1a}$ and $\mathbf{B}_{2a}$, set forth in the previous section, will be recovered in the finishing part of our procedure, as described immediately below. A relatively high order LMFD, while granting a high initial precision fit, will give rise to uncontrollable/unobservable input output paths, because of numerical issues. Therefore the triple $\mathbf{C}_a$, $\mathbf{A}_a$, $\mathbf{B}_a$ of Eq. (3.63) is subsequently reduced to the lowest possible order by using either a Hankel [99, 217] or balanced transformation [218]. Carrying out such a reduction with a third-second order dynamic residualization [153] will eventually bring the missing $\mathbf{B}_{1a}$ term of Eq. (2.7), so recovering the expected fitting structure:

$$\mathbf{H}_a = \mathbf{E}_{0a} + p\mathbf{E}_{1a} + p^2\mathbf{E}_{2a} + \mathbf{C}_a \left(p\mathbf{I} - \mathbf{A}_a\right)^{-1} \left(\mathbf{B}_{0a} + p\mathbf{B}_{1a} + p^2\mathbf{B}_{2a} + p^3\mathbf{B}_{3a}\right) \tag{3.64}$$

The full recovery of the above third-second order residualization will keep the couple $\mathbf{C}_a$, $\mathbf{A}_a$ from the balanced reduction and proceed by identifying all the matrices $\mathbf{E}_a$ and $\mathbf{B}_a$ through a final overall linear LS matrix refitting of Eq. (3.64). A precise fit at zero is imposed through an exact collocation of $\mathbf{H}_a(0)$, $\mathbf{H}'_a(0)$ and $\mathbf{H}''_a(0)$, where the prime denotes the derivative with respect to p:

$$\mathbf{E}_{0a} = \mathbf{H}_a(0) + \mathbf{C}_a\mathbf{A}_a^{-1}\mathbf{B}_{0a} \tag{3.65a}$$

$$\mathbf{E}_{1a} = \mathbf{H}'_a(0) + \mathbf{C}_a\mathbf{A}_a^{-1}\mathbf{B}_{1a} - \mathbf{C}_a\mathbf{A}_a^{-2}\mathbf{B}_{0a} \tag{3.65b}$$

$$\mathbf{E}_{2a} = \frac{1}{2}\mathbf{H}''_a(0) + \mathbf{C}_a\mathbf{A}_a^{-1}\mathbf{B}_{2a} - \mathbf{C}_a\mathbf{A}_a^{-2}\mathbf{B}_{1a} + \mathbf{C}_a\mathbf{A}_a^{-3}\mathbf{B}_{0a} \tag{3.65c}$$

Remarking that $\mathbf{C}_a$ and $\mathbf{A}_a$ are known and $\mathbf{H}_a(0)$, $\mathbf{H}'_a(0)$ and $\mathbf{H}''_a(0)$ are real valued [148], the final form results:

$$\begin{aligned} \mathbf{H}_a - \mathbf{H}_a(0) - p\mathbf{H}'_a(0) - p^2\frac{1}{2}\mathbf{H}''_a(0) = {} & \mathbf{C}_a \left[\left(p\mathbf{I} - \mathbf{A}_a\right)^{-1} + \mathbf{A}_a^{-1} - p\mathbf{A}_a^{-2} + p^2\mathbf{A}_a^{-3}\right] \mathbf{B}_{0a} \\ & + p\,\mathbf{C}_a \left[\left(p\mathbf{I} - \mathbf{A}_a\right)^{-1} + \mathbf{A}_a^{-1} - p\mathbf{A}_a^{-2}\right] \mathbf{B}_{1a} \\ & + p^2\mathbf{C}_a \left[\left(p\mathbf{I} - \mathbf{A}_a\right)^{-1} + \mathbf{A}_a^{-1}\right] \mathbf{B}_{2a} \\ & + p^3\mathbf{C}_a \left(p\mathbf{I} - \mathbf{A}_a\right)^{-1} \mathbf{B}_{3a} \end{aligned} \tag{3.66}$$

which has all of the unknown matrices at the right. It is thus ready for a final linear least squares matrix fit based on the solution of the overdetermined system obtained by collocating Eq. (3.66) along jk, so to match all of the available $\mathbf{H}_a(k)$. The just presented approach makes useless any further overall nonlinear optimization, which was instead found useful in a previous closely related work [148].

It is remarked that the structure of Eq. (3.66) is justified by observing the presented

Galërkin-projection formulation (section 3.1.2), where because of the residualization applied, the aerodynamic transfer matrix has a third-second order residualization (Eq. (3.38)).

Equation (3.66) (or Eq. (3.64)) may eventually be translated back to Eq. (3.55) form as:

$$\begin{aligned}\mathbf{H}_a = \; & [\mathbf{E}_{0a} + \mathbf{C}_a(\mathbf{B}_{1a} + \mathbf{A}_a(\mathbf{B}_{2a} + \mathbf{A}_a\mathbf{B}_{3a}))] + p\,(\mathbf{E}_{1a} + \mathbf{C}_a(\mathbf{B}_{2a} + \mathbf{A}_a\mathbf{B}_{3a})) \\ & + p^2(\mathbf{E}_{2a} + \mathbf{C}_a\mathbf{B}_{3a}) + \mathbf{C}_a(p\mathbf{I} + \mathbf{A}_a)^{-1}\,[\mathbf{B}_{0a} + \mathbf{A}_a(\mathbf{B}_{1a} + \mathbf{A}_a(\mathbf{B}_{2a} + \mathbf{A}_a\mathbf{B}_{3a}))]\end{aligned} \tag{3.67}$$

We can now describe the most demanding part of the LS fitting of an asymptotically stable parent LMFD, with the unknown matrices $\mathbf{N}_i$ and $\mathbf{D}_i$, resulting from the overdetermined nonlinear system of equations obtained by collocating:

$$\mathbf{H}_a(k) = \mathbf{D}^{-1}(jk)\mathbf{N}(jk) \tag{3.68}$$

Such a fitting will cover all of the available $\mathbf{H}_a$, with the exact collocation of $\mathbf{H}_a(0)$ and $\mathbf{H}'_a(0)$ being translated into the constraints:

$$\mathbf{N}_0 = \mathbf{D}_0\mathbf{H}_a(0) \tag{3.69a}$$

$$\mathbf{N}_1 = \mathbf{D}_0\mathbf{H}'_a(0) + \mathbf{D}_1\mathbf{H}_a(0) \tag{3.69b}$$

An alternative way for enforcing such zero frequency constraints is to apply an appropriate high weighting at $k = 0$ and the point next to it. In view of solving the related nonlinear optimization through a Gauss-Newton scheme the collocated fitting is cast in an incremented linearized matrix form:

$$-\mathbf{D}^{-1}(\bar{p})\Delta\mathbf{D}(\bar{p})\mathbf{D}^{-1}(\bar{p})\mathbf{N}(p) + \mathbf{D}^{-1}(\bar{p})\Delta\mathbf{N}(\bar{p}) = \mathbf{H}_a(\bar{p}) - \mathbf{D}^{-1}(\bar{p})\mathbf{N}(\bar{p}) \tag{3.70}$$

where $\bar{p}$ indicates any collocation point jk and the identity, $\partial(\mathbf{D}^{-1}) = -\mathbf{D}^{-1}(\partial\mathbf{D})\mathbf{D}^{-1}$, has been used. No problem is expected by having $\mathbf{D}^{-1}$ in our incremented form. Indeed the aerodynamic subsystem must be asymptotically stable, and we will strive to keep it like that in our iterated solution. The unknown incremental matrices, $\Delta\mathbf{D}(p)$ and $\Delta\mathbf{N}(p)$, are given by:

$$\begin{aligned}\Delta\mathbf{D}(p) &= \sum_{i=0}^{n-1}\Delta\mathbf{D}_i\,p^i = \begin{bmatrix}\Delta\mathbf{D}_0 & \Delta\mathbf{D}_1 & \cdots & \Delta\mathbf{D}_{n-1}\end{bmatrix}\begin{bmatrix}\mathbf{I}\\ p\mathbf{I}\\ \vdots\\ p^{n-1}\mathbf{I}\end{bmatrix} \\ \Delta\mathbf{N}(p) &= \sum_{i=0}^{n+2}\Delta\mathbf{N}_i\,p^i = \begin{bmatrix}\Delta\mathbf{D}_0 & \Delta\mathbf{D}_1 & \Delta\mathbf{N}_2 & \cdots & \Delta\mathbf{N}_{n+2}\end{bmatrix}\begin{bmatrix}\mathbf{H}_a(0) + p\mathbf{H}'_a(0)\\ p\mathbf{H}_a(0)\\ p^2\mathbf{I}\\ \vdots\\ p^{n+2}\mathbf{I}\end{bmatrix}\end{aligned} \tag{3.71}$$

with $\Delta\boldsymbol{\theta}^T = \left[\Delta\mathbf{D}_0^T, \ldots, \Delta\mathbf{D}_{n-1}^T,\, \Delta\mathbf{N}_2^T, \ldots, \Delta\mathbf{N}_{n+2}^T\right]$ and the zero-frequency constraints

identically satisfied. The incremental system is then rewritten as:

$$\mathbf{D}^{-1}(\bar{p})\overline{\Delta\mathbf{D}}\,\mathbf{J}_D(\bar{p}) + \mathbf{D}^{-1}(\bar{p})\overline{\Delta\mathbf{N}}\,\mathbf{J}_N(\bar{p}) = \mathbf{H}_a - \mathbf{D}^{-1}(\bar{p})\mathbf{N}(\bar{p}) \tag{3.72}$$

with:

$$\mathbf{J}_D(p) = \begin{bmatrix} \mathbf{H}_a(0) + p\mathbf{H}'_a(0) - \mathbf{D}^{-1}(p)\mathbf{N}(p) \\ p\left(\mathbf{H}_a(0) - \mathbf{D}^{-1}(p)\mathbf{N}(p)\right) \\ -p^2\mathbf{D}^{-1}(p)\mathbf{N}(p) \\ \vdots \\ -p^{n+2}\mathbf{D}^{-1}(p)\mathbf{N}(p) \end{bmatrix} \qquad \mathbf{J}_N(p) = \begin{bmatrix} p^2\mathbf{I} \\ \vdots \\ p^{n+2}\mathbf{I} \end{bmatrix} \tag{3.73}$$

and the unknown matrix increments

$$\overline{\Delta\mathbf{D}} = [\Delta\mathbf{D}_0, \ldots, \Delta\mathbf{D}_{n-1}] \qquad \text{and} \qquad \overline{\Delta\mathbf{N}} = [\Delta\mathbf{N}_2, \ldots, \Delta\mathbf{N}_{n+2}] \tag{3.74}$$

Unfortunately substantial difficulties arise for a straightforward application of Gauss-Newton iterations, being the unknown parameter matrix $\Delta\mathbf{D}$ in the first term of Eq. (3.70) (or similarly $\overline{\Delta\mathbf{D}}$ in Eq. (3.72)) multiplied both at their left and right sides, whereas it would be easier to solve the associated linearized system of equations if rewritten in a more standard form of the type:

$$\mathbf{J}\Delta\boldsymbol{\theta} = \mathbf{H}_a - \mathbf{D}^{-1}\mathbf{N} \tag{3.75}$$

with $\mathbf{J}$ being the Jacobian matrix matching $\Delta\boldsymbol{\theta}$. To provide such a structure we can devise three possible schemes:

LS1: Reformulate the incremented linear matrix form through the Kronecker product identity [219], $\mathrm{vec}(\mathbf{AXB}) = (\mathbf{B}^T \otimes \mathbf{A})\mathrm{vec}(\mathbf{X})$, combining a vectorization of the unknown matrices, $\mathrm{vec}(\cdot)$, which stacks their columns on top of each other, with the Kronecker product operator, $\otimes$ [220, 221]. Therefore Eq. (3.72) becomes the following sparse system of equations:

$$\mathbf{J}_D^T(\bar{p})\otimes\mathbf{D}^{-1}(\bar{p})\mathrm{vec}\left(\overline{\Delta\mathbf{D}}\right)+\mathbf{J}_N^T(\bar{p})\otimes\mathbf{D}^{-1}(\bar{p})\mathrm{vec}\left(\overline{\Delta\mathbf{N}}\right) = \mathrm{vec}\left(\mathbf{H}_a - \mathbf{D}^{-1}(\bar{p})\mathbf{N}(\bar{p})\right) \tag{3.76}$$

Unfortunately the solution of the above equation cannot exploit fast Kronecker solvers [222–224], leaving a sparse linear system with about $(2n+1)N^2$ unknowns. However, even exploiting such a sparsity the related iterated LS solution time will not match that of the immediately following dense techniques. We remark that the above scheme leads to the minimization of the sum of the squares of each term of the residual matrix.

LS2: The matrix $\mathbf{D}^{-1}(p)$ of Eq. (3.72) may be rewritten in terms of the adjugate matrix: $\mathbf{D}^{-1} = \frac{1}{\det(\mathbf{D})}\mathrm{adj}(\mathbf{D})$, so that, we have:

$$\frac{1}{\det(\mathbf{D}(\bar{p}))}\mathbf{J}_D^T(\bar{p})\,\overline{\Delta\mathbf{D}}^T + \frac{1}{\det(\mathbf{D}(\bar{p}))}\mathbf{J}_N(\bar{p})^T\,\overline{\Delta\mathbf{N}}^T = \left[\mathbf{H}_a - \mathbf{D}^{-1}(\bar{p})\mathbf{N}(\bar{p})\right]^T \mathrm{adj}^{-T}(\mathbf{D}(\bar{p})) \tag{3.77}$$

The adjugate calculation is avoided by reverting the just adopted inversion formula, ending with:

$$\frac{1}{\det(\mathbf{D}(\bar{p}))}\mathbf{J}_D^T(\bar{p})\,\overline{\Delta\mathbf{D}}^T + \frac{1}{\det(\mathbf{D}(\bar{p}))}\mathbf{J}_N(\bar{p})^T\,\overline{\Delta\mathbf{N}}^T = \frac{1}{\det(\mathbf{D}(\bar{p}))}\left[\mathbf{H}_a - \mathbf{D}^{-1}(\bar{p})\mathbf{N}(\bar{p})\right]^T\mathbf{D}^T(\bar{p}) \quad (3.78)$$

This modified Gauss-Newton scheme will likely require more iterations than those needed by the stricter Gauss-Newton form provided by LS1. Nevertheless it is far more efficient, leading to the solution of N dense systems of $(2n+1)N$ equations, all of them having the same full, but N times smaller, matrix of coefficients. Despite the significant simplification it provides, this approach, thanks to the $\frac{1}{\det(\mathbf{D}(\bar{p}))}$ weighting, will progress toward a final solution very close to that of LS1.

LS3: Equation (3.72) may be premultiplied by $\mathbf{D}(\bar{p})$ and transposed to obtain:

$$\mathbf{J}_D^T(\bar{p})\,\overline{\Delta\mathbf{D}}^T + \mathbf{J}_N^T(\bar{p})\,\overline{\Delta\mathbf{N}}^T = \mathbf{H}_a^T\,\mathbf{D}^T(\bar{p}) - \mathbf{N}^T(\bar{p}) \quad (3.79)$$

This is the simpler way of setting our original incremental formulation into the form of a standard linear system of matrix equations, its operation count and solution cost being the same as LS2. Nonetheless it has a residual right hand side which can be significantly different from the original one we would like to minimize. Thus, while keeping its cost to convergence well below that of LS1, it may likely converge to a somewhat different optimal solution.

With the previous recipes our nonlinear LS solution proceeds with the Levenberg-Marquardt method [225, 226]:

$$(\mathbf{J}^T\mathbf{J} + \lambda\,\mathcal{D}(\mathbf{J}^T\mathbf{J}))\overline{\Delta\boldsymbol{\theta}} = \mathbf{J}^T\mathbf{r} \quad (3.80)$$

where λ is a non-negative damping factor, to be adjusted at each iteration, with the unknown parameters being either: $\overline{\Delta\boldsymbol{\theta}}^T = \left[\mathrm{vec}^T\left(\overline{\Delta\mathbf{D}}\right), \mathrm{vec}^T\left(\overline{\Delta\mathbf{N}}\right)\right]$, for LS1, or $\overline{\Delta\boldsymbol{\theta}}^T = \left[\overline{\Delta\mathbf{D}}, \overline{\Delta\mathbf{N}}\right]$ for LS2 and LS3, the Jacobian matrix $\mathbf{J}$ and the residual $\mathbf{r}$ for the three methods being respectively:

$$\mathbf{J} = \begin{cases} \begin{bmatrix}\mathbf{J}_D^T(\bar{p}) & \mathbf{J}_N^T(\bar{p})\end{bmatrix} \otimes \mathbf{D}^{-1}(\bar{p}) \\ \begin{bmatrix}\mathbf{J}_D^T(\bar{p}) & \mathbf{J}_N^T(\bar{p})\end{bmatrix} \det(\mathbf{D}(\bar{p}))^{-1} \\ \begin{bmatrix}\mathbf{J}_D^T(\bar{p}) & \mathbf{J}_N^T(\bar{p})\end{bmatrix} \end{cases} \quad (3.81a)$$

$$\mathbf{r} = \begin{cases} \mathrm{vec}\left(\mathbf{H}_a - \mathbf{D}^{-1}(\bar{p})\mathbf{N}(\bar{p})\right) \\ \left[\mathbf{H}_a - \mathbf{D}^{-1}(\bar{p})\mathbf{N}(\bar{p})\right]^T\mathbf{D}^T(\bar{p})\det(\mathbf{D}(\bar{p}))^{-1} \\ \mathbf{H}_a^T\mathbf{D}^T(\bar{p}) - \mathbf{N}^T(\bar{p}) \end{cases} \quad (3.81b)$$

The initial trial matrices can be obtained by starting any of the three nonlinear Gauss-Newton schemes with null matrices, and LS3. The order n of the MFD approximations

generally used is rarely greater than two/three. Therefore, using LS2/LS3, the number of unknowns is on the order of hundreds, even with a hundred modes. Nonetheless it may be worthwhile to end our identification with a few iterations of the sparse LS1, with constant $\mathbf{J}$, which is anyhow the best way of working with LS1. Using double precision floating point no significant ill conditioning problem is expected, even when n is somewhat higher than two/three [227]. Therefore a very precise model will be supplied to the final identification, without relying on any optimization technique, often involving many thousands of unknowns and therefore a larger computational cost [163, 208, 228, 229].

The asymptotic stability of the state matrix $\mathbf{A}_a$, of Eq. (3.63) [163], is guaranteed at each iteration by [230]:

- determining the full eigensolution, eigenvectors, $\mathbf{V}$, and eigenvalues, $\mathcal{D}(\mathbf{e})$, of $\mathbf{A}_a$;
- setting any real part of the eigenvalues greater than an acceptable negative threshold to that very threshold value, so making $\mathcal{D}(\mathbf{e})$ stable;
- recovering $\mathbf{A}_a = \mathbf{V}\mathcal{D}(\mathbf{e})\mathbf{V}^{-1}$, so maintaining the block structure of $\mathbf{A}_a$ unchanged,
- extracting from $\mathbf{A}_a$, by simple inspection, the new $\mathbf{D}_i$ to be used for the next iteration.

Chapter 4

Reducing Gust Modeling Complexity

An alternative gust formulation, which avoids the embedding of the delay operator in the transfer matrix associated with gust penetration, is here presented. By using gust specific compatible basis functions, dubbed gust modes, such an approach treats gusts much as structural motions attached to the aircraft in the same way as if they were structural modes. Therefore it allows gust/turbulence analyses even if the unsteady aerodynamic tools available can provide only motion related GAFs.

4.1 Gust modeling in computational aeroelasticity

The prediction of unsteady loads caused by atmospheric effects like gusts and atmospheric turbulence is essential for the aircraft design and development, both for the structural design as well as for the layout of the control surfaces and the flight control system aiming to alleviate these additional loads. Within the framework of CFD-based aeroelasticity, gust modeling is a significant technical challenge. In the following subsections some approaches for gust modeling are described.

4.1.1 Resolved Gust Approach

The Resolved Gust Approach (RGA) perform the modeling of atmospheric disturbances and incoming gusts by prescribing unsteady boundary conditions at the inflow and far-field boundaries of the discretized computational fluid domain [231]. Small modifications on the non-reflecting far field boundary condition are required, where the velocity components imposed at the outer side of the discretized domain have to be specified as a function of space and time. Therefore the gust is resolved in the flow field, allowing the simulations of the mutual interaction between the aircraft and the gust, i.e. the influence of the gust on the aircraft loads so as the feedback of the aircraft aerodynamics on the shape of the gust. This approach requires the use of high spatial resolution, i.e. very fine computational meshes, so avoiding too big numerical losses due to the numerical dissipation during the traveling motion of the gust from the inflow boundary to the aircraft.

In order to satisfy this constraint a possible solution may be the use of a chimera overset grid approach [232,233], involving the decomposition of a complex geometry into a number of geometrically and topologically simple overlapping grids to which the flow solution process is applied. The component meshes, which are well suited for vortex dominated flows, can be embedded into Cartesian background meshes. This allows keeping all of the advantages associated with structured data [234], including highly efficient implicit flow solvers, vectorization, and parallelism. Therefore using a chimera approach no remeshing techniques are required and grid generation efforts are reduced, thus allowing easily to perform parametric gust response simulations for different shapes and relative positions of the gust with respect to the aircraft.

In Ref. [231] an Euler simulation is performed using a a chimera technique [231, 235] embedding very fine Cartesian grids, named vortex transport meshes, into the main computational mesh (an hybrid structured/unstructured mesh around the body, placed into a Cartesian background mesh). These high resolution Cartesian meshes were moved with the convection velocity of the flow in order to transport the gust from the inflow boundary to the aircraft geometry,

Higher order spatial discretization schemes together with a local grid refinement strategy may be used as an alternative to chimera grids.

4.1.2 Disturbance Velocity Approach

The gust modeled as a far field boundary condition dissipated in large cells. So, in order to reduce the numerical effort due to the requirement of using fine grids, different methods have been searched as possible alternatives to the full resolution of gust-aircraft flow field with the RGA.

A transpiration technique may be used, where the boundary condition on the solid wall of the aircraft surface are modified introducing disturbance velocities representing the traveling atmospheric effects [236]. The boundary condition changes, for example for Euler equations, from

$$\boldsymbol{v}(\boldsymbol{x},t)\cdot\boldsymbol{n}|_{\mathcal{S}_w}=0 \qquad \text{to} \qquad (\boldsymbol{v}(\boldsymbol{x},t)-\mathbf{v}_{\mathrm{g}}(\boldsymbol{x},t))\cdot\boldsymbol{n}|_{\mathcal{S}_w}=0 \tag{4.1}$$

where $\boldsymbol{v}$ is the flow velocity, $\mathbf{v}_{\mathrm{g}}$ the velocity induced by the gust at the boundary surface wall $\mathcal{S}_w$ having unit normal vector $\boldsymbol{n}$. For this simplified method, grid refinement is not necessary. However loads prediction are good just for small angles of attack with a weak or absent shock waves [236].

A generalization of the transpiration concept leading to better results, may be applied by means of an extension of the ALE formulation [71], which is normally used for moving grids by incorporating the grid velocity in the flux function at any place in the domain. This technique, named disturbance velocity approach (DVA) [235], is a very efficient technique in computational aeroelasticity to model the atmospheric effects perturbing an aircraft. Therefore the disturbance velocity approach requires just little modifications of the standard finite-volume-type flux balancing of flow solvers based on the FP/Euler/RANS equations, where a new velocity decomposition is applied. So the gust is imposed by modifying

the fluxes from:

$$\left\{\begin{array}{c}\rho\boldsymbol{v}\cdot\boldsymbol{n}\\ \rho\boldsymbol{v}\left(\boldsymbol{v}\cdot\boldsymbol{n}\right)+p\boldsymbol{n}\\ \rho E^{\mathrm{t}}\boldsymbol{v}\cdot\boldsymbol{n}+p\boldsymbol{v}\cdot\boldsymbol{n}\end{array}\right\} \quad \text{to} \quad \left\{\begin{array}{c}\rho\left(\boldsymbol{v}-\mathbf{v}_{\mathrm{g}}\right)\cdot\boldsymbol{n}\\ \rho\boldsymbol{v}\left(\left(\boldsymbol{v}-\mathbf{v}_{\mathrm{g}}\right)\cdot\boldsymbol{n}\right)+p\boldsymbol{n}\\ \rho E^{\mathrm{t}}\left(\boldsymbol{v}-\mathbf{v}_{\mathrm{g}}\right)\cdot\boldsymbol{n}+p\boldsymbol{v}\cdot\boldsymbol{n}\end{array}\right\} \tag{4.2}$$

being ρ the density, p the pressure, and E^{t} the total energy per unit mass.

Thus considering a flow solver with ALE formulation, the DVA is obtained by superimposing an additional disturbance velocity field $\mathbf{v}_{\mathrm{g}}(\boldsymbol{x},t)$ to the boundary cell face velocity $\boldsymbol{v}_{\mathrm{b}}(\boldsymbol{x},t)$, so that the convection velocity $(\boldsymbol{v}-\boldsymbol{v}_{\mathrm{b}})$ across the cell interface of a control volume will become $(\boldsymbol{v}-\boldsymbol{v}_{\mathrm{b}}-\mathbf{v}_{\mathrm{g}})$. The resulting extended ALE formulation for gust modeling will be:

$$\frac{d}{dt}\int_{\Omega(t)}\mathbf{x}\,d\Omega+\oint_{\mathcal{S}(t)}\left[\mathbf{f}(\mathbf{x})-\mathbf{x}\left(\boldsymbol{v}_{\mathrm{b}}-\mathbf{v}_{\mathrm{g}}\right)\right]\cdot\boldsymbol{n}\,d\mathcal{S}+\oint_{\mathcal{S}(t)}\mathbf{d}(\mathbf{x})\cdot\boldsymbol{n}\,d\mathcal{S}=0,\qquad\forall\Omega(t)\subseteq\mathbb{R}^{d} \tag{4.3}$$

with thee shape of the gust $\mathbf{v}_{\mathrm{g}}(\boldsymbol{x},t)$ specified as a function of the spatial coordinate $\boldsymbol{x}$ and time t, and the other quantities already defined in Eq. (1.11).

The formulation allows easily to handle any type of atmospheric disturbance (vertical and lateral, single and sequences, uniform and nonuniform gusts and stochastic turbulence) by simply providing its spatial and temporal law. Simulations have been performed for simple airfoils as well as complex cases of industrial relevance, a generic fighter encountering a lateral gust and an aeroelastic analysis of a commercial aircraft in cruise configuration perturbed by a vertical gust [6]. Despite the mutual interaction between the gust and the aircraft is disregarded and cannot be simulated, the DVA gives good results for the forces and moments, capturing the gust effects on the aircraft as good as with the resolved gust approach. A prediction error is expected just for gusts of short wavelength [235].

The efficiency of the approach arises from the fact that no additional mesh refinement or higher-order CFD analysis is needed. The approach allows using normal grid techniques, for example unstructured grids, and standard mesh resolutions and discretization adopted in the regular CFD simulations of aircraft in cruise flight conditions. So a much less computational effort is required with respect to the RGA, which needs very high spatial mesh resolution so that the vortices modeling the gust are not destroyed by numerical dissipation while being transported towards the aircraft.

4.2 Gust modeling approximation via gust modes

A novel method based on the use of spatially fixed shape functions is developed for gust modeling. The approach avoid building an aerodynamic ROM for each different gust profile case considered in the loads database, thus reducing the overall number of gust simulations required in the gust loads analysis process. The method approximates the gust profile traveling towards the aircraft using a series of disturbance velocity shape functions fixed in space, named gust modes. The projected surface covered by the aircraft is further divided in aerodynamic zones, named gust patches, defining the nodes over which the generalized coordinates associated to the gust modes are, in a least-squares sense, interpolated. An impulse response (or its analogue counterpart in the frequency domain, a transfer

function) is obtained from each of the gust modes forcing the aerodynamic model. Being the gust modes spatially fixed, the traveling contribution of the gust running towards the aerodynamic model, as well as the true gust profile shape, is devolved to the generalized coordinates, which are calculated as a post-processing through a least squares interpolation of the gust profile on the gust patches. Different kind of gust profiles may be analyzed without effectively run a simulation for the gusts, but just by using the response of the gust modes.

4.2.1 A Preamble on Boundary Conditions Related to Gusts

Assuming a linearized unsteady aerodynamic formulation, we consider a generic gust field penetrated along the aircraft absolute x coordinate, directed as V_∞, as depicted in Fig. 4.1. Adopting the usual frozen gust formulation, we write a gust velocity profile in the absolute reference system, as:

$$\mathbf{V}_g(x,y,z,t) = \mathbf{N}_{v_g}(x,y,z)\,\mathbf{v}_g(\xi) = \mathbf{N}_{v_g}(x,y,z)\,\mathbf{v}_g(V_\infty t - (x-\mathbf{x}_0)) \tag{4.4}$$

so shaping the frozen patches $\mathbf{N}_{v_g}(x,y,z)$ with gust profiles $\mathbf{v}_g$ progressing along x and having a per patch reference entry point collected in the vector $\mathbf{x}_0$, with the notational freedom of using $\mathbf{v}_g(V_\infty t - (x - \mathbf{x}_0))$ to synthesize all of the components $v_{g_i}(V_\infty t - (x - x_{0_i}))$. The adoption of gust patches can be useful both for modeling non uniform gust distributions and to obtain smoother GAFs [168]. Accepting the further notational freedom of

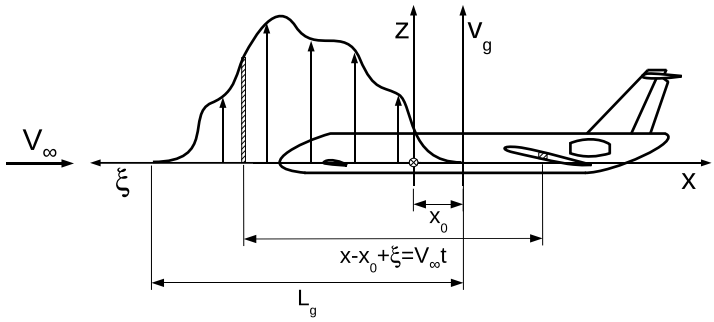

Figure 4.1: *Aircraft penetrating a gust profile.*

using the same symbols for time and frequency domains by explicitly stating the related dependence, we write the Laplace transform of Eq. (4.4)

$$\mathbf{V}_g(x,y,z,s) = \mathbf{N}_{v_g}(x,y,z)\,\mathcal{D}\left(e^{-s\frac{x-\mathbf{x}_0}{V_\infty}}\right)\mathbf{v}_g(s) \tag{4.5}$$

Thus, considering an inviscid flow for sake of brevity, the local gust angle of attack α_g, i.e. the local boundary condition associated to a gust, is:

$$\alpha_g(x,y,z,.) = \frac{\mathbf{n}_0^T(x,y,z)\,\mathbf{V}_g(x,y,z,.)}{V_\infty} \tag{4.6}$$

where the use of the undeformed unit vector normal to the aircraft surface, $\mathbf{n}_0$, is consistent with the assumed linearized formulation and the dummy dots $(.)$ can be either t or s.

In this work we will adopt also a penetration-less gust model, where the local gust angle of attack α_g is approximated with a complete expansion of standing gust modes:

$$\alpha_g(x, y, z, t) = \mathbf{N}_g(x, y, z)\, \mathbf{q}_g(t) \tag{4.7}$$

with $\mathbf{N}_g$ containing the gust shape functions, as depicted in Fig. 4.2, and $\mathbf{q}_g$ their amplitudes. Such an approach can calculate unsteady gust forces using the very same formulation adopted for flutter calculations, with the embedded possibility of treating heterogeneous gust fields, e.g. along large wing spans, whenever such an option is not available in the aerodynamic formulation at hand[1]. Each gust mode $\mathbf{N}_g$ will generate a column of the aerodynamic transfer matrix, leaving the delayed gust modulation amplitude to its input $\mathbf{q}_g$. So the penetration-less approach allows to calculate the generalized gust forces much in the same way as any structural mode. Clearly none of the two gust representations have their own generalized force, but serve only to augment those associated to the motion degrees of freedom.

The true contribution of any gust running along an aircraft is evaluated afterwards, by imposing the equality of the expressions of the related angles of attack:

$$\mathbf{N}_g(x, y, z)\, \mathbf{q}_g(.) = \frac{\mathbf{n}_0^T(x, y, z)\, \mathbf{V}_g(x, y, z, .)}{V_\infty} \tag{4.8}$$

Being difficult to find a penetration-less expansion satisfying the above equation identically, an LS approximation is used. It leads to the solution of the following system of linear equations:

$$\begin{aligned} &\int_{S_0} \mathbf{N}_g^T(x, y, z)\mathbf{N}_g(x, y, z)dS\, \mathbf{q}_g(t) \\ &\qquad = \frac{1}{V_\infty} \int_{S_0} \mathbf{N}_g^T(x, y, z)\, \mathbf{n}_0^T(x, y, z)\, \mathbf{N}_{v_g}(x, y, z)\mathbf{v}_g(V_\infty t - [x - \mathbf{x}_0])dS \end{aligned} \tag{4.9}$$

where S_0 is the undeformed reference surface penetrating the gust, so that:

$$\mathbf{q}_g(t) = \frac{1}{V_\infty} \mathbf{A}_g^{-1}\, \mathbf{b}_g(t) \tag{4.10}$$

being:

$$\mathbf{A}_g = \int_{S_0} \mathbf{N}_g^T\, \mathbf{N}_g dS \tag{4.11a}$$

$$\mathbf{b}_g(t) = \int_{S_0} \mathbf{N}_g^T\, \mathbf{n}_0^T\, \mathbf{N}_{v_g} \mathbf{v}_g dS \tag{4.11b}$$

[1] For example, in Nastran $\mathbf{q}_g$ can be established through extra points, with α_g defined by sampling $\mathbf{N}_g$ at the aerodynamic collocation points (D1JE) [166]. Thus the related generalized aerodynamic forces are obtained as if they were due to structural motions, either for more general gusts or for aerodynamic formulations not supporting their evaluation, without touching any aeroelastic solution sequence. See [237] for an alternative approach within the same context.

with $\mathbf{b}_g(t)$ changing at each time instant. Passing to the complex frequency s we have:

$$\int_{S_0} \mathbf{N}_g^T(x,y,z)\mathbf{N}_g(x,y,z)dS\,\mathbf{q}_g(s) = \frac{1}{V_\infty}\int_{S_0} \mathbf{N}_g^T(x,y,z)\,\mathbf{n}_0^T(x,y,z)\,\mathbf{N}_{v_g}(x,y,z)\,\mathcal{D}\left(\mathrm{e}^{-s\frac{x-\mathbf{x}_0}{V_\infty}}\right)dS\,\mathbf{v}_g(s) \quad (4.12)$$

thus getting:

$$\mathbf{q}_g(s) = \mathbf{A}_g^{-1}\,\mathbf{b}_g(s)\,\frac{\mathbf{v}_g(s)}{V_\infty} \quad (4.13)$$

with:

$$\mathbf{b}_g(s) = \int_{S_0} \mathbf{N}_g^T\,\mathbf{n}_0^T\,\mathbf{N}_{v_g}\mathcal{D}\left(\mathrm{e}^{-s\frac{x-\mathbf{x}_0}{V_\infty}}\right)dS \quad (4.14)$$

Therefore the gust angle of attack in the frequency domain is:

$$\alpha_g(x,y,z,s) = \left[\mathbf{N}_g(x,y,z)\mathbf{A}_g^{-1}\,\mathbf{b}_g(s)\right]\frac{\mathbf{v}_g(s)}{V_\infty} \quad (4.15)$$

Explicitly rewriting Eq. (4.6) as:

$$\alpha_g(x,y,z,s) = \left[\mathbf{n}_0^T(x,y,z)\,\mathbf{N}_{v_g}(x,y,z)\,\mathcal{D}\left(e^{-s\frac{x-\mathbf{x}_0}{V_\infty}}\right)\right]\frac{\mathbf{v}_g(s)}{V_\infty} \quad (4.16)$$

two functionally equivalent gust boundary conditions are obtained, with the penetration-less scheme providing a space filtered delay modulation, having an x resolution hard wired to the chosen shape functions $\mathbf{N}_g(x,y,z)$. Using Eqs. (4.13) and (4.15), the above equivalence allows to easily translate the penetration-less generalized forces into those related to $\mathbf{v}_g$. Indeed the generalized coordinates $\mathbf{q}_g(t)$ and the gust velocity $\mathbf{v}_g(t)$ provides the following two gust transfer matrices:

$$\mathbf{Q}_{ag}(p,M_\infty) = q_\infty\mathbf{H}_{av_g}(p,M_\infty)\,\frac{\mathbf{v}_g(p)}{V_\infty} \quad (4.17a)$$

$$\mathbf{Q}_{ag}(p,M_\infty) = q_\infty\mathbf{H}_{aq_g}(p,M_\infty)\,\mathbf{q}_g(p) \quad (4.17b)$$

hence it is possible to translate the penetration-less approach into the delayed gust penetration form using Eq. (4.13) as:

$$\mathbf{H}_{av_g}(p,M_\infty) = \mathbf{H}_{aq_g}(p,M_\infty)\mathbf{A}_g^{-1}\,\mathbf{b}_g(p) \quad (4.18)$$

4.2.2 Practical Clues for Gust and Turbulence Responses

A concern is often set forth [202] in relation to adopting a single finite state identification of the GAFs related to structural motion and gust, because the oscillating contributions associated to the gust penetration may lead to using an undue number of states to ensure an adequate precision. In practice, even without resorting to multiple gust patches $\mathbf{N}_{v_g}$, such a concern is much mitigated in view of the low range of reduced frequencies required to model the gust boundary conditions and the possibility of choosing an appropriate value

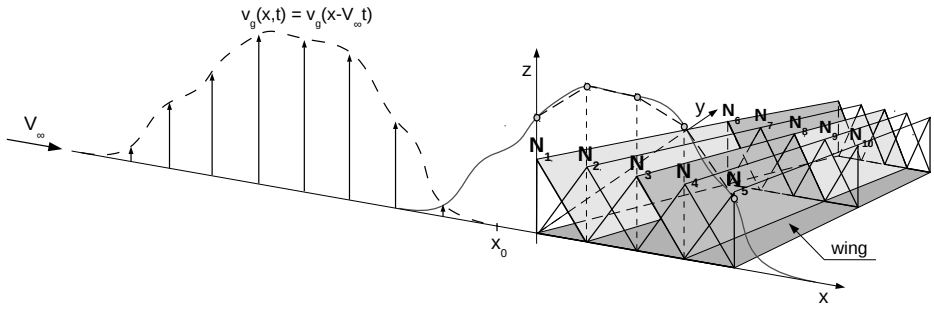

Figure 4.2: *Wing penetrating a gust profile discretized by five linear chordwise and two constant spanwise gust modes.*

for $\mathbf{x}_0$. The latter point is well illustrated by Drischler modified Sears function [238], whereas moving $\mathbf{x}_0$ from the middle of the chord to the leading edge leads to a complete smoothing of an otherwise highly oscillating function. For more complex configurations an approximated optimal $\mathbf{x}_0$ reducing the delay oscillations can be easily inferred by inverse Fourier transforming $\mathbf{H}_{ag}$. Indeed the related time histories will show the presence of delayed impulse gust responses of the various patches, as it will be shown in a few forthcoming examples.

An additional mitigation of such oscillations will also come from the mentioned limited range of required reduced frequencies, as suggested by the frequency content of a Dryden's shaping filter (i.e. a shaping filter commonly used to model typical turbulence power spectral densities):

$$H_w(p) \simeq \sigma_w \sqrt{\frac{L_g}{\pi V_\infty}} \frac{(1+\sqrt{3}\, p\, L_g/l_a)}{(1+p\, L_g/l_a)^2} \tag{4.19}$$

In fact, assuming a conservative reference gust length L_g of about five l_a, a reduced frequency limit of two will be a decade in excess of its double pole at $p = \frac{l_a}{L_g}$. Similar conclusions can be drawn also for short deterministic 1-cos gusts.

A finite state aeroelastic model makes the simulation of any response easy, either deterministic (e.g. a discrete gust or maneuver aimed at determining extreme limit loads), stochastic (e.g. extended time responses for history dependent fatigue load calculations [239]), or a combination of both (e.g. simulations aimed at designing flight flutter tests [240]).

Oftentimes only the variance matrices are needed. In such case they can be straightforwardly determined through the cascaded solution of the following Lyapunov and generalized Sylvester equations [104, 170]:

$$\begin{gathered}
\mathbf{A}_w \boldsymbol{\Sigma}_w + \boldsymbol{\Sigma}_w \mathbf{A}_w^T + \mathbf{B}_w \mathbf{W}\, \mathbf{B}_w^T = 0 \\
\mathbf{A}_{ae} \boldsymbol{\Sigma}_{aew} + \mathbf{E}_{ae} \boldsymbol{\Sigma}_{aew} \mathbf{A}_w^T + \left(\mathbf{A}_{aew} \boldsymbol{\Sigma}_w + \mathbf{B}_{aew} \mathbf{W} \mathbf{B}_w^T\right) = 0 \\
\mathbf{A}_{ae} \boldsymbol{\Sigma}_{ae} \mathbf{E}_{ae}^T + \mathbf{E}_{ae} \boldsymbol{\Sigma}_{ae} \mathbf{A}_{aew}^T + \left(\mathbf{A}_{aew} \boldsymbol{\Sigma}_{aew} \mathbf{E}_{ae}^T + \mathbf{E}_{ae} \boldsymbol{\Sigma}_{aew}^T \mathbf{A}_{aew}^T + \mathbf{B}_{aew} \mathbf{W} \mathbf{B}_{aew}^T\right) = 0
\end{gathered} \tag{4.20}$$

making easier the evaluation of:

$$\begin{aligned}\mathbf{\Sigma}_w &= E(\mathbf{x}_w\mathbf{x}_w^T)\\ \mathbf{\Sigma}_{aew} &= E(\mathbf{x}_{ae}\mathbf{x}_w^T)\\ \mathbf{\Sigma}_{ae} &= E(\mathbf{x}_{ae}\mathbf{x}_{ae}^T)\end{aligned} \tag{4.21}$$

for an assigned intensity $\mathbf{W}$ of the white noise input to the shaping filter.

The above equations can be solved only if the linear(ized) aeroelastic model is asymptotically stable. A flying aircraft without stability augmentation for plunge, side slip and roll mode, does not satisfy this condition. Therefore fictitious corrections are applied, e.g. using dummy low authority controllers or by soft grounding with dummy springs and dampers, while trying to negligibly affect structural deformations. This is hardly possible for an aircraft with very low frequency deformation modes, where such techniques may render it difficult to avoid affecting the structural response. Thus a better procedure is to uncouple the simply stable, ss, from the asymptotically stable, as, part, solving Eq. (4.20) using only the latter. Therefore we apply a slight variation of the approach adopted in [153] to decouple the aeroelastic and shaping filter equations in Eq. (2.11). Considering the generic system:

$$\begin{bmatrix}\mathbf{E}_{11} & \mathbf{E}_{12}\\ \mathbf{0} & \mathbf{E}_{22}\end{bmatrix}\begin{Bmatrix}\dot{\mathbf{x}}_1(t)\\ \dot{\mathbf{x}}_2(t)\end{Bmatrix} = \begin{bmatrix}\mathbf{A}_{11} & \mathbf{A}_{12}\\ \mathbf{0} & \mathbf{A}_{22}\end{bmatrix}\begin{Bmatrix}\mathbf{x}_1(t)\\ \mathbf{x}_2(t)\end{Bmatrix} + \begin{bmatrix}\mathbf{B}_1\\ \mathbf{B}_2\end{bmatrix}\mathbf{u}(t) \tag{4.22}$$

we apply the state (right) transformation:

$$\begin{Bmatrix}\mathbf{x}_1(t)\\ \mathbf{x}_2(t)\end{Bmatrix} = \begin{bmatrix}\mathbf{I} & \mathbf{R}\\ \mathbf{0} & \mathbf{I}\end{bmatrix}\begin{Bmatrix}\mathbf{z}_1(t)\\ \mathbf{x}_2(t)\end{Bmatrix} \tag{4.23}$$

and recombine its equations using a left transformation:

$$\begin{aligned}&\begin{bmatrix}\mathbf{I} & \mathbf{L}\\ \mathbf{0} & \mathbf{I}\end{bmatrix}\begin{bmatrix}\mathbf{E}_{11} & \mathbf{E}_{12}\\ \mathbf{0} & \mathbf{E}_{22}\end{bmatrix}\begin{bmatrix}\mathbf{I} & \mathbf{R}\\ \mathbf{0} & \mathbf{I}\end{bmatrix}\begin{Bmatrix}\dot{\mathbf{z}}_1(t)\\ \dot{\mathbf{z}}_2(t)\end{Bmatrix}\\ &\quad= \begin{bmatrix}\mathbf{I} & \mathbf{L}\\ \mathbf{0} & \mathbf{I}\end{bmatrix}\begin{bmatrix}\mathbf{A}_{11} & \mathbf{A}_{12}\\ \mathbf{0} & \mathbf{A}_{22}\end{bmatrix}\begin{bmatrix}\mathbf{I} & \mathbf{R}\\ \mathbf{0} & \mathbf{I}\end{bmatrix}\begin{Bmatrix}\mathbf{z}_1(t)\\ \mathbf{z}_2(t)\end{Bmatrix} + \begin{bmatrix}\mathbf{I} & \mathbf{L}\\ \mathbf{0} & \mathbf{I}\end{bmatrix}\begin{bmatrix}\mathbf{B}_1\\ \mathbf{B}_2\end{bmatrix}\mathbf{u}(t)\end{aligned} \tag{4.24}$$

obtaining the following transformed coupling $(1,2)$ terms:

$$\mathbf{E}_{11}\mathbf{R} + \mathbf{L}\mathbf{E}_{22} + \mathbf{E}_{12} = 0 \tag{4.25a}$$

$$\mathbf{A}_{11}\mathbf{R} + \mathbf{L}\mathbf{A}_{22} + \mathbf{A}_{12} = 0 \tag{4.25b}$$

Assuming a non singular $\mathbf{A}_{22}$, we can obtain $\mathbf{L}$ as a function of $\mathbf{R}$ from Eq. (4.25b), so that substituted it into Eq. (4.25a) we have:

$$\mathbf{L} = -\mathbf{A}_{22}^{-1}\mathbf{A}_{11}\mathbf{R} - \mathbf{A}_{22}^{-1}\mathbf{A}_{12} \tag{4.26a}$$

$$\mathbf{E}_{11}\mathbf{R} - \mathbf{A}_{22}^{-1}\mathbf{A}_{11}\mathbf{R}\mathbf{E}_{22} + (\mathbf{E}_{12} - \mathbf{A}_{22}^{-1}\mathbf{A}_{12}\mathbf{E}_{22}) = 0 \tag{4.26b}$$

Getting $\mathbf{R}$ from the solution of Eq. (4.26b), a discrete like Sylvester equation, and then $\mathbf{L}$

from Eq. (4.26a), we end with the following decoupled system:

$$\begin{bmatrix} \mathbf{E}_{11} & \mathbf{0} \\ \mathbf{0} & \mathbf{E}_{22} \end{bmatrix} \begin{Bmatrix} \dot{\mathbf{z}}_1(t) \\ \dot{\mathbf{x}}_2(t) \end{Bmatrix} = \begin{bmatrix} \mathbf{A}_{11} & \mathbf{0} \\ \mathbf{0} & \mathbf{A}_{22} \end{bmatrix} \begin{Bmatrix} \mathbf{z}_1(t) \\ \mathbf{x}_2(t) \end{Bmatrix} + \begin{bmatrix} \mathbf{B}_1 + \mathbf{L}\mathbf{B}_2 \\ \mathbf{B}_2 \end{bmatrix} \mathbf{u}(t) \tag{4.27}$$

The above procedure is applied to Eq. (2.11) through the following steps:

1. Obtain a first right and left transformation terms, $\mathbf{R}_1$ and $\mathbf{L}_1$, allowing to write Eq. (2.11) as:

$$\begin{bmatrix} \mathbf{E}_{ae} & \mathbf{0} \\ \mathbf{0} & \mathbf{I} \end{bmatrix} \begin{Bmatrix} \dot{\mathbf{z}}_{ae}(t) \\ \dot{\mathbf{x}}_w(t) \end{Bmatrix} = \begin{bmatrix} \mathbf{A}_{ae} & \mathbf{0} \\ \mathbf{0} & \mathbf{A}_w \end{bmatrix} \begin{Bmatrix} \mathbf{z}_{ae}(t) \\ \mathbf{x}_w(t) \end{Bmatrix} + \begin{bmatrix} \mathbf{B}_{aew} + \mathbf{L}_1\mathbf{B}_w \\ \mathbf{B}_w \end{bmatrix} \mathbf{w}(t) \tag{4.28}$$

2. Calculate an ordered generalized Schur orthogonal decomposition [241] of the couple $\mathbf{E}_{ae}$, $\mathbf{A}_{ae}$:

$$\mathbf{z}_{ae} = \begin{bmatrix} \mathbf{V}_{ss} & \mathbf{V}_{as} \end{bmatrix} \begin{Bmatrix} \mathbf{v}_{ss} \\ \mathbf{v}_{as} \end{Bmatrix} = \mathbf{V}_s \mathbf{v}_s \tag{4.29}$$

where $\mathbf{v}_{ss}$ refers to the simply stable and $\mathbf{v}_{as}$ to the asymptotically stable part. Use it for the already decoupled aeroelastic part, writing:

$$\mathbf{V}_s^T \mathbf{E}_{ae} \mathbf{V}_s \begin{Bmatrix} \dot{\mathbf{v}}_{ss}(t) \\ \dot{\mathbf{v}}_{as}(t) \end{Bmatrix} = \mathbf{V}_s^T \mathbf{A}_{ae} \mathbf{V}_s \begin{Bmatrix} \mathbf{v}_{ss}(t) \\ \mathbf{v}_{as}(t) \end{Bmatrix} + \mathbf{V}_s^T (\mathbf{B}_{aew} + \mathbf{L}_1 \mathbf{B}_w) \mathbf{w}(t) \tag{4.30}$$

to obtain:

$$\begin{bmatrix} \mathbf{T}_{ss} & \mathbf{T}_{ss,as} \\ \mathbf{0} & \mathbf{T}_{as} \end{bmatrix} \begin{Bmatrix} \dot{\mathbf{v}}_{ss}(t) \\ \dot{\mathbf{v}}_{as}(t) \end{Bmatrix} = \begin{bmatrix} \mathbf{S}_{ss} & \mathbf{S}_{ss,as} \\ \mathbf{0} & \mathbf{S}_{as} \end{bmatrix} \begin{Bmatrix} \mathbf{v}_{ss}(t) \\ \mathbf{v}_{as}(t) \end{Bmatrix} + \begin{bmatrix} \mathbf{B}_{ss} \\ \mathbf{B}_{as} \end{bmatrix} \mathbf{w}(t) \tag{4.31}$$

with triangular $\mathbf{T}_{ss}$ and $\mathbf{T}_{as}$ and upper Schur $\mathbf{S}_{ss}$ and $\mathbf{S}_{as}$.

3. Apply the full decoupling procedure again, determining $\mathbf{R}_2$ and $\mathbf{L}_2$, so that Eq. (2.11) will eventually become:

$$\begin{bmatrix} \mathbf{T}_{ss} & \mathbf{0} & \mathbf{0} \\ \mathbf{0} & \mathbf{T}_{as} & \mathbf{0} \\ \mathbf{0} & \mathbf{0} & \mathbf{I} \end{bmatrix} \begin{Bmatrix} \dot{\mathbf{w}}_{ss}(t) \\ \dot{\mathbf{v}}_{as}(t) \\ \dot{\mathbf{x}}_w(t) \end{Bmatrix} = \begin{bmatrix} \mathbf{S}_{ss} & \mathbf{0} & \mathbf{0} \\ \mathbf{0} & \mathbf{S}_{as} & \mathbf{0} \\ \mathbf{0} & \mathbf{0} & \mathbf{A}_w \end{bmatrix} \begin{Bmatrix} \mathbf{w}_{ss}(t) \\ \mathbf{v}_{as}(t) \\ \mathbf{x}_w(t) \end{Bmatrix} + \begin{bmatrix} \mathbf{B}_{ss} + \mathbf{L}_2\mathbf{B}_{as} \\ \mathbf{B}_{as} \\ \mathbf{B}_w \end{bmatrix} \mathbf{w}(t) \tag{4.32}$$

using the following overall right transformation:

$$\begin{Bmatrix} \mathbf{x}_{ae}(t) \\ \mathbf{x}_w(t) \end{Bmatrix} = \begin{bmatrix} \mathbf{T}_{ss} & (\mathbf{T}_{ss}\mathbf{R}_2 + \mathbf{T}_{as}) & \mathbf{R}_1 \\ \mathbf{0} & \mathbf{0} & \mathbf{I} \end{bmatrix} \begin{Bmatrix} \mathbf{w}_{ss}(t) \\ \mathbf{v}_{as}(t) \\ \mathbf{x}_w(t) \end{Bmatrix} \tag{4.33}$$

to recover the original aeroelastic and gust states, as well as any output related to them.

Therefore, thanks to the triangular and Schur form of matrices $\mathbf{T}$ and $\mathbf{S}$, we can easily

solve the following fully uncoupled variance equations for the asymptotically stable part only [104, 170]:

$$\begin{aligned}\mathbf{A}_w\boldsymbol{\Sigma}_w + \boldsymbol{\Sigma}_w\mathbf{A}_w^T + \mathbf{B}_w\mathbf{W}\,\mathbf{B}_w^T &= 0\\ \mathbf{S}_{as}\boldsymbol{\Xi}_{asw} + \mathbf{T}_{as}\boldsymbol{\Xi}_{asw}\mathbf{A}_w^T + \mathbf{B}_{as}\mathbf{W}\mathbf{B}_w^T &= 0\\ \mathbf{S}_{as}\boldsymbol{\Xi}_{as}\mathbf{T}_{as}^T + \mathbf{T}_{as}\boldsymbol{\Xi}_{as}\mathbf{S}_{as}^T + \mathbf{B}_{as}\mathbf{W}\mathbf{B}_{as}^T &= 0\end{aligned} \tag{4.34}$$

recovering the original variances with:

$$\begin{bmatrix}\boldsymbol{\Sigma}_{ae} & \boldsymbol{\Sigma}_{aew}\\ \boldsymbol{\Sigma}_{aew}^T & \boldsymbol{\Sigma}_w\end{bmatrix} = \begin{bmatrix}(\mathbf{T}_{ss}\mathbf{R}_2+\mathbf{T}_{as}) & \mathbf{R}_1\\ \mathbf{0} & \mathbf{I}\end{bmatrix}\begin{bmatrix}\boldsymbol{\Xi}_{as} & \boldsymbol{\Xi}_{asw}\\ \boldsymbol{\Xi}_{asw}^T & \boldsymbol{\Sigma}_w\end{bmatrix}\begin{bmatrix}(\mathbf{T}_{ss}\mathbf{R}_2+\mathbf{T}_{as})^T & \mathbf{0}\\ \mathbf{R}_1^T & \mathbf{I}\end{bmatrix} \tag{4.35}$$

Since the variance of the turbulence, $\boldsymbol{\Sigma}_w$, is a datum of the related shaping filters, the very first Lyapunov equation, identical for both Eq. (4.20) and Eq. (4.34), needs not to be solved.

A couple of remarks about the above decoupling scheme might be of some interest. At first we notice that the Schur decomposition, as for step two, could have been applied directly to Eq. (2.11), getting to the final result of step three in a single shot. However we elected not to do so because keeping an explicit shaping filter has been practically verified to be an advantage. Then, we remark that an eigenvector based decomposition could be adopted in place of Schur's [242], claiming the added advantage of ending with diagonal $\mathbf{T}_{,s}$ and $\mathbf{S}_{,s}$ [243] [2]. That is a viable option for isolated analyses under the control of an aeroelastic analyst, but should be avoided in blind massive calculations, as in optimization procedures or in extended parametric analyses. Indeed the Schur approach is much more stable from the numerical point of view, so avoiding many of the troubles associated to eigenvector based decompositions having coincident/close eigenvalues [244].

A unified identification of motion and gust GAFs is naturally suggested by linearized aerodynamic formulations, nevertheless the GAFs related to motion and gust boundary conditions are often computed in separate phases of the aeroelastic modeling procedure, the motion ones usually coming first. In such cases it might be worth to identify the newly added gust forces only, appending their model to those already available [202]. In this case:

$$\begin{aligned}\mathbf{H}_{amg} = \mathbf{H}_{am}+\mathbf{H}_{ag} = \mathbf{E}_{0am}+p\mathbf{E}_{1am}+p^2\mathbf{E}_{2am}+\mathbf{C}_{am}\left(p\mathbf{I}-\mathbf{A}_{am}\right)^{-1}\left(\mathbf{B}_{0am}+p\mathbf{B}_{1am}\right)\\ +\mathbf{E}_{0ag}+p\mathbf{E}_{1ag}+p^2\mathbf{E}_{2ag}+\mathbf{C}_{ag}\left(p\mathbf{I}-\mathbf{A}_{ag}\right)^{-1}\left(\mathbf{B}_{0ag}+p\mathbf{B}_{1ag}\right)\end{aligned} \tag{4.36}$$

so that, defining $\mathbf{x}_{ae}^T = \{\mathbf{q}^T, \dot{\mathbf{q}}^T, \mathbf{x}_{am}^T, \mathbf{x}_{ag}^T\}$, the separated finite states representation

[2] Two by two block diagonals if one wants to avoid using complex conjugate eigenvalues and eigenvectors.

matrices of Eq. (2.8) are:

$$
\begin{aligned}
\mathbf{E}_{ae} &= \begin{bmatrix} \mathbf{I} & \mathbf{0} & \mathbf{0} & \mathbf{0} \\ \mathbf{0} & \mathbf{M}_{ae} & \mathbf{0} & \mathbf{0} \\ \mathbf{0} & \mathbf{0} & \mathbf{I} & \mathbf{0} \\ \mathbf{0} & \mathbf{0} & \mathbf{0} & \mathbf{I} \end{bmatrix} \\
\mathbf{A}_{ae} &= \begin{bmatrix} \mathbf{0} & \mathbf{I} & \mathbf{0} & \mathbf{0} \\ -\mathbf{K}_{ae} & -\mathbf{C}_{ae} & q_\infty \mathbf{C}_{am} & q_\infty \mathbf{C}_{ag} \\ (V_\infty / l_a)\, \mathbf{B}_{0am} & \mathbf{B}_{1am} & (V_\infty / l_a)\, \mathbf{A}_{am} & \mathbf{0} \\ \mathbf{0} & \mathbf{0} & \mathbf{0} & (V_\infty / l_a)\, \mathbf{A}_{ag} \end{bmatrix} \\
\mathbf{B}_{aeg} &= \begin{bmatrix} \mathbf{0} & \mathbf{0} & \mathbf{0} \\ q_\infty \mathbf{E}_{0ag} & q_\infty\, (l_a/V_\infty)\, \mathbf{E}_{1ag} & q_\infty\, (l_a/V_\infty)^2\, \mathbf{E}_{2ag} \\ \mathbf{0} & \mathbf{0} & \mathbf{0} \\ (V_\infty / l_a)\, \mathbf{B}_{0ag} & \mathbf{B}_{1ag} & \mathbf{0} \end{bmatrix}, \qquad \mathbf{B}_{aef} = \begin{bmatrix} \mathbf{0} \\ \mathbf{B}_h \\ \mathbf{0} \\ \mathbf{0} \end{bmatrix} \\
\mathbf{M}_{ae} &= \mathbf{M} - q_\infty\, (l_a/V_\infty)^2\, \mathbf{E}_{2am}, \\
\mathbf{C}_{ae} &= \mathbf{C} - q_\infty\, (l_a/V_\infty)\, \mathbf{E}_{1am}, \\
\mathbf{K}_{ae} &= \mathbf{K} - q_\infty \mathbf{E}_{0am}
\end{aligned}
\tag{4.37}
$$

Then, while the am part will be determined by an LFMD, as for the unified scheme, the ag part, because of the size of $\mathbf{H}_{ag}$, is better based on a Right Matrix Fraction Description (RMFD):

$$
\mathbf{H}_{ag}(p) = \mathbf{N}(p)\, \mathbf{D}^{-1}(p) = \left(\sum_{i=0}^{n+2} \mathbf{N}_i\, p^i \right) \left(\mathbf{I}\, p^n + \sum_{i=0}^{n-1} \mathbf{D}_i\, p^i \right)^{-1} \tag{4.38}
$$

Making the necessary changes, the related LS identification procedure will closely follow the LMFD one, the only difference being the state matrices produced by the matrix polynomial division:

$$
\mathbf{A}_w = \begin{bmatrix} \mathbf{0} & \mathbf{I} & \mathbf{0} & \dots & \mathbf{0} \\ \mathbf{0} & \mathbf{0} & \mathbf{I} & \dots & \mathbf{0} \\ \vdots & \vdots & \vdots & \ddots & \vdots \\ \mathbf{0} & \mathbf{0} & \mathbf{0} & \dots & \mathbf{I} \\ -\mathbf{D}_0 & -\mathbf{D}_1 & \dots & -\mathbf{D}_{n-2} & -\mathbf{D}_{n-1} \end{bmatrix}, \qquad \mathbf{B}_w = \begin{bmatrix} \mathbf{0} \\ \mathbf{0} \\ \vdots \\ \mathbf{0} \\ \mathbf{I} \end{bmatrix}, \qquad \mathbf{C}_w^T = \begin{bmatrix} \mathbf{R}_{n-1} \\ \mathbf{R}_{n-2} \\ \vdots \\ \mathbf{R}_1 \\ \mathbf{R}_0 \end{bmatrix} \tag{4.39}
$$

The just presented RMFD transfer matrix identification can be used also to identify possible shaping filters for Eq. (2.11) rolling off as $1/s^{ro}$, whose transfer matrix $\mathbf{H}_{sf}$ is obtained by:

- choosing ro and identifying an RMFD of the type:

$$
\mathbf{H}_{sf}(s) = \left(\sum_{i=0}^{n} \mathbf{N}_i\, s^i \right) \left(\sum_{i=0}^{n+ro} \mathbf{D}_i\, s^i \right)^{-1} \tag{4.40}
$$

- executing the needed matrix polynomial division so to obtain:

$$\mathbf{H}_{sf}(s) = \mathbf{C}_w \left(s\mathbf{I} - \mathbf{A}_w\right)^{-1} \mathbf{B}_w \tag{4.41}$$

ending in setting up Eq. (2.11) with either Eq. (2.12), for $ro = 1$, or Eq. (2.13), for $ro = 2$.

The shaping filter approach needs not to be confined to continuous turbulence but can easily be adopted for any finite duration gust profile, e.g. 1-cos gusts. Such discrete filters may be useful in designing optimal multiplant MIMO controllers aimed at gust loads alleviation [153]. To such an end we:

- interpret a finite duration gust profile as an impulse response;
- transform it into the frequency domain;
- choose ro and fitting it with the above RMFD;
- set up Eq. (2.11) as for the chosen ro;
- discard the impulsive solution associated to $ro = 1$, calling V_g the discrete gust amplitude scaling factor, and obtaining the response by integrating with assigning the following initial conditions, see Eq. (2.19):

$$\begin{aligned} \text{if } ro = 1: \qquad \mathbf{x}_{ae}(0^+) &= V_g \mathbf{E}_{ae}^{-1} \left(\mathbf{A}_{ae}\mathbf{E}_{ae}^{-1}\mathbf{B}_{1aew} + \mathbf{B}_{0aew}\right) \\ \mathbf{x}_w(0^+) &= V_g \mathbf{B}_w \end{aligned} \tag{4.42a}$$

$$\begin{aligned} \text{if } ro = 2: \qquad \mathbf{x}_{ae}(0^+) &= V_g \mathbf{E}_{ae}^{-1}\, \mathbf{B}_{0aew} \\ \mathbf{x}_w(0^+) &= V_g \mathbf{B}_w \end{aligned} \tag{4.42b}$$

Figure 4.3 shows the application of this procedure for a two chords length 1-cos gust, to be used in a following example, obtained with an RMFD for $ro = 2$, and order $n = 1$ and $n = 2$. We remark that, even when an analytic expression is available for the gust shape at hand, as for our example, an identification is required anyhow, being necessary having a realizable rational transfer function embedding any delay operator, oftentimes present in the analytic transform.

When a penetration-less gust formulation is adopted we can either use it as an intermediate step leading to the usual $\mathbf{H}_{ag}$ through Eq. (4.18), afterward proceeding as for a penetrating formulation, or work with it directly. So we provide a specific extension to be used for deterministic turbulence simulations and gusts. Such an alternative approach is based on generating the input $\mathbf{q}_g$, either from assigned gust profile or shaping filter, using it directly in the numerical integration. That requires a discretization of Eq. (4.10) so to provide the values $\mathbf{b}_w$ needed by the integrator. Such discretization will clearly depend on the type of expansion $\mathbf{N}_g$ adopted. A possible choice are the locally supported basis functions: piecewise linear, quadratic, hermitian, wavelets [245, 246]. Here we illustrate a specific implementation based on simple, yet efficient, piecewise linear functions N_k, having value

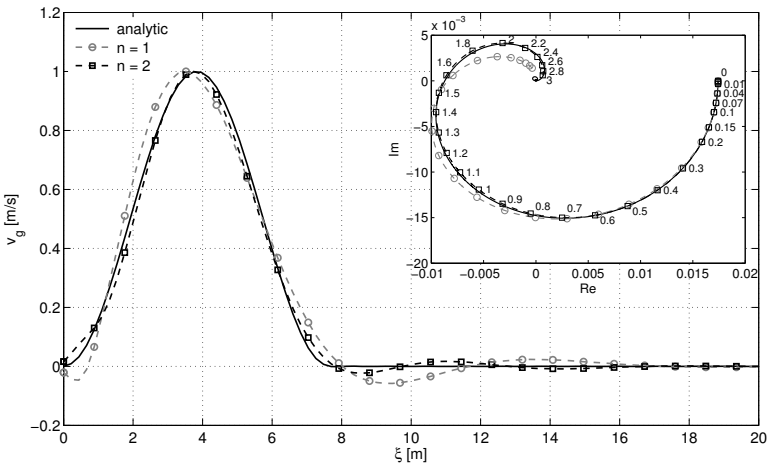

Figure 4.3: *RMFD 1-cos discrete gust filter, time and frequency domain representation.*

1 at each control point x_k and zero at every x_j, $j \neq k$:

$$N_k(x) = \begin{cases} \dfrac{x - x_{k-1}}{x_k - x_{k-1}} & \text{if } x \in [x_{k-1}, x_k], \\ \dfrac{x_{k+1} - x}{x_{k+1} - x_k} & \text{if } x \in [x_k, x_{k+1}], \qquad \text{for } k = 1, ..., n. \\ 0 & \text{otherwise,} \end{cases} \tag{4.43}$$

With such a scheme $\mathbf{A}_g$ is easily calculated and the vector $\mathbf{b}_w(t)$ associated to the convolution part is simply discretized for a finite step integration through:

$$\mathbf{b}_w(t) = \int_0^l \mathbf{N}^T(x)\, \mathbf{v}_g(V_\infty t - x) dx \simeq \lim_{\Delta x \to 0} \sum_{k=0}^{m-1} \mathbf{N}^T(k\Delta x)\, \mathbf{v}_g(V_\infty t - k\Delta x)\Delta x \tag{4.44}$$

with $\mathbf{N}$ being the shorthand: $\mathbf{N}(x, y, z) = \mathbf{N}_g^T(x, y, z)\ \mathbf{n}_0^T(x, y, z)\ \mathbf{N}_{v_g}(x, y, z)$. Such a convolution operation can be constructed as a matrix multiplication, resulting in a delay matrix multiplying the gust vector:

$$\mathbf{b}_{1w}^T(n) = \sum_{k=0}^{m-1} \mathbf{N}_1^T(k\Delta x)\, \mathbf{v}_g(n - k\Delta x)\Delta x = \left[\mathbf{N}_1^T(k\Delta x) * \mathbf{v}_g(n)\right] \Delta x = \mathbf{D}_1\, \mathbf{v}_g(n) \tag{4.45}$$

where the integral related to the discretized first basis function $\mathbf{N}_1$ has been considered

and with the delay matrix $\mathbf{D}_1$ having a Toeplitz matrix structure:

$$\mathbf{D}_1 = \begin{bmatrix} N_1^1 & 0 & \cdots & 0 & 0 \\ N_2^1 & N_1^1 & \cdots & \vdots & \vdots \\ N_3^1 & N_2^1 & \ddots & 0 & 0 \\ \vdots & N_3^1 & \cdots & N_1^1 & 0 \\ N_{m-1}^1 & \vdots & \cdots & N_2^1 & N_1^1 \\ N_m^1 & N_{m-1}^1 & \vdots & \vdots & N_2^1 \\ 0 & N_m^1 & \cdots & N_{m-2}^1 & \vdots \\ 0 & 0 & \ddots & N_{m-1}^1 & N_{m-2}^1 \\ \vdots & \vdots & \vdots & N_m^1 & N_{m-1}^1 \\ 0 & 0 & 0 & \cdots & N_m^1 \end{bmatrix} \Delta x \tag{4.46}$$

The vectors $\mathbf{N}$ and $\mathbf{v}_g$ must have same spatial discretization (i.e. same Δx), so an interpolation is used whenever such a condition is not met.

The procedure is accomplished for every basis function $[\mathbf{N}_1(x), \cdots, \mathbf{N}_n(x)]$, leading to a delay matrix $\hat{\mathbf{D}}$ relating the gust profile and the generalized gust coordinates $\mathbf{q}_g$:

$$\mathbf{q}_g(t) = \hat{\mathbf{D}}\mathbf{v}_g(x) \tag{4.47}$$

the derivatives $\dot{\mathbf{q}}_g$ and $\ddot{\mathbf{q}}_g$ being computed through finite differences. Depending on the spatial step used for the convolution integral the delay matrix may have a large size. Nonetheless, no major problem will arise because of its huge sparsity and diagonally dominant structure.

Chapter 5

Simulations of Linear Reduced Order Aeroelastic Systems

A few examples are presented in order to assess the approaches proposed in chapters 3 and 4.2. In section 5.1 we firstly provide applications of the identification approach through the rational matrix fraction approximation, together with the penetration-less gust approach. The aeroelastic systems thereby considered for these techniques are a plunging typical section in inviscid-incompressible flow, a transonic wing, and a simple aircraft model in incompressible flow. All the examples include the full identification of motion and gust GAFs, followed by either a flutter or a gust/turbulence response analysis. Sucessively in section 5.2 we provide with examples of the penetration-less gust approach for complex cases of industrial relevance, by modeling the aerodynamic subsystem using full-nonlinear compressible Euler equations, and considering two complete aircraft models. In the end, in section 5.3, we provide with results about the projection-based approach exploiting the left/right Schur subspaces, for an airfoil in compressible flow but outside of the transonic region.

5.1 Applications of the system identification and gust modeling approaches

5.1.1 Freely Plunging typical section

The first example is a well known check case for an unrestrained three degrees of freedom (DOF)s airfoil in incompressible flow, representing a two degrees of freedom pitch-plunge aeroelastic problem with an additional fuselage free-free plunge mode. Depending on the adopted stability calculation and the GAFs approximation, differences and inconsistencies may arise in determining a "dynamic divergence" mode and a flutter instability [152, 247, 248], whose best illustration is likely provided by the so called Generalized Aeroelastic Analysis Method (GAAM) [152], combined with an eigenvalue iteration procedure converging onto the true roots of a related complex stability matrix.

The airfoil model [152] has the elastic axis at 40% of the chord, the chord being $2l_a = 1.829\,\mathrm{m}\,(6\,\mathrm{ft})$. Two center of gravity (c.g.) locations will be analyzed, respectively at 37%

and 45% of the chord. The equations of motion are:

$$\left(s^2\begin{bmatrix}1 & x_\alpha & 0\\ x_\alpha & r_\alpha^2 & 0\\ 0 & 0 & \frac{m_f}{m_w}\end{bmatrix}+s\begin{bmatrix}2\zeta\omega_h & 0 & 0\\ 0 & 2\zeta r_\alpha^2\omega_\alpha & 0\\ 0 & 0 & 0\end{bmatrix}+\begin{bmatrix}\omega_h^2 & 0 & -\omega_h^2\\ 0 & r_\alpha^2\omega_\alpha^2 & 0\\ -\omega_h^2 & 0 & \omega_h^2\end{bmatrix}\right)\begin{Bmatrix}h_w(s)\\ \alpha(s)\\ h_f(s)\end{Bmatrix} = \frac{U^2}{\pi\mu l_a^2}\begin{Bmatrix}-c_l(s)l_a\\ c_m(s)\\ 0\end{Bmatrix} \quad (5.1)$$

where the nondimensional radius of gyration is $r_\alpha^2 = 0.25$, the mass ratio $\mu = 20$ and the static unbalance $x_\alpha = -0.06$, for the case with c.g. at 37% chord, and $x_\alpha = 0.10$, for the case with c.g. at 45% chord. The uncoupled bending and torsion frequencies are $\omega_h = 10$ rad/s and $\omega_\alpha = 25$ rad/s. A structural damping coefficient, $\zeta = 0.015$, is applied to both modes. The fuselage mass is assumed to be equal to airfoil mass $m_f = m_w$.

Identification: considering a thin airfoil in a two-dimensional unsteady incompressible inviscid flow, the aerodynamic transfer matrix of the presented three DOFs model is decomposed in its motion and gust dependent parts:

$$\begin{Bmatrix}-c_l(s)l_a\\ c_m(s)\end{Bmatrix} = \begin{bmatrix}\mathbf{H}_{am} & \mathbf{H}_{ag}\end{bmatrix}\begin{Bmatrix}\begin{Bmatrix}h_w(s)\\ \alpha(s)\end{Bmatrix}\\ v_g/V_\infty\end{Bmatrix} = \mathbf{H}_a\begin{Bmatrix}\begin{Bmatrix}h_w(s)\\ \alpha(s)\end{Bmatrix}\\ v_g/V_\infty\end{Bmatrix} \quad (5.2)$$

with $\mathbf{H}_{am}$ derived from the standard Theodorsen theory and $\mathbf{H}_{ag}$ calculated for $\mathbf{x}_0 = 0$, i.e. at the airfoil midchord, as for the Sears function. The penetration-less gust modeling approach is also investigated by verifying the way it reconstructs the Sears function through Eq. (4.18). An asymptotically stable finite state approximation of the aerodynamic transfer matrix is derived by using a second order LFMD, i.e. $n = 2$, which is afterward squeezed to three, two and one state through a Hankel-based reduction. Figure 5.1 depicts the three states approximation of $\mathbf{H}_{am}$, provided by the three proposed LS methods. To display a clear figure, just LS2 is shown, being the differences with LS1 and LS3 unnoticeable. All of them result in a good approximation, not only for the fit along jk but also for a fairly extreme extrapolation along a complex $p = h + jk$ line with $h/k = -0.5$, obtained with the extended Theodorsen function $C(p)$ [152]. Such a full p benchmark is quite significant, because the $p\log(p)$ like singularity at $\mathbf{H}_{am}(0)$ associated to a two dimensional profile is significantly stronger than the $p^2\log(p)$ of three dimensional lifting surfaces [200]. Before calculating the chosen second order parent LMFD we determine as suggested an optimal smoothing $\mathbf{x}_0$. The impulse response associated with the available raw $\mathbf{H}_{ag}$, calculated using the Sears function $S(k)$ [249], as depicted in Fig. 5.2 in the non-dimensionalized time domain $\tau = V_\infty t/l_a$. From it the optimal gust entry point is inferred to be at $x_0 = -0.99$, i.e. quite close to the optimal leading edge smoothing of Drischler modified Sears function. Then the available discrete values of the original raw $\mathbf{H}_{ag}$ are substituted with $\mathbf{H}_{ag}\exp(0.99/V_\infty)$ and used for the unified identification of $\mathbf{H}_a$. Figure 5.3 shows Sears and Drischler functions, along with the smooth gust transfer function inferred from the mentioned gust impulse response. The same figure provides also the results of the unified three state

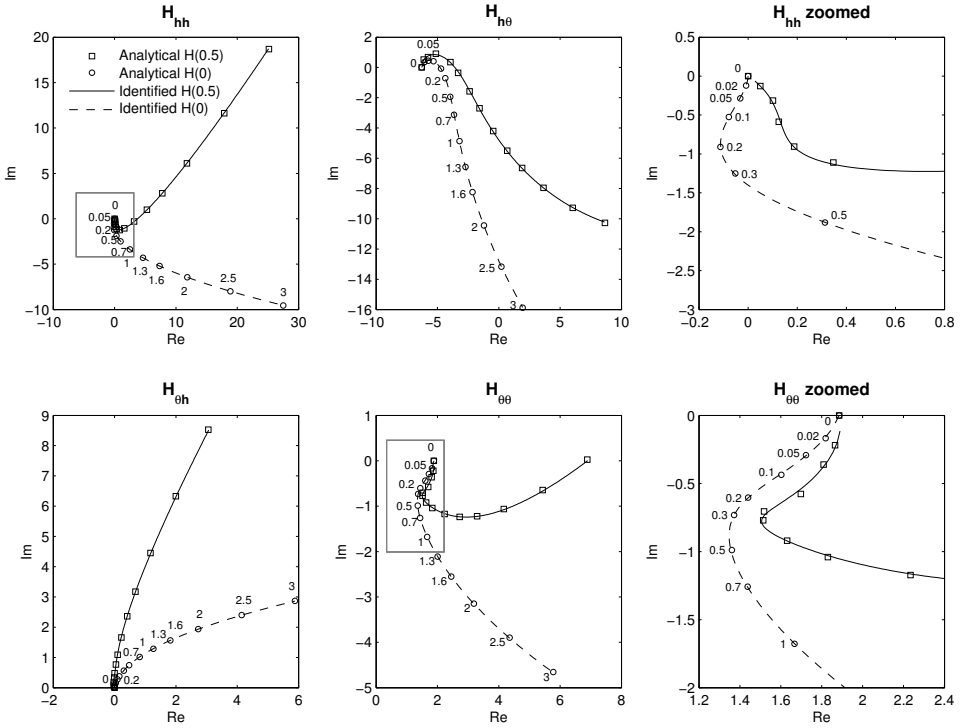

Figure 5.1: *Identification of* $\mathbf{H}_{am}(h + jk)$ *for an airfoil,* $h/k = 0$ *and* 0.5.

approximation provided by the LS2 method, the same as LS1 and LS3 once more.

From the knowledge of the pressure load, Δp, due to an assigned normal harmonic velocity distribution, w_n, over a thin airfoil oscillating in incompressible flow [179]:

$$\frac{\Delta p}{q_\infty} = -\frac{4}{\pi}\sqrt{\frac{1-x}{1+x}}\left[(1-C(k))\int_{-1}^{1}\sqrt{\frac{1+\xi}{1-\xi}}\,w_a(\xi)\,d\xi + \oint_{-1}^{1}\left(\sqrt{\frac{1+\xi}{1-\xi}}\frac{1}{x-\xi} - jk\Lambda_1(x,\xi)\right)w_a(\xi)\,d\xi\right] \tag{5.3}$$

with:

$$\Lambda_1(x,\xi) = \frac{1}{2}\ln\left(\frac{1-x\xi+\sqrt{1-x^2}\sqrt{1-\xi^2}}{1-x\xi-\sqrt{1-x^2}\sqrt{1-\xi^2}}\right) \tag{5.4}$$

$w_a = w_n/V_\infty$, x and ξ the coordinates from the profile midpoint, non-dimensionalized to l_a, it is possible to evaluate $\mathbf{H}_{ag}$ by using the penetration-less approach. The resulting lift and moment $\mathbf{H}_{ag}$ is then obtained by using Eq. (4.18), with $\mathbf{H}_{qg}$ calculated by appropriately integrating the above pressure load generated by each

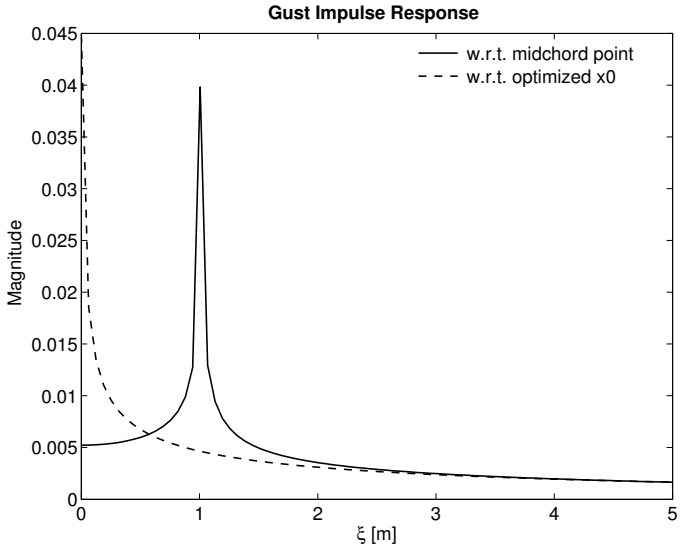

Figure 5.2: *Gust impulse responses of a profile.*

gust mode.

Figure 5.4 shows the comparison between the fully spiraling original Sears function $S(k)$ and its counterpart obtained in such a way, with the perturbation velocities given by using n piecewise linear gust modes. As it can be seen, ten gust modes placed along the airfoil length provide a fairly good accuracy up to $k = 10$, while four are quite adequate within the practical limit of interest of $k = 3$.

Flutter: flutter conditions are obtained through a direct solution of the low order generalized eigenproblem $\mathbf{A}_{ae}\mathbf{x}_{ae} = s\,\mathbf{E}_{ae}\mathbf{x}_{ae}$ for all of the finite state aerodynamic models, i.e. with three, two, one states. Considering the unrestrained three DOFs airfoil case, with c.g. at 37% chord, a "dynamic divergence" instability is found at $V_D = 230.3$ ft/s and frequency $f_D = 1.168$ Hz, whereas a flutter instability has been found at $V_F = 279.9$ ft/s and frequency $f_F = 2.687$ Hz (Fig. 5.6). As highlighted in [247], the divergence instability has a nonzero frequency and could be defined as a low-frequency flutter instability. Table 5.1 summarizes the flutter and divergence calculation for the various cases considered, the two DOFs case being derived from the three DOFs model by constraining the fuselage motion. All of the three, two and one state models predict correctly the flutter and divergence velocities and frequencies, a 4% discrepancy being found for the dynamic divergence prediction of the three DOFs model when using one aerodynamic state. All the identified aerodynamic state space models provide a good approximation over the whole range of frequencies but the very high ones, i.e. at very low airspeeds, as it appears from the root loci of Fig. 5.5.

5.1.2 AGARD 445.6 wing

The three dimensional aeroelastic model of the AGARD 445.6 wing [250], showing a typical flutter dip phenomenon, is used as a further benchmark. The model of the experimental set-up is a sidewall-mounted, semi-span, clean-wing configuration with NACA 65A004 airfoil section, made of laminated mahogany, having a quarter-chord sweep angle $\Lambda_{c/4} = 45\%$, a span $b = 0.762$ m, a root chord $c_r = 0.558$ m and a taper ratio $\lambda = 0.66$. The model selected is the so-called 2.5 ft weakened model number 3 (since all flow conditions, i.e. subsonic, transonic and supersonic, were tested), whose stiffness has been reduced by drilling holes through it and filling them with structural non-cooperating plastic foam to preserve aerodynamic continuity.

The related calculations are carried out on a reduced model based on the first six proper structural modes, whose shapes and generalized mass and stiffness matrices have been determined through Nastran. Since no structural damping is available for the wing model, an estimated value of the modal g-damping coefficient (i.e. minus twice the critical damping ratio of the mode) equal to 0.01 is applied. The structural finite element model uses homogeneous orthotropic triangular plate elements of density $\rho_s = 381.980$ kg/m^3, Young's moduli parallel and orthogonal to the elastic axis $E_{\parallel} = 3.151 \cdot 10^9$ Pa and $E_{\perp} = 4.162 \cdot 10^8$ Pa respectively, tangential elastic modulus $G = 4.392 \cdot 10^8$ Pa and Poisson's coefficient $\nu = 0.310$. The thickness distribution of the plate elements is obtained through a best fit [82] of the available ground vibration results [250]. Table 5.2 summarizes the natural frequencies of the finite element structural model.

The aerodynamic system is based on the unsteady full-potential (FP) equations, so to easily and quickly verify the capability of the proposed reduced order modelling technique for aeroelastic problems characterized by transonic effects. The equations are solved using the

						Improved MFD			
		GAAM [152]		3 states		2 states		1 state	
c.g. [%c]	Instability	V [ft/s]	f [Hz]	V [ft/s]	f [Hz]	V [ft/s]	f [Hz]	V [ft/s]	f [Hz]
					2 DOFs				
37	flutter	257.10	2.489	256.65	2.495	255.01	2.481	252.32	2.421
37	divergence	217.00	—	216.60	—	216.60	—	216.60	—
45	flutter	169.10	2.558	167.83	2.570	169.29	2.501	168.42	2.404
45	divergence	216.60	—	216.60	—	216.60	—	216.60	—
					3 DOFs				
37	flutter	280.50	2.688	279.90	2.687	278.40	2.682	279.40	2.644
37	divergence	230.30	1.156	230.33	1.168	230.30	1.185	221.70	1.154
45	flutter	159.30	2.763	158.08	2.771	159.81	2.718	159.15	2.657
45	divergence	213.50	1.156	213.68	1.142	213.19	1.175	204.67	1.136

Table 5.1: *Flutter and divergence summary of restrained and plunging typical sections.*

S^T solver [49] developed at the *Politecnico di Milano*, which is based on an independent approximation of the density and velocity potential fields. The discretized model, using 46000 nodes and 237000 tetrahedrons, has been provided to the author by A. Parrinello. Flight conditions are analysed at 0 deg angle of attack for three different Mach numbers, 0.678, 0.960 and 1.14, in order to assess the quality of the defined identification procedure in all flow-conditions, subsonic, transonic and weakly supersonic.

The aerodynamic transfer matrix $\mathbf{H}_a(k, M_\infty)$ is evaluated over a discrete set of reduced frequencies, ranging between 0 and 3, through a numerical linearization around a transonic steady reference condition determined by using the unsteady full-potential S^T solver. Such a linearization comes from calculating the response to the imposition of a blended small step, H_j, of the boundary condition associated to each mode j. Then the GAF $\mathbf{h}_{ij}(t)$ associated to each modal form i is computed, and the related $\mathbf{H}_{am}$ column obtained after subtracting from $\mathbf{h}_{ij}(t)$ and H_j their asymptotic values, $\mathbf{h}_{ij\infty}$ and $H_{j\infty}$, leading to:

$$\mathbf{H}_{am}(k)_{ij} = \frac{\mathbf{h}_{ij\infty} + jk\,\mathcal{F}(\mathbf{h}_{ij}(t) - \mathbf{h}_{ij\infty})}{H_{j\infty} + jk\,\mathcal{F}(H_j(t) - H_{j\infty})} \qquad \mathcal{F}(.) \text{ Fourier transform of } (.) \tag{5.5}$$

Since the FP solver can determine just $\mathbf{H}_{am}$, the gust transfer matrix $\mathbf{H}_{ag}$ is calculated by using the usual piecewise linear penetration-less gust modes and Eq. (4.18). For a further check the penetration-less approach is applied at $M_\infty = 0.68$, avoiding any significant transonic effect, making it possible a comparison with a Doublet-Lattice Method (DLM) solution with 260 aerodynamic panels, 20 spanwise and 13 chordwise. The DLM model has been realized using the aerodynamic module of NeoCASS [251], a design tool based on computational methods for the aero-structural analysis and Multi-Disciplinary Optimization (MDO) of aircraft layouts at the conceptual design stage.

Once more the finite state aerodynamic model is identified by using the integrated motion/gust transfer matrix, while presenting only aeroelastic analyses related to the flutter condition.

Identification: the aerodynamic transfer matrix is identified using an LMFD with $n = 3$. The 18 states model so obtained is shrinked to 8 aerodynamic states by using a Hankel-based reduction. The real and imaginary part related to the first two GAFs of $\mathbf{H}_{am}$ are shown in Figs. 5.7 and 5.8, for Mach 0.678, 0.960 and 1.14. Similar results are obtained for the others GAFs. Figure 5.9 shows a comparison between

Mode	Frequency [Hz]		Error	Type
	Experimental	Nastran		
1	9.60	9.46	1.45%	1st bending
2	38.17	39.44	3.32%	1st torsion
3	48.35	49.71	2.81%	2nd bending
4	91.54	94.39	3.11%	2nd torsion

Table 5.2: *Frequencies of the first four structual model of the AGARD 445.6 wing.*

$\mathbf{H}_{ag}$ from a standard DLM with delayed gust penetration beginning at the foremost point of the leading edge and the one obtained through four chordwise gust modes and Eq. (4.18). The fairly good agreement of the result suggests the correctness of the modeling procedure. To show the effect of an appropriate choice of the gust entering point the impulse response associated to $\mathbf{x}_0$ at the leading edge is shown in Fig. 5.10. It suggests a better value of $x_0 = 0.54\,\mathrm{m}$, ending with the significantly decreased oscillatory behavior of $\mathbf{H}_{ag}(k)$ shown in Fig. 5.11, where the first and second mode generalized aerodynamic forces are represented. Anyhow, both the optimized and unoptimized GAFs are well identified, at least within the range of the displayed reduced frequencies. Similar results are found for the other $\mathbf{H}_{ag}$ terms.

Flutter: flutter analyses with the approximated aerodynamic transfer matrices are carried out at several Mach numbers. Experimental data available in literature [250] and numerical results of the Euler/RANS solver AeroFoam [82, 147] and the independent Two-Fields FP solver [49] performed by other authors are summarized in Fig. 5.12 and Table 5.3. The non-dimensional frequency ratio $I_\omega = \omega_F/\omega_\alpha$ and flutter index $I_F = V_F/(l_a\,\omega_\alpha\sqrt{\mu})$ are presented, where V_F is the flutter speed, l_a the mean aerodynamic half chord, ω_α the circular frequency of the first normal torsional mode and μ the mass ratio, i.e. the ratio between the structural mass and the equivalent fluid mass. Flutter results of the current state space formulation completely agree with the p–k analysis based on the same GAFs.

Mach	**Density**	**Flutter speed** $V_F[\mathrm{m/s}]$				**Flutter index** I_F			
	$\rho\,[\mathrm{kg/m^3}]$	FP	$\mathbf{H}_a$ approximation			FP	$\mathbf{H}_a$ approximation		
			LS1	LS2	LS3		LS1	LS2	LS3
0.678	0.208	229.82	229.70	229.78	229.74	0.4141	0.4139	0.4140	0.4139
0.901	0.099	328.09	328.04	328.06	328.05	0.4093	0.4093	0.4093	0.4093
0.960	0.063	300.20	300.52	300.22	300.24	0.2996	0.2999	0.2996	0.2996
1.072	0.056	488.54	488.51	488.53	488.53	0.4532	0.4532	0.4532	0.4532
1.140	0.078	465.25	464.92	465.19	465.18	0.5144	0.5141	0.5144	0.5144

Table 5.3: *Flutter results of AGARD 445.6 wing.*

5.1.3 Complete aircraft model

A gust response analysis based on an LMFD and the penetration-less gust approach is demonstrated on a simple aircraft model, freely available as a Matlab program in Ref. [252], represented in Figure 5.13. It is based on a beam model condensed to five symmetrical degrees of freedom, associated to two rigid and three symmetric deformation modes. The standard unsteady strip theory [179] models the aerodynamics, with a constant lift coefficients along the wing (C_{z,α_w}) and tail span (C_{z,α_t}), the fuselage contribution being approximated through a constant aerodynamic moment coefficient (C_{m,α_f}). The downwash angle ε at the tail is characterized by a downwash coefficient $d\varepsilon/d\alpha = 0.35$. The

main characteristics of the aircraft considered are: wing mean aerodynamic chord (m.a.c.) $c_w = 3.83$ m, wing span $b = 24$ m, wing elastic axis position $e_w = 0.35$ cw, wing surface area $S_w = 91.92$ m^2, stabilizer chord $c_t = 2.29$ m, stabilizer span $b_t = 10$ m, tail elastic axis position $e_t = 0.25\ c_t$, horizontal tail surface area $S_t = 22.90$ m^2, sweepback angle $\Lambda = 17$ deg, stabilizer position $x_t = 17$ m, center of gravity position $x_{cg} = 0.15\ c_w$, aircraft mass $M = 40000$ kg, and inertia moment about lateral axis $I_y = 1.61 \cdot 10^6$ kg m^2.

The strip theory allows exploring a hard test case for the identification process as its $\mathbf{H}_a$ is somewhat less smooth than that provided by many of the previously cited fully interfering computational schemes. So it allows a better check of the way used to determine an appropriate value for the gust entering point $\mathbf{x}_0$ to be adopted to obtain smooth gust GAFs.

Our response analyses will be carried out for one-dimensional (1D) vertical gusts and continuous turbulence, for a flight condition with $V_\infty = 220$ m/s and air density $\rho_\infty = 0.59$ kg/m^3. A deterministic 1-cos gust, having intensity $\bar{v}_g = 1$ m/s and length $L_g = 9.5\ m$, i.e. 2.5 mean aerodynamic chords, is considered, both as a direct input and by means of a discrete shaping filter representation, where an RMFD with $ro = 1$ is used, so to handle the worst approximate case. The continuous gust analysis utilizes a Dryden shaping filter, Eq. (4.19), having root mean square intensity $\sigma_g = 1$ m/s and turbulence scale $L_g = 9.5\ m$. Both a stochastic simulation and Lyapunov equations are used to obtain the turbulence response variances. Since the aircraft model has a simply stable plunge mode, the procedure shown in section 4.2.2 is adopted, resulting in the uncoupled aeroelastic system of Eq. (4.35). The, short, gust/turbulence scale used well stresses the identification process, better results may be obtained by merely assuming a larger L_g.

A smoothing entering point $\mathbf{x}_0$ for a single vertical gust patch is inferred from the impulse response related to $\mathbf{H}_{ag}$ having $\mathbf{x}_0$ placed at the wing root foremost point. Figure 5.14a shows the pitching impulse, which clearly depicts two peaks separated by the distance between wing and tail (17 m). Placing the gust entering point in between them moves the peaks closer, Fig. 5.14a, mitigating the oscillations of $\mathbf{H}_{ag}$, as it appears from Fig. 5.14b, where the identified matrices are also shown. Only the approximation provided by LS1 is presented, being negligible the differences with LS2 and LS3. A better accuracy is achieved when $\mathbf{H}_{ag}$ is based on the "optimized" $\mathbf{x}_0$, the less smooth one producing anyhow quite similar results, at least for the simulations showed afterwards.

Gust responses are carried out by using both a unified identification of $\mathbf{H}_\mathrm{a}$, for structural motions and penetrating gusts, and a penetration less approach with eight gust modes, five for the wing and three for the tail. Both models lead to eight aerodynamic states, obtained after a Hankel based reduction applied to an LMFD with $n = 3$, i.e. with 18 raw states. Deterministic gust responses are determined by using both models, while continuous turbulence variances are calculated by using the former model and Lyapunov equations and by post processing adequately long turbulence response simulations resulting from the penetration-less model.

Sample time responses to a deterministic 1-cos gust are shown in Fig. 5.15. The state space response is calculated by using the smallest order deterministic shaping filter previously shown, i.e. with $n = 1$, and integrating the related LTI system with the initial conditions of Eq. (4.42). The output quantities are the load factor Δn_z, the bending moment M_{b_w} (positive tip down) and torsion moment M_{t_w} (positive leading edge up) at the wing root, and the bending moment M_{b_t} and torsion moment M_{t_t} at the horizontal tail root. The

reference point for wing loads is the intersection of the line of the aerodynamic center with the wing elastic axis, whereas for tail loads is the elastic axis. Small discrepancies in the maximum values, especially for tail loads, are due to the short gust scale used, and come from a relatively poor approximation of the very high frequency content, showing its effect only on the very beginning of the response transient. Slightly increasing the gust length to just three chords would avoid these over predictions. Nevertheless, the double dynamic residualization provides an adequate approximation, down to the used short gust length. Gust response variances to stochastic turbulence are shown in Table 5.4, with the results of the identified state space model obtained by applying the Lyapunov equation to the uncoupled simply stable - asymptotically stable aeroelastic system. Calling $\mathbf{H}_{aeg}$ the aeroelastic transfer matrix from the gust input to a generic output $\mathbf{y}$, the results of the classic approach come from the standard formulae:

$$\mathbf{\Sigma}_{yy} = \frac{1}{2\pi} \int_{-\infty}^{\infty} \mathbf{\Phi}_{yy}(\omega) d\omega \tag{5.6}$$

with

$$\Phi_{yy}(\omega) = \mathbf{H}^{*}_{aeg}(\omega)\, \mathbf{\Phi}_{gg}(\omega)\, \mathbf{H}^{T}_{aeg}(\omega) \tag{5.7}$$

being $\mathbf{\Phi}_{gg}(\omega)$ the PSD of the vertical gust velocity, while those associated to the penetration-less formulation comes from averages over relatively long samples of the deterministic response to a Dryden shaped white noise.

	Classic gust modeling	**Penetration less gust**	**State space (Lyapunov)**
$\sigma(\Delta n_z)$	0.03951	0.03956	0.03919
$\sigma(M_{b_{\text{wing}}})$	4.4307e+04	4.4250e+04	4.3268e+04
$\sigma(M_{t_{\text{wing}}})$	7.0510e+03	7.0355e+03	7.1341e+03
$\sigma(M_{b_{\text{tail}}})$	1.6822e+03	1.6879e+03	1.7069e+03
$\sigma(M_{t_{\text{tail}}})$	2.6829e+01	2.7339e+01	2.5259e+01

Table 5.4: *Standard deviation values for a gust response to a 5 semichords turbulence scale length stochastic gust.*

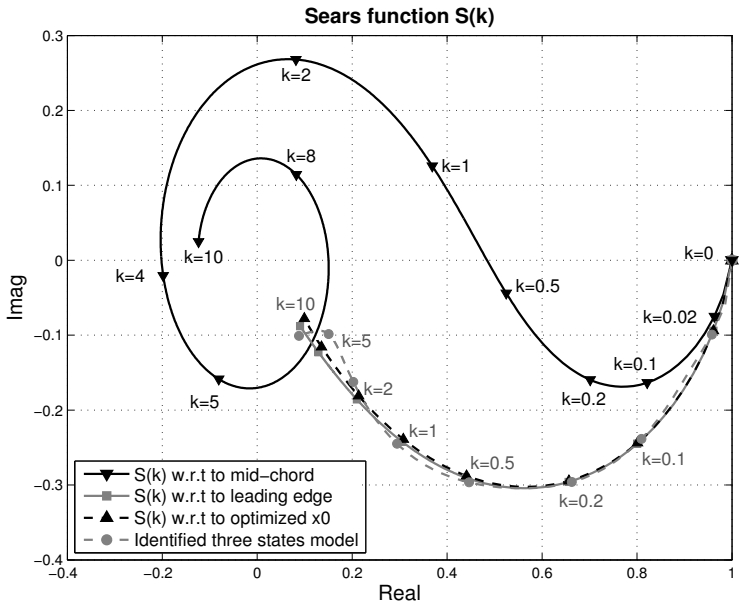

(a) *Sears function in the complex domain.*

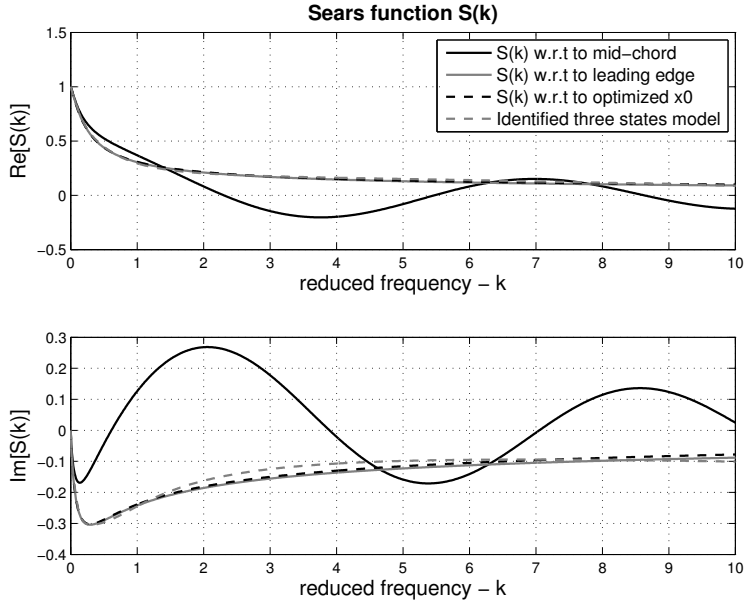

(b) *Real and imaginary part as a function of the reduced frequency.*

Figure 5.3: *Sears function referenced to different values of* $\mathbf{x}_0$.

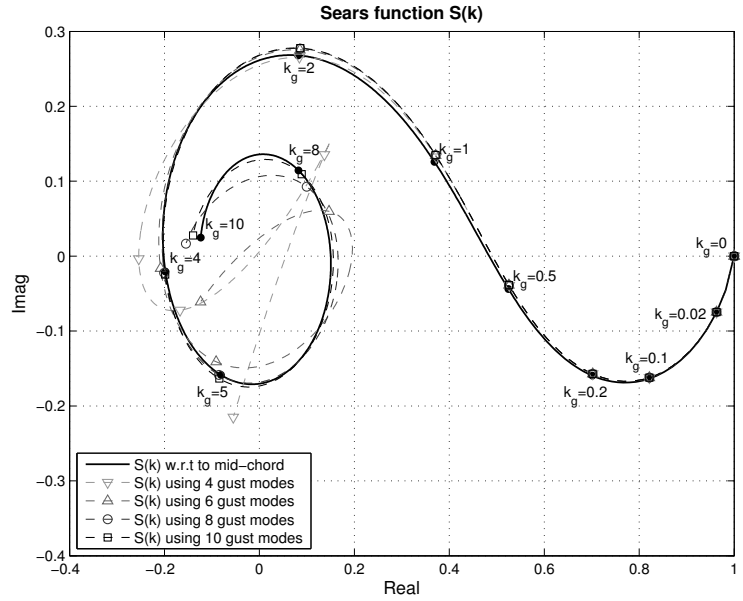

Figure 5.4: *Sears function reconstructed from penetration-less gust modes.*

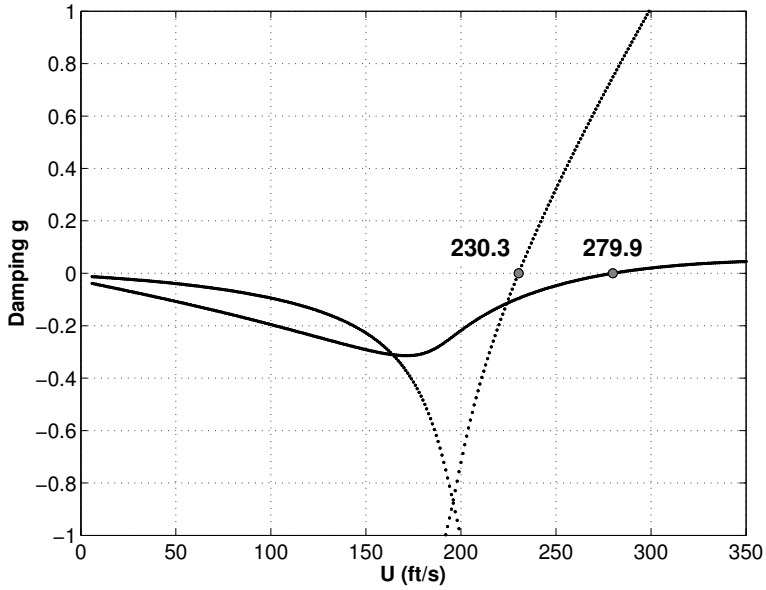

Figure 5.5: *Root loci of a plunging typical section, from the eigenvalues of:* $\mathbf{A}_{ae} = s\,\mathbf{E}_{ae}$.

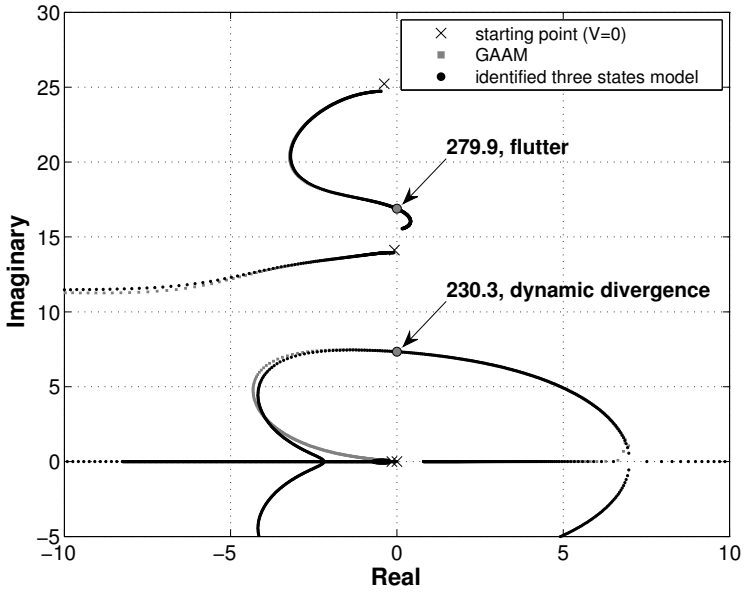

Figure 5.6: *V-g diagram of a plunging typical section, from the eigenvalues of:* $\mathbf{A}_{ae} = s\,\mathbf{E}_{ae}$.

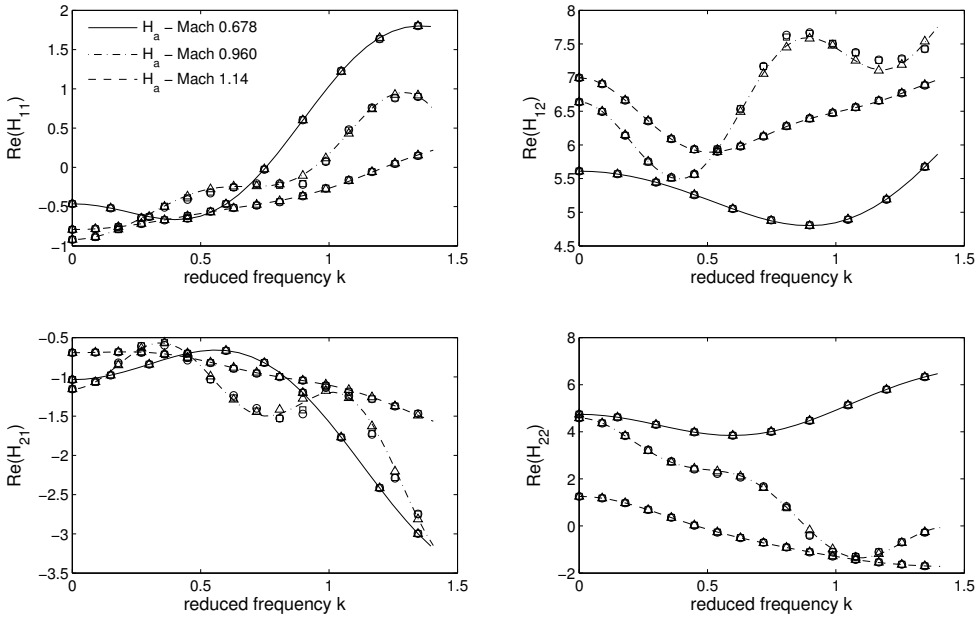

Figure 5.7: *Real part of the AGARD 445.6 wing* $\mathbf{H}_a$ *matrix, LMFD schemes: (△) LS1 – (○) LS2 – (□) LS3. Reduced frequencies dataset:* $k = \{0, 0.005, 0.01, 0.02, 0.05, 0.1, 0.5, 0.7, 1.0, 1.2, 1.5, 1.7, 2.0, 2.3, 2.6, 3.0\}$.

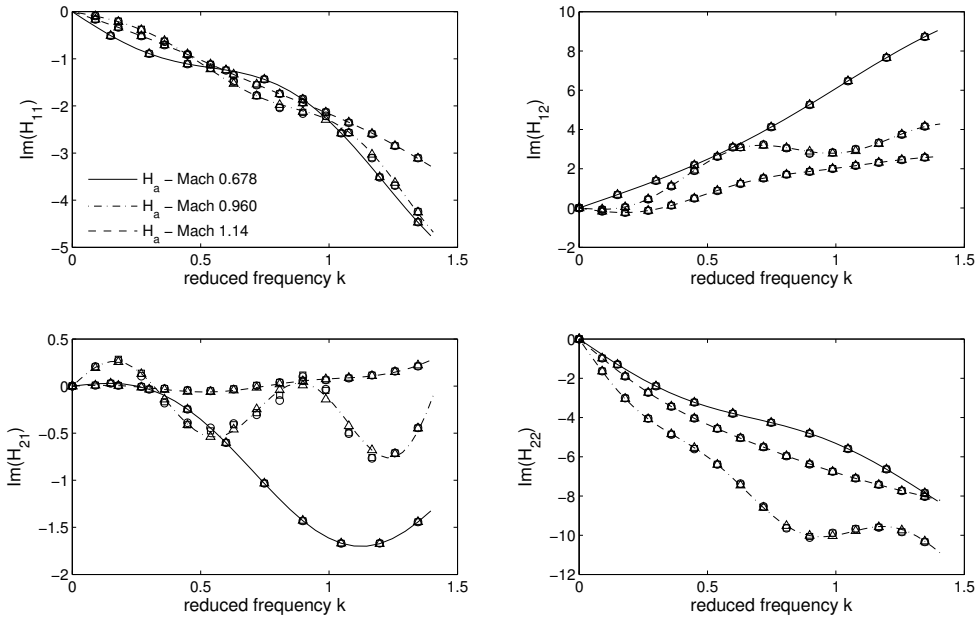

Figure 5.8: *Imaginary part of the AGARD 445.6 wing* $\mathbf{H}_a$ *matrix, LMFD schemes: (△) LS1 – (○) LS2 – (□) LS3.*

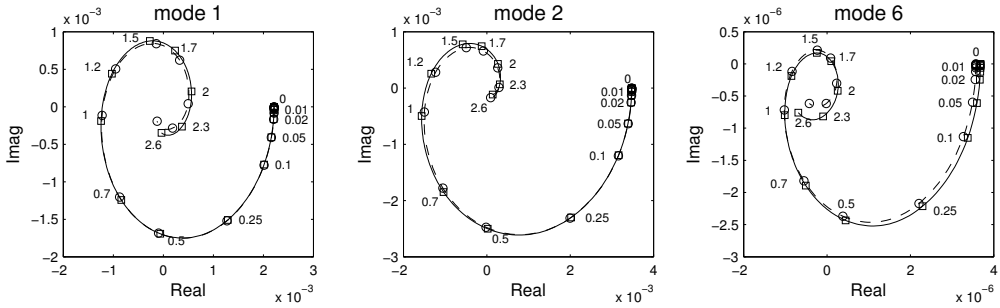

Figure 5.9: $\mathbf{H}_{ag}$ *of the AGARD 445.6 wing, recovered through penetration-less gust modes (dash line).*

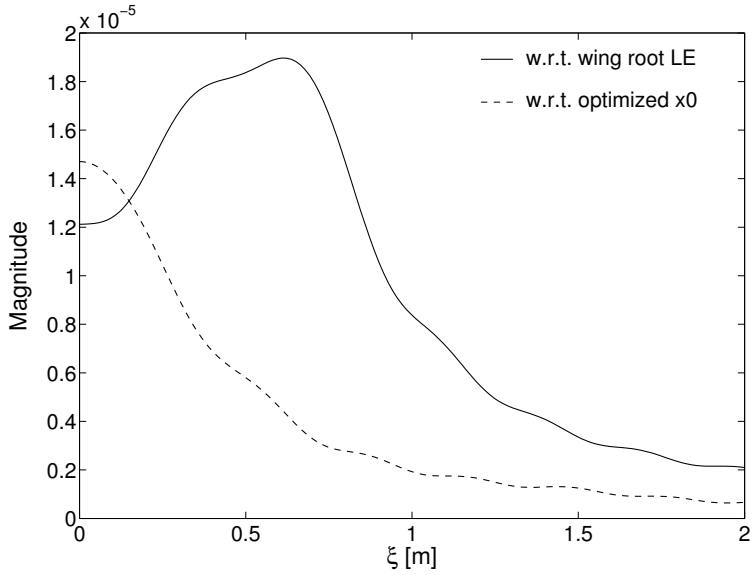

Figure 5.10: *A gust impulse response of the AGARD 445.6 wing.*

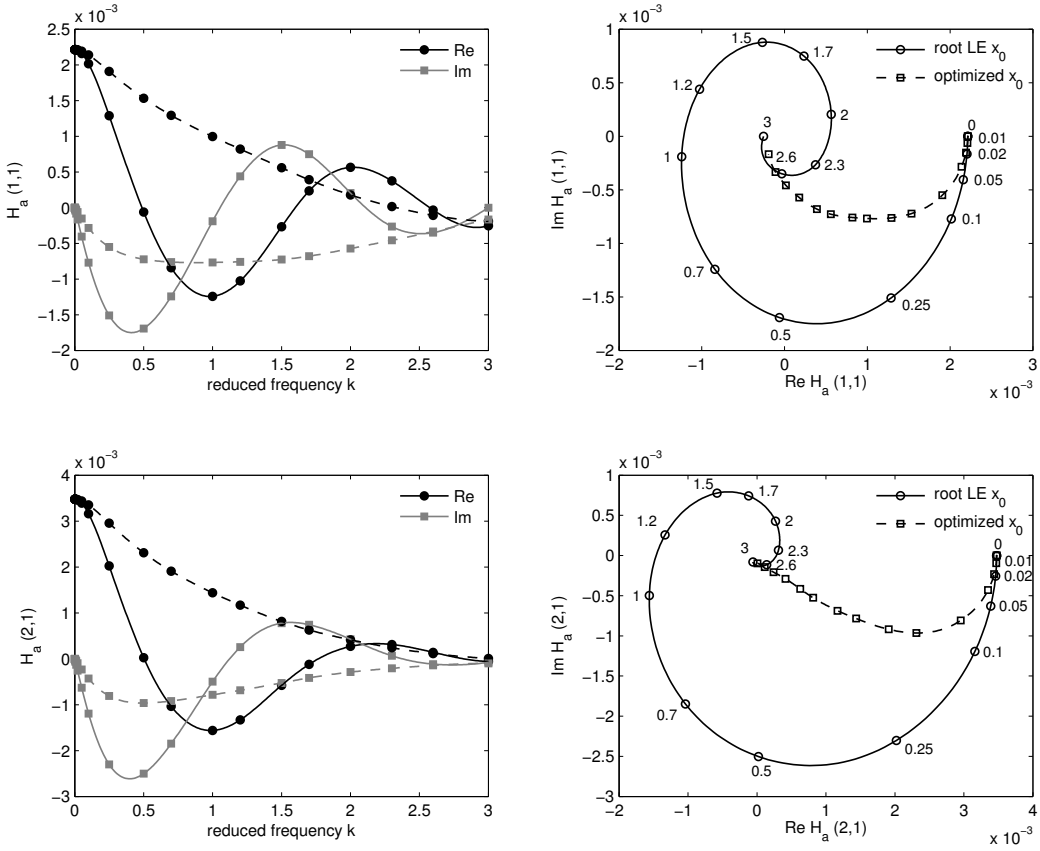

Figure 5.11: *Comparison of the AGARD 445.6 wing* $\mathbf{H}_{ag}$ *matrix, Mach 0.678, w.r.t. the root leading edge, solid line (—) and the optimized* x_0 $(0.54\,m)$*, dash line (- - -).*

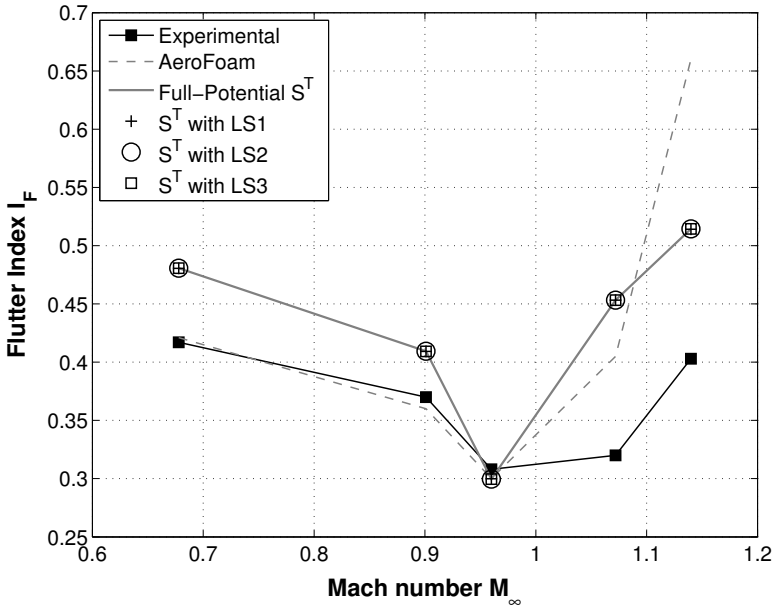

(a) *Flutter index I_F*

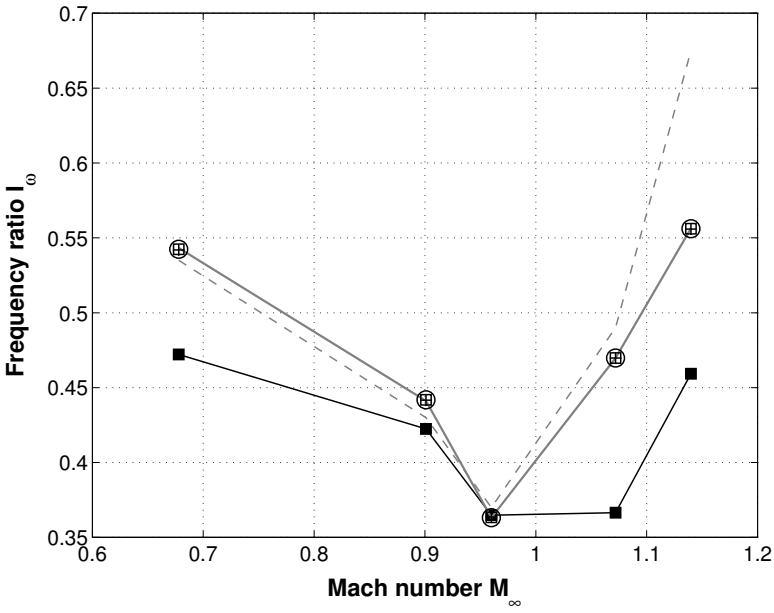

(b) *Frequency ratio I_ω*

Figure 5.12: *Comparison of the flutter index I_F and frequency ratio I_ω obtained with an LMFD model, derived from a linearized full-potential solution, with those of other formulations.*

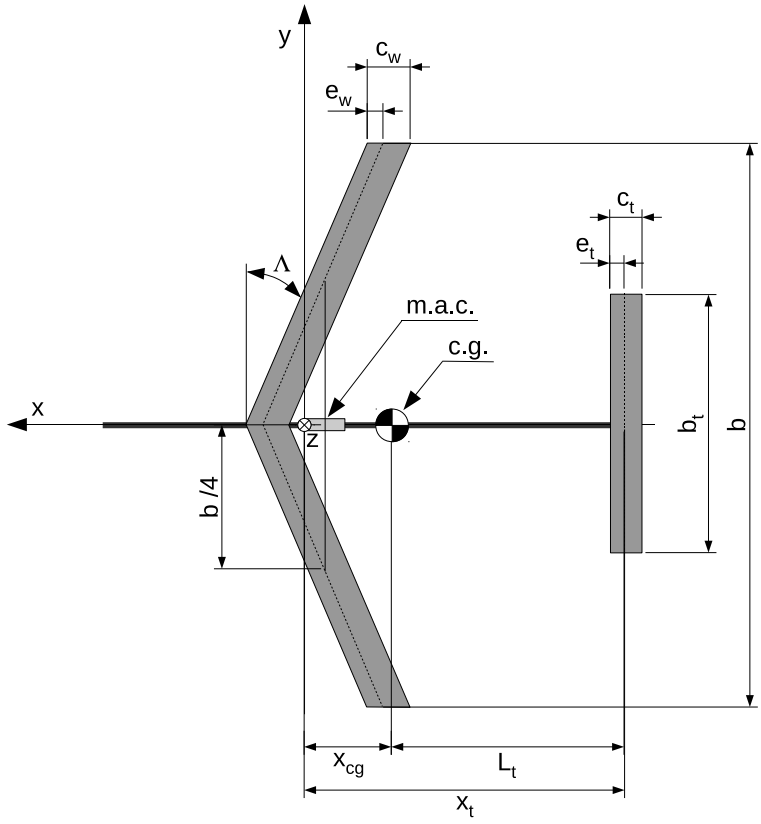

Figure 5.13: *Geometry of the aircraft model.*

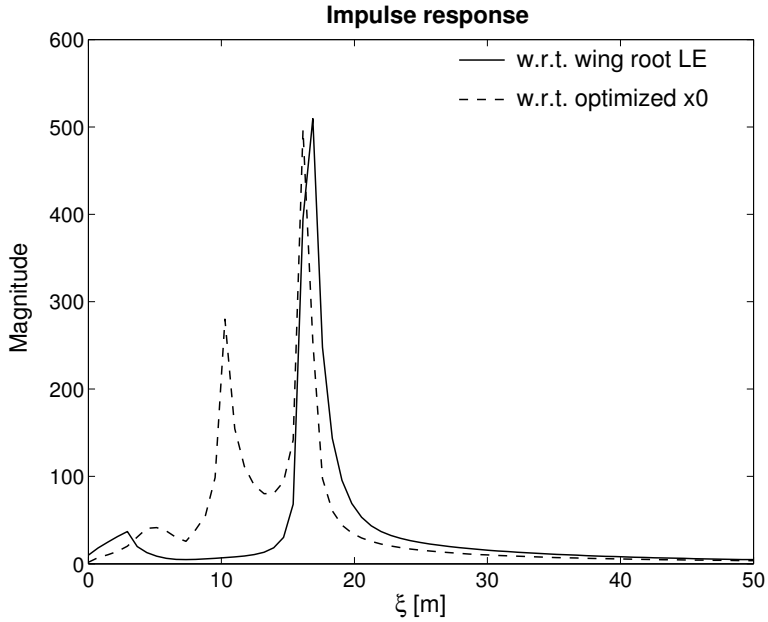

(a) *Pitching mode gust impulse response.*

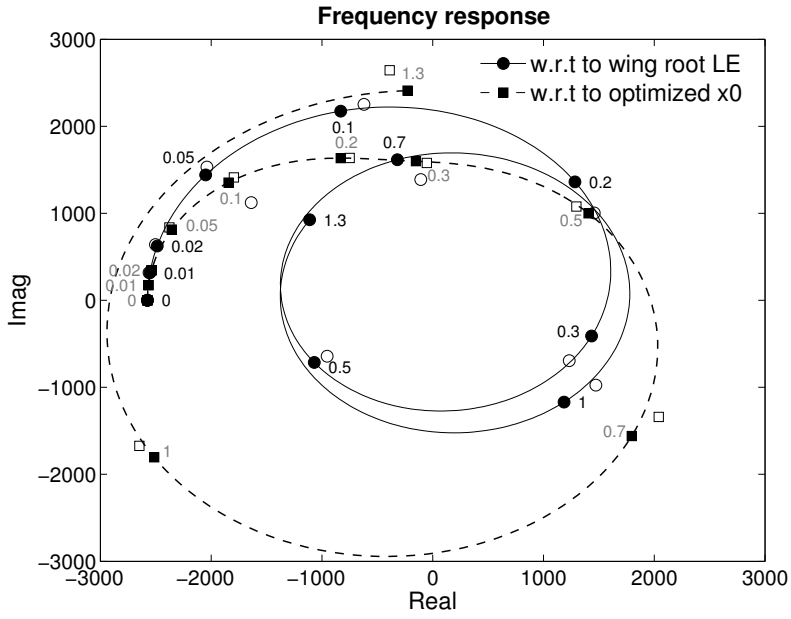

(b) *Pitching mode freq. response: (•) original, (○) identified.*

Figure 5.14: *Pitching mode GAF characterization in time and frequency, referenced to the wing root leading edge and to an "optimized"* $\mathbf{x}_0$.

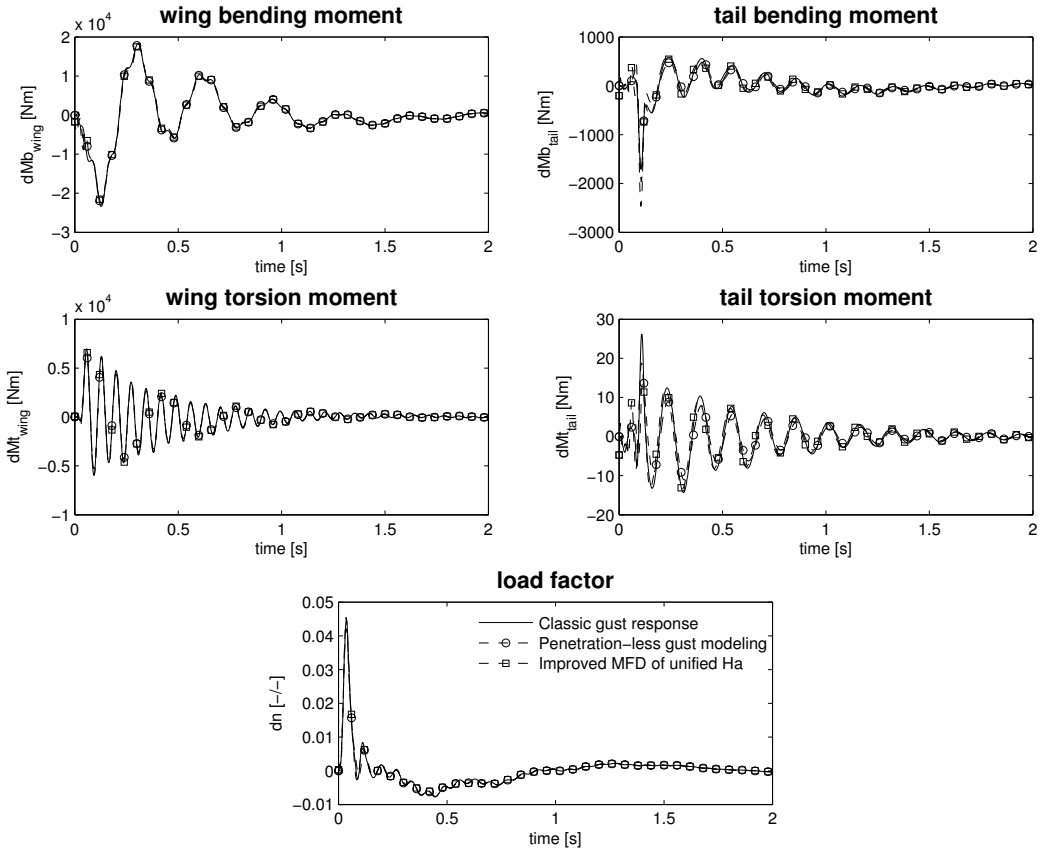

Figure 5.15: *Gust response modeling comparison - deterministic 1-cos gust.*

5.2 Applications of gust modeling approach to complex industrial cases

In section 5.1 the approach has proved its effectiveness in carrying out aerodynamic transfer matrices obtained from low fidelity models (e.g. Theodorsen theory, strip theory, double-lattice method).

In this section the method is applied on high-fidelity aerodynamic models, using Euler equations, on subsonic and transonic flows. The goal was to understand the potential of the method using complex models and if the approach was able to approximate also pressure distributions besides integral quantities as lift and moment. It is remarked that the gust modes approach is naturally formulated for the approximation of integral quantities, being its aim the recovering of the aerodynamic transfer matrix. So no expectations were placed on the approximation of pressure distributions.

The modified gust modeling approach based on shape functions has been implemented in the DLR TAU computational fluid dynamic solver, and gust simulations have been performed. As described in section 4.2, the proposed penetration-less approach calculate the gust response using a convolution in time of the impulse responses of the so called gust modes. The implementation of the method is straightforward. In an aeroelastic simulation environment the approach, if necessary, could even be used without modification of the aerodynamic solver. Indeed it relies on the same concept used for the calculation of the generalized aerodynamic forces, where each structural modes is used to excite the aerodynamic solver with a blended step time history law in order to compute the correspondent column of the aerodynamic tranfer matrix. The gust modes operate in the same way of the structural modes, with the only difference that the gust modes bring just a kinematic contribution to the boundary conditions of the aerodynamic solver, being just disturbance velocity shape functions, whereas the structural modes provides both a geometric (the displacement) and a kinematic (the velocity) contribution.

Nevertheless, in this thesis the penetration-less approach has been implemented directly in the DLR-TAU solver, being the following simulations performed just on rigid aircraft models. The implementation just exploit the available implementation of the disturbance velocity approach (see section 4.1.2) in TAU, by simply providing spatially fixed vertical velocity disturbances with profile as the chosen shape functions (constant or linear). Each shape function excite the aerodynamic model with a step time history law. The correspondent lift and moment time history responses are stored and, in a post-processing step, convoluted in time with the actual gust profile under investigation. For a verification of the implementation, the convolution has been also performed using the pressure time histories, leading to the very same results as those obtained using the lift and the moment.

Two-dimensional test cases such as the NACA 0012 airfoil and a 2D wing-HTP (Horizontal Tail Plane) configuration have been analyzed, showing a good approximation of integral quantities, as well as pressure distribution, for a broad range of gust profiles starting from 2 chords length up to 30 chords lengths. Despite the inherent linearity of the approach, interesting results have been found even for transonic cases. A nonlinear extension by using Volterra series would be straightforward, even if the cost to obtain high order Volterra kernels would compromise the effectiveness of the method. Further complex cases of industrial relevance, considering high fidelity CFD models of aircraft, are examined to verify the soundness of the approach for problems having a far larger order and complexity than academic test cases.

Hereafter are shown some of the results obtained for the two dimensional test cases, analyzed performing sequential simulations on a 2 cores Intel Core2 Duo CPU E6750@ 2.66 GHz. A total number of 27 gust cases having 1-cosine shape are analyzed. The gust length range is from 2 chords to 30 chords length, and the gust amplitude from 5 m/s to 12 m/s. Concerning the NACA 0012 airfoil (modeled using an unstructured grid of 2150 triangles) at subsonic regime (Mach 0.288) the time to process all the 27 gust cases with the disturbance velocity approach (which model the gust as an additional velocity field superimposed, in an Arbitrary-Lagrangian-Eulerian formulation, to the cell face velocity) implemented in the TAU solver is 3177 s (dt = 0.0005 s, 600 time steps). The gust modes approach, using just three gust modes, save up to 87% of the computational time, being required only 392 s (dt = 0.0005 s, 600 time steps) for all the 27 cases. The results are of course approximated, since the method is linear(ized) and make use of a least squares interpolation to approximate the gust profile. However they show the potential of the method which, at least for subsonic flows, may be applied for a worst-case loads prediction as a complementary approach to low-fidelity methods.

Table 5.5 shows the maximum lift and moment relative error (in percentage) between the disturbance velocity approach and the gust modes approach.

	Gust length [chords]								
	2	4	6	8	12	16	20	25	30
					sea level				
gust amplitude [m/s]	7.84	8.81	9.42	9.88	10.57	11.09	11.51	11.95	12.32
lift error [%]	2.41	0.73	0.25	0.17	0.22	0.31	0.39	0.50	0.59
moment error [%]	2.64	1.39	0.43	0.24	0.27	0.39	0.53	0.68	0.83
					15000 ft (4572 m)				
gust amplitude [m/s]	6.16	6.92	7.4	7.76	8.31	8.72	9.05	9.39	9.68
lift error [%]	2.39	0.75	0.25	0.15	0.17	0.23	0.30	0.37	0.43
moment error [%]	2.59	1.40	0.37	0.12	0.09	0.16	0.24	0.34	0.43
					60000 ft (18288 m)				
gust amplitude [m/s]	2.92	3.28	3.51	3.68	3.94	4.13	4.29	4.45	4.59
lift error [%]	2.18	0.65	0.14	0.02	0.01	0.02	0.05	0.09	0.12
moment error [%]	2.33	1.27	0.16	0.15	0.28	0.29	0.28	0.25	0.22

Table 5.5: *Prediction error of the gust mode approach w.r.t. the disturbance velocity approach.*

Figure 5.16 shows the approximation of the lift and the pressure (evaluated at the maximum lift) for the 2 chords length 1-cosine gust profile (at sea level), which is the worst approximate case. Better approximations are obtained for all the others gust lengths and amplitudes cases. A good approximation is obtained, especially considering the computational time saved to run all the 27 gust cases. Also the pressure is quite well approximated, with a relative percentage error of 5.41% w.r.t to the disturbance velocity approach. The transonic case (Mach 0.75) is outside the border limit of applicability of the gust modes approach, which is a linear(ized) approach. However quite good results are found in terms of integral quantities, but for the very short 2 chords length gust. For the transonic case

the worst approximation case in term of pressure distribution is the gust having the greater amplitude, which is the 30 chords length gust, because inducing the greater angle of attack will lead to the strongest shock waves on the airfoil. For this case, the approximation of the pressure evaluated at the maximum load, and the one evaluated at the maximum difference between the disturbance velocity and the gust modes approach are presented in Figure 5.17.

As can be seen a good approximation of the shock wave is obtained at the maximum load, even if the method is linear(ized). This happens because the amplitude of the gust modes used is great enough to excite the nonlinearity of the flow, which will be therefore present in the associated impulse response. However this nonlinearity will remain in the convolution response of the gust modes approach, even when the gust amplitude will decrease under a certain value and a linear response would be expected. This may be seen considering the pressure evaluated in a non dimensional time different from those of the maximum load, as shown looking at the figure of the pressure evaluated at the maximum difference between the disturbance velocity approach and the gust modes approach. Worst results are expected for transonic cases if the gust approach would be applied on more complex cases other than a two dimensional airfoils. However, nonlinear extension of the gust modes approach max be developed using generalized impulse responses (e.g. Volterra series).

Similar results for a subsonic flow (Mach 0.25) are found for the NACA 0012 airfoil with Horizontal Tail Plane (HTP) configuration (Fig. 5.18), where an unstructured hybrid grid (68518 nodes) has been used. Considering one gust profile, the TAU disturbance velocity approach simulate the response of 1 gust profile in 1h 40min (dt = 0.0005 s, 500 time steps). The gust modes approach, using a total of 4 gust modes (3 linear for the wing and 1 constant for the tail) predict the response with a total computational time of 5h 21min (dt = 0.0005 s, 500 time steps). However the main computational time of the gust modes approach is related to the response of the 4 shape functions (5h 20min), while few time is demanded to the post-processing of the traveling contribution of the gust. Therefore, it is expected that analyzing at least 5 gust profiles would be saved the 22% of the computational time (5h 25 min for the gust modes approach and 7h for the disturbance velocity approach), while simulating 10 gust profile would be saved the 65% of the time (5h 30 min for the gust modes approach and 15h 45min for the disturbance velocity approach), and so on. Hereafter are show the results for the worst approximated cases, that is the shortest gust length (2 chords) for integral quantities, leading to a relative error of 4.1%, and the longest gust length (30 chords) for the pressure distribution. The approximation of the pressure at the maximum load for the 30 chords length gust case is shown in Fig. 5.20. As may be seen the tail pressure is not so well approximated. This is because just one constant gust mode is used to approximate the gust response over the tail. Better results are expected using linear modes as for the wing.

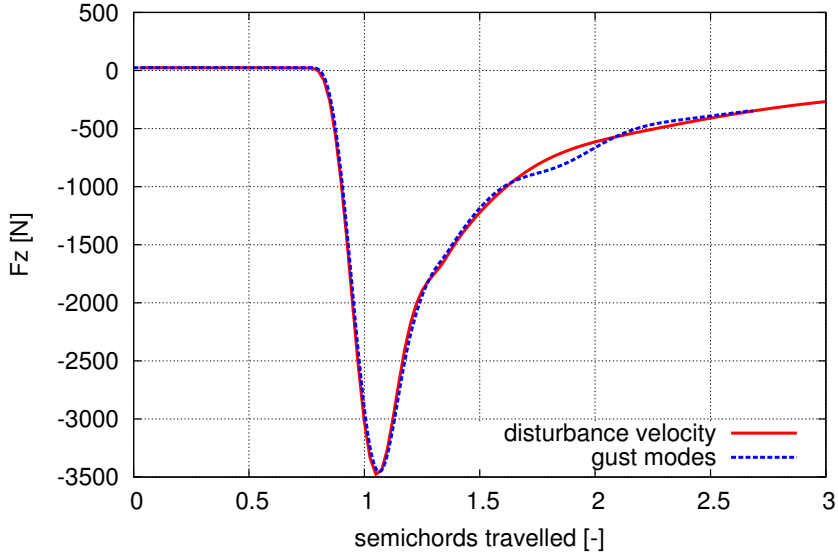

(a) *Lift.*

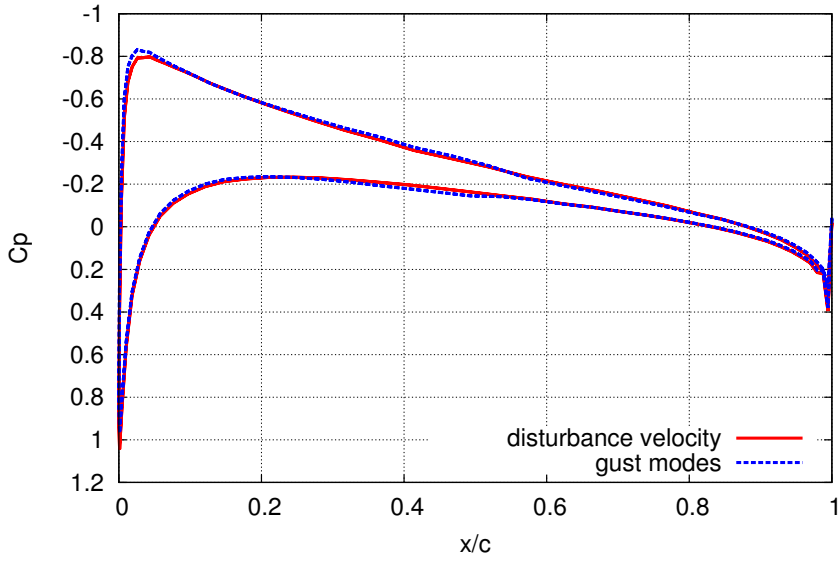

(b) *Pressure distribution at the maximum load.*

Figure 5.16: *Response of the NACA 0012 airfoil to a 2 chord gust at Mach 0.288.*

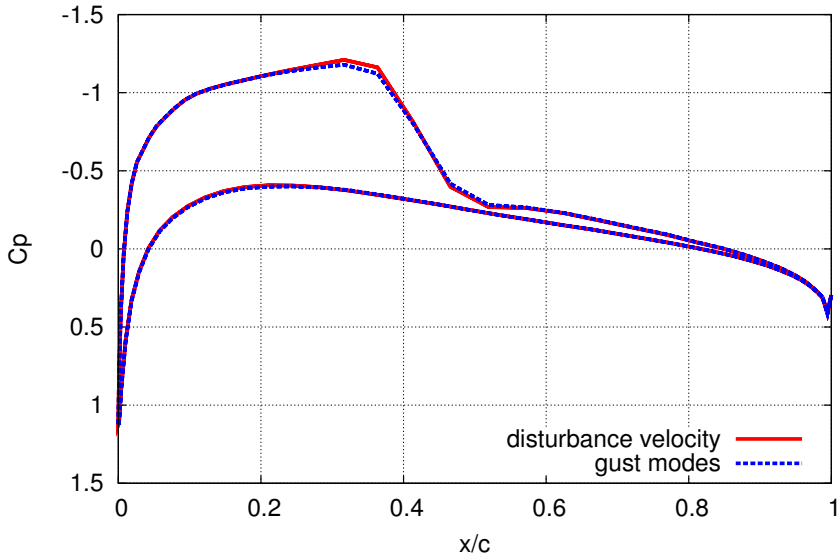

(a) *Pressure distribution at the maximum load.*

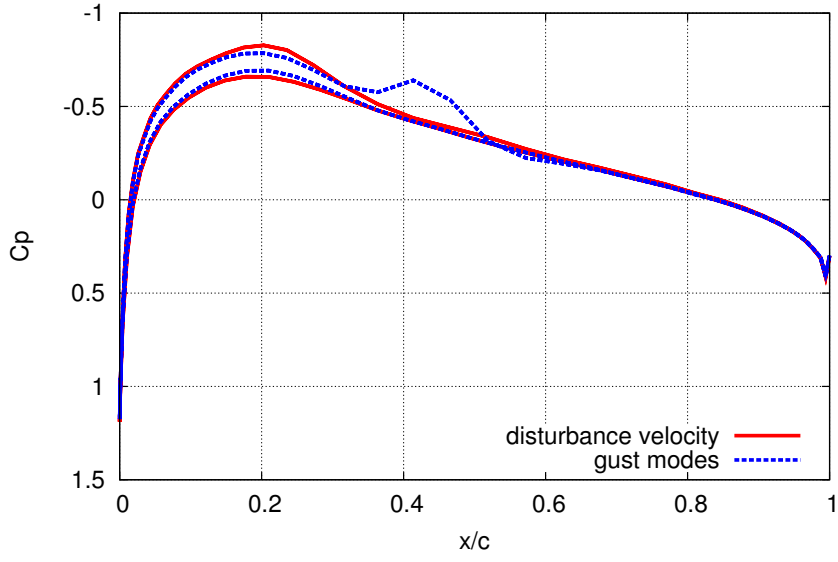

(b) *Pressure distribution at the maximum error.*

Figure 5.17: *Pressure of the NACA 0012 airfoil to a 30 chord gust at Mach 0.75.*

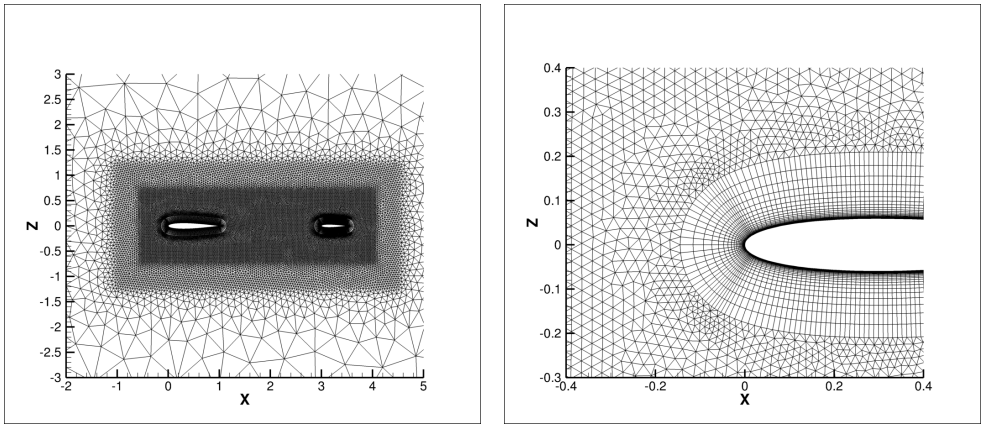

(a) *HTP zoom detail* **(b)** *HTP zoom detail*

Figure 5.18: *Computational grid of the Horizontal Tail Plane (HTP) configuration.*

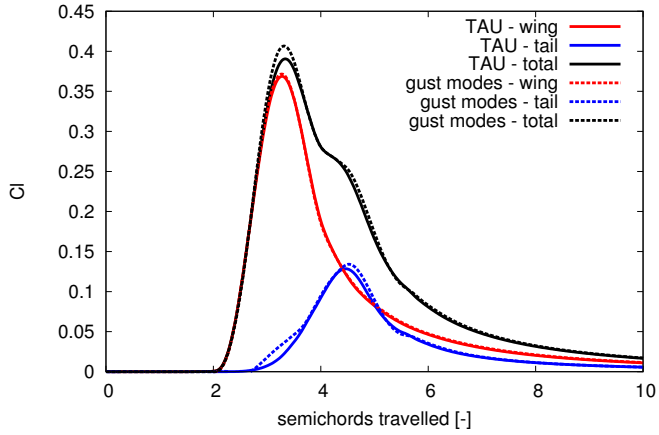

(a) *2 chord length gust*

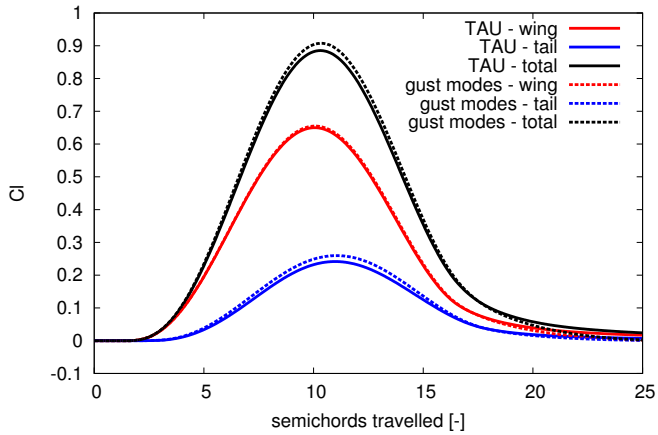

(b) *30 chord length gust*

Figure 5.19: *Lift coefficient for the HTP configuration.*

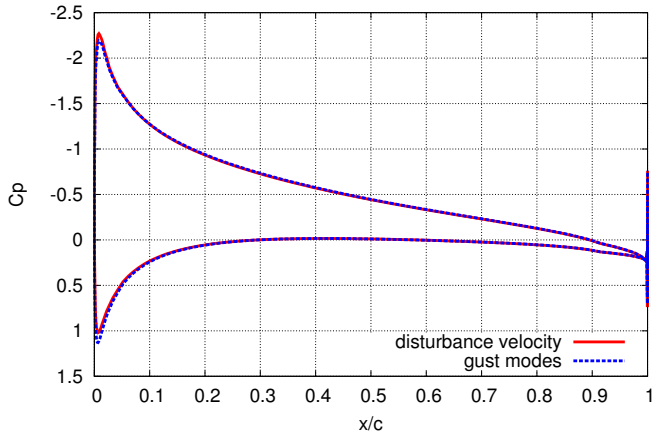

(a) *Wing airfoil.*

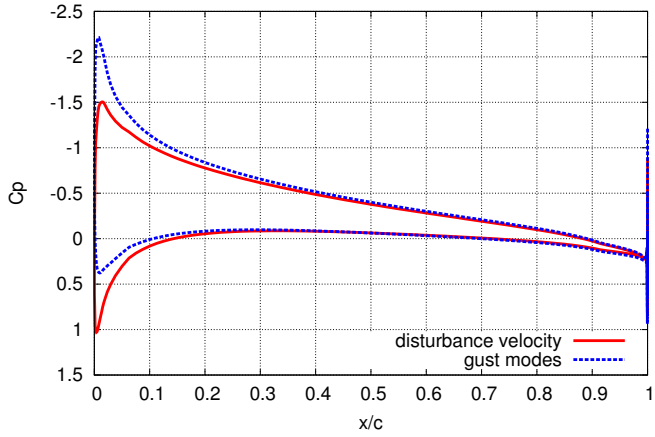

(b) *Tail airfoil.*

Figure 5.20: *Partition of the lift of the HTP config. for a 30 chords length gust.*

Two final complex test cases of industrial relevance are addressed. In both cases the aerodynamic forces are obtained by solving the three-dimensional and time accurate nonlinear Euler equations with the DLR-TAU code [253]. The configurations considered[1] are:

DLR F12 aircraft: is a conventional wing-fuselage-tail configuration for civil passenger transport, selected whitin the SimSAC project as the reference benchmark to compare different dynamic derivatives prediction methods [254]. In this work the aircraft has been used to understand the prediction capability of the proposed alternative gust response approach for high-fidelity aerodynamic models. An unstructured CFD mesh with 6.7 hundred thousands points and 3.5 million tetrahedra elements is used to discretize the aircraft model (Fig. 5.21a). The model is discretized spatially

[1]The aerodynamic computational meshes of the aircraft used as benchmarks have been provided by the DLR Institute of Aerodynamic and Flow Technology of Braunschweig.

with a central scheme with scalar artificial dissipation and temporally with a Backward Euler implicit scheme. The discretized equations are solved with LU-SGS iterations using dual time stepping and a multigrid approach with a 4 levels V-cycle.

Standard Dynamics Model (SDM): is a generic fighter aircraft configuration [255] based on the F-16 plantform, whose geometry has been developed for an international effort to collect wind tunnel data for unsteady aerodynamics [256]. It includes a slender strake-delta wing, horizontal and vertical stabilizers, ventral fin and a blocked off inlet section. However these last two components have been removed in the current model, since the main interest in the gust response contest is to understand the limitation of the gust modes approach when using series of shape function for aircraft with a low aspect-ratio. An unstructured CFD mesh with 6.2 hundred thousands points and 3.4 million tetrahedra elements is used to discretize the aircraft model (Fig. 5.21b). The model is discretized spatially with an upwind scheme with scalar artificial dissipation and temporally with a Backward Euler implicit scheme. The discretized equations are solved with LU-SGS iterations using dual time stepping and a multigrid approach with a 3 levels V-cycle.

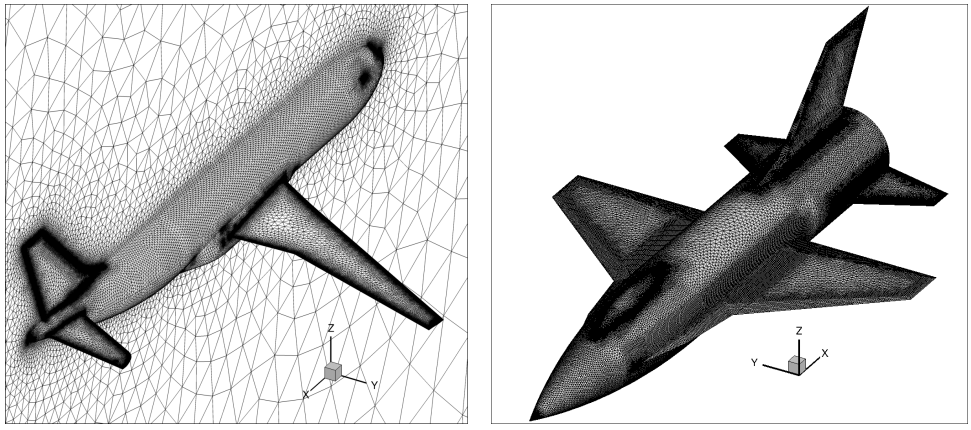

(a) *DLR F12 aircraft* **(b)** *generic fighter configuration*

Figure 5.21: *Computational grids of the aircraft configurations.*

Figure 5.22a shows the results for the simulation of the gust responses for the DLR F12 aircraft in subsonic flow regime, at Mach 0.2, and angle of attack of 7 degrees. Six gust profiles are considered, with a range of lenght running from 4 to 20 reference lengths (i.e. the aerodynamic mean chord, which is 0.253 the length of the aircraft). The responses predicted with the gust modes approach (GMA) are obtained using 6 equally spaced shape functions along the total lenght of the aircraft. Results show an overprediction of 2.5% of the lift coefficient for the longer gusts and small oscillations are found for the shortes gust. In this case 6 unsteady full nonlinear Euler simulations are performed to obtain the impulse responses to the 6 shape functions used to build through the convolution the time history responses. Therefore the gust modes approach in this case require almost the same computational time than computing direcly the responses to the six gusts. Obviously the

proposed method is appealing for CFD calculations just when it is analysed a number of gusts greater than the number of used shape functions. Indeed, any further time history response to gust profiles other than the six considered (potentially even a long sthochastic gust) would be obtained with the GMA in a matter of few seconds (i.e. just the time required by the convolution of the scalar value impulse responses with the new gust profile) with a sequential computation on a local machine, with respect to the hours needed by running, in parallel on a cluster framework, a new full nonlinear unsteady Euler simulations with the TAU code. Similar results are found for the generic fighter SDM configuration in transonic flow regime at Mach 0.78 (Fig. 5.22b), where Six gust modes are used as well.

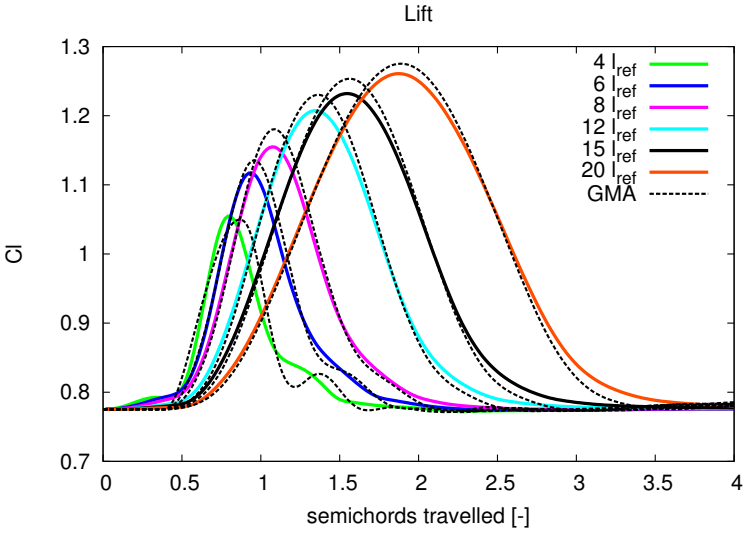

(a) *DLR F12 aircraft.*

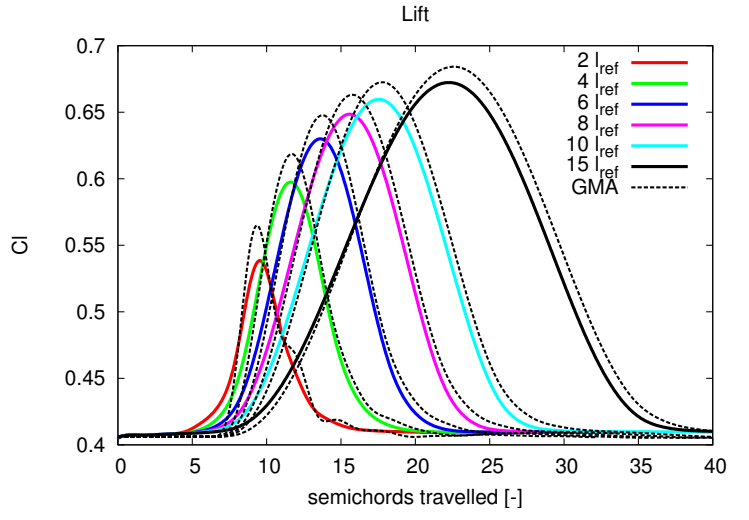

(b) *SDM generic fighter configuration.*

Figure 5.22: *Gust responses of CFD complex models generated using 6 gust modes.*

5.3 Applications of the Schur subspaces projection

Numerical results are obtained for a typical aeroelastic problem, a two degrees of freedom pitch-plunge thin airfoil in full-potential flow, at Mach 0.5 so to avoid relevant transonic effects. This help in better understanding the relevance of the different eigenvalues (acoustics and of pressure). Anyhow, the procedure here developed is suitable also for transonic flows.

Depending on the problem, a typical aerodynamic model may have 10^4 to 10^6 or more degrees of freedoms (DOFs), which may be reduced to only 10 to 10^2 DOFs. In our example, the aerodynamic model is spatially discretized using unstructured O-grids, leading to a coarse model, a medium model and a fine model of respectively 6061, 9336, and 13508 equations. During the generation of the linearized model, the Jacobian matrix may be also carried out by lumping matrices so providing a faster way to calculate the model reduction without leading to any change in the results. The model has been verified by comparing the aerodynamic transfer matrix with analytical models (indicial methods [179]) and other references (AGARD tables [257]). It is shown that the aerodynamic transfer matrix, obtained from both a direct evaluation on selected frequencies or the ratio of the Fourier Transforms of output and input signals, is comparable to the references up to a reduced frequency of 2, as shown in Fig. 5.23 and Fig. 5.24.

The aerodynamic transfer matrix may be also determined by using the Fourier transform on the input-output signals reduced by their asymptotic part. If the system input is a step (Eq. (5.8)), one may remove the asymptotic part (Eq. (5.9)) from the output response and identify the system as if excited from an impulse (Eq. (5.10)), paying attention in recovering then the right input matrix. Therefore, being the output response to a step given by:

$$\mathbf{y} = \mathbf{C}\left(s\mathbf{E} - \mathbf{A}\right)^{-1}\mathbf{B}\,\frac{\mathbf{u}_\infty}{s} \tag{5.8}$$

and the asymptotic value:

$$\mathbf{y}_\infty \underset{s\to 0}{=} -\mathbf{C}\mathbf{A}^{-1}\mathbf{B}\,\frac{\mathbf{u}_\infty}{s} \tag{5.9}$$

the impulse response is:

$$\begin{aligned}\overline{\mathbf{y}} = \mathbf{y} - \mathbf{y}_\infty &= \mathbf{C}\left(s\mathbf{E} - \mathbf{A}\right)^{-1}\left[\mathbf{B} + \left(s\mathbf{E} - \mathbf{A}\right)\mathbf{A}^{-1}\mathbf{B}\right]\frac{\mathbf{u}_\infty}{s} \\ &= \mathbf{C}\left(s\mathbf{E} - \mathbf{A}\right)^{-1}\underbrace{\left(\mathbf{E}\mathbf{A}^{-1}\mathbf{B}\right)}_{\overline{\mathbf{B}}}\mathbf{u}_\infty\end{aligned} \tag{5.10}$$

Thus one identify $\mathbf{E}$, $\mathbf{A}$, $\overline{\mathbf{B}}$, $\mathbf{C}$ and then recover $\mathbf{B}$ as $\mathbf{B} = \mathbf{A}\mathbf{E}^{-1}\overline{\mathbf{B}}$.

In obtaining the aerodynamic reduced order model, the eigenvectors spanning the projection Schur subspace must be chosen. Typically the modes associated to the dominant eigenvalues, i.e. those having the lower absolute value, are selected. Anyhow, to better understanding the nature of the obtained eigenvalues, a first attempt in creating a subspace selecting only the eigenvectors associated to the wake, i.e. those related to the circulation, has been made by simple inspection of the full-potential model with and without wake activated. Generally a disturbance in a compressible flow may be synthesized of three modes of propagation [258], acoustic, vorticity and entropy. The eigenmodes related to the wake

are pressure/vorticity modes, while the others are just acoustics modes and entropy modes. Many of the eigenvalues associated to the system are related to the acoustic and entropic parts, as shown in Fig. 5.25. However the vorticity modes are not enough to describe the aerodynamic response, as may be seen from Fig. 5.26 where the reduced model as been carried out by selecting just the vorticity modes.

A selection of the wake eigenvalues by simple inspection is nevertheless not affordable when others CFD models are used instead of the Full-potential model. Instead the most dominant eigenvalues must be selected, i.e. those closer to the origin. However the eigenvalues and eigenvectors are related to the internal dynamics of the mathematical CFD model, and in particular to its space discretization, which results in mesh depending eigenvalues. In CFD models, the approximation of the space domain arise from both, a discretization of the continuum and a bounded finite dimension representation of an infinite domain. Thus the computational grid determines the frequency or temporal resolution that can be obtained, and the resolution of the eigenvalue distribution.

Finer the grid, greater is the number of eigenvalues appearing about the origin, as may be seen in Fig. 5.27 where the eigenvalues of different grid are represented, along with their indicial responses (Fig. 5.28). As already highlighted by [259], it can be seen that most of the eigenvalues are distributed along lines departing from the origin, which represent a discrete approximation to a branch cut (i.e. a curve in the complex plane such that it is possible to define a single branch of a multi-valued function). Indeed subsonic airflows have a logarithmic branch point at the origin. This can be seen also considering the generalized Theodorsen function $C(s)$ [249] which is defined and analytic throughout the complex s-plane except for a logarithmic branch point at the origin. A branch cut along the negative real axis is required to make the function single valued [260]. The Theodorsen function, although it has no exact analytic poles, may be expressed as a truncated approximation with poles along its branch cut [261]. As the approximation improves, the poles will become infinitely dense.

As a consequence, finer the grid, greater is the number of eigenvectors to be used for projecting the system, as may be seen from the lift responses of a coarse and medium grid models (Fig. 5.29), where a blended step as been used as input. Using a coarse model of n = 6061, the reduced system require the use of 3500 eigenvectors, then further reduced to 30 states through balanced reduction, to have a good approximation of the response of the full model. Using a finer grid model of $n = 9336$, a greater number of eigenvectors (5000) is required to have the same accuracy in approximating the response. In another way, considering a medium model ($n = 9336$) and a fine model ($n = 13508$) reduced utilizing the same number of eigenvectors (6000), and then further reduced through a balancing, the model obtained using the medium grid is more accurate of the fine grid model, as shown in Fig. 5.30, because of the broader spectrum of eigenvalues selected.

A possible strategy to select only the eigenvalues significant for the system response, may be to exploit a multigrid strategy which create by aggregation a coarse mesh from the finer one, thus having an information about the eigenvalues of the system. This information may be then used in generating a coarse subspace projector by extracting only (or the most part of) the pressure/force related eigenvalues from the finer mesh.

Another strategy could relies on the use of the Dominant Poles Algorithm (DPA) [120], which automatically computes an accurate modal equivalent of the transfer function, by

extracting the so called dominant poles, i.e. the eigenvalues λ_j of the approximated transfer function

$$\mathbf{H}(s) = \sum_{j=1}^{n} \mathbf{R}_j/(s - \lambda_j) \tag{5.11}$$

for which the residue matrix

$$\mathbf{R}_j = (\mathbf{C}\mathbf{X}_j)(\mathbf{Y}_j^*\mathbf{B}) \tag{5.12}$$

has a large norm $\mathbf{R}_j/\|\mathrm{Re}(\lambda_j)\|$. However this algorithm computes the dominant poles and the corresponding residue matrices one by one by selecting the most dominant approximation at each iteration of a Newton scheme, so implying a large number of LU factorizations, and thus a large computational cost.

Modal analyses do not consider the matrices $\mathbf{B}$ and $\mathbf{C}$, and so do not take into account the controllability and observability in the definition of the relative importance of the modes. Performing a balanced reduction onto the projected reduced model, and observing the rank of the controllability and observability Gramian matrices, it can be seen (Fig. 5.31) that the controllable part is more important than the observable part. This because the acoustic part does not provide any contribute to the pressure, and so to the forces (lift and moment), of the model. Indeed the response in terms of forces is only due to the circulation, which is related to the wake. This is confirmed by the fact that integral methods does not suffer of the problem of having acoustic eigenvalues.

It is noticed that the dominant eigenvalues are those related to the controllable and observable part of the system. Thus a balanced reduction is required, after reducing the order by projecting the system onto the Schur subspaces. It could be therefore viable to carry out a Krylov subspace with an Arnoldi (or Lanczos) like iterative procedure which select only the controllable and observable subspaces, thus to avoid any additional cost in calculating subspaces not necessary for the dominant dynamic of the system. This would be an advantage, also because the reduced system, arising projecting onto a subspace, could not be richer than the space spanned by the basis used. Related works apply a balanced reduction just after projecting the system, such as the balanced POD. Other methods compute low-rank solutions of the Lyapunov equations [107, 111] or combine SVD-type methods with (rational) Krylov approaches [262], and these methods make it possible to apply balanced truncation to large sparse systems as well [90, 263, 264].

However, generally the order of the model obtained using the RMFA is lower than those obtained with projecting methods followed by balanced reduction or others identification methods based on minimum state. Indeed reduced models arising from identification methods account just for the physical input/output mapping between the generalized model displacement and its generalized integrated forces. Conversely eigenmodes methods account for unimportant details of the flow arising from the internal dynamics of the CFD model, where a large number of states maps a small number of inputs (the generalized displacements) to a small number of outputs (lift and moment). This explain the better performance of the RMFA over the projective eigenmode method.

Figure 5.32, show respectively the eigenvalues of the rational matrix fraction approximation (RMFA) compared to the subspace projective method followed by a balanced reduction, and compared to a subspace identification method (N4SID [265]) build from the time histories responses of the full order model, this last being carried out using the medium

grid. A comparison of the obtained aerodynamic transfer matrix approximations ins shown in Fig. 5.33 and Fig. 5.33, whereas the related step responses are presented in Fig. 5.35 and Fig. 5.36. It must be noted that applying a further balanced reduction to the model obtained from the subspace method does not produce any improvement, being the subspace generated retaining only the eigenvectors of the most important (larger) Hankel singular values, and thus carrying out a minimum state model. Any way one may try to use more states then necessary during the subspace model reduction, and then apply to it the balanced reduction. This would not change the results in term of minimum states.

In considering the performance of the method, one as to take into account also the computational cost to generate the reduced model. In case of the projecting base reduction method, the overall cost is due the operational costs to extract the subspace. Whereas in case of the rational matrix fraction approximation the cost is due to the cost of a matrix-vector multiplication (i.e. the state matrix multiplying the state vector) by the number of times this operation is performed, which depends on the time instants one have to analyze to obtain a suitable time response for constructing the transfer function from the output-input Fourier transform ratio.

Thus, the reduction technique to choose between the projective method and the identification method, is those whom provide, for the problem under investigation, the better compromise between accuracy in prediction and simulation and cost in building the reduced model.

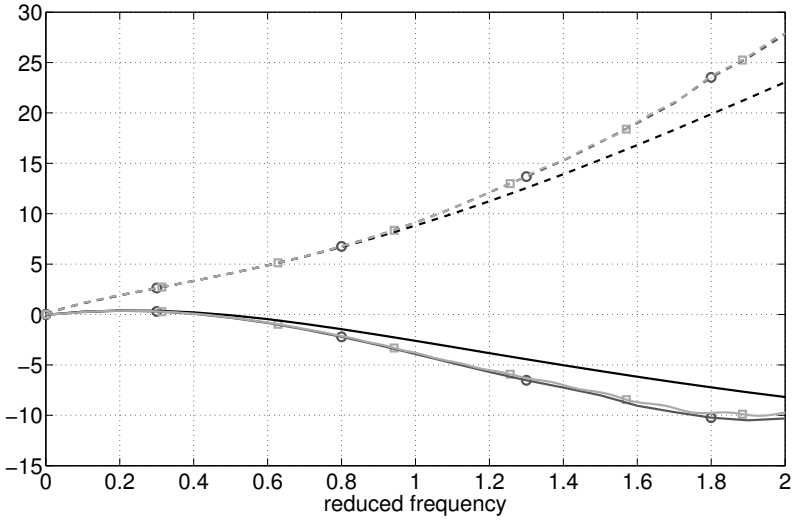

(a) $\mathbf{H}_{hh}$

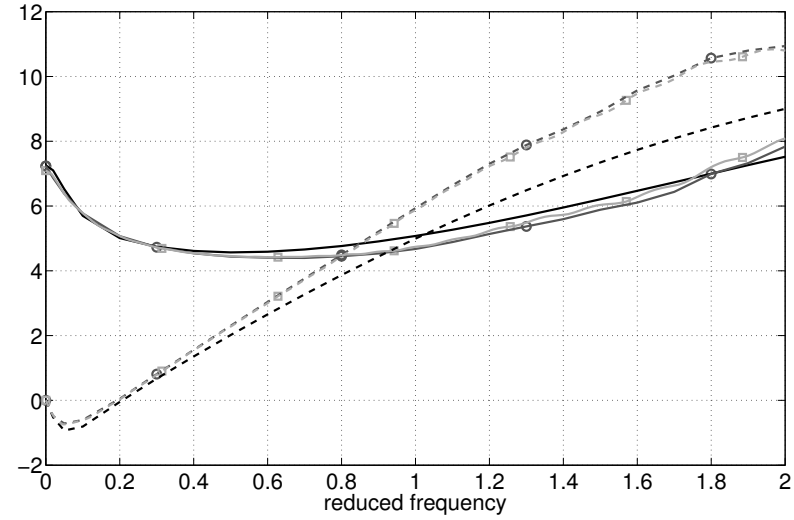

(b) $\mathbf{H}_{h\theta}$

Figure 5.23: *Real part (solid line) and imaginary part (dash line) of the aerodynamic transfer matrix.*

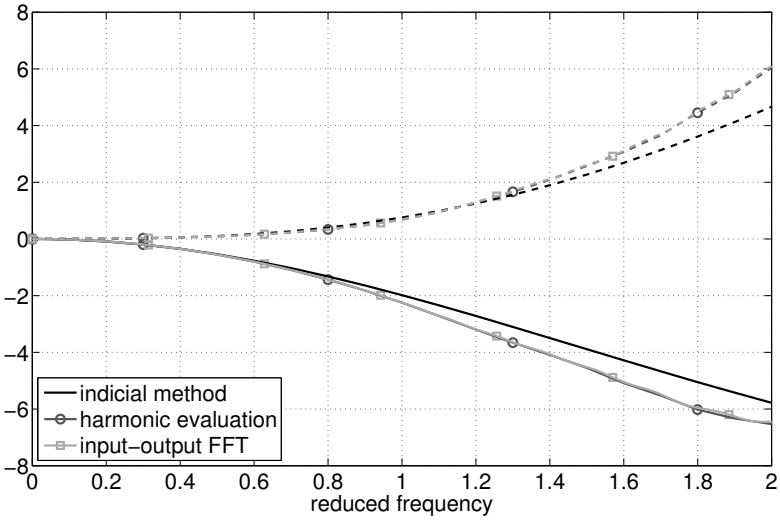

(a) $\mathbf{H}_{\theta h}$

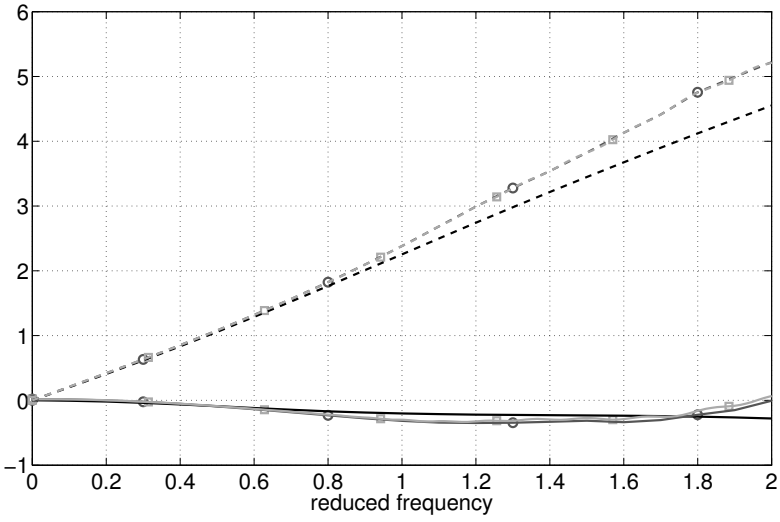

(b) $\mathbf{H}_{\theta\theta}$

Figure 5.24: *Real part (solid line) and imaginary part (dash line) of the aerodynamic transfer matrix.*

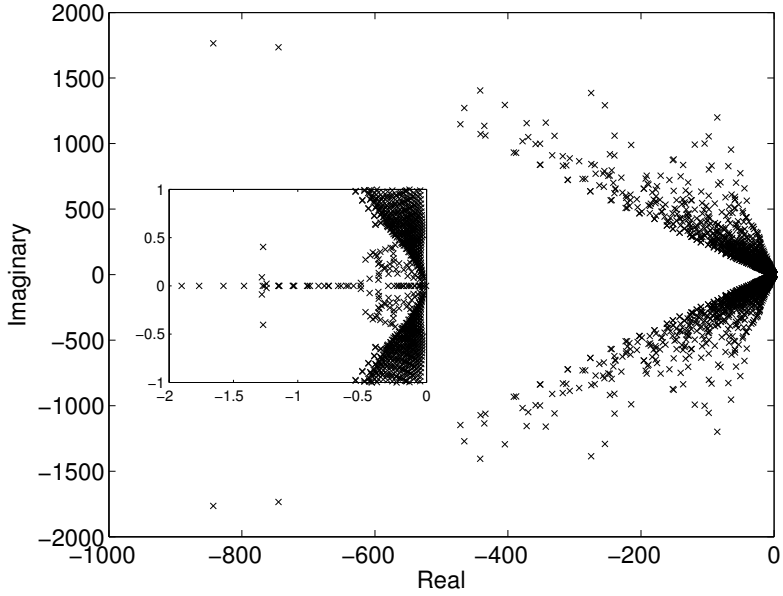

(a) *Complete spectrum of the airfoil model with wake activated.*

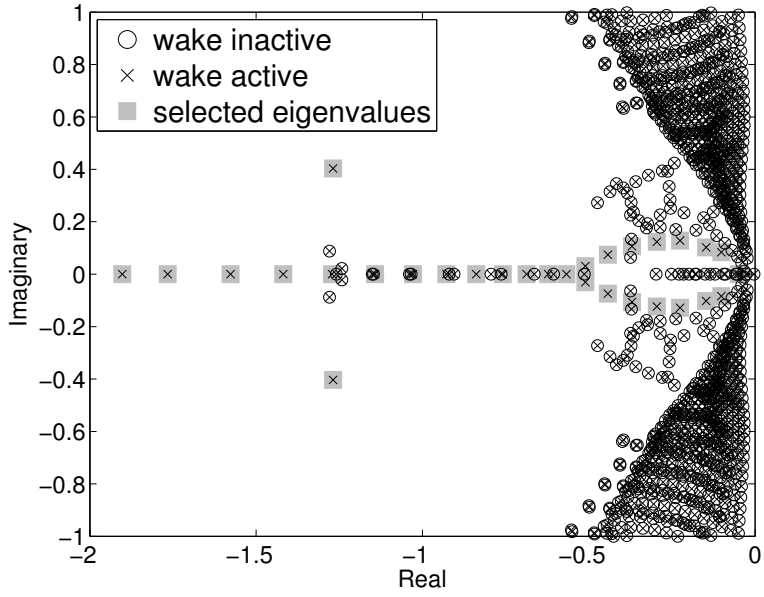

(b) *Selection by inspection of the eigenvalues associated to the wake.*

Figure 5.25: *Eigenvalues associated to the wake.*

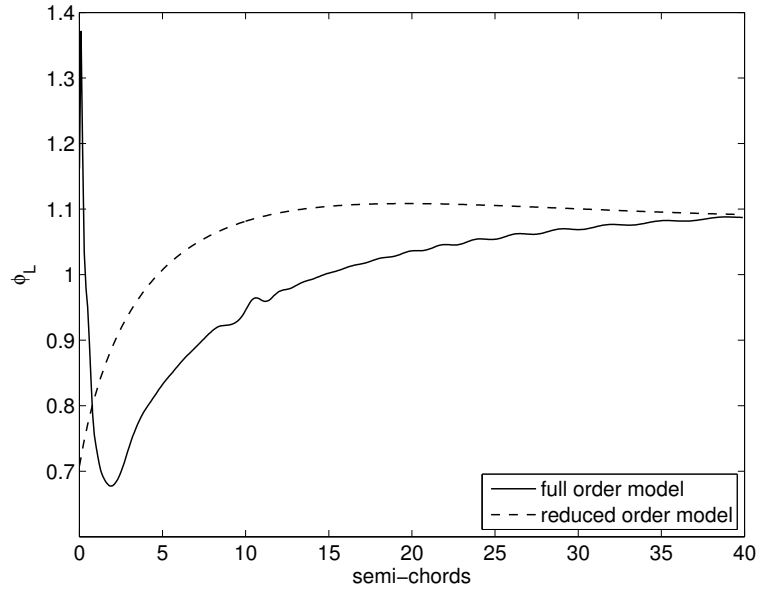

(a) *Lift response ϕ_L to α step.*

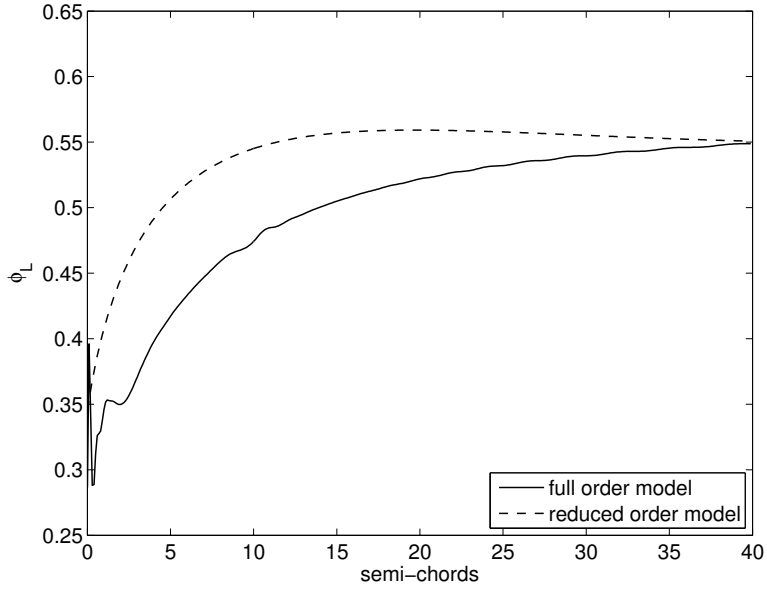

(b) *Lift response ϕ_L to q step.*

Figure 5.26: *Response of the reduced model build with just the vorticity modes.*

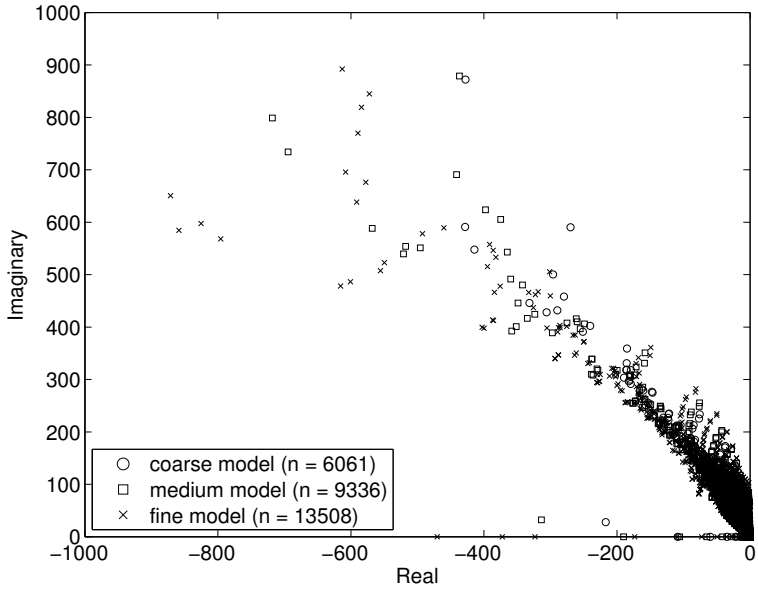

(a) *Complete spectrum.*

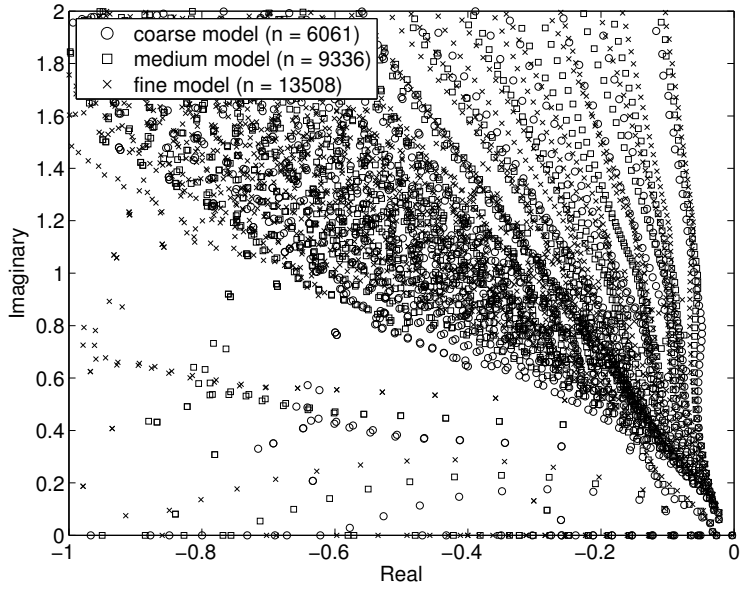

(b) *Zoom detail.*

Figure 5.27: *Eigenvalues of coarse, medium and fine grid models.*

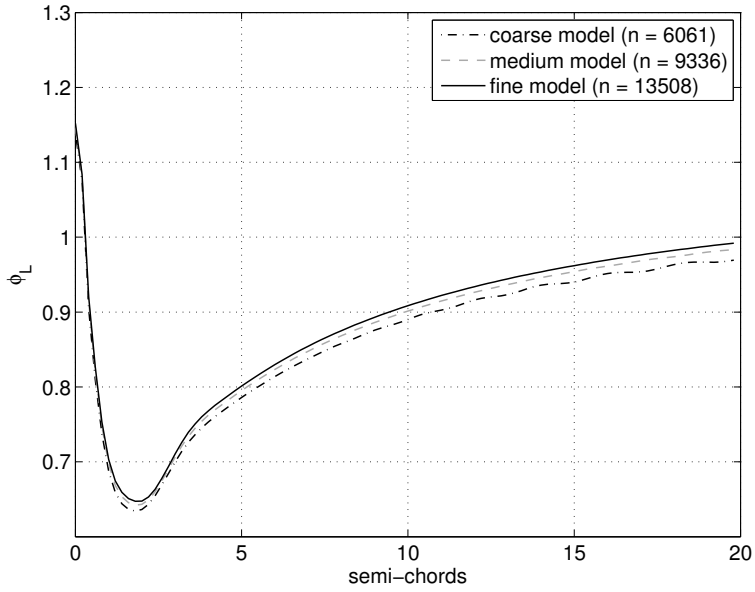

(a) *Indicial lift response to a plunging step.*

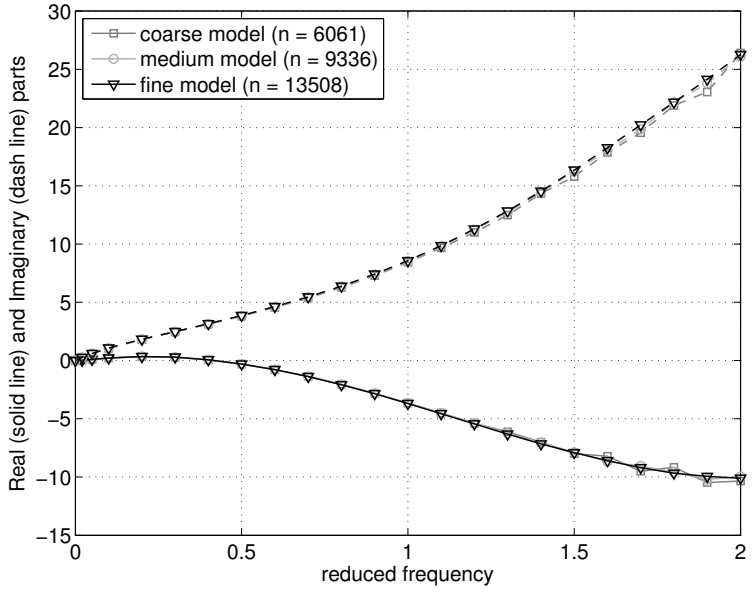

(b) *Lift to plunging aerodynamic transfer function.*

Figure 5.28: *Comparison of coarse, medium and fine grid models.*

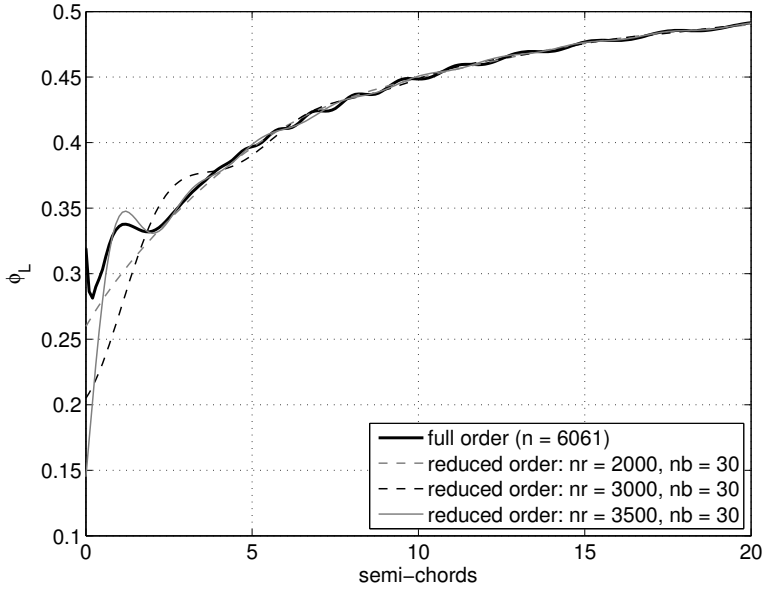

(a) *Coarse model.*

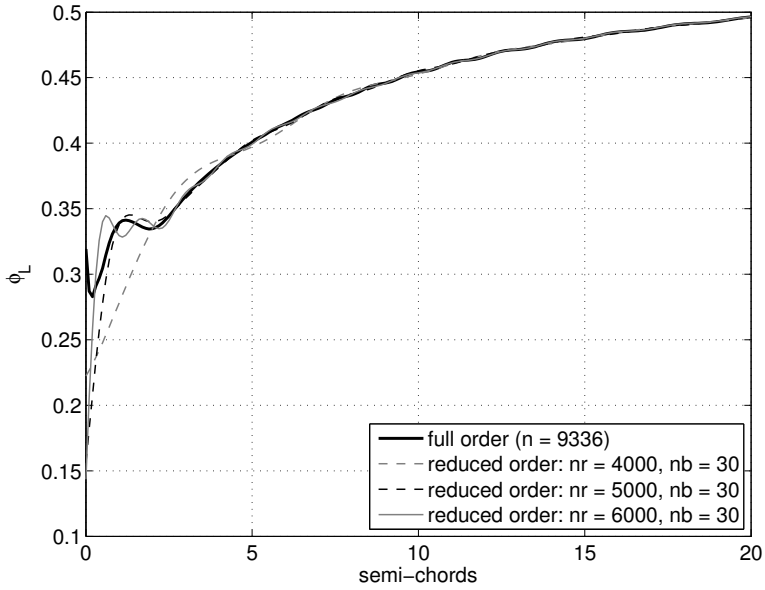

(b) *Medium model.*

Figure 5.29: *Indicial lift response ϕ_L to a pitching step, using different number of eigenvectors.*

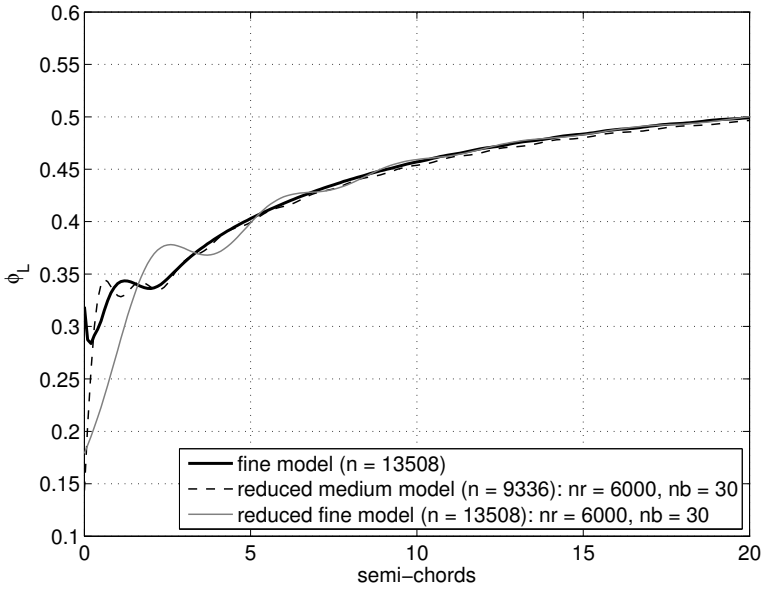

Figure 5.30: *Indicial lift response to a pitching step, using the same number of eigenvectors obtained from different grids.*

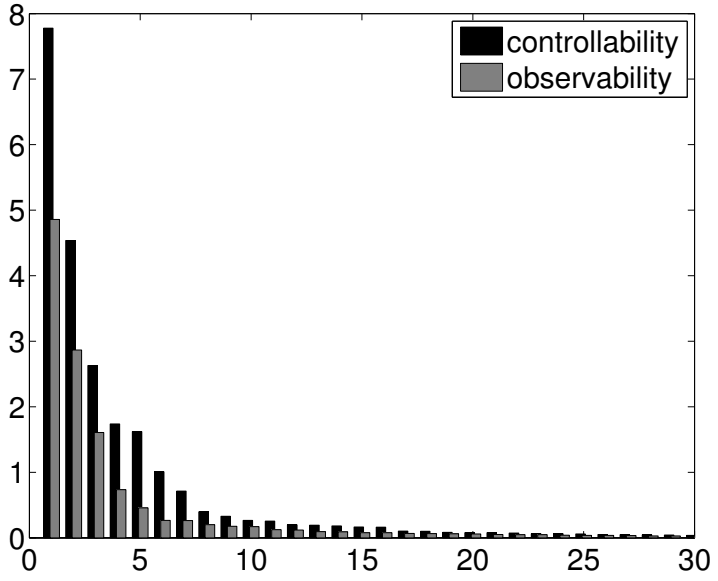

Figure 5.31: *Hankel singular values of controllability and observability Gramian matrices.*

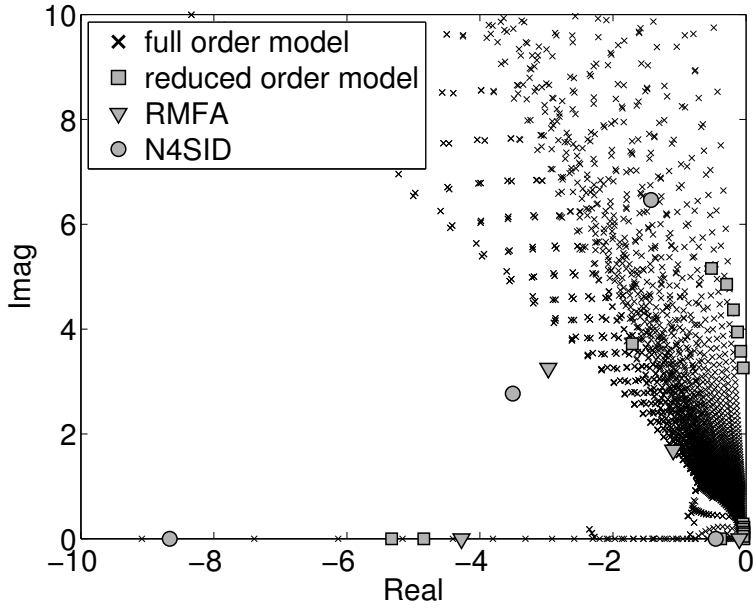

(a) *Eigenvalues.*

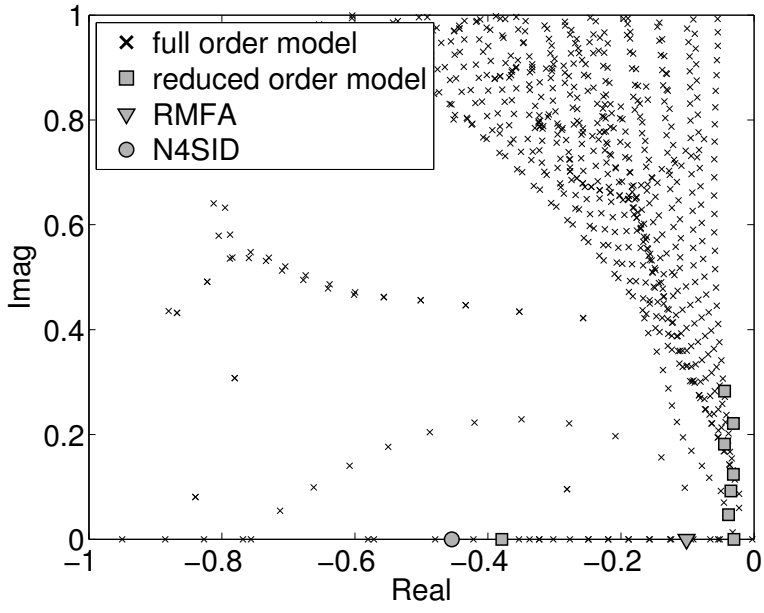

(b) *Zoom detail.*

Figure 5.32: *Eigenvalues of the reduced order model and the identified models.*

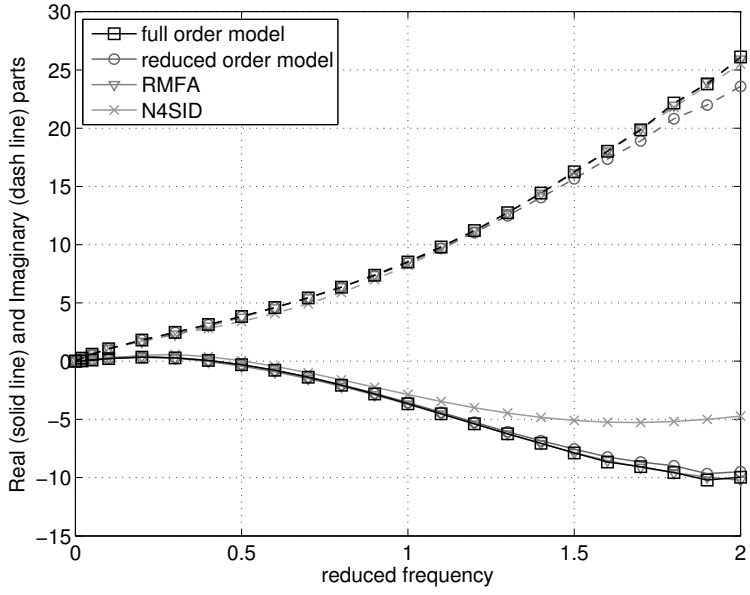

(a) $\mathbf{H}_{hh}$

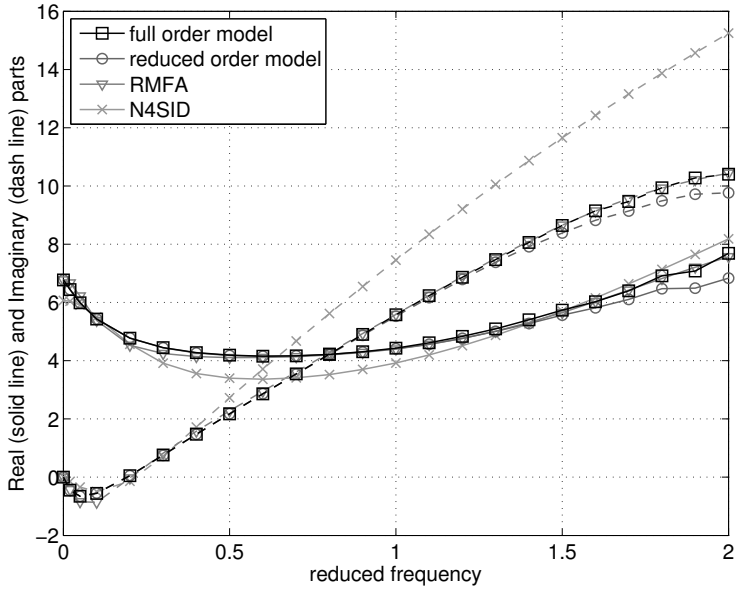

(b) $\mathbf{H}_{h\theta}$

Figure 5.33: *Comparison of the aerodynamic transfer matrix (plunge) obtained from the Schur-based reduced order model and the RMFA and N4SID identified models.*

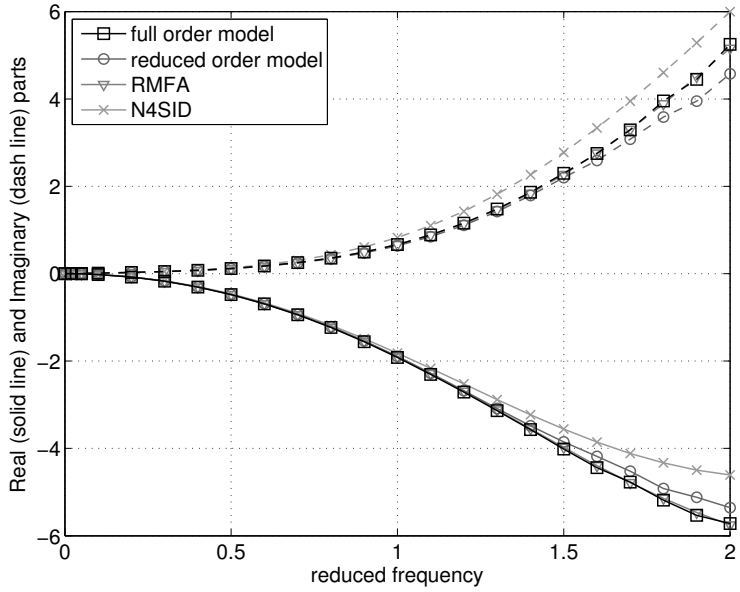

(a) $\mathbf{H}_{\theta h}$

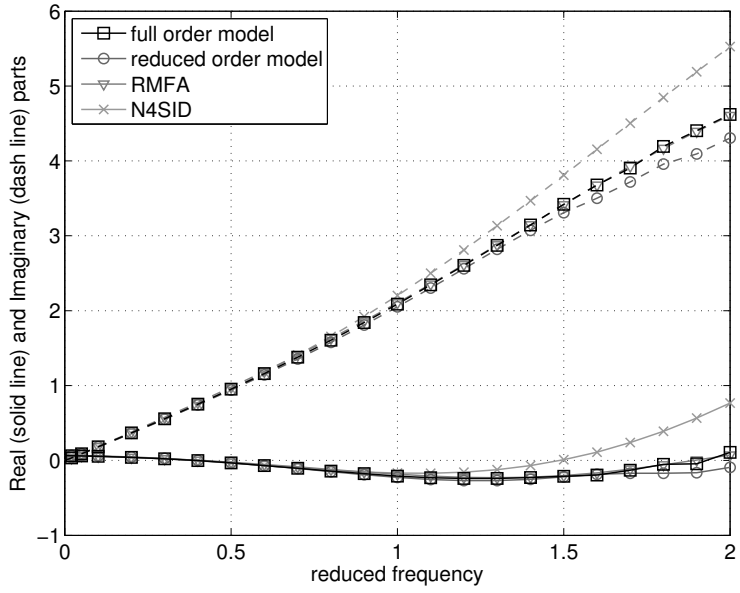

(b) $\mathbf{H}_{\theta\theta}$

Figure 5.34: *Comparison of the aerodynamic transfer matrix (pitch) obtained from the Schur-based reduced order model and the RMFA and N4SID identified models.*

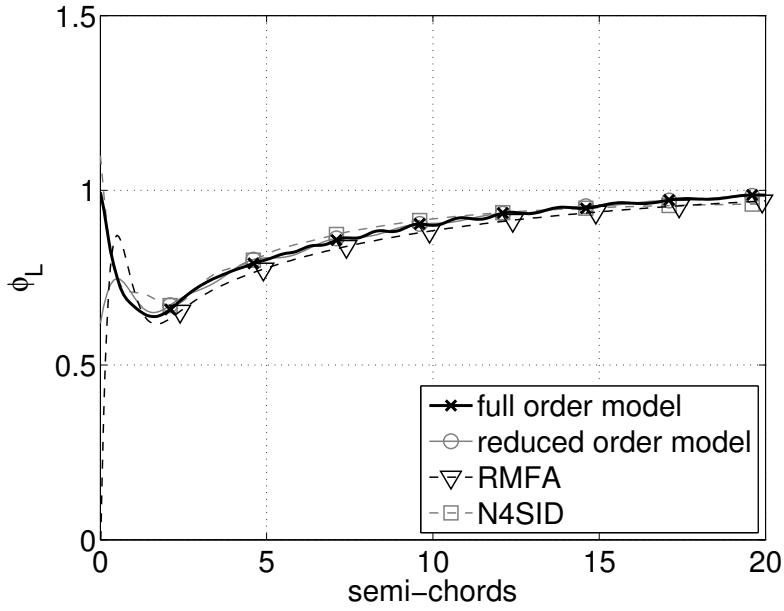

(a) *Lift indicial response to plunging*

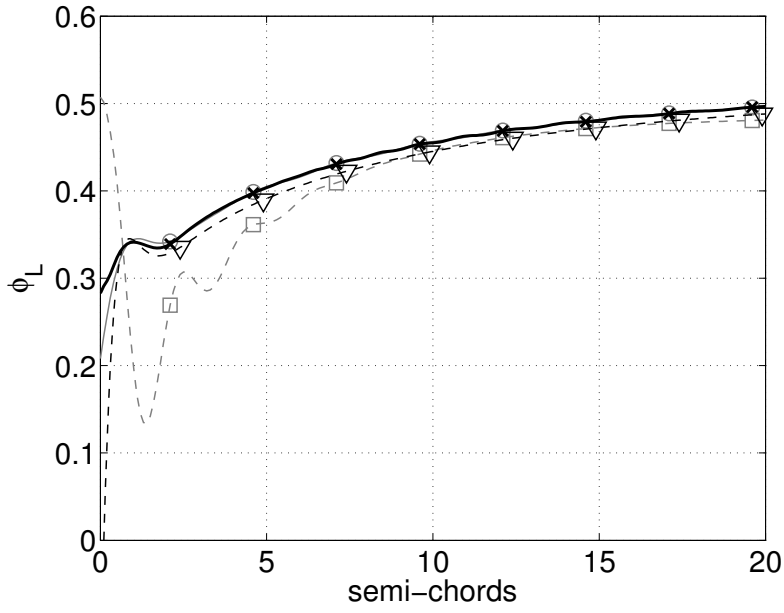

(b) *Lift indicial response to pitching*

Figure 5.35: *Comparison of the lift indicial responses of the Schur-based reduced order model and the RMFA and N4SID identified models.*

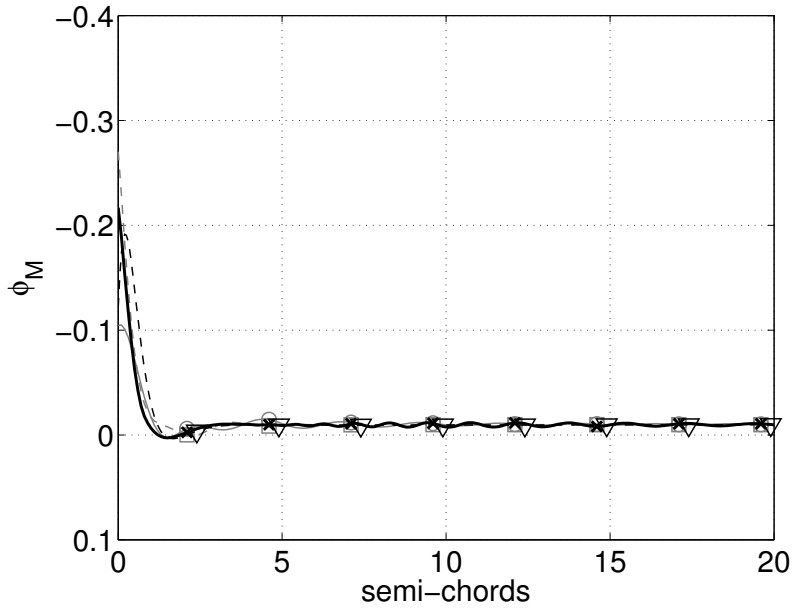

(a) *Moment indicial response to plunging*

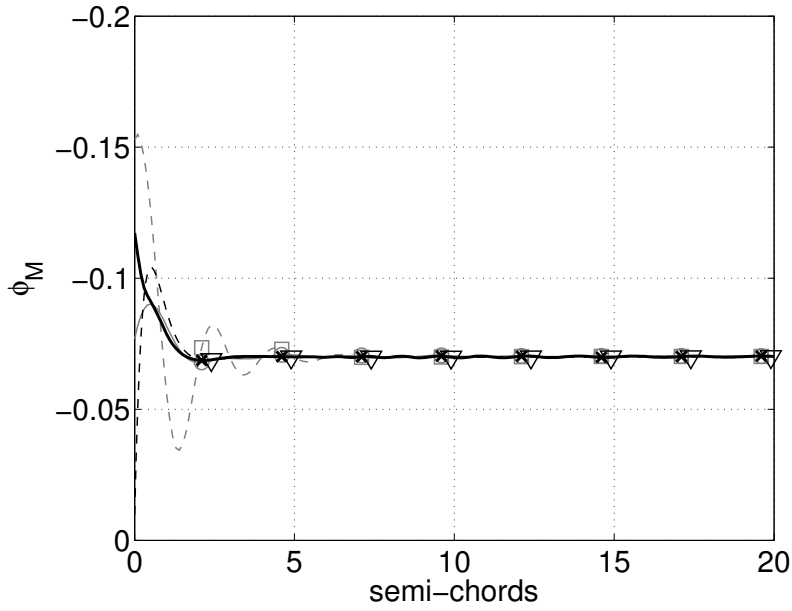

(b) *Moment indicial response to pitching*

Figure 5.36: *Comparison of the moment indicial responses of the Schur-based reduced order model and the RMFA and N4SID identified models.*

Chapter 6

Nonlinear Model Order Reduction

More recent developments and efforts may be found in nonlinear model order reduction of aerodynamic and aeroelastic models. Among the methods considered there are nonlinear identification techniques, such as Volterra series [266–270], indicial functions [271–273] and block-oriented identification [274], generalized POD over nonlinear manifolds [275], Taylor series expansion [276,277], surrogate-based approaches [278] and neural-networks approaches [279–281].

Main challenges on model reduction of nonlinear systems are due to:

canonical form: generally nonlinear systems do not have a universal canonical form (as may be the quadruple $(\mathbf{E}, \mathbf{A}, \mathbf{B}, \mathbf{C})$ for LTI systems written in a state space form, or its correspondent transfer function), completely representing and characterizing explicitly the system. Analytical expressions for the system response cannot be found, but for simple nonlinear systems (e.g. polynomial systems which may be represented using Volterra kernels).

robustness: the behavior of the ROMs may be quantified just locally or with respect to a given set of training data. Therefore global properties of the overall system, such as stability and multiple equilibria, are difficult to analyze.

computational cost: dimensional reduction techniques applied to nonlinear systems often relies on the computation of projective subspaces which can be as expensive to compute as the full model. Nevertheless, these costs are offline costs which do not make less appealing the use of ROMs instead of full order models which, besides having a greater online computational cost compared to ROMs, are burdensome to employ for control system design or within multidisciplinary optimization frameworks.

In section 6.1 a brief overview of the available techniques will be introduced, whereas in section 6.2 and section 6.3, the Ph.D. research work on nonlinear model reduction is presented: a nonlinear identification approach using a polynomial state space model, and an element-based hyper-reduction, that is a reduction of the nonlinearity complexity in a projection-based framework by performing the evaluation onto a subset of the domain.

6.1 Previous works on model order reduction for nonlinear systems

Most of nonlinear model order reduction techniques found their ground on linear methods. For example nonlinear models may be locally approximated in different regions of the state space by linear models (e.g. LTI models or Volterra series), upon which linear dimensionality reduction techniques may be applied.

Many practical nonlinear systems may be well approximated using Linear-Time-Varying (LTV) systems, especially for those systems operating under periodic conditions (e.g. rotorcraft, turbomachinery). A reduced order model whose time-varying transfer matrix (an extension of the notion of transfer matrix for LTI systems to time-varying systems is given in Ref. [282]) approximate the one of the full order model may be obtained using Padè-like approximations [282] or appropriate projections [283].

Research on model reduction for general nonlinear systems have been performed with Volterra series approximating the local behavior of the nonlinear model. Model reduction approaches based on Volterra series [283] built a model matching the moment of the Volterra kernels (i.e. high order transfer functions). The validity of such models holds just locally, since Volterra series converges only for small input signals. The matching of specified moments of Volterra Kernels may be obtained through projection methods, where the system is projected by using appropriate projection matrices covering a series of subspaces (e.g. a series of Krylov subspaces).

Linear or polynomial expansion of the system nonlinearity [284], bi-linearization [285], or Volterra series expansion [283] with subsequent projection, generate reduced models valid only around one operating point of the system, so being applicable only to weakly nonlinear systems and small input disturbances.

Furthermore, computational effort and memory requirements grow exponentially with the order of the polynomial operator, defeating some of the benefits of model reduction.

Unlike these methods generating local ROMs, several global model reduction approaches have been recently proposed to overcome the computational bottleneck for nonlinear systems.

Among these there are the trajectory-based model reduction methods, as the popular Trajectory Piece-Wise Linear (TPWL) [286, 287] method, which generate global reduced models by approximating the nonlinear system at multiple points as it evolves along a training trajectory in the state space. In each of these selected points the full model is linearized and a local linear subspace is extracted, so obtaining a local ROM, having transfer function moments matching those of the full linearized model. All the local subspaces computed along the trajectory are aggregated, so identifying two linear subspaces used to generate the reduced model by linearly projecting the nonlinear system upon them. The nonlinear term is thus approximated by a weighted-summation of linearized systems, so achieving a computationally efficient reduced model. Different linear model order reduction (MOR) techniques (e.g. Krylov subspaces, Truncated Balanced Realization (TRB) [288]) may be used as linear kernel, each one leading to different robustness properties [289] and a different behavior when combined to more complex systems. This approach has been successfully applied to the dynamical problems with low-order or moderate nonlinearities, such as the nonlinear circuit simulations [290].

As an alternative, projection methods may be also applied directly to the nonlinear system of equations. In this case a POD is generally used to obtain the projection basis from time snapshots of the system. The snapshot matrix may be computationally expensive to generate, relying on the simulation of the full order nonlinear model. Moreover the dominant directions of the state evolution extracted with the SVD depend on the particular input used on the system, which should excite a wide range of dynamics.

An additional drawback of projection methods for nonlinear high-dimensional systems is that the system nonlinearity may be represented inefficiently. This may be observed by considering a generic finite-dimensional nonlinear dynamical systems $\dot{\mathbf{x}}(t) = \mathbf{f}_{\mathsf{nl}}(\mathbf{x}(t))$, being $\mathbf{x} \in \mathbb{R}^n$ the state vector and $\mathbf{f}_{\mathsf{nl}} : \mathbb{R}^n \to \mathbb{R}^n$ a nonlinear mapping. Indeed after a state approximation, $\mathbf{x} = \mathbf{V}\mathbf{q}$, with $\mathbf{V} \in \mathbb{R}^{n\times r}$, $r \ll n$ and $\mathbf{q}$ being the reduced state vector, and the projection of the equation onto a low-dimensional (e.g. POD) subspace $\mathbf{W} \in \mathbb{R}^{n\times r}$, the cost of evaluating the reduced form of the nonlinearity, $\mathbf{W}^T\mathbf{f}_{\mathsf{nl}}(\mathbf{V}\mathbf{q})$, still scales as the dimension of the original problem. Hence, despite the subspaces are computed a priori by expensive offline computations, the runtime simulation of the reduced order model:

$$\dot{\mathbf{q}} = \mathbf{f}_r(\mathbf{q}) := \underbrace{\mathbf{W}^T}_{r\times n}\underbrace{\mathbf{f}_{\mathsf{nl}}(\mathbf{V}\mathbf{q})}_{n\times 1} \tag{6.1}$$

still involves the use of the Full Order Model (FOM). During the online stage, at first the large state vector $\mathbf{x}$ must be recovered with a matrix multiplication using $\mathbf{V}$, then the nonlinearity is evaluated and finally it is projected on the subspace $\mathbf{W}$. These matrix-vector operations makes the resulting ROM costly to evaluate.

For this reason, projection-based model reduction approaches are efficient primarily for problems where the matrices are constructed only once or can be assembled a priori. This is the case of systems whose nonlinearity is expressed in a polynomial form, where the projection of each terms of the polynomial may be precomputed, thus alleviating the computational cost of evaluating the reduced nonlinear vector. For general non-polynomial cases, different approaches have been developed in order to efficiently reduce the burden limit of scalability of the nonlinear term.

Research has been performed on methods which, maintaining the nonlinear structure of the system, try to decrease the computational effort by avoiding full evaluations of the nonlinear term and the Jacobian matrix used in the simulation of the nonlinear system. Among them the Missing Point Estimation (MPE) [291, 292], the Empirical Interpolation Method (EIM) [293] and its discrete variants, the Discrete Empirical Interpolation Method (DEIM) [294, 295] and the Unassembled DEIM (UDEIM) [296], which approximate the nonlinear terms via interpolation over a subset of points that are independent of the large-scale full model dimension n.

The missing point estimation method reduces the complexity of the nonlinear term $\mathbf{f}_{\mathsf{nl}}(t)$ via a reduced-basis expansion whose projection matrices are computed over a restricted subset of the spatial domain. The spatial subset samples are selected using an optimization approach aiming to preserve the orthogonality of the subspace $\mathbf{V}^T\mathbf{V} = \mathbf{I}$. All other missing components are then reconstructed by means of a gappy POD [297].

In a similar way the discrete empirical interpolation method utilizes reduced bases (e.g. POD) to approximate both the state variables and the evaluation of the discretized nonlinear term, which is approximated by projection onto a constant reduced basis $\mathbf{\Phi} \in \mathbb{R}^{n\times m}$

with $m \ll n$:

$$\mathbf{f}_{\mathsf{nl}}(t) \approx \mathbf{f}_{\mathsf{nl,r}}(t) = \boldsymbol{\Phi}\,\boldsymbol{\alpha}(t) \tag{6.2}$$

with $\boldsymbol{\alpha}(t) \in \mathbb{R}^m$, so that $\mathbf{f}_{\mathsf{nl,r}}(t)$ can be computed independent of n, because just m evaluations forming $\boldsymbol{\alpha}(t)$ are necessary, being the subspace $\boldsymbol{\Phi}$ precomputed in the off-line phase.

The coefficients $\boldsymbol{\alpha}(t)$ of the reduced basis are obtained by interpolation, enforcing that selected entries of the vector $\mathbf{f}_{\mathsf{nl,r}}(t)$ exactly match the corresponding entries of $\mathbf{f}_{\mathsf{nl}}(t)$ in m indices[1] $p_1, \ldots, p_m$. Such interpolation indices where the approximation is collocated may be selected using different approaches [293, 294, 298], (e.g. a greedy procedure). An extraction matrix $\mathbf{P}$ selecting the m rows of $\boldsymbol{\Phi}$ may be formed as $\mathbf{P} = \left[\mathbf{e}_{p_1}, \ldots, \mathbf{e}_{p_m}\right] \in \mathbb{R}^{n \times m}$, being $\mathbf{e}_i$ the i^{th} canonical vector in $\mathbb{R}^n$. Thus forcing the interpolation at the selected rows it results:

$$\mathbf{P}^T \mathbf{f}_{\mathsf{nl}}(t) = (\mathbf{P}^T \boldsymbol{\Phi})\,\boldsymbol{\alpha}(t) \quad \Rightarrow \quad \boldsymbol{\alpha}(t) = (\mathbf{P}^T \boldsymbol{\Phi})^{-1} \mathbf{P}^T \mathbf{f}_{\mathsf{nl}}(t) \tag{6.3}$$

Therefore, from Eq. (6.2), the interpolate approximation of $\mathbf{f}_{\mathsf{nl}}(t)$ can be computed without the need for $\mathcal{O}(n)$ operations with:

$$\mathbf{f}_{\mathsf{nl,r}}(t) = \boldsymbol{\Phi}\,\boldsymbol{\alpha}(t) = \boldsymbol{\Phi}(\mathbf{P}^T \boldsymbol{\Phi})^{-1} \mathbf{P}^T \mathbf{f}_{\mathsf{nl}}(t) = \mathbb{P}\,\mathbf{f}_{\mathsf{nl}}(t) \tag{6.4}$$

being $\mathbb{P} := \boldsymbol{\Phi}\,\boldsymbol{\alpha}(t) = \boldsymbol{\Phi}(\mathbf{P}^T \boldsymbol{\Phi})^{-1} \mathbf{P}^T$, an oblique projector onto the range of $\boldsymbol{\Phi}$. The component values at other locations are approximated through the reduced basis by an interpolation matrix that can be pre-computed offline.

The direct application of DEIM to FE discretized problems is rather inefficient because each component of the nonlinear force depends on the nodal displacements of all the neighboring elements. This would require to evaluate a relative large number of element functions in order to determine a single component of the nonlinear term. The UDEIM is an alternative formulation of DEIM aiming at preserving the efficiency of the method when applied to a Finite Element (FE) framework by operating on the unassembled vectors, instead that on its assembled DEIM counterpart, so that each selected point is linked to just one element.

Recently a localized discrete empirical interpolation method (LDEIM) [299] has been proposed, where multiple local interpolants, each tailored to a particular system behavior, are constructed instead of global interpolant, therefore avoiding the drawback of DEIM when applied to a system exhibiting a wide range of behaviors, for which many basis vectors and interpolation points are required to accurately approximate the nonlinear term.

Similarly to the previous methods, the work in [300] extends the concept of the empirical interpolation method by approximating the discrete operators via a set of interpolation functionals.

Another approach which approximate the nonlinear term with a sparse sampling is the the Gauss-Newton with approximated tensors (GNAT) method [301, 302]. It achieves a dimension reduction by a Petrov-Galërkin projection scheme along with a gappy POD technique for approximating the nonlinear function and the Jacobian matrix (tangent stiffness matrix).

[1] A least-squares solution may be also considered by selecting a number of entries greater than m, and so framing an overdetermined linear system.

Another family of nonlinear MOR techniques, called the optimizing cubature [303, 304], introduces an optimized quadrature rule for the reduced-order force calculation with an assumption that the reduced-order force density preserves the same form as the full-order model. The method described successively in section 6.3 represents an application of the optimized cubature to a FE-based aeroelastic framework.

An alternative to the runtime simulation of the reduced nonlinear force consists in using a precomputed approximation of the nonlinear term $\mathbf{f}_r(\mathbf{q})$ which is fast to evaluate. Such an approximation may be obtained through system modeling techniques, as data-driven interpolation using radial basis functions or neural networks [89, 305]. In these approximating approaches, challenges include guaranteeing adequate data and model training, supporting high subspace dimensionality, avoiding overfitting, and ensuring energy conservation, passivity, and stability.

6.2 Nonlinear polynomial state space identification

In this section, a method to model nonlinear aeroelastic systems using Polynomial Nonlinear State Space (PNLSS) equations is described. Nonlinear state-space models describe naturally system dynamics and they are proven to be equivalent to several classic block-oriented models [306]. The approach is an identification method applicable to systems presenting a nonlinear behavior of which the nonlinearity term is unknown.

A major problem arising in the nonlinear system identification framework is the selection, based on measured data, of an adequate, low order, model able to characterize the behavior of the original system. The model structure should facilitate the successful estimation of its unknown parameters as well as including good prediction capabilities.

The determination of a model structure for the nonlinear aerodynamic subsystem may involve the postulation of the terms that might enter the model, the selection of an adequate model, and the successive validation of the selected model [307, 308]. However the postulation of the terms to be included in the identified model may be difficult for aerodynamic models arising from high-fidelity CFD formulations. Thus a generic functional expansion of the nonlinear system may be applied. Once selected the basis function of the expansion, e.g. polynomials, the terms of the expansion may be incorporated sequentially, so to have a selection methodical. Therefore at every step the terms already included into the model in previous stages and the new term entering the model are reexamined for their significance.

The method proposed in this thesis follows the framework of the approach developed in Ref. [309], where a discrete in time PNLSS model is identified using Gaussian(-like) signals, such as Gaussian noise and random phase multisines, as excitations input for the training phase. The initial estimation of the model, which is often an issue for nonlinear modeling, is obtained by identifying the linear part of the state space system using a frequency domain subspace identification. All the matrices of the linear part are used as starting values for the estimation, through a nonlinear optimization, of the full nonlinear state space model.

The approach proposed in this thesis extend to continuous in time models the work of Ref. [309]. Moreover, conversely to Ref. [309], a stable state space matrix is identified using the rational matrix fraction approximation presented in section 3.2, leading to a

first/second order dynamic residualization respectively in the state and in the output equations.

Successively, in order to capture the nonlinear behavior, the system is augmented by adding nonlinear polynomial terms whose coefficients are carried out by a nonlinear least squares (NLS) minimization, while maintaining, differently from Ref. [309], the stable state space matrix of the linear part fixed during the iterative fitting procedure of the nonlinear part. A selection of the monomials through the use of a greedy approach is further introduced. Training responses with modulated amplitude and sweeping a given range of reduced frequencies are used in order to identify the nonlinear input-output mapping of the system.

Hence considering a nonlinear state space system written as:

$$\begin{aligned} \dot{\mathbf{x}}(t) &= \mathbf{f}(\mathbf{x}(t),\, \mathbf{u}(t)) \\ \mathbf{y}(t) &= \mathbf{g}(\mathbf{x}(t),\, \mathbf{u}(t)) \end{aligned} \tag{6.5}$$

being $\mathbf{x} \in \mathbb{R}^n$, $\mathbf{u} \in \mathbb{R}^{n_u}$ and $\mathbf{y} \in \mathbb{R}^{n_y}$ the state vector, the input and the output respectively and applying a full polynomial expansion of the function $\mathbf{f}$ and $\mathbf{g}$, the resulting model may be formulated as a Polynomial Non-Linear State Space model, written in the following form:

$$\begin{aligned} \dot{\mathbf{x}} &= \mathbf{A}\,\mathbf{x} + \mathbf{B}\,\mathbf{u} + \mathbf{E}\,\boldsymbol{\zeta}(\mathbf{x}, \mathbf{u}) \\ \mathbf{y} &= \mathbf{C}\,\mathbf{x} + \mathbf{D}\,\mathbf{u} + \mathbf{F}\,\boldsymbol{\eta}(\mathbf{x}, \mathbf{u}) \end{aligned} \tag{6.6}$$

which separate the linear terms from the nonlinear part. The matrices of the linear part in $\boldsymbol{x}(t)$ and $\boldsymbol{u}(t)$ are identified by the improved MFD, whereas the matrices associate to the nonlinear part are obtained successively in a Least-Squares sense. The vectors $\boldsymbol{\zeta}(t) \in \mathbb{R}^{n_\zeta}$ and $\boldsymbol{\eta}(t) \in \mathbb{R}^{n_\eta}$ contain nonlinear monomials in $\mathbf{x}(t)$ and $\mathbf{u}(t)$ of degree two (the monomials of degree one are included in the linear part) up to a chosen degree p. Separating the linear from the nonlinear part helps in the initial estimation of the model, which is performed only onto the linear part. It is worthwhile to note that a different functional expansion, resorting to any kind of basis functions (e.g. orthogonal functions [310]), may be employed instead of the polynomial one. However polynomials are generally easier to compute and manage in multivariable framework.

Using a full polynomial expansion all the monomials up to a chosen degree p are taken in to account. So, defining $\boldsymbol{\xi}(t)$ the concatenation of the state vector and input vector $\boldsymbol{\xi}(t) = \left[\mathbf{x}^T,\, \mathbf{u}^T\right]^T$, the nonlinear vectors $\boldsymbol{\zeta}(t)$ and $\boldsymbol{\eta}(t)$ are given by:

$$\begin{aligned} \boldsymbol{\zeta}(t) &= \boldsymbol{\xi}(t)_{\{p\}} \\ \boldsymbol{\eta}(t) &= \boldsymbol{\xi}(t)_{\{p\}} \end{aligned} \tag{6.7}$$

where the notation $\boldsymbol{\xi}_{\{p\}}$ corresponds to considering all the distinct nonlinear combinations of degree two up to $\{p\}$. Further, $\boldsymbol{\xi}_{(q)}$ is defined as the vector containing all the distinct monomials of degree q (i.e., with multi-index $|\boldsymbol{\alpha}| = q$) composed by the elements of vector $\boldsymbol{\xi}$, having a number of terms given by the binomial coefficient $\binom{N+q-1}{q}$, with N being the sum of the length of the state vector (i.e. the dimension of the system n) and the number

of inputs n_u. For example for a system with $N = 2$ it can be written:

$$\boldsymbol{\xi}_{\{3\}} = \left[\boldsymbol{\xi}_{(2)}^T, \boldsymbol{\xi}_{(3)}^T\right]^T = \left[\xi_1^2,\, \xi_1\xi_2,\, \xi_2^2,\, \xi_1^3,\, \xi_1^2\xi_2,\, \xi_1\xi_2^2,\, \xi_2^3\right]^T \tag{6.8}$$

Thus the total number of terms of the vector $\boldsymbol{\xi}_{\{p\}}$ containing the nonlinear monomials is given by:

$$L_{n,p} = \binom{N+p}{p} - 1 - N \tag{6.9}$$

The overall number of coefficients available to identify the nonlinear behavior of the system, i.e. the coefficients of matrices $\mathbf{E}$ and $\mathbf{F}$, is:

$$N_{\text{nl}} = (n+n_y)\left[\binom{N+p}{p} - 1 - N\right] = (n+n_y)\left[\binom{n+n_u+p}{p} - 1 - n - n_u\right] \tag{6.10}$$

For the sake of a compact formulation the multi-index notation is adopted. An n-dimensional multi-index is an n-tuple $\boldsymbol{\alpha} = [\alpha_1,\, \alpha_2,\, \ldots,\, \alpha_n]$, with $\alpha_k \in \mathbb{N}_0^n$ non-negative integers. For multi-indices $\alpha \in \mathbb{N}_0^n$ and $\mathbf{x} = [x_1,\, x_2,\, \ldots,\, x_n]^T \in \mathbb{R}^n$ a monomial is defined using the power operation:

$$\mathbf{x}^{\boldsymbol{\alpha}} = x_1^{\alpha_1} x_2^{\alpha_2} \ldots x_n^{\alpha_n} = \prod_{k=1}^{n} x_k^{\alpha_k} \tag{6.11}$$

The total degree of the monomial is given by the sum of components of $\boldsymbol{\alpha}$, that in a multi-index notation is given by the absolute value:

$$|\boldsymbol{\alpha}| = \alpha_1 + \alpha_2 + \cdots + \alpha_n = \sum_{k=1}^{n} x_k^{\alpha_k} \tag{6.12}$$

Utilizing a full expansion applied to high dimensional systems may lead to consider many monomials even when a low degree p is considered. Moreover the required state dimension for a good approximation can become quite high, especially when the nonlinearities are concentrated in the states. This require that only the most important monomials retaining and modeling properly the nonlinearity have to be considered. Therefore the monomials to be included for the representation of the nonlinear term are selected by a greedy procedure.

As already said, before selecting the nonlinear monomials, a linear identification is performed using the matrix fraction description approach. The transfer matrix is build using input-output training data. The excitation of each input at the time allow to frame the corresponding column of the transfer matrix by a ratio of the Fourier transform of the input and the Fourier transform of the output.

Once identified a linear state space model, i.e. the matrices $\mathbf{A}$, $\mathbf{B}$, $\mathbf{C}$ and $\mathbf{D}$ in Eq. (6.6), the full nonlinear model may be estimated. The linear matrices may be kept constant, thus proceeding with the only estimation of the matrices $\mathbf{E}$ and $\mathbf{F}$, or included in the identification process starting with initial guess the result obtained from the MFD rational interpolation. Whatever the case a nonlinear least-square minimization is performed using a the Levenberg-Marquardt algorithm. The cost function may be defined as quadratic function of the error $\mathbf{e}(t, \boldsymbol{\theta}) := \mathbf{y}(t, \boldsymbol{\theta}) - \hat{\mathbf{y}}(t)$, with $\hat{\mathbf{y}}$ and $\mathbf{y}$ being respectively the output

of the high-dimensional system and the output of the identified system:

$$\mathcal{F}(\boldsymbol{\theta}) = \frac{1}{2}\int_{t_0}^{t_1} \mathbf{e}(t,\boldsymbol{\theta})^T\, \mathbf{W}_e\, \mathbf{e}(t,\boldsymbol{\theta})\, dt \tag{6.13}$$

where $\mathbf{W}_e$ is an appropriate weighting matrix and the unknown parameters $\boldsymbol{\theta}$ have been vectorized by using the vec$(\cdot)$ operator which orders a matrix stacking its columns:

$$\boldsymbol{\theta} = \left[\text{vec}^T(\mathbf{A}),\, \text{vec}^T(\mathbf{B}),\, \text{vec}^T(\mathbf{C}),\, \text{vec}^T(\mathbf{D}),\, \text{vec}^T(\mathbf{E}),\, \text{vec}^T(\mathbf{F})\right]^T \tag{6.14}$$

A more clever definition of the unknown vector would not take into consideration the state matrix $\mathbf{A}$, which has already been identified and whose stability would be compromised during the re-identification process, so:

$$\boldsymbol{\theta} = \left[\text{vec}^T(\mathbf{B}),\, \text{vec}^T(\mathbf{C}),\, \text{vec}^T(\mathbf{D}),\, \text{vec}^T(\mathbf{E}),\, \text{vec}^T(\mathbf{F})\right]^T \tag{6.15}$$

Further, all the linear matrices identified with the MFD could be left unchanged, leading to a more robust approach using just $\boldsymbol{\theta} = \left[\text{vec}^T(\mathbf{E}),\, \text{vec}^T(\mathbf{F})\right]^T$. Considering that the output is available only at certain sampling points, the cost function may be rewritten in a discretized form as:

$$\mathcal{F}(\boldsymbol{\theta}) = \frac{1}{2}\sum_{k=1}^{N_t} \mathbf{e}(t_k,\boldsymbol{\theta})^T\, \mathbf{W}_e\, \mathbf{e}(t_k,\boldsymbol{\theta}) \tag{6.16}$$

where N_t is the number of sampling points. Therefore the identification problem may be formulated as:

$$\boldsymbol{\theta} = \arg\min_{\boldsymbol{\theta}} \mathcal{F}(\boldsymbol{\theta}) = \arg\min_{\boldsymbol{\theta}} \frac{1}{2}\sum_{k=1}^{N_t} \mathbf{e}(t_k,\boldsymbol{\theta})^T\, \mathbf{W}_e\, \mathbf{e}(t_k,\boldsymbol{\theta}) \tag{6.17}$$

The computation of the Jacobian matrix is needed in order to solve the minimization problem. The Jacobian matrix is the derivative of the system error output with respect to the parameters that have to be changed in order to minimize the cost function:

$$\mathbf{J}_k(t_k,\boldsymbol{\theta}) = \frac{\partial \mathbf{e}(t_k,\boldsymbol{\theta})}{\partial \boldsymbol{\theta}} = \frac{\partial \mathbf{y}(t_k,\boldsymbol{\theta})}{\partial \boldsymbol{\theta}}, \quad k = 1,\ldots,N_t \tag{6.18}$$

Defining the concatenation matrices:

$$\mathbf{e}(\boldsymbol{\theta}) = \left[\mathbf{e}_k^T(t_1,\boldsymbol{\theta}),\, \ldots,\, \mathbf{e}_k^T(t_{N_t},\boldsymbol{\theta})\right]^T \tag{6.19}$$

$$\mathbf{J}(\boldsymbol{\theta}) = \left[\mathbf{J}_k^T(t_1,\boldsymbol{\theta}),\, \ldots,\, \mathbf{J}_k^T(t_{N_t},\boldsymbol{\theta})\right]^T \tag{6.20}$$

the n-th iteration of the LM algorithm [311] is:

$$\Delta\boldsymbol{\theta}_n = -\left[\mathbf{J}(\boldsymbol{\theta}_n)^T\mathbf{J}(\boldsymbol{\theta}_n) + \lambda\mathbf{I}\right]^{-1}\mathbf{J}(\boldsymbol{\theta}_n)^T\mathbf{e}(\boldsymbol{\theta}_n) \tag{6.21}$$

and the solution at the next step is given by:

$$\boldsymbol{\theta}_{n+1} = \boldsymbol{\theta}_n + \Delta\boldsymbol{\theta}_n \tag{6.22}$$

with λ scalar parameter that makes act the algorithm as a modified Newton-Raphson method, when it is very small, and as a gradient descent method, when it is very large.

Indicators such as the significance factor [312] and coherence functions [313, 314] provide a means of determining which terms are significant and which terms can be safely discarded. Alternatively an iterative, greedy, subset-selection algorithm may be employed to chose the monomials that better model the nonlinear behavior of the system. At every iteration, a monomial within the full expansion vector chosen in such a way to mostly decreasing the current Levenberg-Marquardt residual $\mathbf{r}$ is added in the nonlinear term. Then, the residual is updated and the iteration process restart from the begin until the residual becomes lower than a provided tolerance. The main steps are shown in Algorithm 6.1, where $\mathcal{M}$ is the monomial selected at the current iteration which maximize the residual decreasing, $\mathbf{J}_\zeta$ and $\mathbf{e}_\zeta$ are referred to the Jacobian matrix and the error vector updated with the inclusion of the vector $\boldsymbol{\zeta}$ containing the nonlinear monomials in $(\mathbf{x}, \mathbf{u})$. The same procedure is performed using the vector $\boldsymbol{\eta}(\mathbf{x}, \mathbf{u})$.

Algorithm 6.1 Greedy algorithm

Input: $\mathbf{J}(\boldsymbol{\theta}_0), \mathbf{e}(\boldsymbol{\theta}_0), \varepsilon$ ▷ Initial Jacobian matrix, error vector, tolerance
Output: $\boldsymbol{\zeta}(\mathbf{x}, \mathbf{u})$ ▷ vector of monomials

Function GREEDY($\mathbf{J}, \mathbf{e}, \varepsilon$)
  $\boldsymbol{\zeta} \leftarrow \emptyset$
  while $\|\mathbf{r}\| > \varepsilon$ **do**
    $\mathcal{M} \leftarrow$ SELECTMONOMIAL($\mathbf{r}$, $\boldsymbol{\xi}_{\{p\}}$, $\boldsymbol{\zeta}$)
    $\boldsymbol{\zeta} \leftarrow \boldsymbol{\zeta} \cup \{\mathcal{M}\}$
    $(\boldsymbol{\theta}, \mathbf{r}) \leftarrow$ LEVENBERGMARQUARDT($\mathbf{J}_\zeta, \mathbf{e}_\zeta$)
  return $\boldsymbol{\zeta}, \boldsymbol{\theta}$

Algorithm 6.2 Select monomials algorithm

Input: $\mathbf{r}, \boldsymbol{\xi}_{\{p\}}, \boldsymbol{\zeta}$ ▷ residual, all combination of monomials, previously chosen terms
Output: $\mathcal{M}$ ▷ monomial selected among the candidates terms

Function SELECTMONOMIAL($\mathbf{r}, \boldsymbol{\xi}_{\{p\}}, \boldsymbol{\zeta}$)
  $\mathbf{A}_\zeta \leftarrow \mathbf{J}_\zeta^T \mathbf{J}_\zeta$
  $\mathcal{C} \leftarrow \boldsymbol{\xi}_{\{p\}} \setminus \boldsymbol{\zeta}$ ▷ set of candidate monomials
  $\mathcal{M} \leftarrow \arg\max_{\mathcal{M} \in \mathcal{C}} \frac{\mathbf{A}_\zeta^T \mathbf{r}}{\|\mathbf{A}_\zeta\| \|\mathbf{r}\|}$
  return $\mathcal{M}$

The sub-function SELECTMONOMIALS (see Algorithm 6.2) aims in choosing the remaining monomials most likely to reduce the residual error. This is done by selecting among the vector $\boldsymbol{\xi}_{\{p\}}$, containing all the possible combination of monomials up to a degree p, the one whose term $\mathbf{A}_\zeta := \mathbf{J}_\zeta^T \mathbf{J}_\zeta$ maximize the objective function:

$$\mathcal{G} := \frac{\mathbf{A}_\zeta^T \mathbf{r}}{\|\mathbf{A}_\zeta\| \|\mathbf{r}\|} \tag{6.23}$$

Hence:

$$\mathcal{M} = \arg\ \max_{\mathcal{M}\in\boldsymbol{\xi}_{\{\mathrm{P}\}}} \frac{\mathbf{A}_{\zeta}^{T}\mathbf{r}}{\|\mathbf{A}_{\zeta}\|\|\mathbf{r}\|} \tag{6.24}$$

The drawback of the PNLSS approach is that it may carry out identified models whose behavior is not accurate when evaluated outside the region in which they were estimated. This because a polynomial quickly attains large numerical values when its arguments are large. So attention must be paid in its application. Poor numerical conditioning may occur for polynomial series which contain both small and large powers.

Approaches using normalized and pseudo-orthogonal generating functions [315] do not manifest these issues.

Other issues may arise also from the overfitting of the training signals.

Another disadvantage in using polynomial series is that nonlinear characteristics are not necessarily governed by integer power series [316]. There are classes of nonlinearity that cannot be modeled accurately even with high-order polynomial

expansions (e.g, non-smooth nonlinearities in the structural part of the aeroelastic system). Moreover it is quite hard to include high-order polynomial expansions in the states, because the nonlinear behavior of the original system may be represented by several equally good models leading to issues when the identified model will be applied for prediction purposes. An algorithm based on a Bayesian inference approach may alleviate this drawback [317]. by collecting potential models together with their posterior probability instead of the single best model, thus allowing for more flexibility in deciding the most appropriate model of the nonlinearity.

6.2.1 Application of the PNLSS approach for the identification of nonlinear aerodynamic and aeroelastic systems

A first application of the nonlinear identification method presented in the previous section is the Beddoes-Leishman dynamic stall model [318].

The model is identified using monomial up to a degree three in $\boldsymbol{\zeta}$ and a degree two for the monomials in $\boldsymbol{\eta}$.

After being identified with a set of training functions, the aerodynamic model has been applied for a case of an airfoil oscillating ± 10 degrees around a average position of 10 degrees. The results are shown in Fig. 6.1, where the nonlinear state space model has been compared with the linear one arising from the application of the matrix fraction description. As it may be seen the PNLSS approach performs better than matrix fraction description, which can only identify the linear part of the model (i.e. the one arising from the Theodorsen theory).

Another application of the PNLSS identification method is a two-degrees of freedom typical section (a NACA 64A010 airfoil) oscillating in pitch and plunge, subjected to limit-cycle oscillations. The equations of motion of the aeroelastic system are:

$$\begin{bmatrix} 1 & x_\alpha \\ x_\alpha & r_\alpha^2 \end{bmatrix} \begin{Bmatrix} \ddot{h} \\ \ddot{\alpha} \end{Bmatrix} + \begin{bmatrix} 2\zeta\omega_h & 0 \\ 0 & 2\zeta r_\alpha^2 \omega_\alpha \end{bmatrix} \begin{Bmatrix} \dot{h} \\ \dot{\alpha} \end{Bmatrix} + \begin{bmatrix} \omega_h^2 & 0 \\ 0 & r_\alpha^2 \omega_\alpha^2 \end{bmatrix} \begin{Bmatrix} h \\ \alpha \end{Bmatrix} = \frac{U^2}{\pi\mu l_a^2} \begin{Bmatrix} -c_l(t) l_a \\ c_m(t) \end{Bmatrix} \tag{6.25}$$

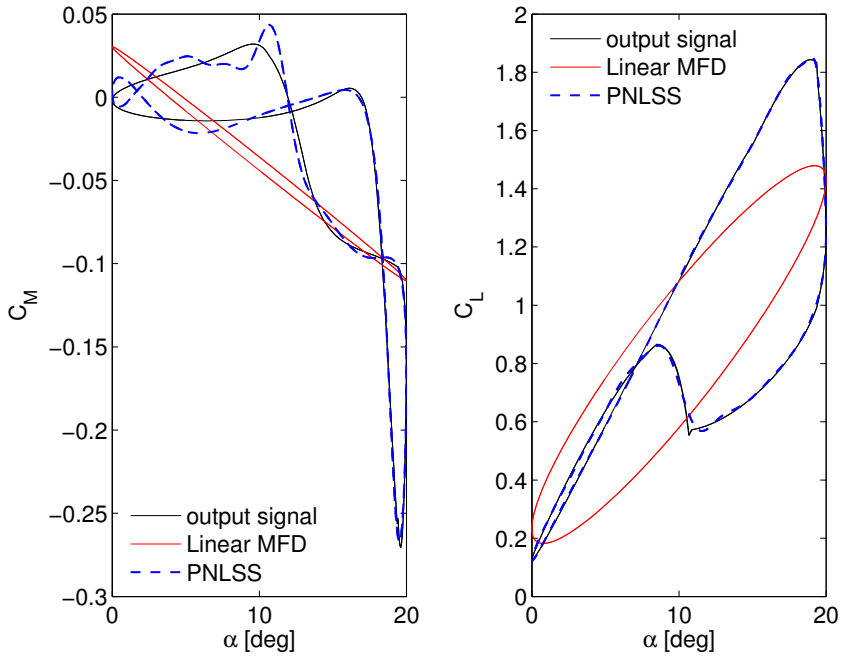

Figure 6.1: *Identification of the dynamic stall.*

where the semi-chord is $b = 0.5$, the nondimensional radius of gyration is $r_\alpha^2 = 0.25$, the mass ratio $\mu = 20$ and the static unbalance $x_\alpha = 0.25$. The ratio between the uncoupled bending and torsion frequencies are $\omega_h/\omega_\alpha = 0.2$. A structural damping coefficient, $\zeta = 0.01$, is applied to both modes. Aerodynamic loads (expressed by the lift and moment coefficients, c_l andc_m) are obtained using Euler equations discretized with 12200 unstructured quadrilateral finite volumes.

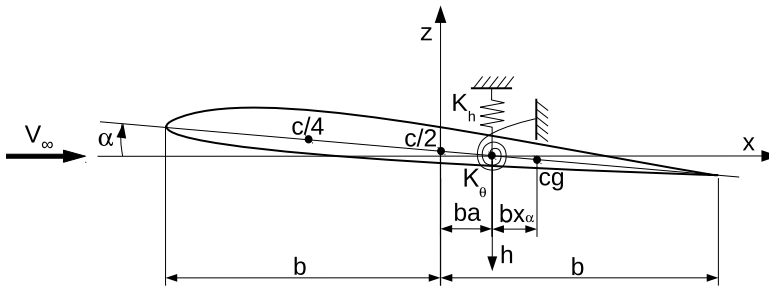

Figure 6.2: *Two degrees of freedom typical section.*

A training signal is used to build the nonlinear state space model. A time period $T_p = (2\pi l_a)/(kV_\infty)$ of the signal, being l_a the aerodynamic reference length, is required to excite a particular reduced frequency k. Specifying the range of reduced frequency that has

to be excited, the training signal can be efficiently created with the correct time steps. A set of reduced frequencies is randomly chosen, each one maintained constant through a period, together with a set of random amplitudes modulated by a gaussian function [305]. In this manner all the frequency of interest should be excited together with a varying amplitude. In Fig. 6.3 is represented the signal used to identify the aerodynamic subsystem.

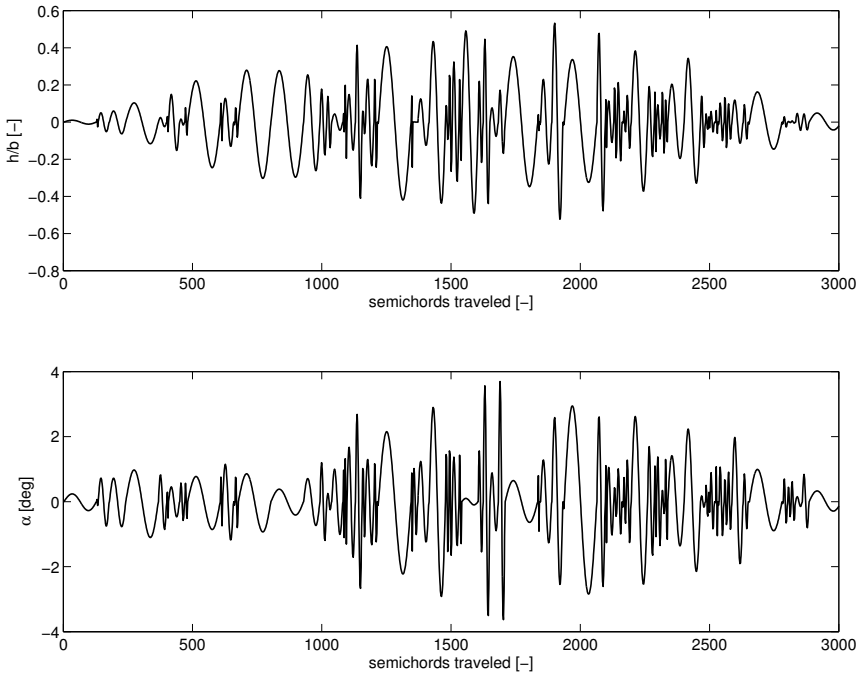

Figure 6.3: *Input training signal to identify the aerodynamic subsystem.*

A PNLSS model using a cubic monomials in the input equation (i.e. in the vector $\boldsymbol{\zeta}$) and quadratic monomials in the output relation (i.e. in the vector $\boldsymbol{\eta}$) is identified through a nonlinear least square approach. The model reproduce accurately the input-output mapping, as may be seen from Fig. 6.4.

The identified nonlinear aerodynamic model is then coupled to the structural part of the typical section, so providing the aeroelastic system to be used in predictive analysis. A limit cycle oscillation is obtained for a flight condition of $M_\infty = 0.8$, and a reduced velocity $V^* := \frac{V_\infty}{b\,\omega_\alpha} = 6$. The simulation show that the identified model is able in catching the LCO response in term of frequency, but not amplitude, as shown in Fig. 6.5.

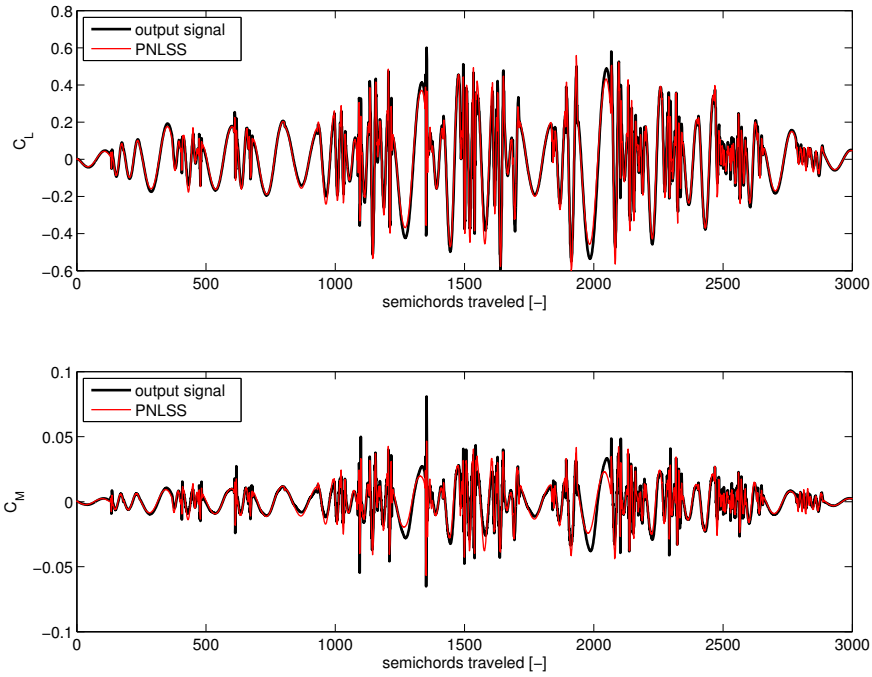

Figure 6.4: *response of the identified aerodynamic subsystem to the training signal.*

6.3 Element-based hyper-reduction

In this section an efficient scheme for evaluating nonlinear forces and their Jacobians associated to finite-element based systems is described. The approach, named element-based hyper-reduction (EBHR), has been presented in Refs. [319, 320], and found its origin in a research work [303] on computer graphics developing a optimized cubature rule for efficient integration of the nonlinear subspace force density, associated with subspace deformations, over a three-dimensional spatial domain. In this thesis, the approach is applied in the context of nonlinear aeroelastic systems.

The method aims at improving the evaluation of the nonlinear terms of reduced order models obtained from the projection of high-dimensional system of equations, whose evaluation has a cost dependent on the dimension n of the original problem. The achieved scalability is obtained through an optimization preprocess that enables a fast n-independent runtime computation of the so called hyper-reduced model.

The approach is focused on cases where the dimensionality burden arises from a detailed finite-element (FE) model. For aeroelastic systems the finite element method is in general applied to the structural model, the aerodynamic subsystem being usually discretized with a finite-volume (FV) method. Therefore the approach shown here its efficiency on the complexity reduction of nonlinear internal structural forces. Nevertheless, it may be

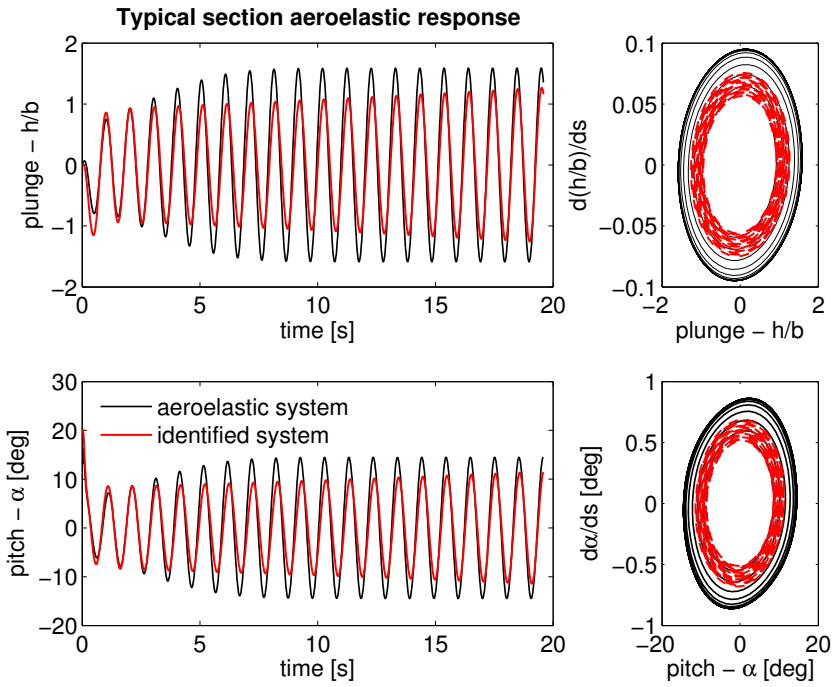

Figure 6.5: *Identification of the limit cycle oscillation.*

directly applied also to FE-based aerodynamic models.

Hence considering the equations governing a general nonlinear aeroelastic system arising from a finite-element discretization:

$$\mathbf{M}\ddot{\mathbf{u}} + \mathbf{C}\dot{\mathbf{u}} + \mathbf{f}(\mathbf{u}) = \mathbf{f}_{\text{ext}} \tag{6.26}$$

being $\mathbf{M}$ and $\mathbf{C}$ the mass matrix and the damping matrix, $\mathbf{f}(\mathbf{u})$ the vector of the nonlinear internal forces, $\mathbf{f}_{\text{ext}}$ the vector of the external forces, and $\mathbf{u} \in \mathbb{R}^n$ the vector of the full states containing the displacements (and in case also rotations) of the finite element nodes.

Expressing the degrees of freedom $\mathbf{u}$ by means of a truncated expansion $\mathbf{u} = \mathbf{V}\mathbf{q}$ using a proper subspace $\mathbf{V} \in \mathbb{R}^{n\times r}$ (e.g. a subset of the eigenvectors corresponding to the structural modes or the POD-based modes, that is empirical eigenvectors, obtained from a SVD applied to a snapshot matrix), being $\mathbf{q} \in \mathbb{R}^r$, with $r \ll n$, the reduced states, i.e. the generalized coordinates associated the chosen subspace, and projecting the transformed equation onto a proper subspace $\mathbf{W} \in \mathbb{R}^{n\times r}$ (e.g. in a Galërkin framework $\mathbf{W} = \mathbf{V}$), it results:

$$\mathbf{M}_r\,\ddot{\mathbf{q}} + \mathbf{C}_r\,\dot{\mathbf{q}} + \mathbf{f}_r(\mathbf{V}\mathbf{q}) = \mathbf{f}_{r,\text{ext}} \tag{6.27}$$

with

$$\mathbf{M}_r := \mathbf{W}^T\mathbf{M}\mathbf{V} \tag{6.28a}$$

$$\mathbf{C}_r := \mathbf{W}^T\mathbf{C}\mathbf{V} \tag{6.28b}$$

$$\mathbf{f}_{r,\text{ext}} := \mathbf{W}^T\mathbf{f}_{\text{ext}} \tag{6.28c}$$

$$\mathbf{f}_r := \underbrace{\mathbf{W}^T}_{r\times n}\underbrace{\mathbf{f}(\mathbf{V}\mathbf{q})}_{n\times 1} \tag{6.28d}$$

where it has been highlighted in Eq. (6.28d) how the computational complexity of nonlinear scales as $\mathcal{O}(n)$.

Similarly to the methods approximating a nonlinear force using a subset of the entire domain (e.g TPWL, missing point estimation, DEIM, unassembled DEIM), the element-based hyper reduction makes use of a Galërkin-projection of the high-dimensional dynamical system onto the POD-based modes, and as a successive step, in order to reduce the complexity of the nonlinear term, it applies an hyper-reduction of the projected system by evaluating the nonlinear internal forces onto a subset of the finite elements. However differently from the previous techniques, the EBHR takes into account the contribution of the discarded elements by weighting the contribution of the retained elements. In this way the reduced nonlinear force term may be written as:

$$\mathbf{f}_r := \mathbf{W}^T\mathbf{f}(\mathbf{V}\mathbf{q}) = \sum_{e=1}^{N_e}\mathbf{W}_e^T\mathbf{f}_e(\mathbf{V}\mathbf{q}) \approx \sum_{e=1}^{n_e\ll N_e}\alpha_e\,\underbrace{\mathbf{W}_e^T}_{r\times m}\underbrace{\mathbf{f}_e(\mathbf{V}\mathbf{q})}_{m\times 1} \tag{6.29}$$

being $\alpha_e > 0$ a positive local weight applied to the retained n_e finite elements, which are a small subset of the overall N_e finite elements $\{\mathcal{E}_e\}_{e=1}^{N_e}$ of the original problem so that the dimension $r = n_e m$ of the reduced system, with m the number of degrees of freedoms of the single element, is much smaller than the dimension of the full order model $n = N_e m$.

The positive weights α_e, and the associated selection of the n_e retained elements, are estimated by minimizing the nonlinear reduced force vector $\mathbf{f}_r(\mathbf{q})$ integration error over a training set of $(\mathbf{q}, \mathbf{f}_r(\mathbf{q}))$ pairs. This is performed using a nonnegative least squares (NNLS) [321], i.e. a constrained LS where the vector $\boldsymbol{\alpha} = [\alpha_1, \ldots, \alpha_{N_e}]^T$ collecting the weights α_e satisfies the vector inequality $\boldsymbol{\alpha} \geq \mathbf{0}$ that is defined componentwise (each component must be either positive or zero), with training forces arising from the n_t snapshots of the time response $\mathbf{u}(t)$ used to obtain the bases $(\mathbf{W}, \mathbf{V})$. Alternatively an iterative, greedy, subset-selection algorithm may be used.

Hence considering the time response evaluated at k-th time step $\mathbf{u}_k = \mathbf{u}(t_k)$, and the corresponding value of the generalized coordinate $\mathbf{q}_k = \mathbf{V}^T\mathbf{u}_k$, the nonlinear reduced force term $\mathbf{f}_r(\mathbf{V}\mathbf{q}_k)$ may be evaluated. Defining:

$$\mathbf{b}_k := \mathbf{W}^T\mathbf{f}(\mathbf{V}\mathbf{q}_k) \qquad \text{and} \qquad \mathbf{A}_k^e := \mathbf{W}_e^T\mathbf{f}_e(\mathbf{V}\mathbf{q}_k) \tag{6.30}$$

the equation (6.29) may be collocated in the n_t time steps used to build the snapshot matrix so forming the following overdetermined linear system:

$$\begin{bmatrix} \mathbf{A}_1^1 & \cdots & \mathbf{A}_1^{N_e} \\ \vdots & & \vdots \\ \mathbf{A}_{n_t}^1 & \cdots & \mathbf{A}_{n_t}^{N_e} \end{bmatrix} \begin{Bmatrix} \alpha_1 \\ \vdots \\ \alpha_{N_e} \end{Bmatrix} = \begin{Bmatrix} \mathbf{b}_1 \\ \vdots \\ \mathbf{b}_{N_e} \end{Bmatrix} \tag{6.31}$$

where all the N_e finite elements are taken under consideration, thus leaving to the NNLS process the task of selecting the most important elements by assigning them a weight $\alpha_e > 0$. Discarding all the elements with an identically null weight α_e, a subset of the original mesh is obtained, so leading to a reduced mesh $\{\mathcal{E}_e\}_{e=1}^{n_e}$, formed by just n_e finite elements, over which to evaluate the nonlinear force.

In the case of high dimensional finite-elements models, a greedy algorithm may be used as an alternative to the brute force NNLS solution, so to incrementally selecting the retained finite elements and estimating their non-negative weights which take into account the contribution of the non-selected elements in forming the model nonlinear behavior.

After the preprocess calculation of the n_e pairs $(\alpha_e, \mathcal{E}_e)$, the runtime simulation of the so obtained hyper-reduced model will consider the evaluation of the nonlinear force assembled using the contribution of just n_e elements.

The EBHR approach avoid the problems related to the approximation of $\mathbf{f}_r(\mathbf{q})$, ensuring energy conservation, passivity, and stability, by exploiting the redundant spatial structure of the generalized displacements $\mathbf{q}$, and the energy associated to the unassembled finite elements.

The subset of elements, and related weights, estimated through the optimization approach are suitable, besides estimating the reduced internal force $\mathbf{f}_r(\mathbf{q})$, to approximate the stiffness matrix (i.e. the Jacobian matrix related to the reduced force vector) as:

$$\mathbf{K}_r(\mathbf{q}) \approx \sum_{e=1}^{n_e} \alpha_e \frac{\partial \mathbf{f}_r^e(\mathbf{q})}{\partial \mathbf{q}^T}, \quad \in \mathbb{R}^{r \times r} \tag{6.32}$$

which thanks to the nonnegative weights, $\alpha_e \geq 0$, inherits the same semi-definiteness properties of the local stiffness matrix $\mathbf{K}_r^e := \partial \mathbf{f}_r^e(\mathbf{q})/\partial \mathbf{q}^T$, of the corresponding finite element.

The evaluation cost of the nonlinear force vector (Eq. (6.29)) using n_e finite elements is $\mathcal{O}(mn_e)$, since each contribution to the force FE assembling can be accumulated in $\mathcal{O}(m)$ operations, being m the number of DOFs of the single element. Evaluating the stiffness matrix approximation (Eq. (6.32)) involves $\mathcal{O}(m^2 n_e)$ operations, since the local stiffness matrix $\mathbf{K}_e$ involves $\mathcal{O}(m)$ operations, but its contribution to the global reduced stiffness matrix $\mathbf{K}_r$ involves a subspace projection computation of the form $\mathbf{K}_r^e = \mathbf{W}_e^T \mathbf{K}_e \mathbf{V}_e$ which requires an $\mathcal{O}(m^2)$ operations. When the stiffness matrix is not needed explicitly (e.g. many iterative Newton-Krylov solvers for nonlinear problems only require evaluation of matrix-vector products, so that it is required the computation of the action of the matrix on an arbitrary vector, but not the explicit storage of the matrix itself), a faster stiffness matrix-vector product is possible using a matrix-free approach [322], where the global reduced stiffness matrix $\mathbf{K}_r$ is never assembled. In any case the cost complexity of the system analysis will be independent from the high dimension n of the original problem.

Chapter 7

Parametric Model Order Reduction

Many relevant applications require the solution of parametrized governing equations over a potentially large range of parameter values. For example optimization processes [323], control design [324], statistical inverse problems [325] (i.e. estimate uncertain inputs from measurements or observations) and uncertainty quantification [326] demand repeated model evaluations for different values of their parameters, which may be material properties, system geometry, system configuration, initial conditions, and boundary conditions. This is computational expensive and very time consuming process when an high-dimensional model is involved. Therefore an accurate way to evaluate the solution for new parameter values having an as reduced complexity as possible is necessary.

Parametric models reduction has emerged recently as an important and vibrant research area among different communities, aiming at generating low cost but accurate models, characterizing the system behavior for different set of parameters. A survey of the state-of-the-art methods in parametric model reduction may be found in Ref. [327]. It describes different approaches within each class of methods handling parametric variation and providing a comparative discussion that lend insights to potential advantages and disadvantages in applying each of the methods.

Assuming that a reduced basis (i.e. a subspace) providing an approximate, but adequately accurate, representation of the state of the full model is available, if the nonlinear term can be computed in a fast way, then a new solutions may be evaluated with a low computational cost.

This may be a successful process if there exist a well structured solution for parameter variation, i.e. the solution varies smoothly on a low-dimensional manifold under parameter variation. A good approximation may be derived for all parameters with an appropriate choice of just some sample points on the manifold.

In building the parametrized ROM, a large up-front cost, the so called off-line cost, may be accepted if a reduced model allowing a rapid yet accurate simulation over the range of parameters, the so called on-line phase, is obtained.

7.1 Linear parametrized dynamical system

A parametrized dynamical system having a large dimension n, linear in the state but generically dependent on a set of d parameters $\mathbf{p} = [p_1, \ldots, p_d]^T \in \Omega \subset \mathbb{R}^d$, may be written in the following state-space formulation:

$$\begin{aligned} \mathbf{E}(\mathbf{p})\,\dot{\mathbf{x}}(t,\mathbf{p}) &= \mathbf{A}(\mathbf{p})\,\mathbf{x}(t,\mathbf{p}) + \mathbf{B}(\mathbf{p})\,\mathbf{u}(t) \\ \mathbf{y}(t,\mathbf{p}) &= \mathbf{C}(\mathbf{p})\,\mathbf{x}(t,\mathbf{p}) \end{aligned} \tag{7.1}$$

where it is assumed that the model is asymptotically stable for every $\mathbf{p} \in \Omega$, being Ω usually bounded. Model reduction aims in finding a model of reduced dimension $r \ll n$:

$$\begin{aligned} \mathbf{E}_r(\mathbf{p})\,\dot{\mathbf{x}}_r(t,\mathbf{p}) &= \mathbf{A}_r(\mathbf{p})\,\mathbf{x}_r(t,\mathbf{p}) + \mathbf{B}_r(\mathbf{p})\,\mathbf{u}(t) \\ \mathbf{y}_r(t,\mathbf{p}) &= \mathbf{C}_r(\mathbf{p})\,\mathbf{x}_r(t,\mathbf{p}) \end{aligned} \tag{7.2}$$

accurately approximating the behavior of the original system, i.e. the output of the reduced system $\mathbf{y}_r(t,\mathbf{p})$ is a good approximation of the output $\mathbf{y}(t,\mathbf{p})$ of the full order model, with respect to an appropriate error measure (e.g. L_2-norm and L_∞-norm in time domain considering the time history responses, or $\mathcal{H}_2$-norm and $\mathcal{H}_\infty$-norm in frequency domain considering the transfer matrices).

In a projection framework for a system with no parametric dependence, the ROM is obtained by approximating the state using a reduced basis $\mathbf{V}$ and projecting the equation (7.1) onto a subspace $\mathbf{W}$, giving rise to a set of reduced matrices $\mathbf{E}_r = \mathbf{W}^T\mathbf{E}\mathbf{V}$, $\mathbf{A}_r = \mathbf{W}^T\mathbf{A}\mathbf{V}$, $\mathbf{B}_r = \mathbf{W}^T\mathbf{B}$ and $\mathbf{C}_r = \mathbf{C}\mathbf{V}$, which are constant matrices precomputed during the off-line phase, so that the reduced model can be evaluated with no further reference to the full model.

Considering a parametrized ROM, proper projection subspaces must be chosen in order to bring the parametric dependence of the original model into the reduced model. The reduced basis matrices $\mathbf{V}$ and $\mathbf{W}$ may be derived by different methods such as rational interpolation methods, balanced truncation and proper orthogonal decomposition (POD). A global or a local approach may be used. In the former approach single global reduced basis matrices $(\mathbf{V},\ \mathbf{W})$ are carried out over the parameter space, i.e. each subspace captures the parametric dependence by embedding information regarding the entire parameter space. This is performed by collecting information coming from the sampling of multiple parameter values. The latter approach carry out multiple local reduced basis matrices $(\mathbf{V}_i,\ \mathbf{W}_i)$ for each sample $\hat{\mathbf{p}}_i$, $i = 1, \ldots, K$, of the parameter space considered. Then the parametric ROM may be built by directly interpolating the local subspaces over the parameter space, so constructing a single reduced model, otherwise by interpolating local reduced models each one carried out by projection onto the related local basis matrices.

An efficient evaluation of the parametric reduced model must be pursued, trying to obtain a model that does not scale as the high dimensions n of the original problem. Indeed, whatever the approach, global or local, for a generic parameter dependent systems the reduced matrices $(\mathbf{E},\mathbf{A})_r = \mathbf{W}^T\left(\mathbf{E}(\mathbf{p}),\mathbf{A}(\mathbf{p})\right)\mathbf{V}$ cannot be precomputed, and would require the evaluation of the original model for each parameter $\mathbf{p}$, and the multiplication for the reduced basis matrices $(\mathbf{V},\ \mathbf{W})$.

In the specific case of an affine parameter dependence, that is a system for which:

$$(\mathbf{E}(\mathbf{p}), \mathbf{A}(\mathbf{p})) = (\mathbf{E}_0, \mathbf{A}_0) + \sum_{i=1}^{M} f_i(\mathbf{p}) \, (\mathbf{E}_i, \mathbf{A}_i) \tag{7.3}$$

the reduced model for a given parameter may be obtained with just a summation of pre-computed (i.e. computed in an off-line step) reduced order matrices weighted by the term $f_i(\mathbf{p})$, without referring back to the original system, thus having a small on-line cost:

$$\begin{aligned} (\mathbf{E}(\mathbf{p}), \mathbf{A}(\mathbf{p}))_r &= \mathbf{W}^T \, (\mathbf{E}(\mathbf{p}), \mathbf{A}(\mathbf{p})) \, \mathbf{V} \\ &= \mathbf{W}^T \, (\mathbf{E}_0, \mathbf{A}_0) \, \mathbf{V} + \sum_{i=1}^{M} f_i(\mathbf{p}) \mathbf{W}^t \, (\mathbf{E}_i, \mathbf{A}_i) \, \mathbf{V} \\ &= (\mathbf{E}_0, \mathbf{A}_0)_r + \sum_{i=1}^{M} f_i(\mathbf{p}) \, (\mathbf{E}_i, \mathbf{A}_i)_r \end{aligned} \tag{7.4}$$

The so constructed ROM will maintain the affine structure of the original problem, thus avoiding changes in designing frameworks and tools developed to handle such model structures.

Approximations like those applied in nonlinear model reduction (see section 6.1) are usually introduced for generic non-affine parameter dependent systems, thus avoiding costly $\mathcal{O}(n)$ evaluations in forming the reduced order matrices for each different parameter value. Thus a Taylor series expansion may be used to provide an approximate affine decomposition of the system matrices [326]. Otherwise interpolation approaches as the Missing Point Estimation [291], the GNAT [302] or the empirical interpolation based methods (EIM, DEIM, UDEIM, LDEIM) [300] may be employed. These interpolation methods may be interpreted as projection methods where an oblique projector is used [294].

7.1.1 Using a single global basis

Single global reduced basis matrices may be carried out by concatenating the local bases obtained from multiple parameter sample $\mathbf{p}_1, \ldots, \mathbf{p}_K$, so that $\mathbf{V} = [\mathbf{V}_1, \ldots, \mathbf{V}_K]$ and $\mathbf{W} = [\mathbf{W}_1, \ldots, \mathbf{W}_K]$, and applying to them an SVD in order to remove the possible rank deficient components from $\mathbf{V}$ and $\mathbf{W}$, leading to matrices having orthonormal columns. If the local matrices will come from a rational interpolation approach the resulting global subspace will maintain the characteristics of the local subspaces, i.e. it will still interpolate (or approximately interpolate if small non-zeros singular values and associate vectors will be removed after the SVD) the full order model at each combination of frequency and parameter used in building every local basis matrix [323]. Otherwise if the local matrices are carried out using projection methods, e.g. a balanced truncation, the global reduced parametric model, even if it yields to a good approximation of the full model, is no longer guaranteed to maintain the properties (e.g. balancing) of each local subspace in the correspondent parameter.

7.1.2 Using multiple local bases

Interpolating among local bases

The set of local basis matrices $\{\mathbf{V}_i\}_{i=1}^K$ and $\{\mathbf{W}_i\}_{i=1}^K$ obtained by sampling the parameter space at points $p_1, \ldots, p_K$, may be directly interpolated, as opposed to constructing fixed global basis matrices $\mathbf{V}$ and $\mathbf{W}$, in order to find local reduced bases for a new parameter value. The interpolation is often performed on a space tangent to a chosen manifold of the local bases [328], so to preserve desired properties (e.g. orthogonality) of the interpolated quantity.

For example a new local basis $\hat{\mathbf{V}}$ preserving the orthonormality property of the $\mathbf{V}_i$, $i = 1, \ldots, K$, orthonormal basis may be obtained by interpolating on the tangent space $\mathcal{T}_{\mathcal{P}}$, at the point $\mathcal{P}$, to the Stiefel manifold $\mathcal{S}_{n,r}$ [329] (i.e. the set of all r-dimensional orthonormal bases of $\mathbb{R}^n$, for $1 < r < n$). An orthonormal basis $\mathbf{V}_i \in \mathbb{R}^{n \times r}$ is a point on $\mathcal{S}_{n,r}$. Considering the tangent space to the Stiefel manifold in a reference point, for simplicity $\mathbf{V}_1$, all the neighborhood points $\mathbf{V}_i \in S_{n,r}$ can be mapped to the tangent space by a logarithmic map:

$$\mathbf{T}_i = \mathrm{Log}_{\mathbf{V}_1}(\mathbf{V}_i) \in \mathcal{T}_{\mathbf{V}_1} \tag{7.5}$$

defining a geodesic on the tangent manifold from $\mathbf{V}_1$ to $\mathbf{V}_i$. A basis $\hat{\mathbf{V}}$ in a new parameter $\hat{\mathbf{p}}$ is carried out by interpolating the local bases in their mapped representation:

$$\mathbf{T}(\hat{\mathbf{p}}) = \sum_{i=1}^{K} l_i(\hat{\mathbf{p}}) \mathbf{T}_i \in \mathcal{T}_{\mathbf{V}_1} \tag{7.6}$$

where $l_i(\hat{\mathbf{p}})$ are the Lagrange basis functions, and using an exponential map to obtain the correspondent point onto the original Stiefel manifold $\mathcal{S}_{n,r}$:

$$\hat{\mathbf{V}} = \mathrm{Exp}_{\mathbf{V}_1}(\mathbf{T}(\hat{\mathbf{p}})) \in \mathcal{S}_{n,r} \tag{7.7}$$

preserving the desired properties (i.e. orthonormality). Numerically the mapping step is accomplished as follows:

$$\mathbf{T}_i = \mathbf{U}_i \tan^{-1}(\mathbf{\Sigma}_i) \mathbf{Z}_i^T \tag{7.8}$$

with $\mathbf{U}_i$ and $\mathbf{Z}_i$ coming from the following thin SVD [330]:

$$(\mathbf{I} - \mathbf{V}_1 \mathbf{V}_1^T) \mathbf{V}_i (\mathbf{V}_1^T \mathbf{V}_i)^{-1} = \mathbf{U}_i \mathbf{\Sigma}_i \mathbf{Z}_i^T \tag{7.9}$$

Conversely, the mapping back operation is achieved by:

$$\mathbf{V}(\hat{\mathbf{p}}) = \mathbf{V}_1 \hat{\mathbf{Z}} \cos(\hat{\mathbf{\Sigma}}) + \hat{\mathbf{U}} \sin(\hat{\mathbf{\Sigma}}) \tag{7.10}$$

where $\hat{\mathbf{U}}$ and $\hat{\mathbf{Z}}$ are computed with a thin SVD applied to the interpolated mapped basis:

$$\mathbf{T}(\hat{\mathbf{p}}) = \hat{\mathbf{U}} \hat{\mathbf{\Sigma}} \hat{\mathbf{Z}}^T \tag{7.11}$$

Interpolating among local reduced-order model matrices

The direct interpolation of the local basis matrices may require, for a generic non-affine system, to recompute expensive multiplications involving the full order large dimensional system $\mathbf{W}^T(\mathbf{E}(\hat{\mathbf{p}}), \mathbf{A}(\hat{\mathbf{p}}))\mathbf{V}$, whenever a new local reduced model is searched for a given parameter value $\hat{\mathbf{p}}$. This issue may be addressed for an affine parametric dependence by precomputing those quantities that do not depend on the parameters [331].

An alternative for generic systems consists of interpolating the local reduced state-space quantities [332–336]. as opposed to the basis matrices themselves. A congruence transformation of the local bases is necessary before the interpolation, in order to express the reduced systems in the same generalized coordinate system. The resulting transformed projection matrices are then used to carry out the calculation of local ROMs, whose matrices can be directly interpolated [333, 335, 336] otherwise interpolated after been mapped to a proper manifold [334].

Starting by selecting a reference basis, for example $(\mathbf{V}_1, \mathbf{W}_1)$, the congruence transformation matrices $\mathbf{Q}_i, \mathbf{P}_i \in \mathbb{R}^{r\times r}$ for $i = 1, \ldots, K$, to be applied at the local reduced matrices $\mathbf{E}_r := \mathbf{W}_i^T\mathbf{E}(\mathbf{p}_i)\mathbf{V}_i$ and $\mathbf{A}_r := \mathbf{W}_i^T\mathbf{A}(\mathbf{p}_i)\mathbf{V}_i$ related to the set of parameters $\{\mathbf{p}_i\}_{i=1}^K$, are obtained by solving the following optimization problems:

$$\mathbf{Q}_i = \arg\min_{\mathbf{Q}} \|\mathbf{V}_i\,\mathbf{Q} - \mathbf{V}_1\|_2 \qquad \text{subject to} \quad \mathbf{Q}^T\mathbf{Q} = \mathbf{I}_r \tag{7.12a}$$

$$\mathbf{P}_i = \arg\min_{\mathbf{P}} \|\mathbf{W}_i\,\mathbf{P} - \mathbf{W}_1\|_2 \qquad \text{subject to} \quad \mathbf{P}^T\mathbf{P} = \mathbf{I}_r \tag{7.12b}$$

which are solved through the use of a singular value decompositions for each basis. The resulting congruence transformation applied to the local bases is:

$$\widetilde{\mathbf{V}}_i := \mathbf{V}_i\mathbf{Q}_i \quad \text{and} \quad \widetilde{\mathbf{W}}_i := \mathbf{W}_i\mathbf{P}_i \quad \text{for } i = 1, \ldots, K \tag{7.13}$$

Hence the local ROMs, for the set of parameters $\{\mathbf{p}_i\}_{i=1}^K$, lying in the same generalized coordinate system are:

$$\begin{aligned} \widetilde{\mathbf{E}}_r(\mathbf{p}_i)\,\dot{\widetilde{\mathbf{x}}}_r(t, \mathbf{p}_i) &= \widetilde{\mathbf{A}}_r(\mathbf{p}_i)\,\widetilde{\mathbf{x}}_r(t, \mathbf{p}_i) + \widetilde{\mathbf{B}}_r(\mathbf{p}_i)\,\mathbf{u}(t) \\ \widetilde{\mathbf{y}}_r(t, \mathbf{p}_i) &= \widetilde{\mathbf{C}}_r(\mathbf{p}_i)\,\widetilde{\mathbf{x}}_r(t, \mathbf{p}_i) \end{aligned} \tag{7.14}$$

with matrices $\widetilde{\mathbf{E}}_r(\mathbf{p}_i) := \mathbf{P}_i^T\mathbf{E}_r(\mathbf{p}_i)\mathbf{Q}_i$, $\widetilde{\mathbf{A}}_r(\mathbf{p}_i) := \mathbf{P}_i^T\mathbf{A}_r(\mathbf{p}_i)\mathbf{Q}_i$, $\widetilde{\mathbf{B}}_r(\mathbf{p}_i) := \mathbf{P}_i^T\mathbf{B}_r(\mathbf{p}_i)$, $\widetilde{\mathbf{C}}_r(\mathbf{p}_i) := \mathbf{C}_r(\mathbf{p}_i)\mathbf{Q}_i$, and state $\widetilde{\mathbf{x}}_r(t, \mathbf{p}_i) := \mathbf{Q}_i^T\mathbf{x}_r(t, \mathbf{p}_i)$ A reduced order model for a new given parameter value $\hat{\mathbf{p}}$ may be obtained using a manifold interpolation approach (as previously described in section 7.1.2), when the matrices are non-singular and square, or a direct interpolation [334], when the matrices are singular or not square, onto the set of local congruence-transformed matrices.

A different congruence transformation is proposed in Ref. [333], where the dominant left singular vectors of the matrix concatenating the local bases $\{\mathbf{V}_i\}_{i=0}^K$ is used. It is worthwhile to notice that the congruence transformation is not necessary when a global basis, obtained by concatenating the local basis, is used as a projection subspace [332].

Interpolating the local transfer functions

In a system identification framework, a parametric reduced order model may be obtained by interpolating the transfer functions $\mathbf{H}_i(s, \mathbf{p}_i)$ identified at the set of parameters $\mathbf{p}_i$, $i = 1, \ldots, K$. The local transfer functions may be obtained directly from an identification process, so that the knowledge of the model matrices $(\mathbf{E}, \mathbf{A}, \mathbf{B}, \mathbf{C})$ is not strictly necessary. Nevertheless the interpolation process may be applied also on transfer functions obtained by:

$$\mathbf{H}_i(s, \mathbf{p}_i) = \mathbf{C}(\mathbf{p}_i)(s\,\mathbf{E}(\mathbf{p}_i) - \mathbf{A}(\mathbf{p}_i))^{-1}\mathbf{B}(\mathbf{p}_i), \quad i = 1, \ldots, K \tag{7.15}$$

where the model matrices may be those of the full order model as well as of a reduced order model determined with another model order reduction process (e.g. a projection method).

The transfer function evaluated in a new parameter point $\hat{\mathbf{p}}$ can be obtained by the following interpolation:

$$\widehat{\mathbf{H}}(s, \hat{\mathbf{p}}) = \sum_{i=1}^{K} L_i(\hat{\mathbf{p}})\, \mathbf{H}_i(s, \mathbf{p}_i) \tag{7.16}$$

being $L_i(\mathbf{p}_j) = \delta_{ij}$, with $i, j = 1, \ldots, K$. It is worthwhile to note that this representation separates the variables s and $\mathbf{p}$.

Any multivariate interpolation technique satisfying the condition $\hat{\mathbf{H}}(s, \mathbf{p}_i) = \mathbf{H}_i(s, \mathbf{p}_i)$ may be used. For example Lagrange polynomials, Lagrange interpolation [337], Hermite interpolation [338], rational interpolation [339, 340] and spline techniques may be exploited for simple scalar dependent systems. More sophisticated approaches (e.g. tensorization [341] which, using the Kronecker identity $\mathrm{vec}(\mathbf{AXB}) = (\mathbf{B}^T \otimes \mathbf{A})\mathrm{vec}(\mathbf{X})$, forms system of linear equations having a tensor product structure) may be used in case of general system depending on multiple parameters. Hermite and spline interpolation may be employed for regular grids of parameters, whereas Interpolation methods based on radial basis function [342] may be used for irregular grids. Sparse grids interpolation [340] is preferable, since the resulting interpolation of the reduced models become more complex as the model depend on more parameters.

Hereafter a transfer function having scalar parametric dependence is obtained through an interpolation process in order to show some of the properties connected with the approach. The parametric interpolated transfer function may be written with the following realization:

$$\widehat{\mathbf{H}}(s, \mathbf{p}) = \widehat{\mathbf{C}}(\mathbf{p})(s\,\widehat{\mathbf{E}} - \widehat{\mathbf{A}})^{-1}\widehat{\mathbf{B}} \tag{7.17}$$

with matrices concatenating the information of the local models (full or reduced) at the different parameter values:

$$\begin{aligned}
\widehat{\mathbf{E}} &= \mathrm{diag}(\mathbf{E}_r(\mathbf{p}_1), \ldots, \mathbf{E}_r(\mathbf{p}_K)) \\
\widehat{\mathbf{A}} &= \mathrm{diag}(\mathbf{A}_r(\mathbf{p}_1), \ldots, \mathbf{A}_r(\mathbf{p}_K)) \\
\widehat{\mathbf{B}} &= \left[\mathbf{B}_r^T(\mathbf{p}_1), \ldots, \mathbf{B}_r^T(\mathbf{p}_K)\right]^T \\
\widehat{\mathbf{C}}(\mathbf{p}) &= [L_1(\mathbf{p})\mathbf{C}_r(\mathbf{p}_1), \ldots, L_K(\mathbf{p})\mathbf{C}_r(\mathbf{p}_K)]
\end{aligned} \tag{7.18}$$

Since the representation separates the variables s and $\mathbf{p}$ it is possible to include the para-

metric dependence on $\mathbf{p}$ as more suitable. In this case, for sake of example, it has been included in forming the output matrix $\widehat{\mathbf{C}}(\mathbf{p})$.

Hence evaluating the ROM in a new parameter would require just the evaluation of the function $L_i(\mathbf{p})$. Moreover the concatenating structure adopted for the representation of the ROM will allow using local reduced models of different dimensions. An important advantage of the block-diagonal structure is that the final system will inherit the stability properties of the local models. Thus the parametric ROM $(\widehat{\mathbf{E}}, \widehat{\mathbf{A}})$ will be stable whenever the full order model is uniformly stable in the parameter domain or, if local reduced models are used, whenever stable local $(\mathbf{E}_r(\mathbf{p}_i), \mathbf{A}_r(\mathbf{p}_i))$ matrices are obtained for each parameter $\mathbf{p}_i$. Depending on the chosen interpolation method, an error bound and a proper distribution of the parameters $\mathbf{p}_i$ may be obtained.

Representing the parametric ROM as in Eq. (7.17) leads to a model whose dimensions grow rapidly with the number of parameter samples $\mathbf{p}_i$. Nevertheless the realization obtained concatenating the local system is not necessary to be formed explicitly, so that the evaluation of the parametric transfer function $\widehat{\mathbf{H}}(s, \mathbf{p})$ in a new parameter $\hat{\mathbf{p}}$ would just require the evaluation of the scalar parametric functions $L_i(\mathbf{p})$ at the given parameter and the evaluation of the local transfer functions $\mathbf{H}_i(s, \mathbf{p}_i)$ along the frequency points s. The realization however would lead to a parametric model whose poles does not depend on the parameter, being the dependence not included in the state matrices $(\widehat{\mathbf{E}}, \widehat{\mathbf{A}})$. Moreover the parametric transfer function may have spurious poles if the local models possess same poles, for example when some poles of the original model are duplicated in several of the local reduced models.

7.2 Nonlinear parametrized dynamical systems

In this section the thesis contributes in extending the work of Refs. [319, 320] to the generation of parametric reduced-order models (PROMs) for nonlinear aeroelastic systems.

7.2.1 Parametric Element-Based Hyper Reduction

As highlighted in section 7.1, different strategies may be used in building the basis needed for the EBHR framework, starting from snapshots of the full order model (FOM). In a local bases approach, a basis $\mathbf{V}_j$ is carried out for each parameter $\mathbf{p}_j$ considered, as depicted qualitatively in the scheme of Fig. 7.1, where the element-based hyper-reduction block may be schematically represented as a function requiring in input the time history response of the displacement obtained for the given parameter $\mathbf{p}_j$ and the corresponding local basis generated from the POD of its snapshot matrix. The disadvantages of the local basis approach is that it may generate different reduced meshes, because the elements of the mesh model selected by the element-based hyper-reduction method depend indirectly (through the local basis $\mathbf{V}(\mathbf{p}_j)$ and the time response $\mathbf{q}(t, \mathbf{p}_j)$) on the parameter under analysis, i.e. $n_e(\mathbf{p})$. Therefore the interpolation of the bases may be difficult to handle when the response to a new parameter $\hat{\mathbf{p}}$ is searched.

In a global basis approach the basis $\mathbf{V}$ is carried out by using a snapshots matrix built considering all the time responses of the system for all the set of parameters $\{\mathbf{p}_j\}_{j=1}^{N}$.

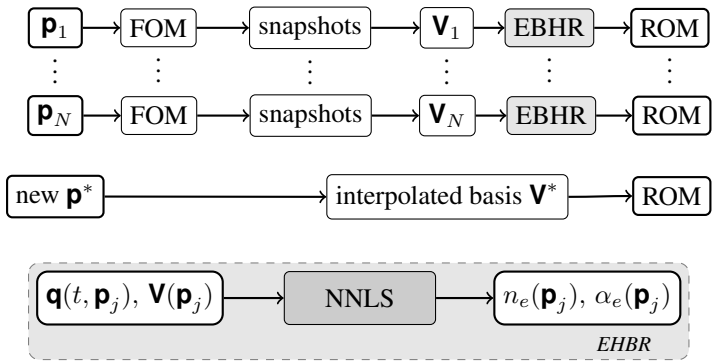

Figure 7.1: *Qualitative scheme of a EBHR applied to a local bases approach.*

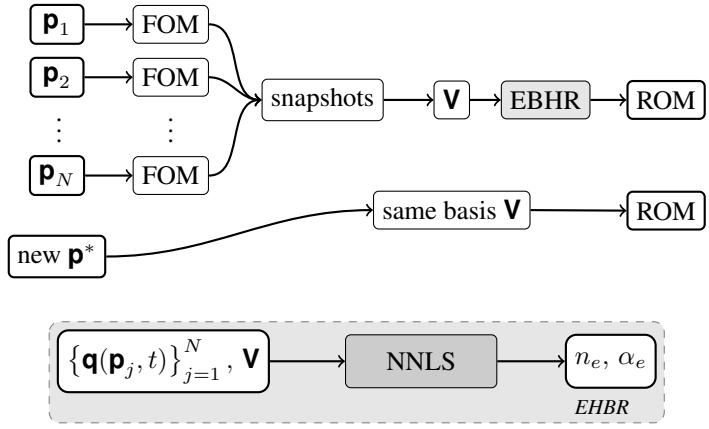

Figure 7.2: *Qualitative scheme of a EBHR applied to a global basis approach.*

7.2.2 Application of the EBHR to an aeroelastic system subjected to limit cycle oscillations

This subsection applies the element-based hyper reduction approach described in section 6.3 to an aeroelastic system that exhibits limit cycle oscillations (LCO). A simplified aeroelastic model consisting of a rectangular cantilevered plate, of 0.3 m chord, in quasi-steady supersonic flow is considered, with model data coming from Refs. [343, 344]. The governing equations are given by the von Karman's large deflection plate theory [345]:

$$\rho_s h \frac{\partial^2 w}{\partial t^2} + D\boldsymbol{\nabla}^4 w = \frac{12D}{h^2}\left[(\varepsilon_{xx} + \nu\varepsilon_{yy})\frac{\partial^2 w}{\partial x^2} + 2(1-\nu)\varepsilon_{xy}\frac{\partial^2 w}{\partial x \partial y} + (\varepsilon_{yy} + \nu\varepsilon_{xx})\frac{\partial^2 w}{\partial y^2}\right] + p_{\text{aero}} \tag{7.19a}$$

$$\frac{\partial}{\partial x}(\varepsilon_{xx} + \nu\varepsilon_{yy}) + (1-\nu)\frac{\partial \varepsilon_{xy}}{\partial y} = 0 \tag{7.19b}$$

$$\frac{\partial}{\partial y}(\varepsilon_{yy} + \nu\varepsilon_{xx}) + (1-\nu)\frac{\partial \varepsilon_{xy}}{\partial x} = 0 \tag{7.19c}$$

being $\rho_s = 2800\,\mathrm{kg/m^3}$ the density of the plate and $D = \frac{Eh^3}{12(1-\nu^2)}$ the plate rigidity, with elastic modulus $E = 70\,\mathrm{G\,Pa}$, Poisson's ratio $\nu = 0.3$ and plate thickness $h = 0.001\,\mathrm{m}$. The in-plane and out-of-plane deformations are coupled by the internal strains ε_{xx}, ε_{yy} and ε_{xy}, thus providing the structural nonlinearity necessary to bound the growth of vibrational amplitude and giving rise to the possibility for the system to exhibit a LCO behavior. The internal strains in the plate are:

$$\varepsilon_{xx} = \frac{\partial^2 u}{\partial x^2} + \frac{1}{2}\left(\frac{\partial^2 w}{\partial x^2}\right)^2 \tag{7.20a}$$

$$\varepsilon_{yy} = \frac{\partial^2 v}{\partial y^2} + \frac{1}{2}\left(\frac{\partial^2 w}{\partial y^2}\right)^2 \tag{7.20b}$$

$$\varepsilon_{xy} = \frac{1}{2}\left(\frac{\partial^2 v}{\partial x^2} + \frac{\partial^2 u}{\partial y^2} + \frac{\partial^2 w}{\partial x^2}\frac{\partial^2 w}{\partial y^2}\right)^2 \tag{7.20c}$$

where u, v and w are the plate displacements along the x, y and z coordinates respectively.

The external load over the wing is provide by the aerodynamic pressure p_{aero}, which is computed with a quasi-steady piston theory in supersonic flow [179, 346]:

$$p_{\mathsf{aero}} = \frac{2\rho_\infty V_\infty^2}{\sqrt{M_\infty^2 - 1}}\frac{\partial w}{\partial x} + \frac{2\rho_\infty V_\infty (M_\infty - 2)}{(M_\infty^2 - 1)^{3/2}}\frac{\partial w}{\partial t} \tag{7.21}$$

with ρ_∞, V_∞ and M_∞ the freestream air density, airspeed and Mach number respectively. A supersonic flight condition of $M_\infty = 2$, non-dimensional dynamic pressure $\lambda = \frac{2\rho_\infty V_\infty^2 c^3}{D\sqrt{M_\infty^2-1}} = 90$ and non-dimensional mass ratio $\mu = (2\rho_\infty c)/(\rho_s h) = 0.2$ is considered.

Spatially discretizing the structural model with a Finite Element approach brings to the following system of nonlinear second-order ODEs:

$$\mathbf{M}\ddot{\mathbf{u}}(t) + \mathbf{C}\dot{\mathbf{u}}(t) + \mathbf{f}_{\mathsf{nl}}(\mathbf{u}) = \mathbf{f}_{\mathsf{aero}}(\mathbf{u}, \dot{\mathbf{u}}, M_\infty) \tag{7.22}$$

being $\mathbf{M}$ and $\mathbf{C}$ the finite element mass and damping matrices and $\mathbf{f}_{\mathsf{nl}}$ the nonlinear internal force vector, function of the structural deformation vector $\mathbf{u}$, containing the FE nodes degrees of freedoms (three translations and two rotations for each node, being a plane plate). The aerodynamic load is approximated as:

$$\mathbf{f}_{\mathsf{aero}}(\mathbf{u}, \dot{\mathbf{u}}, M_\infty) = \mathbf{K}_{\mathsf{a}}\mathbf{u} + \mathbf{C}_{\mathsf{a}}\dot{\mathbf{u}} \tag{7.23}$$

where the aerodynamic stiffness matrix $\mathbf{K}_{\mathsf{a}}$ and aerodynamic damping matrix $\mathbf{C}_{\mathsf{a}}$ are given by:

$$\mathbf{K}_{\mathsf{a}} = \frac{2\rho_\infty V_\infty^2}{\sqrt{M_\infty^2 - 1}}\boldsymbol{\mathcal{I}}_p\frac{\partial \mathbf{N}_w}{\partial x} \tag{7.24}$$

$$\mathbf{C}_{\mathsf{a}} = \frac{2\rho_\infty V_\infty (M_\infty - 2)}{(M_\infty^2 - 1)^{3/2}} \boldsymbol{\mathcal{I}}_p \mathbf{N}_w \tag{7.25}$$

with $\boldsymbol{\mathcal{I}}_p$ being an interpolation matrix computing the work-equivalent forces of the pressure integrated over the elements, and $\mathbf{N}_w$ being the shape function related to the out-of-plane displacement w.

The nonlinear aeroelastic equation of motion is thus:

$$\mathbf{M}\ddot{\mathbf{u}} + (\mathbf{C} - \mathbf{C}_{\mathsf{a}})\,\dot{\mathbf{u}} - \mathbf{K}_{\mathsf{a}}\mathbf{u} + \mathbf{f}_{\mathsf{nl}}(\mathbf{u}) = 0 \tag{7.26}$$

which can be integrated using a second-order accurate, A/L-stable multistep integration scheme [347], with asymptotic spectral radius $\rho = 0.6$, with Newton-Raphson sub-iterations within each time step so obtaining the time history response.

The response of the aeroelastic system will depend upon the dynamic pressure parameter λ (considering the other parameters constant). Limit cycle oscillations will arise when λ will be greater the critical dynamic pressure λ^*, i.e. the flutter point or Hopf-bifurcation point. A direct flutter computation is used to obtain the flutter points via eigenanalysis of the aeroelastic system. Then the system is simulated at airspeeds for which there is an LCO.

The element-based hyper reduction approach is applied to reduce the computational costs for the simulation of the system. A fixed parameter, as well as a parameter dependent, aeroelastic model is considered to show the soundness of the approach. Two responses at dynamic pressure $\lambda = 60$ and $\lambda = 120$ are carried out for the original system. A snapshot matrix and the corresponding POD-basis are obtained for each one of the two responses. The so obtained subspaces are used in building two EBHR models, at the correspondent λ parameter. A comparison of the response of the two hyper-reduced models with their full order model counterpart is shown in Fig. 7.4 and Fig. 7.5. As may be seen a very good approximation of the responses is obtained with percentage relative errors of $8.2 \cdot 10^{-3}\,\%$ and $6.0 \cdot 10^{-3}\,\%$, having use an error metric of the form:

$$\varepsilon = \left(\frac{1}{N_s} \sum_{k=1}^{N_s} \frac{\|\mathbf{f}(t_k) - \mathbf{f}_r(t_k)\|}{\|\mathbf{f}(t_k)\|} \right)^{1/2} \tag{7.27}$$

The parametric hyper-reduced model is carried out using a global basis approach where a global subspace is obtained concatenating the local basis arising from the cases at $\lambda = 60$ and $\lambda = 120$, ad applying an SVD so discarding redundant informations. The resulting model consists of a reduced mesh having just 25% of the elements of the original finite element model. The parametrized EBHR model has been successively evaluated for a given parameter value $\lambda = 90$ in order to asses its prediction capability. The comparison of the response with the time history simulated using the full order model show a good agreement, with a percentage relative error of $1.82 \cdot 10^{-2}$. As shown in Fig. 7.6, both frequency and amplitude of the LCO are well approximated, but an initial transitory which results in a different phase of the response. A speed up factor of almost 40 is obtained using the hyper-reduced model instead of the full order model.

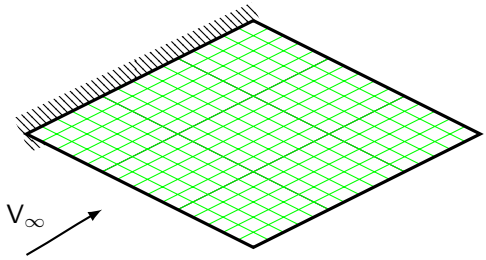

Figure 7.3: *Representation of the structural model of the plate.*

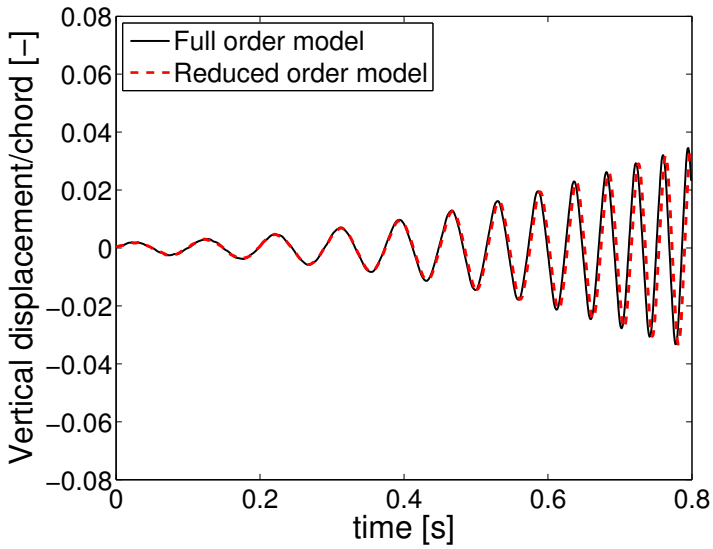

Figure 7.4: *Trailing edge panel tip vertical displacement at dynamic pressure* $\lambda = 60$

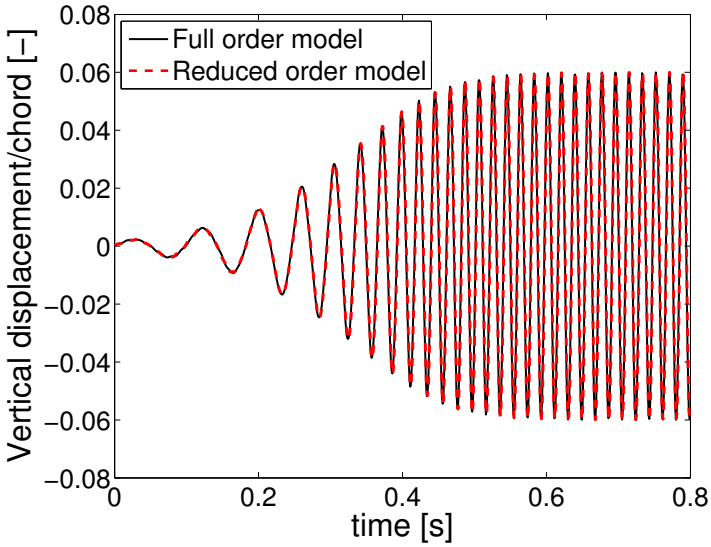

Figure 7.5: *Trailing edge panel tip vertical displacement at dynamic pressure* $\lambda = 120$

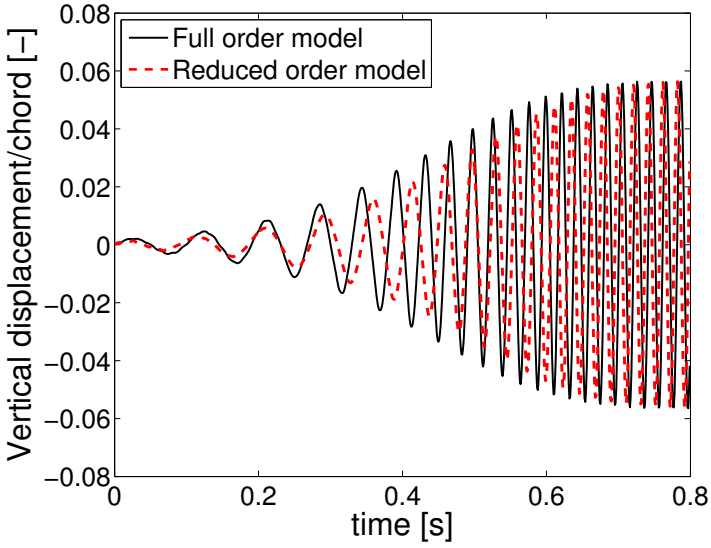

Figure 7.6: *Trailing edge panel tip vertical displacement at dynamic pressure* $\lambda = 90$

Conclusion and Recommendations

This thesis developed model order reduction techniques to reduce the dimensionality and complexity of high-dimensional computational aeroelastic models. Projection methods as well as identification techniques have been proposed and applied to linear an nonlinear aeroelastic systems.

A Petrov-Galërkin, as well as a Bubnov-Galërkin, projection-based model order reduction method is proposed, where the aerodynamic system is projected onto aerodynamic Schur subspaces obtained trough a left/right Schur decomposition. The reduced Schur bases are first manipulated in such a way to obtain a state transformation and a projection matrix decoupling completely the slow-fast dynamics of the system. This allows to easily introduce a residualization of the state associate to the high frequencies leading to more accurate results. The drawback in using aerodynamic modes is that the spectrum of the eigenvalues becomes richer as the computational grid is refined. However the enrichment will involve fast frequencies as well as slow frequencies, yielding to bigger projective subspaces and thus a less efficient reduction. In order to avoid this problem a dominant pole criteria relying on controllability and observability concepts is used to select the eigenvalues mainly contributing to the input-output mapping of the system. Using the correspondent Schur subspaces of the dominant poles allows to obtain a low order model which provide accurate results. However a deeper investigation should be directed to alternative methods for the computation of the low frequency, observable-controllable subspace simultaneously. Indeed the dominant poles approximation algorithm computes the dominant poles one by one by selecting the most dominant approximation at each iteration of a Newton scheme, so implying a large number of LU factorizations, and thus a large computational cost. A procedure based on the Jacobi-Davidson subspace iteration method for generalized eigenproblem, which iteratively construct a (generalized) partial Schur form, should be devised.

Concerning the identification techniques, the improved matrix fraction description developed in this work allows to obtain a unified low-order, asymptotically stable, linear time invariant approximation of the linear(ized) aerodynamic transfer matrices. It is based on three efficient nonlinear least squares methods, combined with a model order reduction providing a double dynamic residualization, which maintains an accurate fitting up to relatively high frequencies. It significantly improves a previous matrix fraction description formulation through: the adoption of a more appropriate performance index, the avoidance of a tweaked iterated weighting to ensure the identification of a stable model, the obtainment of either lower order models for an assigned precision or a better fitting for a given order, and the omission of a costly final constrained nonlinear optimization. Hence, thanks to the combination of the iterative solution to find a stable state space matrix, and the fi-

nal refitting step improving the accuracy to the high frequencies, the approach has been demonstrated to provide an effective fitting of the aerodynamic transfer matrices, thus leading to accurate results in flutter analyses and gust responses. Within such a framework it is also suggested a possible way to determine a nearly optimal gust entering location, aimed at providing smoother gust generalized aerodynamic forces. Hence the aerodynamic matrix function could be described using a lower number of sample reduced frequencies, that in a context of expensive high-fidelity aeroelastic analysis, allows a further reduction in the overall computational time to carry out the reduced model.

Moreover, the thesis proposes an alternative penetration-less gust formulation. The approach is based on spatially-fixed shape functions called gust modes, which can be used either to approximate any gust profile or to obtain the usual gust transfer matrices, enabling the analysis of gust responses even without resorting to standard delayed gust penetration schemes. Even if does not involve a direct dimensional reduction of the model, the procedure may be framed as a method reducing the complexity of gust simulations. Indeed the approach avoids building an aerodynamic reduced model for each different gust profile considered in the loads database, thus reducing the overall number of gust simulations required in the gust response analysis process.

The soundness of the proposed gust formulation has proved its effectiveness in carrying out aerodynamic transfer matrices obtained from low fidelity models (e.g. Theodorsen theory, strip theory, double-lattice method), and it has been verified through applications on complex cases of industrial relevance, such as complete aircraft with aerodynamic modeled using high-fidelity computational fluid dynamic. The approach allows to perform efficient and accurate aeroelastic gust responses, thanks to the resulting quite good approximation of the generalized aerodynamic forces. Intrinsic errors may arise from the least-squares interpolation when short length gusts are considered, which however does not affect the aeroelastic response but in the initial transient part of it. The method allows to easily compute the response to stochastic turbulence, being the modeling of the disturbance velocity profile performed as a post processing after the computation of the impulse (or step/blended step) response to each gust modes activation. This is quite a good advantage in the context of high-fidelity CFD, being the unsteady full nonlinear simulation to be performed just until the steady state response to the impulse, and not for the entire duration of the turbulence. The formulation, although devised to reconstruct the generalized aerodynamic forces, has shown in the airfoil test case to be effective even in the approximation of the pressure distribution, at least in correspondence of the temporal instant for which there are maximum loads, whereas spurious oscillations are present in other part of the time history pressure response. The behavior of the pressure distribution for the complete aircraft application have still to be investigated. Moreover, despite the inherent linearity of the method, which stands on a superposition approach, promising results have been shown on both subsonic and transonic cases, for the latter being more marked the poor approximation of the pressure distribution far from the maximum load time instant. This issue could be of relatively limited importance within the contest of the aircraft design, where critical loads are considered. Nevertheless, an extension of the approach could be devised for nonlinear problems using convolution type multi-input Volterra integral equations. Approximate representation (polynomial expansions or sparse representations) of the Volterra series should be used, so avoiding large numbers of CFD computations to determine Volterra high-order kernels. The remaining limitation, inherent to the approach,

in not to be able to simulate gust-aircraft mutual interaction responses cannot be fixed.

Widely available numerical examples, fully documented in the open literature, demonstrate the features and capabilities of the proposed projection-based model reduction, identification technique and gust modeling formulation. Generally speaking identification methods have shown to lead to smaller models than projecting methods, because they account just for the physical input/output behavior of the system. Indeed the numerical complexity is sometimes much higher than the physical complexity, because of the numerical constraints due to the accuracy and the consistency which must be satisfied, and this leads to high-fidelity models whose discretization brings a very densely distributed eigenvalues spectrum. Identification methods are thus more suitable when integral quantities, i.e. generalized forces, are quantities of interest, or when the aerodynamic system is available trough its transfer matrices or input-output responses. Whereas projection methods are more suitable when the pressure distribution or flow structures are the interesting quantities. In this prospective, simulations of three-dimensional cases should be performed with the Schur-based projection method, so to better highlight more the performances or drawbacks of the approach.

It is remarked that the most suitable order reducing techniques depend on the problem under investigation, and must be chosen as a compromise between the obtainable prediction accuracy and the order reduction cost. In particular the costs associated to identification methods are mainly due in generating the time history responses to be use to build an input/output mapping, whereas the costs of projection-based reduced models are mainly related to the extraction of the subspace, which may require a simulation of the system as well, upon which to project the original model.

In addition to linear techniques, also nonlinear model order reduction methods have been taken into account. An identification approach for nonlinear aeroelastic systems is proposed, whereas a linear state space model is identified through the used of the presented matrix fraction description and extended to model nonlinearities using a polynomial expansion on the state and input. The unknown coefficient matrices are determined through the use of a least square minimization, after selecting training input signals exciting the nonlinearity of the system over a wide range of frequencies. Separating the linear and nonlinear part in a state space form, allows the identification of a stable state space matrix which leads to a more robust identification of the remaining nonlinear unknown coefficients. Such an approach has been applied to the identification of a Beddoes-Leishman dynamic stall model as well as to a typical section in transonic flow subjected to limit cycle oscillations. The dynamic stall application has achieved accurate results, while the limit cycle test has resulted in a good match of its frequency with an underestimate of the related amplitude. Despite the identification of a stable state matrix, the technique is prone to numerical difficulties in the convergence of the iterative fitting algorithm, especially when the nonlinearities are modeled with polynomial terms in the states. So it is generally advisable to avoid to use polynomial terms in the states within the state equation, but for low degrees up to three, or better to use them just within the output equation. Further, the application of the method to large systems presenting strong nonlinearities may lead to a high number of parameters of the model because of the possible combinations that could arise. This issue could be solved by modeling the nonlinear term by using structured/block-structured matrices, with only few static nonlinear blocks, so allowing a model with fewer unknown parameters which are easier to identify.

Within the projection reduction framework the application of the hyper-reduction procedure to a nonlinear finite element model has been used. Indeed, the projection of a large order nonlinear aeroelastic model onto a reduced subspace does not necessarily lead to a reduction of the complexity associated with solving the model, and an additional reduction procedure, the hyper-reduction, is required. The method is based on a Galërkin projection, achieving a dimensionality reduction through the use of a precomputed POD subspace. Further on, the nonlinear term is approximated by using an oblique projection constructed by properly selecting a subset of finite elements of the full model, while preserving important properties of the high-dimensional finite element model to be reduced. As the hyper-reduction operates on a much reduced computational domain, the reduced mesh, the complexity in solving the hyper-reduced order model does not scale with the large dimension any more, leading to important computational speedups. The procedure is demonstrated in building an accurate hyper-reduced model of an aeroelastic panel in supersonic flow subjected to limit cycle oscillations. Then a parametric hyper-reduced model is carried out using pre-computed snapshot solutions for a chosen set of parameters, afterward compressed into a global reduced-order basis. The predictive capability of the model has been demonstrated in simulating the response of the system at a given parameter outside those of the chosen set. The proposed nonlinear model reduction framework reduces the computational time required by a typical high-dimensional model while maintaining a good level of accuracy. A-posteriori error estimate could be devised so to found an error bounding function for the discrepancy between the exact and approximated nonlinear term. This error bound could also suggest appropriate choices for the training vectors and to be extended to nonlinear parametrized problems.

The proposed nonlinear and parametric reduction methods, being the last development of the thesis work, still require further analyses and improvements, including the investigation of their robustness, sensitivity and stability.

Concerning the parametric model reduction, a multi-parametric dependence have to be considered, where the parametrized reduced model should be obtained from the interpolation of reduced basis or reduced matrices over a multiple set of parameters, e.g. the Mach number, the angle of attack and structural properties as the plate thickness and stiffness. Interpolation of reduced local bases may also be considered in place of using global bases, including hybrid local-global bases where local basis are used for some parameters (e.g. flight condition parameters) and global basis for others (e.g. structural parameters).

Because of the data-dependent nature of the POD basis, the EBHR approach did not provide good approximations for systems whose parameters lies outside of the sampling parameter domains from which a POD basis is constructed. An adaptive approach could be therefore devised to handle this issue incorporating procedures to efficiently update the reduced basis, and thus improving the accuracy of the parametric ROM. The POD basis could be derived from a set of sampled solution trajectories (snapshots) from linearized models so reducing the computational cost compared to use the original large-scale nonlinear system. Other possible future research includes the combination of the element-based hyper-reduction approach with other projection-based model reduction techniques such as Krylov-based approximation methods or methods making use of controllability and observability concepts to better capture the input-output behavior. For specific applications to dynamical systems exhibiting limit-cycle oscillations, a combination of the parametric EBHR with the Harmonic-Balance method could be devised.

Bibliography

[1] Bennett, R. M. and Edwards, J. W., "An Overview of Recent Developments in Computational Aeroelasticity," *Proceedings of the 29 th AIAA Fluid Dynamics Conference*, Albuquerque, NM, June 15-18 1998, pp. 98–2421.

[2] Schuster, D. M., Liu, D. D., and Huttsell, L. J., "Computational Aeroelasticity: Success, Progress, Challenge," *Journal of Aircraft*, Vol. 40, No. 5, 2003, pp. 843–856. doi:10.2514/2.6875.

[3] Bendiksen, O. O., "Modern developments in computational aeroelasticity," *Proceedings of the Institution of Mechanical Engineers, Part G: Journal of Aerospace Engineering*, Vol. 218, No. 3, 2004, pp. 157–177.

[4] Bartels, R. E. and Sayma, A. I., "Computational aeroelastic modelling of airframes and turbomachinery: progress and challenges," *Phil. Trans. R. Soc. A*, Vol. 365, No. 1859, October 2007, pp. 2469–2499.

[5] de C. Henshaw, M. J., Badcock, K. J., Vio, G. A., Allen, C. B., Chamberlain, J., Kaynes, I., Dimitriadis, G., Cooper, J. E., Woodgate, M. A., Rampurawala, A. M., Jones, D., Fenwick, C., Gaitonde, A. L., Taylor, N. V., Amor, D. S., Eccles, T. A., and Denley, C. J., "Non-linear aeroelastic prediction for aircraft applications," *Progress in Aerospace Sciences*, Vol. 43, No. 4-6, 2007, pp. 65–137. doi:10.1016/j.paerosci.2007.05.002.

[6] *Computational Flight Testing — Results of the Closing Symposium of the German Research Initiative ComFliTe, Braunschweig, Germany, June 11th-12th, 2012*, edited by N. Kroll, R. Radespiel, J. W. van der Burg, and K. Sorensen, Vol. 123 of *Notes on Numerical Fluid Mechanics and Multidisciplinary Design*, Springer, 2013.

[7] Heeg, J., Chwalowski, P., Florance, J. P., Wieseman, C. D., Schuster, D. M., and Perry, B., "Overview of the Aeroelastic Prediction Workshop," *Proceedings of the 51st AIAA Aerospace Sciences Meeting including the New Horizons Forum and Aerospace Exposition*, Grapevine (Dallas/Ft. Worth Region), Texas, January 7-10 2013.

[8] Heeg, J., Chwalowski, P., Schuster, D., and Dalenbring, M., "Overview and Lessons Learned from the Aeroelastic Prediction Workshop," *Proceedings of the 54th AIAA/ASME/ASCE/AHS/ASC Structures, Structural Dynamics, and Materials Conference*, April 8-11 2013.

[9] Edwards, J. W. and Malone, J. B., "Current status of computational methods for transonic unsteady aerodynamics and aeroelastic applications," *Computing Systems in Engineering*, Vol. 3, No. 5, 1992, pp. 545–569. doi:10.1016/0956-0521(92)90025-E.

[10] Dowell, E. H. and Tang, D., "Nonlinear Aeroelasticity and Unsteady Aerodynamics," *AIAA Journal*, Vol. 40, No. 9, 2002, pp. 1697–1707.

[11] Dowell, E., Edwards, J., and Strganac, T., "Nonlinear Aeroelasticity," *Journal of Aircraft*, Vol. 40, No. 5, 2003, pp. 857–874.

[12] Bendiksen, O. O., "Review of unsteady transonic aerodynamics: Theory and applications," *Progress in Aerospace Sciences*, Vol. 47, No. 2, 2011, pp. 135–167. doi:10.1016/j.paerosci.2010.07.001.

[13] Beckert, A. and Wendland, H., "Multivariate interpolation for fluid-structure-interaction problems using radial basis functions," *Aerospace Science and Technology*, Vol. 5, No. 2, 2001, pp. 125–134. doi:10.1016/S1270-9638(00)01087-7.

[14] Degand, C. and Farhat, C., "A three-dimensional torsional spring analogy method for unstructured dynamic meshes," *Computers and Structures*, Vol. 80, No. 3-4, 2002, pp. 305–316. doi:10.1016/S0045-7949(02)00002-0.

[15] de Boer, A., van der Schoot, M. S., and Bijl, H., "Mesh deformation based on radial basis function interpolation," *Computers & Structures*, Vol. 85, No. 11-14, 2007, pp. 784–795. doi:10.1016/j.compstruc.2007.01.013.

[16] Cizmas, P. G. A. and Gargoloff, J. I., "Mesh Generation and Deformation Algorithm for Aeroelasticity Simulations," *Journal of Aircraft*, , No. 3, 2008, pp. 1062–1066.

[17] Rendall, T. C. S. and Allen, C. B., "Efficient mesh motion using radial basis functions with data reduction algorithms," *Journal of Computational Physics*, Vol. 228, No. 17, 2009, pp. 6231–6249. doi:10.1016/j.jcp.2009.05.013.

[18] Rendall, T. C. S. and Allen, C. B., "Reduced surface point selection options for efficient mesh deformation using radial basis functions," *Journal of Computational Physics*, Vol. 229, No. 8, 2010, pp. 2810–2820. doi:10.1016/j.jcp.2009.12.006.

[19] Smith, M., Cesnik, C., and Hodges, D., "Evaluation of Some Data Transfer Algorithms for Noncontiguous Meshes," *Journal of Aerospace Engineering*, Vol. 13, No. 2, April 2000, pp. 52–58. doi:10.1061/(ASCE)0893-1321(2000)13:2(52).

[20] Beckert, A., "Coupling fluid (CFD) and structural (FE) models using finite interpolation elements," *Aerospace Science and Technology*, Vol. 4, No. 1, 2000, pp. 13–22. doi:10.1016/S1270-9638(00)00111-5.

[21] Zwaan, R. J. and Prananta, B. B., "Fluid/structure interaction in numerical aeroelastic simulation," *International Journal of Non-Linear Mechanics*, Vol. 37, No. 4-5, 2002, pp. 987–1002. doi:10.1016/S0020-7462(01)00110-X.

[22] Cavagna, L., Quaranta, G., and Mantegazza, P., "Application of Navier-Stokes simulations for aeroelastic stability assessment in transonic regime," *Computers & Structures*, Vol. 85, No. 11-14, 2007, pp. 818–832. doi:10.1016/j.compstruc.2007.01.005.

[23] de Boer, A., van Zuijlen, A. H., and Bijl, H., "Review of coupling methods for non-matching meshes," *Computer Methods in Applied Mechanics and Engineering*, Vol. 196, No. 8, 2007, pp. 1515–1525. doi:10.1016/j.cma.2006.03.017.

[24] de Boer, A., van Zuijlen, A. H., and Bijl, H., "Comparison of conservative and consistent approaches for the coupling of non-matching meshes," *Computer Methods in Applied Mechanics and Engineering*, Vol. 197, No. 49-50, 2008, pp. 4284–4297. doi:10.1016/j.cma.2008.05.001.

[25] McNamara, J. J. and Friedmann, P. P., "Flutter Boundary Identification for Time-Domain Computational Aeroelasticity," *AIAA Journal*, Vol. 45, No. 7, 2007, pp. 1546–1555.

[26] Hirsch, C., *Numerical Computation of Internal and External Flows: The Fundamentals of Computational Fluid Dynamics*, Butterworth-Heinemann, 2007.

[27] Tezduyar, T., Behr, M., and Liou, J., "A new strategy for finite element computations involving moving boundaries and interfaces – The deforming-spatial-domain/space-time procedure: I. The concept and the preliminary numerical tests," *Computer Methods in Applied Mechanics and Engineering*, Vol. 94, No. 3, 1992, pp. 339–351. doi:10.1016/0045-7825(92)90059-S.

[28] Tezduyar, T. E., Sathe, S., Keedy, R., and Stein, K., "Space-time finite element techniques for computation of fluid-structure interactions," *Computer Methods in Applied Mechanics and Engineering*, Vol. 195, No. 17-18, 2006, pp. 2002–2027. doi:10.1016/j.cma.2004.09.014.

[29] Guruswamy, G. P., "Unsteady aerodynamic and aeroelastic calculations for wings using Euler equations," *AIAA Journal*, Vol. 28, No. 3, 1990, pp. 461–469. doi:10.2514/3.10415.

[30] Robinson, B. A., Yang, H. T. Y., and Batina, J. T., "Aeroelastic analysis of wings using the Euler equations with a deforming mesh," *Journal of Aircraft*, Vol. 28, No. 11, 1991, pp. 781–788. doi:10.2514/3.46096.

[31] Lee-Rausch, E. M. and Batina, J. T., "Wing flutter boundary prediction using unsteady Euler aerodynamic method," *Journal of Aircraft*, Vol. 32, No. 2, 1995, pp. 416–422. doi:10.2514/3.46732.

[32] Lee-Rausch, E. and Batina, J. T., "Wing flutter computations using an aerodynamic model based on the Navier-Stokes equations," *Journal of Aircraft*, Vol. 33, No. 6, 1996, pp. 1139–1147. doi:10.2514/3.47068.

[33] Rausch, R. D., Batina, J. T., and Yang, H. T. Y., "Three-dimensional time-marching aeroelastic analyses using an unstructured-grid Euler method," *AIAA Journal*, Vol. 31, No. 9, 1993, pp. 1626–1633. doi:10.2514/3.11824.

[34] Farhat, C., Geuzaine, P., and Brown, G., "Application of a three-field nonlinear fluid-structure formulation to the prediction of the aeroelastic parameters of an F-16 fighter," *Computers & Fluids*, Vol. 32, No. 1, 2003, pp. 3–29. doi:10.1016/S0045-7930(01)00104-9.

[35] Berglind, T., "A hybrid structured-unstructured grid method for aerodynamic flow simulations," *Proceedings of the 33rd Aerospace Sciences Meeting and Exhibit*, Reno, NV, 1995. doi:10.2514/6.1995-51.

[36] Khawaja, A. and Kallinderis, Y., "Hybrid grid generation for turbomachinery and aerospace applications," *International Journal for Numerical Methods in Engineering*, Vol. 49, No. 1-2, 2000, pp. 145–166. doi:10.1002/1097-0207(20000910/20)49:1/2<145::AID-NME927>3.0.CO;2-W.

[37] Jameson, A., "Time dependent calculations using multigrid, with applications to unsteady flows past airfoils and wings," *Proceedings of the AIAA 10th Computational Fluid Dynamics Conference*, AIAA, Honolulu, HI, 1991. doi:10.2514/6.1991-1596.

[38] Zhou, L. and Walker, H., "Residual Smoothing Techniques for Iterative Methods," *SIAM Journal on Scientific Computing*, Vol. 15, No. 2, 1994, pp. 297–312. doi:10.1137/0915021.

[39] Trottenberg, U., Oosterlee, C. W., and Schüller, A., *Multigrid*, Academic Press, 2000.

[40] Pope, S. B., *Turbulent Flows*, Cambridge University Press, 2000.

[41] Wilcox, D. C., *Turbulence Modeling for CFD*, DCW Industries, Inc., 2006.

[42] Strelets, M., "Detached eddy simulation of massively separated flows," *39th Aerospace Sciences Meeting and Exhibit*, Reno, NV, January 2001. doi:10.2514/6.2001-879.

[43] Squires, K. D., "Detached-Eddy Simulation: Current Status and Perspectives," *Direct and Large-Eddy Simulation V*, edited by R. Friedrich, B. J. Geurts, and O. Métais, Vol. 9 of *ERCOFTAC Series*, Springer Netherlands, 2004, pp. 465–480. doi:10.1007/978-1-4020-2313-2_49.

[44] Piomelli, U., "Large-eddy simulation: achievements and challenges," *Progress in Aerospace Sciences*, Vol. 35, No. 4, 1999, pp. 335–362. doi:10.1016/S0376-0421(98)00014-1.

[45] Zhang, Z., Liu, F., and Schuster, D., "An Efficient Euler Method on Non-Moving Cartesian Grids with Boundary-Layer Correction for Wing Flutter Simulations," *Proceedings of the 44th AIAA Aerospace Sciences Meeting and Exhibit*, Reno, Nevada, January 9-12 2006. doi:10.2514/6.2006-884.

[46] Morino, L., "Boundary Integral Equations in Aerodynamics," *Applied Mechanics Reviews*, Vol. 46, No. 8, 1993, pp. 445–466. doi:10.1115/1.3120373.

[47] Anderson, J., *Modern compressible flow: with historical perspective*, Mcgraw Hill, 2002.

[48] Parrinello, A. and Mantegazza, P., "Independent Two-Fields Solution for Full-Potential Unsteady Transonic Flows," *AIAA Journal*, Vol. 48, No. 7, 2010, pp. 1391–1402. doi:10.2514/1.J050013.

[49] Parrinello, A. and Mantegazza, P., "Improvements and Extensions to a Full-Potential Formulation Based on Independent Fields," *AIAA Journal*, Vol. 50, No. 3, 2012, pp. 571–580. doi:10.2514/1.J051270.

[50] Nitzsche, F. and Voss, R., "Development of a solution for the transonic flutter analysis of finite wings," *Proceedings of the Int. Forum on Aeroelasticity and Structural Dynamics*, Amsterdam, The Netherlands, 2003.

[51] Batina, J. T., "Advanced small perturbation potential flow theory for unsteady aerodynamic and aeroelastic analyses," Tech. Rep. NASA TM 2005-213908, November 2005.

[52] Katz, J. and Plotkin, A., *Low-Speed Aerodynamics*, Cambridge Aerospace Series, Cambridge University Press, February 5 2001.

[53] Ehlers, F. E., Epton, M. A., Johnson, F. T., Magnus, A. E., and Rubbert, P. E., "Improved Higher-Order Panel Method for Linearized Supersonic Flow," *AIAA Journal*, Vol. 17, No. 3, 1979, pp. 225–226. doi:10.2514/3.61104.

[54] Roughen, K. M., Baker, M. L., and Fogarty, T., "Computational Fluid Dynamics and Doublet-Lattice Calculation of Unsteady Control Surface Aerodynamics," *Journal of Guidance, Control, and Dynamics*, Vol. 24, No. 1, 2001, pp. 160–166. doi:10.2514/2.4697.

[55] Lesoinne, M. and Farhat, C., "Higher-Order Subiteration-Free Staggered Algorithm for Nonlinear Transient Aeroelastic Problems," *AIAA Journal*, Vol. 36, No. 9, 1998, pp. 1754–1757. doi:10.2514/2.7555.

[56] Farhat, C. and Lesoinne, M., "Two efficient staggered algorithms for the serial and parallel solution of three-dimensional nonlinear transient aeroelastic problems," *Computer Methods in Applied Mechanics and Engineering*, Vol. 182, No. 3-4, 2000, pp. 499–515. doi:10.1016/S0045-7825(99)00206-6.

[57] Degroote, J., Bathe, K.-J., and Vierendeels, J., "Performance of a new partitioned procedure versus a monolithic procedure in fluid-structure interaction," *Computers & Structures*, Vol. 87, No. 11-12, 2009, pp. 793–801. doi:10.1016/j.compstruc.2008.11.013.

[58] Demasi, L. and Livne, E., "Aeroelastic Coupling of Geometrically Nonlinear Structures and Linear Unsteady Aerodynamics: Two Formulations," *Proceedings of the 49th AIAA/ASME/ASCE/AHS/ASC Structures, Structural Dynamics, and Materials Conference*, Schaumburg, IL, April 2008.

[59] Morton, S. A., Melville, R. B., and Visbal, M. R., "Accuracy and Coupling Issues of Aeroelastic Navier-Stokes Solutions on Deforming Meshes," *Journal of Aircraft*, Vol. 35, No. 5, 1998, pp. 798–805. doi:10.2514/2.2372.

[60] Yee, H. C., Torczynski, J. R., Morton, S. A., Visbal, M. R., and Sweby, P. K., "On spurious behavior of CFD simulations," *International Journal for Numerical Methods in Fluids*, Vol. 30, No. 6, 1999, pp. 675–711. doi:10.1002/(SICI)1097-0363(19990730)30:6<675::AID-FLD857>3.0.CO;2-V.

[61] Farhat, C., van der Zee, K. G., and Geuzaine, P., "Provably second-order time-accurate loosely-coupled solution algorithms for transient nonlinear computational aeroelasticity," *Computer Methods in Applied Mechanics and Engineering*, Vol. 195, No. 17-18, 2006, pp. 1973–2001. doi:10.1016/j.cma.2004.11.031.

[62] Farhat, C., Lesoinne, M., and Tallec, P. L., "Load and motion transfer algorithms for fluid/structure interaction problems with non-matching discrete interfaces: Momentum and energy conservation, optimal discretization and application to aeroelasticity," *Computer Methods in Applied Mechanics and Engineering*, Vol. 157, No. 1-2, 1998, pp. 95–114. doi:10.1016/S0045-7825(97)00216-8.

[63] Samareh, J. and Bhatia, K., "A unified approach to modeling multidisciplinary interactions," *Proceedings of the 8th Symposium on Multidisciplinary Analysis and Optimization*, AIAA, Long Beach, CA, September 2000. doi:10.2514/6.2000-4704.

[64] Harder, R. L. and Desmarais, R. N., "Interpolation using surface splines," *Journal of Aircraft*, Vol. 9, No. 2, 1972, pp. 189–191. doi:10.2514/3.44330.

[65] Maman, N. and Farhat, C., "Matching fluid and structure meshes for aeroelastic computations: A parallel approach," *Computers & Structures*, Vol. 54, No. 4, 1995, pp. 779–785. doi:10.1016/0045-7949(94)00359-B.

[66] Jiao, X. and Heath, M. T., "Common-refinement-based data transfer between non-matching meshes in multiphysics simulations," *International Journal for Numerical Methods in Engineering*, Vol. 61, No. 14, 2004, pp. 2402–2427. doi:10.1002/nme.1147.

[67] Cebral, J. R. and Lohner, R., "Conservative Load Projection and Tracking for Fluid-Structure Problems," *AIAA Journal*, Vol. 35, No. 4, 1997, pp. 687–692. doi:10.2514/2.158.

[68] Chadwick, P., *Continuum Mechanics: Concise Theory and Problems*, Dover books on physics, Dover Publications, 1998.

[69] Malvern, L. E., *Introduction to the Mechanics of a Continuous Medium*, Prentice-Hall, Englewood Cliffs, New Jersey, 1969.

[70] Hirt, C. W., Amsden, A. A., and Cook, J. L., "An arbitrary Lagrangian-Eulerian computing method for all flow speeds," *Journal of Computational Physics*, Vol. 14, No. 3, 1974, pp. 227–253. doi:10.1016/0021-9991(74)90051-5.

[71] Donea, J., Giuliani, S., and Halleux, J. P., "An arbitrary lagrangian-eulerian finite element method for transient dynamic fluid-structure interactions," *Computer Methods in Applied Mechanics and Engineering*, Vol. 33, No. 1-3, 1982, pp. 689–723. doi:10.1016/0045-7825(82)90128-1.

[72] Fanion, T., Fernández, M., and Le Tallec, P., "Deriving Adequate Formulations for Fluid-Structure Interaction Problems: from ALE to Transpiration," *Revue Européenne des Éléments*, Vol. 9, No. 6-7, 2000, pp. 681–708. doi:10.1080/12506559.2000.10511481.

[73] Formaggia, L. and Nobile, F., "Stability analysis for the arbitrary Lagrangian Eulerian formulation with finite elements," *East-West Journal of Numerical Mathematics*, Vol. 7, No. 2, 1999, pp. 105–131.

[74] Étienne, S., Garon, A., and Pelletier, D., "Perspective on the geometric conservation law and finite element methods for ALE simulations of incompressible flow," *Journal of Computational Physics*, Vol. 228, No. 7, 2009, pp. 2313–2333. doi:10.1016/j.jcp.2008.11.032.

[75] Farhat, C., Geuzaine, P., and Grandmont, C., "The Discrete Geometric Conservation Law and the Nonlinear Stability of ALE Schemes for the Solution of Flow Problems on Moving Grids," *Journal of Computational Physics*, Vol. 174, No. 2, 2001, pp. 669–694. doi:10.1006/jcph.2001.6932.

[76] Geuzaine, P., Grandmont, C., and Farhat, C., "Design and analysis of ALE schemes with provable second-order time-accuracy for inviscid and viscous flow simulations," *Journal of Computational Physics*, Vol. 191, No. 1, 2003, pp. 206–227. doi:10.1016/S0021-9991(03)00311-5.

[77] Shyy, W., Smith, R. W., Udaykumar, H. S., and Rao., M. M., *Computational Fluid Dynamics with Moving Boundaries*, Dover Books on Engineering, Dover Publications, 2007.

[78] Mavriplis, D. J. and Yang, Z., "Construction of the discrete geometric conservation law for high-order time-accurate simulations on dynamic meshes," *Journal of Computational Physics*, Vol. 213, No. 2, 2006, pp. 557–573. doi:10.1016/j.jcp.2005.08.018.

[79] Farhat, C., Lesoinne, M., and Maman, N., "Mixed explicit/implicit time integration of coupled aeroelastic problems: Three-field formulation, geometric conservation and distributed solution," *International Journal for Numerical Methods in Fluids*, , No. 10, 1995, pp. 807–835. doi:10.1002/fld.1650211004.

[80] Batina, J. T., "Unsteady Euler airfoil solutions using unstructured dynamic meshes," *AIAA Journal*, Vol. 28, No. 8, 1990, pp. 1381–1388. doi:10.2514/3.25229.

[81] Bottasso, C. L. and Detomi, D., "A Procedure for Tetrahedral Boundary Layer Mesh Generation," *Engineering with Computers*, Vol. 18, No. 1, 2002, pp. 66–79. doi:10.1007/s003660200006.

[82] Romanelli, G., *Computational Aeroservoelasticity of Free-Flying Deformable Aircraft*, Phd thesis, Politecnico di Milano, March 2012, URL `http://hdl.handle.net/10589/56884`.

[83] Witteveen, J. and Bijl, H., "Explicit Mesh Deformation Using Inverse Distance Weighting Interpolation," *19th AIAA Computational Fluid Dynamics*, San Antonio, Texas, 22-25 June 2009. doi:10.2514/6.2009-3996.

[84] Mavriplis, D. J., "Adaptive meshing techniques for viscous flow calculations on mixed element unstructured meshes," *International Journal for Numerical Methods in Fluids*, Vol. 34, No. 2, 2000, pp. 93–111. doi:10.1002/1097-0363(20000930)34:2<93::AID-FLD48>3.0.CO;2-3.

[85] Guardone, A., Isola, D., and Quaranta, G., "Arbitrary Lagrangian Eulerian formulation for two-dimensional flows using dynamic meshes with edge swapping," *Journal of Computational Physics*, Vol. 230, August 2011, pp. 7706–7722. doi:10.1016/j.jcp.2011.06.026.

[86] Söderström, T. and Stoica, P., *System Identification*, Prentice Hall, Upper Saddle River, N.J., 1989.

[87] Ljung, L., *System Identification–Theory for the User*, Prentice-Hall, Upper Saddle River, N.J., 2nd ed., 1999.

[88] Pintelon, R. and Schoukens, J., *System Identification: A Frequency Domain Approach*, IEEE Press, New York, 2001.

[89] Nelles, O., *Nonlinear System Identification. From Classical Approaches to Neural Networks and Fuzzy Models*, Springer, 2001.

[90] Antoulas, A. C., *Approximation of Large-Scale Dynamical Systems*, Society for Industrial and Applied Mathematics, Philadephia, PA, 2005.

[91] Schilders, W. H., van der Vorst, H. A., and Rommes, J., *Model Order Reduction: Theory, Research Aspects and Applications*, Vol. 13 of *Mathematics in Industry*, Springer, 2008.

[92] de villemagne, C. and Skelton, R. E., "Model reductions using a projection formulation," *26th IEEE Conference on Decision and Control, 1987*, Vol. 26, December 1987, pp. 461–466. doi:10.1109/CDC.1987.272862.

[93] Kunisch, K. and Volkwein, S., "Galerkin Proper Orthogonal Decomposition Methods for a General Equation in Fluid Dynamics," *SIAM Journal on Numerical Analysis*, Vol. 40, No. 2, 2002, pp. 492–515. doi:10.1137/S0036142900382612.

[94] Sirovich, L., "Turbulence and the dynamics of coherent structures. I - Coherent structures. II - Symmetries and transformations. III - Dynamics and scaling," *Quarterly of Applied Mathematics*, Vol. 45, 1987, pp. 561–571, 573–590.

[95] Gragg, W. B. and Lindquist, A., "On the partial realization problem," *Linear Algebra and Its Applications*, Vol. 50, 1983, pp. 277–319. doi:10.1016/0024-3795(83)90059-9.

[96] Lanczos, C., "An iteration method for the solution of the eigenvalue problem of linear differential and integral operators," *Journal of Research of the National Bureau of Standards*, Vol. 45, No. 4, 1950, pp. 225–280.

[97] Arnoldi, W. E., "The principle of minimized iterations in the solution of the matrix eigenvalue problem," *Quarterly of Applied Mathematics*, Vol. 9, No. 17, 1951, pp. 17–29.

[98] Ruhe, A., "Rational Krylov: A Practical Algorithm for Large Sparse Nonsymmetric Matrix Pencils," *Siam Journal on Scientific Computing*, Vol. 19, 1998. doi:10.1137/S1064827595285597.

[99] Glover, K., "All Optimal Hankel Norm Approximation of Linear Multivariable Systems and their L_∞-Error Bounds," *International Journal of Control*, Vol. 39, No. 6, 1984, pp. 1145–1193. doi:10.1080/00207178408933239.

[100] Moore, B., "Principal component analysis in linear systems: Controllability, observability, and model reduction," *IEEE Transactions on Automatic Control*, Vol. 26, 1981, pp. 17–32. doi:10.1109/TAC.1981.1102568.

[101] Safonov, M. G. and Chiang, R. Y., "A Schur method for balanced-truncation model reduction," *IEEE Transactions on Automatic Control*, Vol. 34, No. 7, jul 1989, pp. 729 –733. doi:10.1109/9.29399.

[102] Laub, A., Heath, M., Paige, C., and Ward, R., "Computation of system balancing transformations and other applications of simultaneous diagonalization algorithms," *IEEE Transactions on Automatic Control*, Vol. 32, 1987, pp. 115–122. doi:10.1109/TAC.1987.1104549.

[103] Varga, A., "Minimal Realization Procedures Based on Balancing and Related Techniques," *Conference On Computer Aided Systems Theory*, 1991, pp. 733–761. doi:10.1007/BFb0021056.

[104] Penzl, T., "Numerical Solution of Generalized Lyapunov Equations," *Advances in Computational Mathematics*, Vol. 8, No. 1-2, 1998, pp. 33–48. doi:10.1023/A:1018979826766.

[105] Stykel, T., "Gramian-Based Model Reduction for Descriptor Systems," *MCSS Mathematics of Control, Signals and Systems*, Vol. 16, No. 4, 2004, pp. 297–319. doi:10.1007/s00498-004-0141-4.

[106] Penzl, T., "A Cyclic Low-Rank Smith Method for Large Sparse Lyapunov Equations," *SIAM Journal on Scientific Computing*, Vol. 21, No. 4, 1999, pp. 1401–1418. doi:10.1137/S1064827598347666.

[107] Li, J.-R. and White, J., "Low Rank Solution of Lyapunov Equations," *Siam Journal on Matrix Analysis and Applications*, Vol. 24, 2002, pp. 260–280. doi:10.1137/S0895479801384937.

[108] Sorensen, D. C. and Antoulas, A. C., "The Sylvester equation and approximate balanced reduction," *Linear Algebra and its Applications*, Vol. 351-352, No. 0, 2002, pp. 671–700. doi:10.1016/S0024-3795(02)00283-5.

[109] Gugercin, S., Sorensen, D. C., and Antoulas, A. C., "A Modified Low-Rank Smith Method for Large-Scale Lyapunov Equations," *Numerical Algorithms*, Vol. 32, 2003, pp. 27–55. doi:10.1023/A:1022205420182.

[110] Grasedyck, L., "Existence of a low rank or $\mathcal{H}$-matrix approximant to the solution of a Sylvester equation," *Numerical Linear Algebra with Applications*, Vol. 11, No. 4, 2004, pp. 371–389. doi:10.1002/nla.366.

[111] Penzl, T., "Algorithms for model reduction of large dynamical systems," *Linear Algebra and its Applications*, Vol. 415, No. 2-3, 2006, pp. 322–343. doi:10.1016/j.laa.2006.01.007.

[112] Simoncini, V., "A New Iterative Method for Solving Large-Scale Lyapunov Matrix Equations," *Siam Journal on Scientific Computing*, Vol. 29, 2007, pp. 1268–1288. doi:10.1137/06066120X.

[113] Davison, E., "A method for simplifying linear dynamic systems," *IEEE Transactions on Automatic Control*, Vol. 11, 1966, pp. 93–101. doi:10.1109/TAC.1966.1098264.

[114] Marschall, S. A., "An approximate method for reducing the order of a linear system," *Contr. Eng.*, Vol. 10, 1966, pp. 642–648.

[115] Kokotovic, P. V., Jr., R. E. O., and Sannuti, P., "Singular perturbations and order reduction in control theory–An overview," *Automatica*, Vol. 12, No. 2, 1976, pp. 123–132. doi:10.1016/0005-1098(76)90076-5.

[116] Liu, Y. and Anderson, B. D. O., "Singular perturbation approximation of balanced systems," *Proceedings of the 28th IEEE Conference on Decision and Control*, Vol. 2, dec 1989, pp. 1355–1360. doi:10.1109/CDC.1989.70360.

[117] Benner, P., Quintana-Orti, E. S., and Quintana-Orti, G., "Singular perturbation approximation of large, dense linear systems," *Proceedings of the 2000 IEEE International Symposium on Computer-Aided Control System Design*, Anchorage, Alaska, USA, September 25-27 2000, pp. 255–260. doi:10.1109/CACSD.2000.900220.

[118] Stewart, G., "A Krylov–Schur Algorithm for Large Eigenproblems," *SIAM Journal on Matrix Analysis and Applications*, Vol. 23, No. 3, 2002, pp. 601–614. doi:10.1137/S0895479800371529.

[119] Stewart, G., "Addendum to "A Krylov–Schur Algorithm for Large Eigenproblems"," *SIAM Journal on Matrix Analysis and Applications*, Vol. 24, No. 2, 2002, pp. 599–601. doi:10.1137/S0895479802403150.

[120] Rommes, J. and Martins, N., "Efficient Computation of Multivariable Transfer Function Dominant Poles Using Subspace Acceleration," *IEEE Transactions on Power Systems*, Vol. 21, No. 4, nov. 2006, pp. 1471–1483. doi:10.1109/TPWRS.2006.881154.

[121] Kosambi, D. D., "Statistics in function space," *Journal of the Indian Mathematical Society*, Vol. 7, 1943, pp. 76–88.

[122] Karhunen, K., "Zur Spektraltheorie Stochastischer Prozesse," *Annales Academiæ Scientiarum Fennicæ*, 1946.

[123] Loève, M., "Fonctions aléatoires de seconde ordre," *Revue Scientifique*, Vol. 84, 1946, pp. 195–206.

[124] Loève, M., *Probability Theory I, II*, Vol. 45 of *Graduate Texts in Mathematics*, Springer-Verlag, 4th ed., 1977, Originally published as a monograph.

[125] Pearson, K., "LIII. On lines and planes of closest fit to systems of points in space," *Philosophical Magazine Series 6*, Vol. 2, 1901, pp. 559–572. doi:10.1080/14786440109462720.

[126] Hotelling, H., "Analysis of a complex of statistical variables into principal components," *Journal of Educational Psychology*, Vol. 24, 1933, pp. 417–441. doi:10.1037/h0071325.

[127] Jolliffe, I. T., *Principal Component Analysis*, Springer Series in Statistics, Springer, NY, 2nd ed., 2002.

[128] Willcox, K. and Peraire, J., "Balanced Model Reduction via the Proper Orthogonal Decomposition," *AIAA Journal*, Vol. 40, 2002, pp. 2323–2330. doi:10.2514/2.1570.

[129] Rowley, C., "Model Reduction for fluids, Using Balanced Proper Orthogonal Decomposition," *International Journal of Bifurcation and Chaos*, Vol. 15, 2005, pp. 997–1013. doi:10.1142/S0218127405012429.

[130] Hwang, H. and Lan, C. E., "Direct solution of unsteady transonic flow equations in frequency domain," *27th Aerospace Sciences Meeting*, No. AIAA Paper 89-0641, AIAA, Reno, Nevada, January 9-12 1989.

[131] Greco, P., Lan, C. E., and Lim, T., "Frequency domain unsteady transonic aerodynamics for flutter and limit cycle oscillation prediction," *AIAA, 35th Aerospace Sciences Meeting & Exhibit*, No. AIAA Paper 97-0835, AIAA, Reno, NV, Jan. 6-9 1997. doi:10.2514/6.1997-835.

[132] Hall, K. C., Thomas, J. P., and Clark, W. S., "Computation of Unsteady Nonlinear Flows in Cascades Using a Harmonic Balance Technique," *AIAA Journal*, Vol. 40, No. 5, 2002, pp. 879–886. doi:10.2514/2.1754.

[133] Hyvärinen, A., Karhunen, J., and Oja, E., *Independent Component Analysis*, John Wiley & Sons, Inc. doi:10.1002/0471221317.

[134] Julier, S. J. and Uhlmann, J. K., "Unscented filtering and nonlinear estimation," *Proceedings of the IEEE*, Vol. 92, No. 3, 2004, pp. 401–422. doi:10.1109/JPROC.2003.823141.

[135] Jensen, F. V. and Nielsen, T. D., *Bayesian Networks and Decision Graphs*, Information Science and Statistics, Springer, July 2007.

[136] Schoukens, J., Pintelon, R., and Renneboog, J., "A maximum likelihood estimator for linear and nonlinear systems-a practical application of estimation techniques in measurement problems," *Instrumentation and Measurement, IEEE Transactions on*, Vol. 37, No. 1, 1988, pp. 10–17. doi:10.1109/19.2655.

[137] Draper, N. R. and Smith, H., *Applied Regression Analysis*, Wiley, 3rd ed., May 1998.

[138] Åström, K.-J. and Bohlin, T., "Numerical Identification of Linear Dynamic Systems from Normal Operating Records," *IFAC Symposium on Self-Adaptive Systems*, Teddington, England, 1965.

[139] Junge, T. F. and Unbehauen, H., "Online identification of nonlinear time-variant systems using structurally adaptive radial basis function networks," *Proceedings of the American Control Conference*, Vol. 2, jun 1997, pp. 1037–1041. doi:10.1109/ACC.1997.609685.

[140] Kortmann, P. and Unbehauen, H., "Structure identification of functional-type fuzzy models with application to modelling nonlinear dynamic plants," *Computational Intelligence Theory and Applications*, edited by B. Reusch, Vol. 1226 of *Lecture Notes in Computer Science*, Springer Berlin Heidelberg, 1997, pp. 35–45. doi:10.1007/3-540-62868-1_95.

[141] Billings, S. A., "Identification of nonlinear systems–a survey," *Control Theory and Applications, IEE Proceedings D*, Vol. 127, No. 6, November 1980, pp. 272–285. doi:10.1049/ip-d:19800047.

[142] Wiener, N., *Nonlinear problems in random theory*, MIT Press, Cambridge, MA, 1958.

[143] Chen, P. C., Sarhaddi, D., and Liu, D. D., "Transonic-Aerodynamic-Influence-Coefficient Approach for Aeroelastic and MDO Applications," *Journal of Aircraft*, Vol. 37, 2000.

[144] Chen, P. C., Sarhaddi, D., Liu, D. D., and Karpel, M., "Unified Aerodynamic-Influence-Coefficient Approach for Aeroservoelastic and Multidisciplinary Optimization Applications," *Journal of Aircraft*, Vol. 37, 2000, pp. 260–265. doi:10.2514/2.2589.

[145] Isogai, K., "On the Transonic-Dip Mechanism of Flutter of a Sweptback Wing," *AIAA Journal*, Vol. 17, No. 7, 1979, pp. 793–795. doi:10.2514/3.61226.

[146] Dowell, E. H., Clark, R., Cox, D., Jr., H. C. C., Edwards, J. W., Hall, K. C., Peters, D. A., Scanlan, R., Simiu, E., Sisto, F., and Strganac, T. W., *A Modern Course in Aeroelasticity*, Vol. 116 of *Solid Mechanics and Its Applications*, Springer, September 2004.

[147] Romanelli, G. and Serioli, E., "AeroFoam," 2008, [retrieved May 2012], URL `http://www.aero.polimi.it/freecase/`.

[148] Pasinetti, G. and Mantegazza, P., "Single Finite States Modeling of Aerodynamic Forces Related to Structural Motions and Gusts," *AIAA Journal*, Vol. 37, No. 5, 1999, pp. 604–612. doi:10.2514/2.760.

[149] Mantegazza, P., "Identification of Generalized Unsteady Aerodynamic Forces from Harmonic Aerodynamic Loadings," *L'Aerotecnica - Missili e Spazio*, Vol. 60, No. 3, 1981, pp. 154–160.

[150] Mantegazza, P. and Cardani, C., "An Iterative Technique to Compute Flutter Speed through the Simultaneous Solution of Each Aeroelastic Mode and Frequency at Increasing Speed," *L'Aerotecnica - Missili e Spazio*, Vol. 54, No. 5-6, 1975, pp. 286–291.

[151] Cardani, C. and Mantegazza, P., "Continuation and Direct Solution of the Flutter Equation," *Computers and Structures*, Vol. 8, No. 2, 1978, pp. 185–192. doi:10.1016/0045-7949(78)90021-4.

[152] Edwards, J. W. and Wieseman, C. D., "Flutter and Divergence Analysis using the Generalized Aeroelastic Analysis Method," *Journal of Aircraft*, Vol. 45, No. 3, 2008, pp. 906–915. doi:10.2514/1.30078.

[153] Ghiringhelli, G. L., Lanz, M., Mantegazza, P., and Ricci, S., "Active Flutter Suppression Techniques in Aircraft Wings," *Integrated Technology Methods and Applications in Aerospace Systems Design*, Vol. 52 of *Control and Dynamic Systems Series*, Academic Press, 1992, pp. 57–115.

[154] Gage, S., "Creating a Unified Graphical Wind Turbulence Model from Multiple Specifications," *AIAA Modeling and Simulation Technologies Conference and Exhibit*, No. AIAA-2003-5529, Austin, Texas, USA, August 2003.

[155] Justus, C. G., Campbell, C. W., Doubleday, M. K., and Johnson, D. L., "New Atmospheric Turbulence Model for Shuttle Applications," Tech. Rep. NASA TM-4168, NASA, 1990.

[156] Bianchin, M., Quaranta, G., and Mantegazza, P., "State Space Reduced Order Models for the Static Aeroelasticity and Flight Mechanics of Flexible Aircraft," *Proceedings of the 17th Congresso Nazionale AIDAA*, Associazione Italiana di Aeronautica e Astronautica, Rome, September 2003.

[157] Meijer, J. J. and Zwaan, R. J., "Calculation of Frequency Response Functions for Flexible Aircraft," Tech. Rep. TR 75147 U, Nationaal Lucht- En Ruimtevaartlaboratorium (NLR), 1975.

[158] Gupta, K. K., Brenner, M. J., and Voelker, L. S., "Development of an Integrated Aeroservoelastic Analysis Program and Correlation with Test Data," Tech. Rep. NASA TP 3120, NASA, 1991.

[159] Lanz, M. and Mantegazza, P., "Numerical Methods for Predicting the Aeroelastic Stability and Response of Flexible Airplanes," *L'Aerotecnica - Missili e Spazio*, Vol. 63, No. 2, 1984, pp. 105–118.

[160] Lanz, M. and Mantegazza, P., "Modern Methods for the Analysis of the Dynamic Response of Aeroelastic Systems," *L'Aerotecnica - Missili e Spazio*, Vol. 64, No. 3, 1985, pp. 170–176.

[161] Mantegazza, P., "Interpolation and Extrapolation of Transfer Functions," *L'Aerotecnica - Missili e Spazio*, Vol. 59, No. 2, 1980, pp. 69–75.

[162] Ghiringhelli, G. L. and Mantegazza, P., "Interpolation, Extrapolation and Modelling of Unsteady Linearized Aerodynamic Forces," *Proceedings of the International Forum on Aeroelasticity and Structural Dynamics*, Strasbourg, France, 1993, pp. 207–221.

[163] Morino, L., Mastroddi, F., De Troia, R., Ghiringhelli, G. L., and Mantegazza, P., "Matrix Fraction Approach for Finite-State Aerodynamic Modeling," *AIAA Journal*, Vol. 33, No. 4, 1995, pp. 703–711. doi:10.2514/3.12381.

[164] Nissim, E., "Flutter Analisys using Unsteady Aerodynamics in Non-Padé Form," *Journal of Aircraft*, Vol. 34, No. 1, 1997, pp. 133–136. doi:10.2514/2.2147.

[165] Hoblit, F. M., *Gust Loads on Aircraft: Concepts and Applications*, AIAA Education Series, Washington, D.C., 1988.

[166] MSC Nastran (2010) User Documentation, *MSC.Nastran Version 68, Aeroelastic Analysis User's Guide*, MSC.Software, Santa Ana, CA, October 2004.

[167] ZONA Technology, Inc., Scottsdale, AZ, *ZAERO Version 8.5 Theoretical Manual*, June 2011.

[168] Karpel, M., Moulin, B., and Chen, P. C., "Dynamic Response of Aeroservoelastic Systems to Gust Excitation," *Journal of Aircraft*, Vol. 42, No. 5, 2005, pp. 1264–1272. doi:10.2514/1.6678.

[169] Ripepi, M. and Mantegazza, P., "Improved Matrix Fraction Approximation of Aerodynamic Transfer Matrices," *AIAA Journal*, Vol. 51, No. 5, May 2013, pp. 1156–1173. doi:10.2514/1.J052009.

[170] Gardiner, J. D., Laub, A. J., Amato, J. J., and Moler, C. B., "Solution of the Sylvester Matrix Equation $\mathrm{AXB^T + CXD^T = E}$," *ACM Trans. Math. Softw.*, Vol. 18, No. 2, jun 1992, pp. 223–231. doi:10.1145/146847.146929.

[171] Parameswaran, V. and Baeder, J. D., "Indicial Aerodynamics in Compressible Flow-Direct Computational Fluid Dynamic Calculations," *Journal of Aircraft*, Vol. 34, No. 1, 1997, pp. 131–133. doi:10.2514/2.2146.

[172] Wales, C., Gaitonde, A., and Jones, D., "Reduced order modelling for aeroelastic aerofoil response to a gust," *Proceedings of the 51st AIAA Aerospace Sciences Meeting including the New Horizons Forum and Aerospace Exposition*, AIAA, January 2013. doi:10.2514/6.2013-790.

[173] Tang, D., Kholodar, D., Juang, J.-N., and Dowell, E. H., "System Identification and Proper Orthogonal Decomposition Method Applied to Unsteady Aerodynamics," *AIAA Journal*, Vol. 39, No. 8, 2001, pp. 1569–1576. doi:10.2514/2.1482.

[174] Ronch, A. D., Tantaroudas, N. D., Timme, S., and Badcock, K. J., "Model reduction for linear and nonlinear gust loads analysis," *Proceedings of the 54th AIAA/ASME/ASCE/AHS/ASC Structures, Structural Dynamics, and Materials Conference*, AIAA Paper 2013-1492, April 2013. doi:10.2514/6.2013-1492.

[175] Raveh, D. E., "CFD-Based Models of Aerodynamic Gust Response," *Journal of Aircraft*, Vol. 44, No. 3, 2007.

[176] Fung, Y. C., *An Introduction to the Theory of Aeroelasticity*, Dover Publications, Inc., 1993.

[177] Raveh, D. E., "Gust-Response Analysis of Free Elastic Aircraft in the Transonic Flight Regime," *Journal of Aircraft*, Vol. 48, No. 4, 2011, pp. 1204–1211. doi:10.2514/1.C031224.

[178] Sitaraman, J. and Baeder, J. D., "Computational-Fluid-Dynamics-Based Enhanced Indicial Aerodynamic Models," *Journal of Aircraft*, Vol. 41, No. 4, 2004, pp. 798–810.

[179] Bisplinghoff, R. L., Ashley, H., and Halfman, R. L., *Aeroelasticity*, Dover, 1996, pp. 251–293, 380–400.

[180] Bartels, R. E., "Developing an Accurate CFD Based Gust Model for the Truss Braced Wing Aircraft," *Proceedings of the 31st AIAA Applied Aerodynamics Conference*, No. AIAA 2013-3044, San Diego, CA, 24-27 June 2013. doi:10.2514/6.2013-3044.

[181] Hall, K. C., "Eigenanalysis of unsteady flows about airfoils, cascades, and wings," *AIAA Journal*, Vol. 32, 1994, pp. 2426–2432. doi:10.2514/3.12309.

[182] Hall, K. C., Florea, R., and Lanzkron, P. J., "A reduced order model of unsteady flows in turbomachinery," *Journal of Turbomachinery-transactions of The Asme*, Vol. 117, 1995. doi:10.1115/1.2835672.

[183] Florea, R. and Hall, K. C., "Eigenmode Analysis of Unsteady Flows about Airfoils," *Journal of Computational Physics*, Vol. 147, 1998, pp. 568–593. doi:10.1006/jcph.1998.6102.

[184] Romanowski, M. C. and Dowell, E. H., "Reduced Order Euler Equations for Unsteady Aerodynamic Flows: Numerical Techniques," *AIAA Journal*, , No. AIAA Paper 96-0528, Jan. 1996.

[185] Dowell, E. H., Hall, K. C., and Romanowski, M. C., "Eigenmode Analysis in Unsteady Aerodynamics: Reduced Order Models," *Applied Mechanics Reviews*, Vol. 50, 1997. doi:10.1115/1.3101718.

[186] Lumley, J. L., "The Structure of Inhomogeneous Turbulent Flows," *Atmospheric turbulence and radio propagation*, edited by A. M. Yaglom and V. I. Tatarski, Nauka, Moscow, 1967, pp. 166–178.

[187] Berkooz, G., Holmes, P., and Lumley, J. L., "The proper orthogonal decomposition in the analysis of turbulent flows," *Annual Review of Fluid Mechanics*, Vol. 25, 1993, pp. 539–575. doi:10.1146/annurev.fl.25.010193.002543.

[188] Poje, A. C. and Lumley, J. L., "A model for large-scale structures in turbulent shear flows," *Journal of Fluid Mechanics*, Vol. 285, 1995. doi:10.1017/S0022112095000577.

[189] Moin, P. and Moser, R. D., "Characteristic-eddy decomposition of turbulence in a channel," *Journal of Fluid Mechanics*, Vol. 200, 1989, pp. 471–509. doi:10.1017/S0022112089000741.

[190] Rempher, D. and Fasel, H. F., "Evolution of three-dimensional coherent structures in a flat-plate boundary layer," *Journal of Fluid Mechanics*, Vol. 260, 1994, pp. 351–375. doi:10.1017/S0022112094003551.

[191] Rempher, D. and Fasel, H. F., "Dynamics of three-dimensional coherent structures in a flat-plate boundary layer," *Journal of Fluid Mechanics*, Vol. 275, 1994, pp. 257–283. doi:10.1017/S0022112094002351.

[192] Deane, A. E., Kevrekidis, I. G., Karniadakis, G. E., and Orszag, S. A., "Low-dimensional models for complex geometry flows: Application to grooved channels and circular cylinders," *Physics of Fluids*, Vol. 3, 1991, pp. 2337–2354. doi:10.1063/1.857881.

[193] Tang, K. Y., Graham, W. R., and Peraire, J., "Active Flow Control using a Reduced Order Model and Optimum Control," No. AIAA Paper 96-1946, 1996.

[194] Holmes, P., Lumley, J. L., Berkooz, G., and Rowley, C. W., *Turbulence, Coherent Structures, Dynamical Systems and Symmetry, 2nd edn.*, Vol. 53, 2012. doi:10.1080/00107514.2012.699471.

[195] Romanowski, M. C., "Reduced Order Unsteady Aerodynamic and Aeroelastic Models Using Karhunen-Loève Eigenmodes," No. AIAA Paper 96-3981, 1996.

[196] Kim, T., "Frequency-Domain Karhunen-Loève Method and Its Application to Linear Dynamic Systems," *AIAA Journal*, Vol. 36, 1998, pp. 2117–2123. doi:10.2514/2.315.

[197] Hall, K. C., Thomas, J. P., and Dowell, E. H., "Reduced order-modelling of unsteady small-disturbance flows using a frequency-domain proper orthogonal decomposition technique," *37th Aerospace Sciences Meeting and Exhibit*, No. AIAA 99-0655, Reno, NV, January 11-14 1999.

[198] Epureanu, B. I., Dowell, E. H., and Hall, K. C., "Reduced-Order Models of Unsteady Transonic Viscous Flows in Turbomachinery," *Journal of Fluids and Structures*, Vol. 14, 2000, pp. 1215–1234. doi:10.1006/jfls.2000.0320.

[199] Juang, J.-N. and Pappa, R. S., "An eigensystem realization algorithm for modal parameter identification and model reduction," *Journal of Guidance Control and Dynamics*, Vol. 8, 1985, pp. 620–627. doi:10.2514/3.20031.

[200] Milne, R. D., "Asymptotic Behavior of Linear Stationary Integro-Differential Equations," Tech. Rep. 3548, Aeronautical Research Council Reports and Memoranda, London, July 1968.

[201] Sevart, F. D., "Development of Active Flutter Suppression Wind Tunnel Testing Technology," Tech. Rep. AFFDL-TR-74-126, U.S. Air Force, Jan. 1975.

[202] Abel, I., "An Analytical Technique for Predicting the Characteristics of a Flexible Wing Equipped with an Active Flutter-Suppression System and Comparison with Wind-Tunnel Data," Tech. Rep. NASA TP-1367, NASA, 1979.

[203] Roger, K. L., "Airplane Math Modeling and Active Aeroelastic Control Design," Tech. Rep. AGARD CP-228, AGARD, August 1977.

[204] Lyons, M. G., Vepa, R., Mcintosh, S. C., J., and Debra, D. B., "Control Law Synthesis and Sensor Design for Active Flutter Suppression," *Guidance and Control Conference*, No. AIAA Paper 73-832, Key Biscayne, FL, August 1973.

[205] Vepa, R., "On the Use of Padé Approximants to Represent Unsteady Aerodynamic Loads for Arbitrarily Small Motion of Wings," *14th Aerospace Sciences Meeting*, No. AIAA Paper 76-17, Washington, D.C., January 1976.

[206] Vepa, R., "Finite State Modeling of Aeroelastic Systems," Tech. Rep. NASA CR 2779, NASA, 1977.

[207] Edwards, J. W., "Unsteady Aerodynamic Modeling and Active Aeroelastic Control," Tech. Rep. NASA-CR-148019, NASA, Feb. 1977.

[208] Dunn, H. J., "An Analytical Technique for Approximating Unsteady Aerodynamics in the Time Domain," Tech. Rep. NASA TP-1738, NASA, 1980.

[209] Dunn, H. J., "An Assessment of Unsteady Aerodynamic Approximations for Time Domain Analysis," *Proceedings of the Aeroservoelasticity Specialist Meeting*, Vol. 1, U.S. Air Force, October 1984, pp. 98–115.

[210] Karpel, M., "Design for Active and Passive Flutter Suppression and Gust Alleviation," Tech. Rep. NASA CR-3482, NASA, 1981.

[211] Tiffany, S. H. and Karpel, M., "Aeroservoelastic Modeling and Applications using Minimum-State Approximations of the Unsteady Aerodynamics," Tech. Rep. NASA TM-101574, NASA Langley Research Center Hampton, VA 23665-5225, April 1989.

[212] Karpel, M., "Time Domain Aeroservoelastic Modeling using Weighted Unsteady Aerodynamic Forces," *Journal of Guidance, Control, and Dynamics*, Vol. 13, No. 1, 1990, pp. 30–37. doi:10.2514/3.20514.

[213] Burkhart, T. M., "Subsonic Transient Lifting Surface Aerodynamics," *Journal of Aircraft*, Vol. 14, No. 1, 1977, pp. 44–50. doi:10.2514/3.58748.

[214] Richardson, J. R., "A More Realistic Method for Routine Flutter Calculations," *AIAA Symposium of Structural Dynamics and Aeroelasticity*, AIAA, Boston, Massachusetts, 1965, pp. 10–17.

[215] Lawrence, A. J. and Jackson, P., "Comparison of Different Methods of Assessing the Free Oscillatory Characteristics of Aeroelastic Systems," No. CP-1084, Aeronautical Research Council, H.M. Stationery Off. in London, 1970.

[216] Thomas E. Noll and Boyd Perry III and Michael G. Gilbert, "Recent Activities in Aeroservoelasticity at the NASA Langley Research Center," Tech. Rep. NASA-TM-101582, NASA, May 1989.

[217] Safonov, M. G., Chiang, R. Y., and Limebeer, D. J. N., "Optimal Hankel Model Reduction for Nonminimal Systems," *Automatic Control, IEEE Transactions on*, Vol. 35, No. 4, apr 1990, pp. 496 –502. doi:10.1109/9.52314.

[218] Safonov, M. G. and Chiang, R. Y., "A Schur Method for Balanced-Truncation Model Reduction," *IEEE Transactions on Automatic Control*, Vol. 34, No. 7, July 1989, pp. 729–733. doi:10.1109/9.29399.

[219] de Callafon, R. A., de Roover, D., and Van den Hof, P. M. J., "Multivariable Least Squares Frequency Domain Identification using Polynomial Matrix Fraction Descriptions," *35th IEEE Conference on Decision and Control*, Vol. 2, Kobe, Japan, December 1996, pp. 2030–2035. doi:10.1109/CDC.1996.572883.

[220] Brewer, J., "Kronecker Products and Matrix Calculus in System Theory," *IEEE Transactions on Circuits and Systems*, Vol. 25, No. 9, 1978, pp. 772–781. doi:10.1109/TCS.1978.1084534.

[221] Loan, C. V. and Pitsianis, N., "Approximation with Kronecker Products," *Linear Algebra for Large Scale and Real Time Applications*, Kluwer Publications, 1993, pp. 293–314.

[222] Buis, P. E. and Dyksen, W. R., "Efficient Vector and Parallel Manipulation of Tensor Products," *ACM Trans. Math. Softw.*, Vol. 22, No. 1, March 1996, pp. 18–23. doi:10.1145/225545.225548.

[223] Fausett, D. W. and Fulton, C. T., "Large Least Squares Problems Involving Kronecker Products," *SIAM J. Matrix Anal. Appl.*, Vol. 15, No. 1, January 1994, pp. 219–227. doi:10.1137/S0895479891222106.

[224] Fausett, D. W., Fulton, C. T., and Hashish, H., "Improved Parallel QR Method for Large Least Squares Problems Involving Kronecker Products," *Journal of Computational and Applied Mathematics*, Vol. 78, No. 1, 1997, pp. 63–78. doi:10.1016/S0377-0427(96)00109-4.

[225] Moré, J., "The Levenberg-Marquardt Algorithm: Implementation and Theory," *Numerical Analysis*, edited by G. Watson, Vol. 630 of *Lecture Notes in Mathematics*, Springer Berlin/Heidelberg, 1978, pp. 105–116. doi:10.1007/BFb0067700.

[226] Wright, S. J. and Holt, J. N., "An Inexact Levenberg-Marquardt Method for Large Sparse Nonlinear Least Squares," *The ANZIAM Journal*, Vol. 26, No. 04, 1985, pp. 387–403. doi:10.1017/S0334270000004604.

[227] Feldmann, P. and Freund, R. W., "Efficient Linear Circuit Analysis by Padé Approximation via the Lanczos Process," *IEEE Transactions on Computer-aided Design of Integrated Circuits and Systems*, Vol. 14, No. 5, 1995, pp. 639–649. doi:10.1109/43.384428.

[228] Karpel, M., "Design for Active Flutter Suppression and Gust Alleviation using State-Space Aeroelastic Modeling," *Journal of Aircraft*, Vol. 19, No. 3, 1982, pp. 221–227. doi:10.2514/3.57379.

[229] Tiffany, S. H. and Adams, W. M., "Non-Linear Programming Extensions to Rational Function Approximation Methods for Unsteady Aerodynamic Forces," Tech. Rep. NASA TP-2776, NASA, July 1988.

[230] Andrighettoni, M. and Mantegazza, P., "Multi-Input/Multi-Output Adaptive Active Flutter Suppression for a Wing Model," *Journal of Aircraft*, Vol. 35, No. 3, 1998, pp. 462–469. doi:10.2514/2.2319.

[231] Heinrich, R., "Numerical Simulation of Wake-Vortex Encounters Using the Chimera-Technique," *New Results in Numerical and Experimental Fluid Mechanics III*, edited by S. Wagner, U. Rist, H.-J. Heinemann, and R. Hilbig, Vol. 77 of *Notes on Numerical Fluid Mechanics (NNFM)*, Springer Berlin Heidelberg, 2002, pp. 74–81. doi:10.1007/978-3-540-45466-3_10.

[232] Benek, J., Buning, P., and Steger, J., "A 3-D chimera grid embedding technique," *Prooceedings of the 7th Computational Physics Conference*, Cincinnati, OH, USA, 15-17 July 1985. doi:10.2514/6.1985-1523.

[233] Chesshire, G. and Henshaw, W. D., "Composite overlapping meshes for the solution of partial differential equations," *Journal of Computational Physics*, Vol. 90, No. 1, 1990, pp. 1–64. doi:10.1016/0021-9991(90)90196-8.

[234] Heinrich, R. and Kalitzin, N., "Numerical Simulation of Three-Dimensional Flows Using the Chimera-Technique," *New Results in Numerical and Experimental Fluid Mechanics II*, edited by W. Nitsche, H.-J. Heinemann, and R. Hilbig, Vol. 72 of *Notes on Numerical Fluid Mechanics (NNFM)*, Vieweg+Teubner Verlag, 1999, pp. 226–233. doi:10.1007/978-3-663-10901-3_30.

[235] Heinrich, R. and Reimer, L., "Comparison Of Different Approaches For Gust Modeling In The CFD Code TAU," *Proceedings of the International Forum on Aeroelasticity and Structural Dynamics*, Bristol, UK, 24-27 June 2013.

[236] Struijs, R., Jonville, G., Darracq, D., and Heinrich, R., "Inviscid Computation of Effect of Wake Vortices on a Scale-Model Airplane," *Journal of Aircraft*, Vol. 40, No. 1, 2003, pp. 100–109.

[237] Crimaldi, J. P., Britt, R. T., and Rodden, W. P., "Response of B-2 Aircraft to Nonuniform Spanwise Turbulence," *Journal of Aircraft*, Vol. 30, No. 5, 1993, pp. 652–659. doi:10.2514/3.46394.

[238] Drischler, J. A., "Calculation and Compilation of the Unsteady-Lift Functions for a Rigid Wing Subjected to Sinusoidal Gusts and to Sinusoidal Sinking Oscillations," Tech. Rep. NACA TN 3748, NACA, 1956.

[239] Prananta, B. B., Veul, R. P. G., Houwink, R., Hounjet, M. H. L., and van Muijden, J., "A Generic Flexible Aircraft Loads Database System for Fatigue Analysis," *Proceedings of the International Forum on Aeroelasticity and Structural Dynamics 2007*, Stockholm, June 2007. doi:10921/413.

[240] Vacher, P. and Bucharles, A., "Realistic Simulation of Flutter Flight Tests," *Proceedings of the International Conference on Noise and Vibration Engineering, ISMA 2008*, Leuven, Belgium, September 2008.

[241] Golub, G. H. and Loan, C. F. V., *Matrix Computations*, Johns Hopkins University Press, MD, 1996, pp. 308–390.

[242] Livne, E., "Alternative Approximations for Integrated Control/Structure Aeroservoelastic Synthesis," *AIAA Journal*, Vol. 31, No. 6, 1993, pp. 1100–1108. doi:10.2514/3.49052.

[243] Lancaster, P., *Lambda-matrices and Vibrating Systems*, Dover, New York, 2002, pp. 23–41.

[244] Datta, B. N., *Numerical Methods for Linear Control Systems Design and Analysis*, Elsevier Academic Press, New York, 2003, 79–104.

[245] Percival, D. B. and Walden, A. T., *Wavelet Methods for Time Series Analysis*, Cambridge University Press, New York, 2000, pp. 59–158, 457–500.

[246] Daubechies, I., "Orthonormal Bases of Compactly Supported Wavelets," *Communications on Pure and Applied Mathematics*, Vol. 41, No. 7, 1988, pp. 909–996. doi:10.1002/cpa.3160410705.

[247] Rodden, W. P. and Bellinger, E. D., "Unrestrained Aeroelastic Divergence in a Dynamic Stability Analysis," *Journal of Aircraft*, Vol. 19, No. 9, 1982, pp. 796–797. doi:10.2514/3.61559.

[248] Van Zyl, L. H. and Maserumule, M. S., "Unrestrained Aeroelastic Divergence and the p-k Flutter Equation," *Journal of Aircraft*, Vol. 38, No. 3, 2001, pp. 588–590. doi:10.2514/2.2808.

[249] Fung, Y. C., *An Introduction to the Theory of Aeroelasticity*, Dover, New York, 2008, pp. 407–412.

[250] Yates, E. C., "AGARD Standard Aeroelastic Configurations for Dynamic Response. I-Wing 445.6," Tech. Rep. AGARD R 765, AGARD, 1985.

[251] Cavagna, L., Ricci, S., and Travaglini, L., "NeoCASS: An integrated tool for structural sizing, aeroelastic analysis and MDO at conceptual design level," *Progress in Aerospace Sciences*, Vol. 47, No. 8, 2011, pp. 621–635. doi:10.1016/j.paerosci.2011.08.006.

[252] Vink, W. J. and Jonge, J. B. D., "A MATLAB Program to Study Gust Loading on a Simple Aircraft Model," Tech. Rep. NLR TP 97379, Nationaal Lucht- En Ruimtevaartlaboratorium (NLR), 1998.

[253] Schwamborn, D., Gerhold, T., and Heinrich, R., "The DLR TAU-Code: Recent Applications in Research and Industry," *Proceedings of the "European Conference on Computational Fluid Dynamics" ECCOMAS CDF 2006*, The Netherland, 2006.

[254] Mialon, B., Khrabrov, A., Khelil, S. B., Huebner, A., Ronch, A. D., Badcock, K., Cavagna, L., Eliasson, P., Zhang, M., Ricci, S., Jouhaud, J.-C., Rogé, G., Hitzel, S., and Lahuta, M., "Validation of numerical prediction of dynamic derivatives: The DLR-F12 and the Transcruiser test cases," *Progress in Aerospace Sciences*, Vol. 47, No. 8, 2011, pp. 674–694. doi:10.1016/j.paerosci.2011.08.010, Special Issue - Modeling and Simulating Aircraft Stability and Control Special Issue - Modeling and Simulating Aircraft Stability and Control.

[255] Ghoreyshi, M., Badcock, K. J., Ronch, A. D., Marques, S., Swift, A., and Ames, N., "Framework for Establishing Limits of Tabular Aerodynamic Models for Flight Dynamics Analysis," *Journal of Aircraft*, Vol. 48, No. 1, 2011, pp. 42–55.

[256] Huang, X. Z., Tech. rep.

[257] Pike, E. C., "Manual on Aeroelasticity," Tech. Rep. AGARD-R-578-71, AGARD, 1971.

[258] Chu, B.-T. and Kovásznay, L. S. G., "Non-linear interactions in a viscous heat-conducting compressible gas," *Journal of Fluid Mechanics*, Vol. 3, 1 1958, pp. 494–514. doi:10.1017/S0022112058000148.

[259] Heeg, J. and Dowell, E., "Aerodynamic and aeroelastic insights using eigenanalysis," No. AIAA Paper 99-1472, 1999. doi:10.2514/6.1999-1472.

[260] Cunningham, H. J. and Desmarais, R. N., "Generalization of the Subsonic Kernel Function in the S-Plane, with Applications to Flutter Analysis," Tech. Rep. NASA TP-2292, NASA, March 1984.

[261] Desmarais, R. N., "A continued fraction representation for Theodorsen's circulation function," Tech. Rep. NASA-TM-81838, NASA Langley Research Center, Sep 1 1980.

[262] Gugercin, S. and Antoulas, A. C., "Model reduction of large-scale systems by least squares," *Linear Algebra and Its Applications*, Vol. 415, 2006, pp. 290–321. doi:10.1016/j.laa.2004.12.022.

[263] Benner, P., Mehrmann, V., and Sorensen, D. C., *Dimension Reduction of Large-Scale Systems*, Vol. 45 of *Lecture Notes in Computational Science and Engineering*, Springer, 2005.

[264] Benner, P., "Numerical linear algebra for model reduction in control and simulation," *GAMM Mitteilungen*, Vol. 29, No. 2, 2006, pp. 275–296.

[265] Overschee, P. V. and Moor, B. D., "N4SID: Subspace algorithms for the identification of combined deterministic-stochastic systems," *Automatica*, Vol. 30, No. 1, 1994, pp. 75–93. doi:10.1016/0005-1098(94)90230-5, Special issue on statistical signal processing and control.

[266] Silva, W. A., "Reduced-Order Models Based on Linear and Nonlinear Aerodynamic Impulse Responses," *40th AIAA/ASE/ASCE/AHS/ASC Structures, Structural Dynamics, and Materials Conference*, No. AIAA Paper No. 99-1262, St. Louis, Missouri, April 12-15 1999.

[267] Raveh, D. E., Levy, Y., , and Karpel, M., "Efficient Aeroelastic Analysis Using Computational Unsteady Aerodynamics," Vol. 38, No. 3, 2001, pp. 547–556.

[268] Silva, W., "Identification of Nonlinear Aeroelastic Systems Based on the Volterra Theory: Progress and Opportunities," *Nonlinear Dynamics*, Vol. 39, 2005, pp. 25–62. doi:10.1007/s11071-005-1907-z.

[269] Lucia, D. and Beran, P., "Reduced-Order Model Development Using Proper Orthogonal Decomposition and Volterra Theory," *AIAA Journal*, Vol. 42, 2004, pp. 1181–1190. doi:10.2514/1.10419.

[270] Marzocca, P., Lazzaro, R., and Librescu, L., "Flutter/Aeroelastic Response of Panels via a Combined Galerkin-Volterra Series Approach," *45th AIAA/ASME/ASCE/AHS/ASC Structures, Structural Dynamics, and Materials Conference*, No. AIAA Paper 2004-1855, Palm Springs, California, 19-22 April 2004.

[271] Ballhaus, W. F. and Goorjian, P. M., "Computation of Unsteady Transonic Flows by the Indicial Method," *AIAA Journal*, Vol. 16, No. 2, 1978, pp. 117–124.

[272] Silva, W. A., "Identification of Linear and Nonlinear Aerodynamic Impulse Responses Using Digital Filter Techniques," Tech. rep., NASA Langley Research Center, Aeroelasticity Branch, August 1997.

[273] Marzocca, P., Librescu, L., Kim, D.-H., and Lee, L., "Supersonic Flutter and LCO of Airfoils via CFD/Analytical Combined Approach," *46th AIAA/ASME/ASCE/AHS/ASC Structures, Structural Dynamics, and Materials Conference*, No. AIAA Paper 2005-2298, 18-21 April 2005.

[274] Baldelli, D. H., Brenner, M., and Lind, R., "Nonlinear Aeroelastic/Aeroservoelastic Modeling by Block-Oriented Identification," *Journal of Guidance Control and Dynamics*, Vol. 28, 2005, pp. 1056–1064. doi:10.2514/1.11792.

[275] Sahyoun, S. and Djouadi, S. M., "Nonlinear model reduction for fluid flows," *American Control Conference (ACC), 2011*, San Francisco, CA, USA, June 29 - July 1 2011, pp. 1765–1769.

[276] Thomas, J. P., Dowell, E. H., and Hall, K. C., "Using Automatic Differentiation to Create a Nonlinear Reduced-Order-Model Aerodynamic Solver," *AIAA Journal*, Vol. 48, 2010, pp. 19–24. doi:10.2514/1.36414.

[277] Ronch, A. D., Badcock, K., Wang, Y., Wynn, A., and Palacios, R., "Nonlinear Model Reduction for Flexible Aircraft Control Design," Minneapolis, Minnesota, 13-16 August 2012. doi:10.2514/6.2012-4404.

[278] Glaz, B., Liu, L., and Friedmann, P. P., "Reduced-Order Nonlinear Unsteady Aerodynamic Modeling Using a Surrogate-Based Recurrence Framework," *AIAA Journal*, Vol. 48, 2010, pp. 2418–2429. doi:10.2514/1.J050471.

[279] Marques, F. and Anderson, J., "Identification and Prediction of Unsteady Transonic Aerodynamic Loads by Multi-Layer Functionals," *Journal of Fluids and Structures*, Vol. 15, No. 1, 2001, pp. 83–106. doi:10.1006/jfls.2000.0321.

[280] Denegri, C. M. and Johnson, M. R., "Limit Cycle Oscillation Prediction Using Artificial Neural Networks," *Journal of Guidance Control and Dynamics*, Vol. 24, 2001, pp. 887–895. doi:10.2514/2.4824.

[281] Voitcu, O. and Wong, Y. S., "Neural Network Approach for Nonlinear Aeroelastic Analysis," *Journal of Guidance Control and Dynamics*, Vol. 26, 2003, pp. 99–105. doi:10.2514/2.5019.

[282] Roychowdhury, J., "Reduced-order modeling of time-varying systems," *IEEE Transactions on Circuits and Systems II: Analog and Digital Signal Processing*, Vol. 46, No. 10, 1999, pp. 1273–1288. doi:10.1109/82.799678.

[283] Phillips, J. R., "Projection-based approaches for model reduction of weakly nonlinear, time-varying systems," *IEEE Transactions on Computer-Aided Design of Integrated Circuits and Systems*, Vol. 22, No. 2, 2003, pp. 171–187. doi:10.1109/TCAD.2002.806605.

[284] Chen, Y., *Model Order Reduction for Nonlinear Systems*, Master's thesis, Massachusetts Institute of Technology, Cambridge, MA, September 1999.

[285] Bai, Z., "Krylov subspace techniques for reduced-order modeling of large-scale dynamical systems," *Applied Numerical Mathematics*, Vol. 43, No. 1-2, 2002, pp. 9–44. doi:10.1016/S0168-9274(02)00116-2.

[286] Rewieński, M., *A trajectory piecewise-linear approach to model order reduction of nonlinear dynamical systems*, Ph.D. thesis, Massachusetts Institute of Technology, June 2003.

[287] Rewieński, M. and White, J., "A trajectory piecewise-linear approach to model order reduction and fast simulation of nonlinear circuits and micromachined devices," *IEEE Transactions on Computer-Aided Design of Integrated Circuits and Systems*, Vol. 22, No. 2, 2003, pp. 155–170. doi:10.1109/TCAD.2002.806601.

[288] Phillips, J. R. and Silveira, L. M., "Poor man's TBR: a simple model reduction scheme," *IEEE Transactions on Computer-Aided Design of Integrated Circuits and Systems*, Vol. 24, No. 1, 2005, pp. 43–55. doi:10.1109/TCAD.2004.839472(410) 24.

[289] Mohaghegh, K., Striebel, M., ter Maten, E. J. W., and Pulch, R., "Nonlinear Model Order Reduction Based on Trajectory Piecewise Linear Approach: Comparing Different Linear Cores," *Scientific Computing in Electrical Engineering SCEE 2008*, edited by J. Roos and L. R. J. Costa, Mathematics in Industry, Springer Berlin Heidelberg, 2010, pp. 563–570. doi:10.1007/978-3-642-12294-1_69.

[290] Rewieński, M. and White, J., "Model order reduction for nonlinear dynamical systems based on trajectory piecewise-linear approximations," *Linear Algebra and its Applications*, Vol. 415, No. 2-3, 2006, pp. 426–454. doi:10.1016/j.laa.2003.11.034, Special Issue on Order Reduction of Large-Scale Systems.

[291] Astrid, P., Weiland, S., Willcox, K., and Backx, T., "Missing Point Estimation in Models Described by Proper Orthogonal Decomposition," *IEEE Transactions on Automatic Control*, Vol. 53, No. 10, 2008, pp. 2237–2251. doi:10.1109/TAC.2008.2006102.

[292] Bui-Thanh, T., Damodaran, M., and Willcox, K., "Proper Orthogonal Decomposition Extensions for Parametric Applications in Compressible Aerodynamics," *Proceedings of the 21st AIAA Applied Aerodynamics Conference*, AIAA, Orlando, Florida, 23-26 June 2003. doi:10.2514/6.2003-4213.

[293] Barrault, M., Maday, Y., Nguyen, N. C., and Patera, A. T., "An "empirical interpolation method": application to efficient reduced-basis discretization of partial differential equations," *Comptes Rendus Mathematique*, Vol. 339, No. 9, 2004, pp. 667–672. doi:10.1016/j.crma.2004.08.006.

[294] Chaturantabut, S. and Sorensen, D. C., "Nonlinear Model Reduction via Discrete Empirical Interpolation," *SIAM Journal on Scientific Computing*, Vol. 32, No. 5, 2010, pp. 2737–2764. doi:10.1137/090766498.

[295] Chaturantabut, S., *Nonlinear Model Reduction via Discrete Empirical Interpolation*, Ph.D. thesis, Department of Computational and Applied Mathematics, Rice University, Houston, Texas, May 2011.

[296] Tiso, P. and Rixen, D. J., "Discrete Empirical Interpolation Method for Finite Element Structural Dynamics," *Topics in Nonlinear Dynamics, Volume 1*, edited by G. Kerschen, D. Adams, and A. Carrella, Vol. 35 of *Conference Proceedings of the Society for Experimental Mechanics Series*, Springer New York, 2013, pp. 203–212. doi:10.1007/978-1-4614-6570-6_18.

[297] Everson, R. and Sirovich, L., "Karhunen–Loève procedure for gappy data," *J. Opt. Soc. Am. A*, Vol. 12, No. 8, Aug 1995, pp. 1657–1664. doi:10.1364/JOSAA.12.001657.

[298] Nguyen, N. C., Patera, A. T., and Peraire, J., "A "best points" interpolation method for efficient approximation of parametrized functions," *International Journal for Numerical Methods in Engineering*, Vol. 73, No. 4, 2008, pp. 521–543. doi:10.1002/nme.2086.

[299] Peherstorfer, B., Butnaru, D., Willcox, K., and Bungartz, H.-J., "Localized Discrete Empirical Interpolation Method," Tech. Rep. TR-13-1, MIT Aerospace Computational Design Laboratory, June 2013.

[300] Drohmann, M., Haasdonk, B., and Ohlberger, M., "Reduced Basis Approximation for Nonlinear Parametrized Evolution Equations based on Empirical Operator Interpolation," *SIAM Journal on Scientific Computing*, Vol. 34, No. 2, 2012, pp. A937–A969. doi:10.1137/10081157X.

[301] Carlberg, K., Bou-Mosleh, C., and Farhat, C., "Efficient non-linear model reduction via a least-squares Petrov-Galerkin projection and compressive tensor approximations," *International Journal for Numerical Methods in Engineering*, Vol. 86, No. 2, 2011, pp. 155–181. doi:10.1002/nme.3050.

[302] Carlberg, K., Farhat, C., Cortial, J., and Amsallem, D., "The GNAT method for nonlinear model reduction: Effective implementation and application to computational fluid dynamics and turbulent flows," *Journal of Computational Physics*, Vol. 242, No. 0, 2013, pp. 623–647. doi:10.1016/j.jcp.2013.02.028.

[303] An, S. S., Kim, T., and James, D. L., "Optimizing Cubature for Efficient Integration of Subspace Deformations," *ACM Trans. Graph.*, Vol. 27, No. 5, December 2008, pp. 165:1–165:10. doi:10.1145/1409060.1409118.

[304] Antil, H., Field, S. E., Herrmann, F., Nochetto, R. H., and Tiglio, M., "Two-Step Greedy Algorithm for Reduced Order Quadratures," *Journal of Scientific Computing*, Vol. 57, No. 3, 2013, pp. 604–637. doi:10.1007/s10915-013-9722-z.

[305] Mannarino, A., *Reduced order aeroelastic models through continuous time neural networks*, Master's thesis, Politecnico di Milano, December 2012, URL `http://hdl.handle.net/10589/71915`.

[306] Paduart, J., *Identification of nonlinear systems using polynomial nonlinear state space models*, Phd thesis, Vrije Universiteit Brussel, 2008.

[307] Morelli, E. A. and Klein, V., "Application of System Identification to Aircraft at NASA Langley Research Center," *Journal of Aircraft*, Vol. 42, No. 1, 2005, pp. 12–25. doi:10.2514/1.3648.

[308] Klein, V. and Morelli, E. A., *Aircraft System Identification: Theory And Practice*, AIAA Educational Series, 2006.

[309] Paduart, J., Lauwers, L., Swevers, J., Smolders, K., Schoukens, J., and Pintelon, R., "Identification of nonlinear systems using Polynomial Nonlinear State Space models," *Automatica*, Vol. 46, No. 4, 2010, pp. 647–656. doi:10.1016/j.automatica.2010.01.001.

[310] Morelli, E. A., "Global nonlinear aerodynamic modeling using multivariate orthogonal functions," *Journal of Aircraft*, Vol. 32, No. 2, 1995, pp. 270–277. doi:10.2514/3.46712.

[311] Marquardt, D. W., "An Algorithm for Least-Squares Estimation of Nonlinear Parameters," *Journal of the Society for Industrial and Applied Mathematics*, Vol. 11, No. 2, 1963, pp. 431–441.

[312] Atkins, P. and Worden, K., "Identification of a multi-degree-of-freedom nonlinear system," *Proceedings of the 15th International Modal Analysis Conference - IMAC*, Vol. 3089, Orlando, 1997, pp. 1023–1028.

[313] Richards, C. M. and Singh, R., "Feasibility of Identifying Non-Linear Vibratory Systems Consisting of Unknown Polynomial Forms," *Journal of Sound and Vibration*, Vol. 220, No. 3, 1999, pp. 413–450. doi:10.1006/jsvi.1998.1918.

[314] Bendat, J. S. and Piersol, A. G., *Random Data: Analysis and Measurement Procedures*, Wiley Series in Probability and Statistics, Wiley, March 2010.

[315] Adams, D. E. and Allemang, R. J., "Polynomial, non-polynomial, and orthogonal polynomial generating functions for nonlinear system identification," *Proceedings of the International Seminar on Modal Analysis (ISMA)*, Leuven, 2000.

[316] Kerschen, G., Worden, K., Vakakis, A. F., and Golinval, J.-C., "Past, present and future of nonlinear system identification in structural dynamics," *Mechanical Systems and Signal Processing*, Vol. 20, No. 3, 2006, pp. 505–592. doi:10.1016/j.ymssp.2005.04.008.

[317] Kerschen, G., Hemez, F. M., and Golinval, J.-C., "Bayesian Model Screening for the Identification of Nonlinear Mechanical Structures," *Journal of Vibration and Acoustics*, Vol. 125, June 2003, pp. 389–397. doi:10.1115/1.1569947.

[318] Leishman, J. G. and Beddoes, T. S., "A Semi-Empirical Model for Dynamic Stall," *Journal of the American Helicopter Society*, Vol. 34, No. 3, 1989, pp. 3–17. doi:doi:10.4050/JAHS.34.3.

[319] Farhat, C., Cortial, J., and Chapman, T., "A Hyper-Reduction Method for Nonlinear Structural Dynamics Reduced-Order Models," *Tenth World Congress on Computational Mechanics (WCCM X)*, Sao Paolo, Brazil, July 8-13 2012.

[320] Amsallem, D., Cortial, J., Deolalikar, S., Coderre, A., and Farhat, C., "Error Estimates for Element-Based Hyper-Reduction of Nonlinear Dynamic Finite Element Models," *Proceedings of the European Numerical Mathematics and Advanced Applications (ENUMATH) conference*, Lausanne, Switzerland, August 26-30 2013.

[321] Lawson, C. L. and Hanson, R. J., *Solving Least Squares Problems*, Society for Industrial and Applied Mathematics, 1995. doi:10.1137/1.9781611971217.

[322] Knoll, D. A. and Keyes, D. E., "Jacobian-free Newton-Krylov methods: a survey of approaches and applications," *Journal of Computational Physics*, Vol. 193, No. 2, 2004, pp. 357–397. doi:10.1016/j.jcp.2003.08.010.

[323] Baur, U., Beattie, C., Benner, P., and Gugercin, S., "Interpolatory Projection Methods for Parameterized Model Reduction," *SIAM Journal on Scientific Computing*, Vol. 33, No. 5, 2011, pp. 2489–2518. doi:10.1137/090776925.

[324] Chen, G., Sun, J., and Li, Y.-M., "Adaptive Reduced-Order-Model-Based Control-Law Design for Active Flutter Suppression," *Journal of Aircraft*, Vol. 49, No. 4, 2012, pp. 973–980.

[325] Galbally, D., Fidkowski, K., Willcox, K., and Ghattas, O., "Non-linear model reduction for uncertainty quantification in large-scale inverse problems," *International Journal for Numerical Methods in Engineering*, Vol. 81, No. 12, 2010, pp. 1581–1608. doi:10.1002/nme.2746.

[326] Bui-Thanh, T., Willcox, K., and Ghattas, O., "Parametric Reduced-Order Models for Probabilistic Analysis of Unsteady Aerodynamic Applications," *AIAA Journal*, Vol. 46, No. 10, 2008, pp. 2520–2529.

[327] Benner, P., Gugercin, S., and Willcox, K., "A Survey of Model Reduction Methods for Parametric Systems," Max Planck Institute Magdeburg Preprint MPIMD/13-14, August 2013, Available from `http://www.mpi-magdeburg.mpg.de/preprints/`.

[328] Amsallem, D. and Farhat, C., "Interpolation Method for Adapting Reduced-Order Models and Application to Aeroelasticity," *AIAA Journal*, Vol. 46, No. 7, 2008, pp. 1803–1813.

[329] Amsallem, D., Cortial, J., Carlberg, K., and Farhat, C., "A method for interpolating on manifolds structural dynamics reduced-order models," *International Journal for Numerical Methods in Engineering*, Vol. 80, No. 9, 2009, pp. 1241–1258. doi:10.1002/nme.2681.

[330] Begelfor, E. and Werman, M., "Affine Invariance Revisited," *Prooceedings of the 2006 IEEE Computer Society Conference on Computer Vision and Pattern Recognition*, Vol. 2, 2006, pp. 2087–2094. doi:10.1109/CVPR.2006.50.

[331] Son, N. T., "A real time procedure for affinely dependent parametric model order reduction using interpolation on Grassmann manifolds," *International Journal for Numerical Methods in Engineering*, Vol. 93, No. 8, 2013, pp. 818–833. doi:10.1002/nme.4408.

[332] Degroote, J., Vierendeels, J., and Willcox, K., "Interpolation among reduced-order matrices to obtain parameterized models for design, optimization and probabilistic analysis," *International Journal for Numerical Methods in Fluids*, Vol. 63, No. 2, 2010, pp. 207–230. doi:10.1002/fld.2089.

[333] Panzer, H., Mohring, J., Eid, R., and Lohmann, B., "Parametric Model Order Reduction by Matrix Interpolation," 2010.

[334] Amsallem, D. and Farhat, C., "An Online Method for Interpolating Linear Parametric Reduced-Order Models," *SIAM Journal on Scientific Computing*, Vol. 33, No. 5, 2011, pp. 2169–2198. doi:10.1137/100813051.

[335] Brillante, C., *Interpolazione di modelli aeroelastici parametrizzati*, Master's thesis, Politecnico di Milano, December 2012, URL `http://hdl.handle.net/10589/71884`.

[336] Geuss, M., Panzer, H., and Lohmann, B., "On parametric model order reduction by matrix interpolation," *Proceeding of the 2013 European Control Conference (ECC)*, Zürich, Switzerland, July 17-19 2013, pp. 3433–3438.

[337] Berrut, J. and Trefethen, L., "Barycentric Lagrange Interpolation," *SIAM Review*, Vol. 46, No. 3, 2004, pp. 501–517. doi:10.1137/S0036144502417715.

[338] Sadiq, B. and Viswanath, D., "Barycentric Hermite Interpolation," *SIAM Journal on Scientific Computing*, Vol. 35, No. 3, 2013, pp. A1254–A1270. doi:10.1137/110833221.

[339] Berrut, J.-P., Baltensperger, R., and Mittelmann, H. D., "Recent Developments in Barycentric Rational Interpolation," *Trends and Applications in Constructive Approximation*, edited by D. H. Mache, J. Szabados, and M. G. Bruin, Vol. 151 of *ISNM International Series of Numerical Mathematics*, Birkhäuser Basel, 2005, pp. 27–51. doi:10.1007/3-7643-7356-3_3.

[340] Baur, U., Benner, P., Greiner, A., Korvink, J., Lienemann, J., and Moosmann, C., "Parameter preserving model order reduction for MEMS applications," *Mathematical and Computer Modelling of Dynamical Systems*, Vol. 17, No. 4, 2011, pp. 297–317. doi:10.1080/13873954.2011.547658.

[341] Benner, P. and Breiten, T., "Low rank methods for a class of generalized Lyapunov equations and related issues," *Numerische Mathematik*, Vol. 124, No. 3, 2013, pp. 441–470. doi:10.1007/s00211-013-0521-0.

[342] van Bühren, G., Hornung, N., Clees, T., and Nikitina, L., "Aspects of adaptive hierarchical RBF metamodels for optimization," *Journal of Computational Methods in Science and Engineering*, Vol. 12, 2012, pp. 5–23. doi:10.3233/JCM-2012-0401.

[343] Dowell, E. H., "Nonlinear oscillations of a fluttering plate," *AIAA Journal*, Vol. 4, No. 7, 1966, pp. 1267–1275. doi:10.2514/3.3658.

[344] Stanford, B. and Beran, P., "Limit Cycle Oscillations of a Structurally-Optimized Cantilevered Wing," *Proceedings of the 13th AIAA/ISSMO Multidisciplinary Analysis Optimization Conference*, No. AIAA 2010-9124, AIAA, Fort Worth, Texas, 13-15 September 2010.

[345] Amabili, M., *Nonlinear Vibrations and Stability of Shells and Plates*, Cambridge University Press, 2008. doi:10.1017/CBO9780511619694.

[346] Ashley, H. and Zartarian, G., "Piston Theory-A New Aerodynamic Tool for the Aeroelastician," *Journal of the Aeronautical Sciences (Institute of the Aeronautical Sciences)*, Vol. 23, No. 12, 1956, pp. 1109–1118.

[347] Pierangelo, M., Massimiliano, L., and Paolo, M., "Multistep integration of ordinary, stiff and differential-algebraic problems for multibody dynamics applications," *Proceedings of the XVI Congresso Nazionale AIDAA*.

Symbols and Abbreviations

General Notation

Fields

$\mathbb{R}$	Set of real numbers
$\mathbb{R}_+$	Set of non-negative real numbers
$\mathbb{R}^n$	Set of n-dimensional real numbers
Ω	subset of $\mathbb{R}^n$

Constants and Indices

n	size of the full order model
l	size of the low order model
r	size of the reduced order model
N	number of the generalized degrees of freedom
I_n	Identity matrix of dimension $n \times n$
0_n	Null matrix of dimension $n \times n$

Subscript

ae	aeroelastic system
a	aerodynamic
am	aerodynamic related to structural motions
ag	aerodynamic related to gust
amg	unified aerodynamic (i.e. related to structural motions and to gust)
δ	Dirac function
θ	pitch
h	plunge
s	slow frequency content part
f	fast frequency content part
ss	simply stable part of a matrix
as	asymptotically stable part of a matrix
r	reduced system
nl	nonlinear term

Operations on Vectors, Matrices, and functions

$\|\|a\|\|$	Euclidean norm
vec$(\cdot)$	vectorization operator stacking the matrix columns on top of each other
$\otimes$	Kronecker product operator
$\dot{(\cdot)}$	$:= d(\cdot)/d(t)$, differentiation in the time domain
$(\cdot)'$	$:= d(\cdot)/d(jk)$, differentiation in the frequency domain
$\Delta(\cdot)$	difference operator in the iterative procedures
$\mathcal{D}(\cdot)$	either a diagonal matrix or the diagonal of a matrix

Aeroelastic System

t	time instant
τ	$= V_\infty t/l_a$, non-dimensionalized time domain
M_∞	freestream Mach number
Re_∞	freestream Reynolds number
V_∞	constant aircraft speed or freestream airspeed
q_∞	$= \frac{1}{2}\rho V_\infty^2$, freestream dynamic pressure
$\mathbf{v}_g$	gust/continuous turbulence velocity
$\mathbf{q}$	set of the generalized degrees of freedom
$\mathbf{N}_q$	structural modes
$\mathbf{M}$	generalized mass matrix
$\mathbf{C}$	generalized damping matrix
$\mathbf{K}$	generalized linear stiffness matrix
$\mathbf{f}_{\mathsf{nl}}$	vector of the generalized nonlinear internal forces of the structure
$\mathbf{Q}$	generalized aerodynamic forces
$\mathbf{u}$	vector of input of the state space system
$\mathbf{y}$	vector of output of the state space system
$\mathbf{x}$	vector of state variables of the system
$\mathbf{A}, \mathbf{B}, \mathbf{C}, \mathbf{D}$	state space representation matrices of the LTI system
$\mathbf{E}$	dynamic matrix, square and possibly singular, of models represented in a descriptor state-space form
$\mathbf{H}(s)$	generic transfer function associated to the linear system

Chapter 1

Symbols in order of appearance

$\mathbf{x}$	flow variables
$\mathbf{F}(\mathbf{x})$	vector including terms due to flow field nonlinearity (i.e. inviscid fluxes), flow field viscosity and other body forces
$\mathbf{G}(t)$	motion of the boundaries at the fluid-structure interfaces
$\mathbf{f}(\mathbf{x})$	inviscid fluxes
$\mathbf{d}(\mathbf{x})$	viscous fluxes
$\rho(\boldsymbol{x}, t)$	fluid density
$\boldsymbol{v}(\boldsymbol{x}, t)$	flow velocity
$E^{\mathsf{t}}(\boldsymbol{x}, t)$	total energy per unit volume
$P(\boldsymbol{x}, t)$	pressure
$\boldsymbol{\tau}(\boldsymbol{x}, t)$	viscous stresses tensor
$\boldsymbol{q}(\boldsymbol{x}, t)$	power exchanged by conduction
ϕ	scalar velocity potential function
c_∞	free-stream speed of sound
γ	heat capacity ratio
$c(\boldsymbol{x}, t)$	the local celerity of sound
$E(\boldsymbol{x}, t)$	domain function taking values 1 and 0 respectively outside and inside the body surface
$\mathcal{S}_{\mathsf{b}}$	body surface
G_{A}	fundamental solution for acoustic waves equation
$\mathcal{V}_{\mathsf{f}}$	fluid volume
$\mathcal{S}_{\mathsf{w}}$	wake surface
$\boldsymbol{v}_{\mathsf{b}}(\boldsymbol{x}, t)$	local velocity of the moving boundaries at $\boldsymbol{x}$
$\boldsymbol{n}(\boldsymbol{x}, t)$	normal unit vector to $\mathcal{S}_{\mathsf{b}}$ at $\boldsymbol{x}$, assumed positive when pointing outside the fluid domain
$\boldsymbol{v}_t$	transpiration velocity through the surface, equal to zero for impermeable surfaces
$\Omega(t)$	arbitrary control volume

$\mathcal{Y}_r$	generic subspace of the original phase space over which the full order system is projected
$\mathbf{Y}_r$	orthonormal basis spanning $\mathcal{Y}_r$
$\mathcal{X}_r$	generic subspace used for the state transformation
$\mathbf{X}_r$	orthonormal basis spanning $\mathcal{X}_r$
$\mathbf{G}_c$	controllability Gramian
$\mathbf{G}_o$	observability Gramian
$\mathbf{K}$	correlation matrix
$\mathbf{w}(t)$	white noise disturbance
$\mathbf{H}_w$	linear filter shaping the white noise disturbance $\mathbf{w}$
$\boldsymbol{\theta}$	parameter vector
δ	backward-shift (delay) operator

Abbreviations

CFD	Computational Fluid Dynamics
CAE	Computational Aeroelasticity
FSI	Fluid Structure Interaction
FEM	Finite Element Modeling
CSD	computational structural dynamics
MOR	Model Order Reduction
PDE	Partial Differential Equation
RANS	Reynolds Averaged Navier-Stokes
FP	Full Potential
DLM	Doublet Lattice Method
ALE	Arbitrary Lagrangian-Eulerian
DOFs	Degrees Of Freedoms
DAEs	Differential Algebraic Equations
ODEs	Ordinary Differential Equations
LTI	Linear Time Invariant
ROM	Reduced Order Modeling
SVD	Singular Value Decomposition
POD	Proper Orthogonal Decomposition
PCA	Principal Component Analysis
LS	Least-Squares
MIMO	Multi Input Multi Output

Chapter 2

Symbols in order of appearance

j	$=\sqrt{-1}$, imaginary unit
s	circular complex frequency
l_a	aerodynamic reference length (usually the mean aerodynamic semi-chord)
p	$= sl_a/V_\infty = h + jk$, complex reduced frequency
k	$= \omega l_a/V_\infty$, harmonic reduced frequency
$\mathbf{Q}_{amg}$	$= \mathbf{Q}_{am} + \mathbf{Q}_{ag}$, total generalized unsteady aerodynamic forces
$\mathbf{H}_{amg}$	$= [\mathbf{H}_{am}\, \mathbf{H}_{ag}]$, unified aerodynamic transfer matrix
$\mathbf{A}_w$, $\mathbf{B}_w$,$\mathbf{C}_w$	matrices of the state space realization of the continuous turbulence shaping filters
$H(t)$	Heaviside step function
$\delta(t)$	impulse function (Dirac delta)
h	plunge motion (i.e. rigid downward vertical translation)
θ	pitch motion (i.e. pure upward rigid plane rotation)
F_h	physical downward force
M_θ	pitch up moment
L	lift
$\boldsymbol{r}_i(\bar{\boldsymbol{x}})r_i$	generic rigid body modes

$\boldsymbol{r}_i(\bar{\boldsymbol{x}})$	shape of the rigid body modes
r_i	amplitudes of the rigid body modes
$\bar{\boldsymbol{x}}$	aerodynamic reference point
α	aircraft incidence
q	aircraft pitching rate
F_y	physical side force
M_ψ	yaw moment
M_ϕ	roll moments
v	rigid side motion
ψ	rigid yaw
ϕ	rigid roll
β	side slip angle
r	yaw rates
p	roll rates
V_F	flutter airspeed
λ	eigenvalues
$\mathbf{R}(\mathbf{x})$	generic nonlinear function
β	the bifurcation parameters
$\widehat{\mathbf{x}}$	equilibrium solution
$\mathbf{J}$	system Jacobian matrix

Abbreviations

LCFD	Linearized Computational Fluid Dynamics
GAAM	Generalized Aeroelastic Analysis Method
GAF	Generalized Aerodynamic Force
PSD	Power Spectral Density
FVM	Field Velocity Method
SVM	Split Velocity Method
LCO	Limit Cycle Oscillation

Chapter 3

Symbols in order of appearance

$\mathbf{S}$	real upper Schur matrix
$\mathbf{X}_s$	right Schur subspace
$\mathbf{Y}_s$	left Schur subspace
$\mathbf{X}_r$	right residual basis complementing $\mathbf{X}_s$
$\mathbf{Y}_r$	left residual basis complementing $\mathbf{Y}_s$
$\mathbf{X}_f$	right basis associated to the fast dynamic
$\mathbf{Y}_f$	left basis associated to the fast dynamic
m	order of the residualization
z	discrete frequency domain
n_k	number of harmonic reduced frequencies k
$\mathbf{W}$	appropriately assigned weighting matrix
n	order of the MFD
$\mathbf{N}_i$	numerator matrix term of the MFD
$\mathbf{D}_i$	quotient matrix term of the MFD
$\mathbf{R}_i$	remainder matrix term of the MFD
$\bar{p}$	collocation point jk
$\boldsymbol{\theta}$	unknown parameters assembled in a matricial form
$\mathbf{J}$	Jacobian matrix
λ	non-negative damping factor of the Levenberg-Marquardt method
$\mathbf{r}$	residual vector
$\mathbf{V}$	matrix of the eigenvectors
$\mathbf{e}$	vector of the eigenvalues

Abbreviations

ERA	Eigensystem Realization Algorithm
RMFA	Rational Matrix Fraction Approximation
MS	Minimum State
MFD	Matrix Fraction Description
LMFD	Left Matrix Fraction Description
RMFD	Right Matrix Fraction Description
MPA	Matrix Padé Approximation
LS1	First Least Squares Fitting Algorithm
LS2	Second Least Squares Fitting Algorithm
LS3	Third Least Squares Fitting Algorithm

Chapter 4

Symbols in order of appearance

x	abscissa coordinate of aircraft reference frame
$\mathbf{x}_0$	vector of gust patches distances from the aircraft reference frame
$\mathbf{V}_g(x, y, z, t)$	gust velocity profile in the absolute reference system
$V_g(\omega)$	Fourier transform of the gust spatial profile
$\mathbf{N}_{v_g}(x, y, z)$	frozen patches of the gust profile
ξ	abscissa coordinate of a local reference frame travelling with the gust
$\mathbf{v}_g(\xi)$	gust velocity profile in a local reference frame
α_g	local gust angle of attack (i.e. the local boundary condition associated to a gust)
$\mathbf{n}_0$	undeformed unit vector normal to the aircraft surface
$\mathbf{N}_g$	matrix containing the spatially fixed standing gust shape functions
N_k	k-th gust shape function
$\mathbf{q}_g$	vector of the amplitudes of the gust shape functions
S_0	undeformed reference surface penetrating the gust
$H_w(p)$	continuous turbulence's shaping filter (e.g. Dryden's)
L_g	reference gust length
$\mathbf{W}$	assigned intensity of the white noise input to the shaping filter
$\mathbf{\Sigma}_w$	variance of the continuous turbulence
$\mathbf{H}_{sf}$	transfer matrix of general shaping filters
ro	rolling off parameter of the shaping filter
V_g	discrete gust amplitude scaling factor
$\mathbf{q}_g$	generalized gust degrees of freedom
$\mathbf{Q}_a$	generalized unsteady aerodynamic forces
$\mathbf{x}_a$	aerodynamic state vector
$\mathbf{x}_{ae}$	aeroelastic state vector

Abbreviations

RGA	Resolved Gust Approach
DVA	Disturbance Velocity Approach

Chapter 5

Symbols in order of appearance

c.g.	center of gravity
r_α^2	nondimensional radius of gyration
μ	mass ratio
x_α	static unbalance

ω_h	uncoupled bending frequency
ω_α	uncoupled torsion frequency
ζ	structural damping coefficient
m_f	fuselage mass
m_w	airfoil mass
$S(k)$	Sears function
Δp	pressure load
w_n	normal harmonic velocity distribution
x, ξ	coordinates from the profile midpoint, non-dimensionalized to l_a
V_D	"dynamic divergence" instability velocity
V_F	flutter instability velocity
f_F	flutter frequency
$\Lambda_{c/4}$	sweepback angle
b	wing span
c_r	root chord
λ	taper ratio
ρ_s	density of the structure
$E_\parallel$	Young's moduli parallel to the elastic axis
$E_\perp$	Young's moduli orthogonal to the elastic axis
G	tangential elastic modulus
ν	Poisson's coefficient
I_ω	$= \omega_F/\omega_\alpha$, non-dimensional frequency ratio
I_F	$= V_F/(l_a\,\omega_\alpha\sqrt{\mu})$, flutter index
ω_α	circular frequency of the first normal torsional mode
C_{z,α_w}	lift coefficients along the wing span
C_{z,α_t}	lift coefficients along the tail span
C_{m,α_f}	aerodynamic moment coefficient of the fuselage
ε	downwash angle at the tail
$d\varepsilon/d\alpha$	downwash coefficient
c_w	wing mean aerodynamic chord (m.a.c.)
e_w	wing elastic axis position
S_w	wing surface area
c_t	tail stabilizer chord
b_t	tail stabilizer span
e_t	tail elastic axis position
S_t	horizontal tail surface area
x_t	stabilizer position
x_{cg}	center of gravity position
M	aircraft mass
I_y	inertia moment about lateral axis
Δn_z	load factor
M_{b_w}	bending moment (positive tip down) at the wing root
M_{t_w}	torsion moment (positive leading edge up) at the wing root
M_{b_t}	bending moment at the horizontal tail root
M_{t_t}	torsion momentat the horizontal tail root

Abbreviations

GMA	Gust Modes Approach
HTP	Horizontal Tail Plane
DPA	Dominant Poles Algorithm
N4SID	Numerical algorithms for Subspace State Space System IDentification

Chapter 6

Symbols in order of appearance

$\mathbf{f}_{\text{nl}}$	nonlinear mapping

$\mathbf{q}$	reduced state vector
$\mathbf{V}$	state transformation global basis
$\mathbf{W}$	projection subspace global basis
$\boldsymbol{\Phi}$	reduced basis over which to project the nonlinear term
$\boldsymbol{\alpha}(t)$	coefficients of the reduced basis $\boldsymbol{\Phi}$
P	projection matrix extracting selected rows of a given matrix
$\mathbf{e}_i$	i^{th} canonical vector in $\mathbb{R}^n$
$\mathbb{P}$	oblique projector
$\boldsymbol{\zeta}(t)$	vector in the state equation containing nonlinear monomials in the state and the input
$\boldsymbol{\eta}(t)$	vector in the output equation containing nonlinear monomials in the state and the input
$\mathbf{E}$	matrix of the coefficients of the monomials in $\boldsymbol{\zeta}$
$\mathbf{F}$	matrix of the coefficients of the monomials in $\boldsymbol{\eta}$
$\boldsymbol{\xi}_{\{p\}}$	all the distinct nonlinear combinations of degree two up to $\{p\}$
$\boldsymbol{\xi}_{(q)}$	vector containing all the distinct monomials of degree q composed by the elements of vector $\boldsymbol{\xi}$
$\mathbf{e}(t, \boldsymbol{\theta})$	error between the measured output and those of the identified system
$\mathbf{W}_e$	weighting matrix
$\boldsymbol{\theta}$	unknown parameters
$\mathcal{F}(\boldsymbol{\theta})$	cost function
N_t	number of sampling points
$\mathbf{u}$	vector of the state of the full order model
$\mathbf{f}(\mathbf{u})$	vector of the nonlinear internal forces
$\mathbf{f}_{\text{ext}}$	vector of the external forces
$\mathbf{f}_r$	reduced nonlinear force term
α_e	positive local weight applied to the retained finite elements
n_e	number of retained finite elements
N_e	overall number of finite elements
m	number of degrees of freedoms of a single finite element
$\mathbf{K}_r$	global reduced stiffness matrix

Abbreviations

LTV	Linear-Time-Varying
FOM	Full Order Model
MPE	Missing Point Estimation
EIM	Empirical Interpolation Method
DEIM	Discrete Empirical Interpolation Method
UDEIM	Unassembled Discrete Empirical Interpolation Method
GNAT	Gauss-Newton with Approximated Tensors
PNLSS	Polynomial Non-Linear State Space
NLS	Nonlinear Least Squares
EBHR	Element-Based Hyper-Reduction
FE	Finite Element
FV	Finite Volume
NNLS	Non-Negative Least Squares

Chapter 7

Symbols in order of appearance

d	number of the set of parameters
$\mathbf{p}$	vector of the parameters
$\widehat{(\cdot)}$	interpolated quantity
$\mathbf{V}_i$	i-th state transformation local basis
$\mathbf{W}_i$	i-th projection subspace local basis

$\mathcal{T}_{\mathcal{P}}$	tangent space at the point $\mathcal{P}$
$\mathcal{S}_{n,r}$	Stiefel manifold (i.e. set of all r-dimensional orthonormal bases of $\mathbb{R}^n$, for $1 < r < n$)
$\mathbf{Q}_i$, $\mathbf{P}_i$	congruence transformation matrices for the local reduced order models
D	plate rigidity
h	plate thickness
ε_{xx}, ε_{yy}, ε_{xy}	plate internal strains
u, v, w	plate displacements
p_{aero}	aerodynamic pressure load
λ	non-dimensional dynamic pressure
$\mathbf{K}_{\mathsf{a}}$	aerodynamic stiffness matrix
$\mathbf{C}_{\mathsf{a}}$	aerodynamic damping matrix
$\boldsymbol{\mathcal{I}}_p$	interpolation matrix
$\mathbf{N}_w$	shape function related to the out-of-plane displacement w
λ^*	critical dynamic pressure

Abbreviations

PROM	Parametric Reduced Order Model

Summary

Model Order Reduction for Computational Aeroelasticity

Matteo Ripepi

This thesis presents a few approaches to reduced order models within the framework of computational aeroelasticity.

The advent and development of high-performance computing is requiring, more and more, procedures and techniques aimed at reducing the computational effort of high-fidelity high-dimensional computational fluid dynamic based aeroelastic systems, in order to afford accurate and fast evaluation of the load databases essential for aircraft design. The adoption of reduced order modeling techniques represents a promising approach to achieve this goal. The generation of low-dimensional models preserving the main behavior and the features of the original problem may be realized in many ways.

In this thesis, the model order reduction of the aerodynamic subsystem, aimed at obtaining accurate aerodynamic generalized forces, is addressed through the use of both identification techniques as well as projection methods. Linearized aerodynamic models are at first considered, both in a state-space form or through their transfer matrix representation. A Petrov-Galërkin approach is developed where the linearized aerodynamic subsystem is projected onto left/right Schur subspaces. Global reduced bases are obtained from an eigenanalysis of the state space matrices of the system. The method proposes a Schur-based formulation, completely decoupling the low and fast subspaces of the system spectrum. This allows an efficient residualization of the fast dynamic, contributing to more accurate reduced order models. The drawback of the eigenbased model reduction for an aerodynamic subsystem is that the dominant spectrum becomes more and more rich as the computational grid is refined. Therefore a proper selection of the aerodynamic modes must be devised in order to avoid retaining in the subspace many worthless eigenvectors which would make the reduced model larger than necessary. Hence, instead of focusing on the dominant state dynamics, the proposed method tries to complements the low frequency Schur subspace by further mapping the input-output behavior, which is the key parameter to be captured by the reduced model. This is achieved through a dominant pole criterion plus, the controllability and observability, thus selecting the global modes which are likely to contribute more to the input-output relation of the aerodynamic model.

Differently, identification methods are more suitable whenever the aerodynamic subsystem is available through its transfer matrices, related to structural motions and gusts, thus

requiring the identification of an asymptotically stable finite state aerodynamic subsystem. To such an aim the thesis develops an improved rational matrix approximation, combining three nonlinear least squares identification techniques with a system reduction based on a double dynamic residualization, which maintains an accurate fitting up to relatively high frequencies. It significantly improves a previous matrix fraction description formulation through: the adoption of a more appropriate performance index, the avoidance of a tweaked iterated weighting to ensure the identification of a stable model, the obtainment of either lower order models for an assigned precision or a better fitting for a given order, and the omission of a costly final constrained nonlinear optimization.

An alternative gust formulation is also proposed which approximates the gust profile traveling towards the aircraft using a series of disturbance velocity shape functions fixed in space, named gust modes. The approach, reconstructing generalized gust forces through these special structural motion like modes, makes it possible to determine a gust response even without the usual gust penetration model. In the time domain an impulse response is then obtained from each of the gust modes, so recovering the aerodynamic load response using a convolution technique. The traveling contribution of the gust running towards the aerodynamic model, as well as the true gust shape profile, is devolved to generalized coordinates calculated as a post-processing through a least squares interpolation of the gust profile. The approach avoids building an aerodynamic reduced model for each different gust profile case considered in the loads database, thus reducing the overall number of gust simulations required in the gust loads analysis process. The procedure has proved its effectiveness in carrying out aerodynamic transfer matrices obtained from low fidelity models (e.g. Theodorsen theory, strip theory, double-lattice method), as well as reconstructing loads responses of high-fidelity aerodynamic models, based on Euler equation, for complete aircraft cases of industrial relevance.

In order to include nonlinear effects, necessary to better predict important aeroelastic and aerodynamic phenomena (e.g. limit cycle oscillations), reduction techniques for nonlinear systems have been also developed. A method identifying a nonlinear state-space model approximating the behavior of nonlinear aeroelastic systems from input-output time histories training signals is proposed. The procedure carries out a linear state space using the matrix fraction description, which is then extended with polynomials nonlinear terms in the state and the input, whose unknown coefficient matrices are obtained through a least-squares fitting.

Alternatively, within projection based framework, a recently developed model reduction approach for the efficient and fast solution of nonlinear finite-element based dynamical systems is exploited for nonlinear aeroelastic systems. Such a model reduction relies on a Galërkin projection of the high-dimensional dynamical system onto a set of Proper Orthogonal Decomposition modes, followed by an hyper-reduction carried out with a weighted evaluation of the nonlinear terms onto a subset of the finite elements. The weights, taking into account for the contribution of the discarded elements, are precomputed using a non-negative least-squares problem minimizing the discrepancy between the nonlinear term and its approximation onto the elements subset. This hyper-reduction step enables an online evaluation of the reduced-order model that does not scale with the large dimension of the original problem. Afterwards a parametric reduced order model is obtained using a global reduced basis carried out by considering reduced bases computed after simulating the system on a set of parameters.

Sommario

Riduzione d'Ordine dei Modelli per Aeroelasticità Computazionale

Matteo Ripepi

Questa tesi presenta alcuni approcci per la riduzione dell'ordine dei modelli sviluppati nell'ambito dell'aeroelasticità computazionale.

L'avvento e lo sviluppo del calcolo ad alte prestazioni sta richiedendo sempre più l'uso di procedure e tecniche per la riduzione del costo computazionale di sistemi aeroelastici di ordine elevato, basati sulla fluidodinamica computazionale, allo scopo di rendere possibile la valutazione dei carichi dimensionanti, essenziali per il progetto di velivoli, in maniera accurata e veloce. L'adozione di tecniche di modellazione ridotta rapresenta un approccio promettente per raggiungere tale obiettivo. La generazione di modelli ridotti, che preservino il comportamento principale e le caratteristiche del problema originale, può essere ottenuta in molti modi.

In questa tesi, la modellazione ridotta del sottosistema aerodinamico, al fine di ottenere forze aerodinamiche generalizzate, è ottenuta attraverso tecniche di identificazione e metodi proiettivi. Modelli aerodinamici linearizzati sono considerati, sia nello spazio degli stati che attraverso la loro matrice di trasferimento. Viene sviluppato un approccio alla Petrov-Galërkin dove il sottosistema aerodinamico è proiettato su sottospazi di Schur destri e sinistri. Basi ridotte globali sono ottenute da un'analisi agli autovalori delle matrici agli stati del sistema. Il metodo propone una formulazione basata su sottospazi di Schur che realizzano un disaccoppiamento completo della dinamica lenta e veloce del sistema. Questo permette una residualizzazione efficiente della dinamica veloce, portando a modelli di ordine ridotto più accurati. Lo svantaggio di formulazioni di modellazione ridotta basate su modi aerodinamici è che lo spettro dominante diventa via via più ricco con il raffinamento della griglia di calcolo. Quindi una selezione dei modi aerodinamici deve essere concepita per evitare di tenere nel sottospazio autovettori che non portano informazioni aggiuntive e implicherebbero modelli ridotti di dimensioni più grandi del necessario. Il metodo proposto complementa la dinamica di bassa frequenza dei sottospazi di Schur, cercando una mappatura del comportamento ingresso-uscita attraverso il criterio dei poli dominanti ed i concetti di controllabilità e osservabilità, in tal modo selezionando i modi globali che contribuiscono maggiormente alla relazione ingresso-uscita del modello aerodinamico.

Diversamente, le techniche di identificazione sono più adatte ogniqualvolta il sottositema aerodinamico è disponibile attraverso le sue matrici di transferimento, relative alla dinamica strutturale e ai disturbi da raffica, rendendo così necessario l'identificazione di un

sottosistema aerodinamico agli stati asintoticamente stabile. A tale scopo la tesi sviluppa un'approssimazione mediante rappresentazioni matriciali fratte, combinando tre tecniche di identificazione ai minimi quatrati nonlineari con un processo di riduzione basato su una residualizzazione dinamica doppia, che mantiene una curva interpolante accurata fino a frequenze relativamente alte. Il metodo migliora una precedente formulazione attraverso: l'adozione di un indice di prestazione più appropriato, evitando l'uso di tecniche di pesatura che assicurano l'identificazione di un modello stabile, l'ottenimento di modelli ridotti di basso ordine, assegnata la pecisione, o un'interpolazione più accurata, assegnato l'ordine, e infine l'omissione di una costosa ottimizzazione nonlineare vincolata.

La tesi propone anche una formulazione alternativa di risposta alla raffica, in cui la raffica in moto relativo verso il velivolo è approssimata attraverso una serie di funzioni di forma rappresentanti disturbi di velocià fissi nello spazio, nominati modi di raffica. L'approccio, ricostruendo le forze generalizzate attraverso questi simil modi strutturali, rende possibile determinare la risposta alla raffica anche senza l'uso del classico metodo di penetrazione. Nel dominio del tempo una risposta impulsiva è poi ottenuta per ogni modo di raffica, ricostruendo la risposta del carico aerodinamico usando una convoluzione. Il contributo di moto della raffica viaggiante verso il modello aerodinamico, così come l'effettivo profilo della raffica, è devoluto a coordinate generalizzate calcolate a posteriori attraverso un'interpolazione ai minimi quadrati del profilo di raffica. L'approccio evita di costruire un modello aerodinamico ridotto per ogni profilo di raffica considerato nel database dei carichi, in tal modo riducendo il numero totale di simulazioni richieste nel processo di generazione dei carichi da raffica. L'efficacia della procedura è stata provata nell'ottenere matrici di trasferimento dell'aerodinamica per modelli a bassa fedeltà (e.g. la teoria di Theodorsen, la teoria delle strisce, il metodo a reticolo di doppiette), così come nel ricostruire la risposta dei carichi di modelli aerodinamici ad alta fedeltà, basati sulle equazioni di Eulero, per casi di velivoli completi.

Allo scopo di introdurre efetti nonlineari, necessari per una miglior predizione di importanti fenomeni aeroelastici (e.g. cicli limite) ed aerodinamici, sono anche state sviluppate tecniche di riduzione per sistemi nonlineari. La tesi propone un metodo che identifica un modello nonlinear agli stati approssimante il comportamento di sistemi aeroelastici nonlineari da storie temporali di ingresso-uscita. La procedura identifica dapprima un modello lineare nello spazio degli stati, che succesivamente estende con termini nonlineari polinomiali nello stato e nell'ingresso, i cui coefficienti incogniti sono ottenuti attraverso un'interpolazione ai minimi quadrati.

In alternativa, nell'ambito dei metodi proiettivi, la tesi esplora un recente approccio di modellazione ridotta per la soluzione efficiente e veloce di sistemi dinamici modellati con elementi finiti, applicandolo a sistemi aeroelastici nonlineari. Il metodo usa una proiezione alla Galërkin del sistem dinamico di ordine elevato su un insieme di modi derivanti da una decomposizione ortogonale propria, seguita da una hyper-riduzione compiuta con una valutazione pesata del termine nonlineare su un sottoinsieme degli elelemtni finiti. I pesi, tenendo conto del contributo degli elementi scartati, sono pre-calcolati usando minimi quadrati non-negativi minimizzanti la discrepanza tra il termine nonlineare e la sua approssimazione sul sottoinsieme di elementi. Questa hyper-riduzione consente una valutazione del modello ridotto indipendente dalle dimensioni del problema originale. Successivamente un modello ridotto parametrico è ottenuto usando una base ridotta globale realizzata da basi ridotte calcolate da simulazioni del sistema per un insieme di parametri.

Curriculum Vitae

I was born in October 10th, 1983 in Busto Arsizio (VA), Italy. I started my journey in the aeronautical world in the high-school years becoming an industrial technician in aeronautical constructions at the Giacomo Fauser technical institute, Novara, Italy. After that, I got my B.Sc. in Aerospace Engineering with full marks at Politecnico di Milano in 2005. From the end of 2005 I was enrolled in the master program of Politecnico di Milano and I earned my M.Sc. in Aeronautical Engineering with honors in October 2008. The title of the thesis was: "Nonlinear Aeroservoelastic Analysis of a Highly-Flexible Aircraft" supervised by Prof. P. Mantegazza. In the same period I had a research visiting experience at the Daniel Guggenheim School of Aerospace Engineering at Georgia Institute of Technology, Atlanta, GA, USA, under the supervision of Prof. D. H. hodges. After the degrees I spent two years as a junior aeroelastic engineer in the Sistemi Dinamici S.p.A., an Engineering Company between Ingegneria dei Sistemi S.p.A. and AgustaWestland, supporting AW in its business for product innovation.

Since September 2011 I have been working towards my Ph.D. degree at the Dipartimento di Scienze e Tecnologie Aerospaziali, Politecnico di Milano, Milano, Italy. The Ph.D. research has been focused on approaches to generate and apply reduced order models for aeroelastic computations, with a focus on gust loads, and it has been supervised by Prof. P. Mantegazza. During my Ph.D. project I spent a four-months stay at the Institute of Aerodynamics and Flow Technology of DLR, the German Aerospace Center, Braunschweig, Germany, collaborating with Dr. S. Görtz, and a three-months stay at the Department of Aeronautics & Astronautics of Stanford University, Stanford, CA, USA, collaborating with Dr. D. Amsallem in the Farhat Research Group.

"The gulls who scorn perfection for the sake of travel go nowhere, slowly. Those who put aside travel for the sake of perfection go anywhere, instantly."

— Richard Bach, Jonathan Livingston Seagull (1970)